Influence of Seasonally Variable Hypoxia on Epibenthic Communities in a Coastal Ecosystem, British Columbia, Canada

by

Jackson Wing Four Chu
B.Sc., Simon Fraser University, 2006
M.Sc., University of Alberta, 2010

A Dissertation Submitted in Partial Fulfillment
of the Requirements for the Degree of

DOCTOR OF PHILOSOPHY

in the Department of Biology

Supervisory Committee

Influence of Seasonally Variable Hypoxia on Epibenthic Communities in a Coastal Ecosystem, British Columbia, Canada

by

Jackson Wing Four Chu
B.Sc., Simon Fraser University, 2006
M.Sc., University of Alberta, 2010

Supervisory Committee

Dr. Verena Tunnicliffe (Department of Biology, School of Earth and Ocean Sciences)
Supervisor

Dr. Francis Juanes (Department of Biology)
Departmental Member

Dr. Rana El-Sabaawi (Department of Biology)
Departmental Member

Dr. Roberta Hamme (School of Earth and Ocean Sciences)
Outside Member

Abstract

Supervisory Committee
Dr. Verena Tunnicliffe (Department of Biology, School of Earth and Ocean Sciences)
Supervisor
Dr. Francis Juanes (Department of Biology)
Departmental Member
Dr. Rana El-Sabaawi (Department of Biology)
Departmental Member
Dr. Roberta Hamme (School of Earth and Ocean Sciences)
Outside Member

Natural cycles of environmental variability and long-term deoxygenation in the ocean impose oxygen deficiency (hypoxia) on marine communities. My research exploits a naturally occurring hypoxia cycle in Saanich Inlet, British Columbia, Canada where I combined spatial surveys with remotely operated vehicles, ecological time-series from the subsea cabled observatory VENUS, and lab-based respirometry experiments to examine the influence of seasonally variable oxygen conditions on epibenthic communities.

In situ oxygen thresholds established for dozens of fish and invertebrate species in this system show they naturally occur in lower oxygen levels than what general lethal and sublethal thresholds would predict. Expansion of hypoxic waters induced a loss of community structure which was previously characterized by disjunct distributions among species. Communities in variable hypoxia also have scale-dependent structure across a range of time scales but are primarily synchronized to a seasonal oscillation between two phases. Time-series revealed timing of diurnal movement in the slender sole *Lyopsetta exilis* and reproductive behavior of squat lobster *Munida quadrispina* in the hypoxia cycle. Hypoxia-induced mortality of sessile species slowed the rate of community recovery after deoxygenation. The 10-year oxygen time-series from VENUS, revealed a significant increase in the annual low-oxygen period in Saanich Inlet and that deoxygenation has occurred in this system since 2006. Differences in the critical oxygen thresholds (O_2^{crit}) and standard metabolic rates of key species (spot prawn *Pandalus platyceros*, slender sole, and squat lobster) determined the lowest *in situ* oxygen at which populations occurred and explained disproportionate shifts in distributions and

community respiration. Finally, a meta-analysis on global O_2^{crit} reported for crustaceans showed that hypoxia tolerance differs among major ocean basins.

Long-term trends of deoxygenation suggest a future regime shift may occur when the duration at which a system remains below critical oxygen levels exceeds the time needed for communities to recover. Species-specific traits will determine the critical threshold and the nature of the community response in systems influenced by variable states of oxygen deficiency. However, oceanographic and evolutionary history provides context when determining the regional response of benthic communities influenced by rapidly changing environments.

Table of Contents

List of Tables

List of Figures

Acknowledgments

My research would not have been possible without my supervisor, Verena Tunnicliffe. She created the foundation, freedom, and endless opportunities to find my own way and followed the three strikes rule in regards to the live animal experiments. I express my sincere thanks to my committee members, Roberta Hamme, Francis Juanes, and Rana El-Sabaawi for their feedback as I meandered through each step of my degree. Thank you especially to Francis for letting me "squat" in his lab while my fish continued to "flatline". Thank you to Lisa Levin; our brief chats gave me insight and direction. And my utmost gratitude goes to Jonathan Rose for his technical diversity, even persona, and consistent support.

The constant professionalism of CSSF/ROPOS and the Captains and crew of the CCGS JP Tully, CCGS Vector, RV Thompson, and RV Falkor contributed immensely to my research. I am grateful to staff at VENUS for the ship and ROV support during their hectic maintenance cruises. I was able to focus on research for almost the entirety of my degree because of the generous funding provided by NSERC, University of Victoria, Marine Technology Society, and CHONe,

My family has been a continued source of stability during all my academic pursuits and I thank them for patience and understanding. My partner, Katie Gale, reminded me of the small things in life which brought a balance to my big picture pursuits. S.T. Bear helped me stay creative. Finally, thanks to *Neovision vision* for a story that I will keep telling for the rest of my career.

Chapter 1: General Introduction

Background

Oxygen loss in the ocean

Rising atmospheric CO_2 is projected to increase stratification of surface waters, decrease the strength of thermohaline circulation, and shift the distribution and concentration of oxygen in the ocean (Keeling *et al.*, 2010; Gattuso *et al.*, 2015). As a result, the volume of naturally-occurring oxygen minimum zones in the deep ocean is predicted to expand (Bopp *et al.*, 2013). In coastal waters, regional-scale drivers such as the relaxation of wind-driven upwelling events, localized changes in rainfall, and increased nutrient flux can further reduce the amount of environmental oxygen ($[O_2]_{env}$) (Rabalais *et al.*, 2002; Chan *et al.*, 2008; Levin *et al.*, 2009b). As a consequence of changes in environmental forcing, the worldwide occurrence of hypoxic systems ($[O_2]_{env}$ < 1.4 ml l^{-1}) has increased and its severity is predicted to worsen (Diaz & Rosenberg, 2008; Keeling *et al.*, 2010). Model consensus predicts average $[O_2]_{env}$ in the global ocean will continue to decline by a further 1.8 to 3.5 % by the year 2100 (Bopp *et al.*, 2013). Under the most stringent scenario of climate change mitigation, $[O_2]_{env}$ in the ocean is not projected to recover by the end of the 21st century (Bopp *et al.*, 2013; Gattuso *et al.*, 2015).

Distribution of oxygen in the northern Pacific Ocean

At the scale of the Northern Pacific Ocean, oxygenated deep waters are formed in the Sea of Okhotsk, Russia, where atmospheric oxygen enters into the ocean surface. The

denser, oxygenated water sinks into deeper depths and, through advection, travels eastwards towards North America (Whitney *et al.*, 2007). Oxygen is lost through biological conversion of organic to inorganic compounds (remineralization) during the multidecadal transit to reach the eastern Pacific Ocean. Here, the oxygen-depleted water combines with water carried by the California undercurrent, which also becomes oxygen-depleted through remineralization as it flows northward along the western continental shelf of North America. Wind-driven upwelling along the continental shelf and high productivity conditions (Hales *et al.*, 2006) can result in the expansion of oxygen-depleted waters into shallower depths which reduces the extent of aerobically viable habitat for populations of benthic invertebrates and demersal fish. Such was the case for the Oregon coast in 2002, where the upwelling of severely deoxygenated waters into surface depths caused the acute response of massive mortality in local crab and fish populations (Grantham *et al.*, 2004; Chan *et al.*, 2008). Oxygen levels along the Canadian Pacific coast have persistently declined in the past 30 years (Crawford & Peña, 2013). While the impacts of oxygen deficiency are well-established for many systems across the globe (Diaz & Rosenberg, 2008), the consequences of oxygen deficiency for benthic communities in the northeast Pacific waters of Canada have not been addressed and will be the primary focus of my dissertation.

Multi-level response of metazoan life to low oxygen

Apart from possibly a few extreme species (Danovaro *et al.*, 2010), modern metazoans have evolved to require oxygen to varying degrees (Thannickal, 2009). Oxygen has a central role in aerobic metabolism; it is used as a terminal electron acceptor

in the electron transport chain which occurs in the mitochondria. Through a series of high energy-yielding processes (i.e., ATP creation), electrons are transported by the coenzymes NADH and $FADH_2$, which regenerate to NAD and FAD when they donate their electrons, forming H_2O as a by-product. When oxygen supply is too low to allow regeneration of the finite supply of NAD and FAD, no ATP can be formed and cell death can occur (Hill *et al.*, 2008). Although alternative anaerobic pathways exist to create ATP in aerobic metazoans, they are generally much less energy efficient. For most animals, exposure to $[O_2]_{env}$ outside the normal range of variability can be considered stressful and invokes responses at the physiological, population, and community level.

Most animals live within a 'safety range' of $[O_2]_{env}$, or normoxia, and homeostasis is maintained by the regulatory capacity of each species' internal milieu. When exposed to $[O_2]_{env}$ that is outside the range of normoxia, acclimatization is the 'first line of defense' (Hochachka & Somero, 2002). Physiological responses include biochemical modifications to the structure and function of oxygen carrying proteins, such as hemoglobin and hemocyanin, which increase their oxygen affinity in the circulatory system. This phenomenon is particularly well understood in several species of fish and crustaceans (Mcmahon, 2001; Wells, 2009). When $[O_2]_{env}$ conditions shift below the safety range (i.e., into hypoxia), mobile animals can migrate into more oxygenated waters or adapt to living under stress by either improving the efficiency of oxygen delivery or by reducing overall energy demand (Hochachka, 1997; Childress & Seibel, 1998). Physiological delivery of oxygen to the cells depends on both blood O_2 concentration and cardiac output; adaptations to increase oxygen delivery can manifest as changes in morphology and behavior (Farrell & Richards, 2009). Organism-level responses to

hypoxia reported in fish and crustaceans include increases in gill ventilation, gill perfusion, cardiac output, hemoglobin/hemocyanin concentration, and tissue oxygen (Mcmahon, 2001; Farrell & Richards, 2009). Metabolic suppression as a response to low $[O_2]_{env}$ is also suggested to be a common strategy in both fish and invertebrate species (Richards, 2010; Seibel, 2011). Species from most invertebrate phyla other than Echinodermata have been reported to depress their metabolism by 60-100% of their standard rate under environmental stress (Guppy *et al.*, 1994). A few marine organisms such as European eel *Anguilla anguilla* (van Ginnekan *et al.*, 2001) and the galatheid crab *Munida rugosa* (Zainal *et al.*, 1992) can temporarily exploit anaerobic metabolism when exposed to sublethal levels of $[O_2]_{env}$ (Hill *et al.*, 1991; Sato *et al.*, 1993), but these pathways are unlikely to be permanently sustainable due to their lower ATP yield compared to aerobic metabolism.

Physiological responses to hypoxia can eventually drive changes observed at the population level. Increased mortality and reduced metabolism can decrease the biomass of populations and shift them towards smaller body sizes. As less energy may be available for the development of reproductive structures (Wu, 2009), annual events such as spawning seasons may be affected. To avoid metabolically unfavorable areas, poleward shifts in the populations of mobile species may result (Deutsch *et al.*, 2015). However, because hypoxia tolerance differs among animal groups (Vaquer-Sunyer & Duarte, 2008), the response in feeding, growth, reproduction, and survival in future oxygen deficient conditions will also vary among species.

The community level response to hypoxia may best address the broad-scale influence of hypoxia because shifts in the identity, abundance, and spatial arrangement of

species (i.e., compositional heterogeneity) can be linked back to changes in the environment. Although random processes can also predict patterns of species relative abundance (Hubbell, 1997; Bell, 2001), this would also predict no relationship among species traits, abundances, community composition, and conditions in the environment. However, physiological trait differences among species can mechanistically explain community assembly patterns along environmental gradients (McGill *et al.*, 2006; Pörtner & Farrell, 2008). Because of metabolic limitations in low oxygen, deoxygenation can restructure communities by excluding hypoxia sensitive species (e.g., due to death or migration) which may create a new niche for new, hypoxia-tolerant species to exploit. When ocean oxygen decreases to the point of severe hypoxia ($[O_2]_{env} < 0.5$ ml l^{-1}), the diversity and biomass of benthic metazoan species linearly decrease and chemosynthetic, sulfur-oxidizing bacterial mats (*Thioploca* or *Beggiatoa* spp.) emerge to utilize the appearance of H_2S (Rabalais *et al.*, 2002). Chronic severe hypoxia eventually alters trophic structure as energy does not transfer up to the higher levels of the food chain due to the absence of the larger animals (Diaz & Rosenberg, 2008). Continued depletion of $[O_2]_{env}$ towards zero shifts the energetics of the system as alternative electron acceptors sequentially replace O_2 (*in decreasing order of energy yield*: NO_3^-, NO_2^-, Mn^{+4}, Fe^{+3}, SO_4^{2-}, Froelich *et al.*, 1979). The ecosystem shifts from a state of interactions dominated by larger metazoans to one driven by microbial activity, and possibly by eukaryotic microorganisms (Edgcomb *et al.*, 2010). A net loss of ecosystem function results from the overall reduction in biomass.

Seasonal hypoxia cycle in Saanich Inlet

My dissertation takes advantage of a naturally occurring hypoxia cycle in Saanich Inlet, British Columbia, Canada. Saanich Inlet is a 24-km long basin, with a maximum depth of 230 m and nested within the Salish Sea (Fig. 1.1a). At the mouth of Saanich Inlet, a shallow sill at 75 m depth (Fig.1.1b) restricts deep water circulation and exchange with source waters outside the inlet (Gargett *et al.*, 2003). Deoxygenation at depth occurs when the high productivity in the inlet (Timothy & Soon, 2001; Grundle *et al.*, 2009) sinks and is consumed by microbial respiration (Zaikova *et al.*, 2010).

Below sill depths, the inlet transitions from oxygenated ($[O_2]_{env} > 1.4$ ml l^{-1}) to hypoxic to anoxic ($[O_2]_{env} = 0$). The anoxic water is eventually flushed with dense, oxygenated water during renewal events that can occur in spring and fall (Anderson & Devol, 1973; Manning *et al.*, 2010). In 2006, the Victoria Experimental Network under the Sea (VENUS) observatory was installed in Saanich Inlet and began capturing high frequency oxygen and water column data (most data are collected per minute). The VENUS time-series resolves the seasonally alternating phases of deoxygenation and reoxygenation as well as the magnitude of the hourly oxygen fluctuations (Fig. 1.2a). The natural, multi-scale variability of $[O_2]_{env}$ has not been addressed as a driver of community-level patterns because of the lack of permanent, *in situ* monitoring and concomitant biological measurements. The location and technological infrastructure of VENUS in Saanich Inlet provide a globally unique opportunity to study the spatio-temporal patterns of benthic communities influenced by rapidly fluctuating $[O_2]_{env}$

conditions. The length of the continuous VENUS time-series also allows me to examine oxygen trends in Saanich Inlet over 10 years.

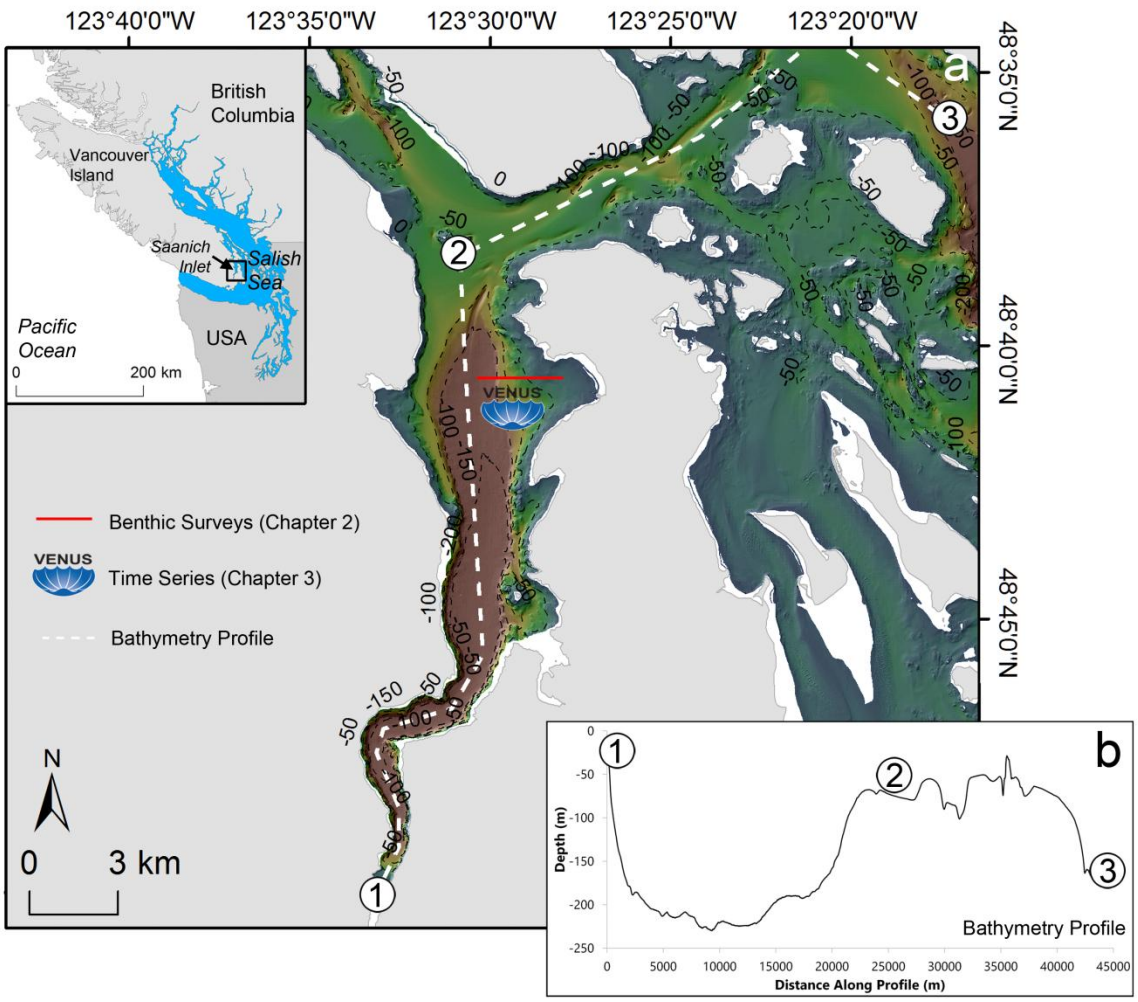

Figure 1.1. Field sites of my dissertation. (a) Saanich Inlet is located in Vancouver Island, nested within the Salish Sea (inset in blue) and on the Pacific coast of British Columbia, Canada. (b) A shallow sill at 75 m depth restricts circulation which results in a seasonal hypoxia cycle occurring in the deeper waters of the inlet. Circled numbers correspond to points along the bathymetry profile. *In situ* data in this dissertation came from benthic imagery surveys with remotely operated vehicles (Chapter 2) and time-series from the VENUS cabled observatory (Chapter 3).

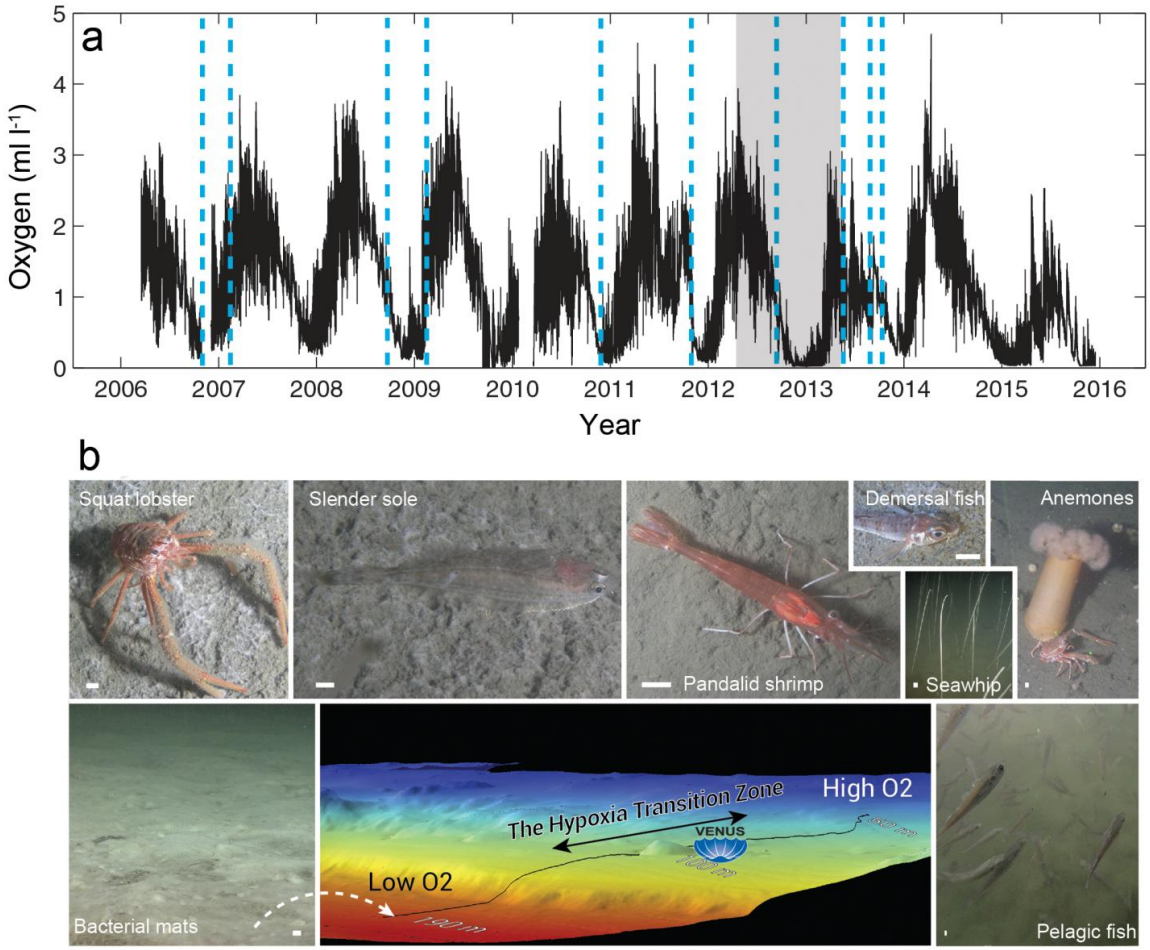

Figure 1.2. Spatio-temporal sampling in Saanich Inlet. (a) The 10-year VENUS oxygen time-series resolves a seasonally predictable hypoxia cycle at 96 m depth. Vertical blue dashed lines indicate timing of benthic surveys described in Chapter 2. The grey band indicates the 14-month period of the *in situ* ecological-time series described in Chapter 3. (b) Some representative species of the benthic community in Saanich Inlet. Note that pelagic fish (e.g., hake) are often seen exhibiting demersal behavior in Saanich Inlet.

Research objectives

The primary goal of my dissertation was to determine the patterns and processes that can structure epibenthic communities living in highly variable oxygen conditions. Specific objectives were to (1) characterize changes in community structure along a spatially shifting hypoxia gradient, (2) relate changes in compositional heterogeneity to a

temporally variable hypoxia cycle, and (3) determine if community-level patterns are linked to species-specific differences in metabolic responses to hypoxia.

My dissertation has three data chapters:

(1) Chapter 2: *Oxygen limitations on marine animal distributions and the collapse of epibenthic community structure during shoaling hypoxia.* Camera systems and oxygen sensors mounted onto ROVs mapped the distribution of the epibenthic species assemblage along the same benthic hypoxia gradient from 2006-2013. I determined the *in situ* lower limits of $[O_2]_{env}$ at which dozens of fish and invertebrate species naturally occur. I used these *in situ* oxygen limits to test the applicability of several hypoxia thresholds from the literature. I conducted three of these benthic transects in 2013: before deoxygneation, after deoxygenation, and during the onset of reoxygenation to determine if the relative distribution, abundance, and spatial arrangement of co-occurring species change as a result of spatially shifting hypoxia boundaries.

(2) Chapter 3: *Scale-dependent response of epibenthic communities in a temporally variable hypoxic environment.* My goal was to use high frequency VENUS data to determine the scale-dependent processes influencing community structure over a range of temporal scales. I used an ecological time-series generated from the deployment of a novel camera platform tethered to the VENUS cabled observatory. I synthesized a suite of multivariate methods primarily designed for spatial data and

applied this workflow for analyzing ecological time-series. I tested if the inclusion of short-term measurements of environmental variability (e.g., max, min, sd) would improve the explanatory power of my analyses. I also addressed whether scale-dependent processes structure compositional heterogeneity at different temporal scales and the role of dominant species in the rates of community response in seasonal hypoxia. Lastly, I used the 10-year oxygen time-series from VENUS to determine if oxygen loss has occurred in Saanich Inlet and if the annual hypoxic period has increased during this period.

(3) Chapter 4: *Ecophysiological limits to aerobic metabolism in hypoxia determine epibenthic distributions and energy sequestration in the northeast Pacific Ocean.* I hypothesized that species-specific differences in physiological traits linked to aerobic metabolism could explain the community-level response to deoxygenation. From the field surveys, I identified three key species influencing the spatio-temporal patterns in community structure: spot prawn *Pandalus platyceros*, slender sole *Lyopsetta exilis*, and squat lobster *Munida quadrispina*, and measured the critical oxygen thresholds and standard metabolic rates of each using lab-based respirometry. I integrated my respirometry data with my *in situ* distribution data to test if critical oxygen thresholds would predict shifts in distributions among co-existing species and to calculate the overall shifts in their relative contribution to respiration in the field during several transitional points in the Saanich Inlet hypoxia cycle. Lastly, I grounded my ecophysiological approach with a global meta-analysis on crustaceans and determined if hypoxia tolerance differs among major ocean basins.

Methodological approach

A secondary goal of my dissertation was to establish a framework for applied use of advanced technology to address ecological questions in the deep sea. I used the location of the VENUS infrastructure and predictability of the seasonal hypoxia cycle in Saanich Inlet to address how temporal scale relates to community turnover and diversity in epibenthic systems. Data came from the deployment of a novel camera platform that took images coupled with water column properties over the 14-month period of the 2012-2013 hypoxia cycle (Fig. 1.2a). The synthesis of processing and analyzing ecological time-series from benthic camera deployments are summarized in my methods section of Chapter 3. The timing of the hypoxia cycle also allowed me to use remotely operated vehicles equipped with onboard oxygen sensors and high-definition camera systems to map community structure across environmental gradients (Fig. 1.2a). Part of my methods for using ROVs during benthic research is summarized in Appendix E. The natural hypoxia gradient allowed me to measure the lower oxygen thresholds for dozens of benthic species that are common to the continental shelf and slope of the northeast Pacific Ocean (Fig. 1.2b). By focusing at the community level in my response data, I was able to identify the species with key roles in driving community structure over space and time. Populations of deep-sea species that occur in Saanich Inlet represent a diverse assemblage of fish and invertebrates that are common throughout the continental shelf and slope of the northeast Pacific Ocean. Because continuous observations of live, deep-sea animals are rare, I took advantage of the tractable locations and accessibility of these populations in my live animal experiments, expanded our overall knowledge of several

ecologically important species, and potentially established new model species for deep-sea biology (Chapter 4, Appendix D).

I designed my dissertation to improve our understanding of the scales at which epibenthic metazoan communities respond to changes in oceanic oxygen. My results establish oxygen threshold ranges applicable to benthic marine megafauna and establish a framework for advancing applied use of submersible (Appendix E) and subsea observatory technology (Chapter 3) to address ecological questions. The larger question of how environmental forcing can impact ecosystem function has been identified as a priority research theme for ocean science in Canada (CCA, 2012). My dissertation quantifies and establishes the research foundation needed to address this issue in the context of oxygen loss on the Pacific coast of Canada.

Literature cited

Anderson JJ, Devol AH (1973) Deep Water Renewal in Saanich Inlet , an Intermittently Anoxic Basin. *Estuarine, Coastal & Shelf Science*, **16**, 1–10.

Bell G (2001) Neutral Macroecology. *Science*, **293**, 2413–2418.

Bopp L, Resplandy L, Orr JC et al. (2013) Multiple stressors of ocean ecosystems in the 21st century: projections with CMIP5 models. *Biogeosciences*, **10**, 6225–6245.

CCA (Council of Canadian Academies) (2012) 40 Priority Research Questions for Ocean Science in Canada. Ottawa, ON: CCA, The Core Group on Ocean Science in Canada. 22 pp.

Chan F, Barth JA, Lubchenco J, Kirincich A, Weeks H, Peterson WT, Menge BA (2008) Emergence of anoxia in the California current large marine ecosystem. *Science*, **319**, 920.

Childress JJ, Seibel BA (1998) Life At Stable Low Oxygen Levels: Adaptations of Animals To Oceanic Oxygen Minimum Layers. *Journal of Experimental Biology*, **1232**, 1223–1232.

Crawford WR, Peña MA (2013) Declining Oxygen on the British Columbia Continental Shelf Declining Oxygen on the British Columbia Continental Shelf. *Atmosphere-Ocean*, **51**, 88–103.

Danovaro R, Dell'Anno A, Pusceddu A, Gambi C, Heiner I, Kristensen RM (2010) The first metazoa living in permanently anoxic conditions. *BMC Biology*, **8**, 30.

Deutsch C, Farrel A, Seibel B, Portner H-O, Huey RB (2015) Climate change tightens a metabolic constraint on marine habitats. *Science*, **348**, 1132–1136.

Diaz RJ, Rosenberg R (2008) Spreading dead zones and consequences for marine ecosystems. *Science*, **321**, 926–929.

Edgcomb VP, Breglia SA, Yubuki N, Beaudoin D, Patterson DJ, Leander BS (2010) Identity of epibiotic bacteria on symbiontid euglenozoans in O 2 -depleted marine sediments: evidence for symbiont and host co-evolution. *ISME Journal*, **5**, 231–243.

Farrell AP, Richards JG (2009) Defining Hypoxia: An integrative synthesis of the responses of fish to hypoxia. In: *Fish Physiology - Hypoxia*, **27**, pp. 487–503. Elsevier Inc.

Froelich PN, Klinkhammer GP, Bender ML, Luedtke NA, Heath GR, Cullen D, Dauphin P (1979) Early oxidation of organic matter in pelagic sediments of the eastern equatorial Atlantic: suboxic diagenesis. *Geochimica et Cosmochimica Acta*, **43**, 1075-1090.

Gargett AE, Stucchi D, Whitney F (2003) Physical processes associated with high primary production in Saanich Inlet, British Columbia. *Estuarine, Coastal & Shelf Science*, **56**, 1141–1156.

Gattuso J-P, Magnan A, Bille R et al. (2015) Contrasting futures for ocean and society from different anthropogenic CO2 emissions scenarios. *Science*, **349**, aac4722–1–aac4722–10.

Grantham BA, Chan F, Nielsen KJ et al. (2004) Upwelling-driven nearshore hypoxia signals ecosystem and oceanographic changes. *Nature*, **429**, 749–754.

Grundle DS, Timothy DA, Varela DE (2009) Variations of phytoplankton productivity and biomass over an annual cycle in Saanich Inlet, a British Columbia fjord. *Continental Shelf Research*, **29**, 2257–2269.

Guppy M, Fuery CJ, Flanigan JE (1994) Biochemical principles of metabolic depression. *Comparative Biochemistry & Physiology. Part B, Biochemistry & Molecular Biology*, **109**, 175–89.

Hales B, Karp-Boss L, Perlin A, Wheeler PA (2006) Oxygen production and carbon

sequestration in an upwelling coastal margin. *Global Biogeochemical Cycles*, **20**, GB3001.

Hill AD, Taylor AC, Strang RHC (1991) Physiological and metabolic responses of the shore crab Carcinus maenas (L.) during environmental anoxia and subsequent recovery. *Journal of Experimental Marine Biology & Ecology*, **150**, 31–50.

Hill AD, Wyse GA, Anderson M (2008) *Animal Physiology*, 2nd edn. Harper & Row, New York, 770 pp.

Hochachka PW (1997) Oxygen - A key regulatory metabolite in metabolic defense against hypoxia. *American Zoologist*, **37**, 595–603.

Hochachka PW, Somero GN (2002) *Biochemical adaptation, Mechanism and Process in Physiological Evolution*. Oxford University Press, Oxford, 478 pp.

Hubbell SP (1997) A unified theory of biogeography and relative species abundance and its application to tropical rain forests and coral reefs. *Coral Reefs*, **16**, S9–S21.

Keeling RF, Körtzinger A, Gruber N (2010) Ocean Deoxygenation in a Warming World. *Annual Review of Marine Science*, **2**, 199–229.

Levin LA, Ekau W, Gooday AJ et al. (2009) Effects of natural and human-induced hypoxia on coastal benthos. *Biogeosciences*, **6**, 2063–2098.

Manning CC, Hamme RC, Bourbonnais A (2010) Impact of deep-water renewal events on fixed nitrogen loss from seasonally-anoxic Saanich Inlet. *Marine Chemistry*, **122**, 1–10.

McGill BJ, Enquist BJ, Weiher E, Westoby M (2006) Rebuilding community ecology from functional traits. *Trends in Ecology & Evolution*, **21**, 178–185.

Mcmahon BR (2001) Respiratory and circulatory compensation to hypoxia in crustaceans. *Respiration Physiology*, **128**, 349–364.

Pörtner HO, Farrell AP (2008) Physiology and Climate Change. *Science*, **322**, 690–692.

Rabalais NN, Turner RE, Wiseman WJ (2002) Gulf of Mexico Hypoxia, a.k.a. "the Dead Zone." *Annual Review of Ecology & Systematics*, **33**, 235–263.

Richards JG (2010) Metabolic Rate Suppression as a mechanism for surviving environmental challenge in fish. In: *Aestivation: Molecular and Physiological Aspects, Progress in Molecular and Subcellular Biology* (eds Navas CA, Carvalho JE), pp. 113–139. Springer-Verlag, Berlin.

Sato M, Takeuchi M, Kanno N, Nagahisa E, Sato Y (1993) Distribution of opine

dehydrogenases and lactate dehydrogenase activities in marine animals. *Comparative Biochemistry & Physiology Part B: Comparative Biochemistry*, **106B**, 955–960.

Seibel BA (2011) Critical oxygen levels and metabolic suppression in oceanic oxygen minimum zones. *Journal of Experimental Biology*, **214**, 326–336.

Thannickal VJ (2009) Oxygen in the Evolution of Complex Life and the Price We Pay. *American Journal of Respiratory Cell & Molecular Biology*, **40**, 507–510.

Timothy DA, Soon MYS (2001) Primary production and deep-water oxygen content of two British Columbian fjords. *Marine Chemistry*, **73**, 37–51.

Van Ginneken VJT, Onderwater M, Olivar OL, van den Thillart GEEJM (2001) Metabolic depression and investigation of glucose/ethanol conversion in the European eel (*Anguilla anguilla* Linnaeus 1758) during anaerobiosis. *Thermochimica Acta* **373**, 23–30.

Vaquer-Sunyer R, Duarte CM (2008) Thresholds of hypoxia for marine biodiversity. *Proceedings of the National Academy of Sciences of the United States of America*, **105**, 15452–15457.

Wells RMG (2009) Blood, Gas Transport and Hemoglobin Function: Adaptations for Functional and Environmental Hypoxia. In: *Fish Physiology - Hypoxia*, **27**, pp. 255–299. Elsevier Inc.

Whitney FA, Freeland HJ, Robert M (2007) Persistently declining oxygen levels in the interior waters of the eastern subarctic Pacific. *Progress in Oceanography*, **75**, 179–199.

Wu RSS (2009) Effects of Hypoxia on Fish Reproduction and Development. In: *Fish Physiology - Hypoxia*, **27**, pp. 79–141. Elsevier Inc.

Zaikova E, Walsh D a, Stilwell CP, Mohn WW, Tortell PD, Hallam SJ (2010) Microbial community dynamics in a seasonally anoxic fjord: Saanich Inlet, British Columbia. *Environmental Microbiology*, **12**, 172–191.

Zainal KAY, Taylor AC, Atkinson RJA (1992) The effect of temperature and hypoxia on the respiratory physiology of the squat lobster *Munida rugosa* and *Munida sarsi* (Anomura, Galatheidae). *Comparative Biochemistry & Physiology Part A: Physiology*, **101A**, 557–567.

Chapter 2: Oxygen limitations on marine animal distributions and the collapse of epibenthic community structure during shoaling hypoxia

Preface

Chapter 2 is a research article in Global Change Biology: Chu JWF, Tunnicliffe V (2015) Oxygen limitations on marine animal distributions and the collapse of epibenthic community structure during shoaling hypoxia. Global Change Biology 21, 2989-3004. Raw data are published in the Dryad Data Repository: doi:10.5061/dryad.1p55v

Verena Tunnicliffe (dissertation supervisor, University of Victoria) contributed to the original survey design, was responsible for transects prior to 2011, provided resources for this study, and gave input during the writing of the article.

I performed transects from 2011-2013, generated and analyzed the data, interpreted the results, and wrote the article.

Abstract

Deoxygenation in the global ocean is predicted to induce ecosystem-wide changes. Analysis of multi-decadal oxygen time-series projects the Northeast Pacific to be a current and future hot spot of oxygen loss. However, the response of marine communities to deoxygenation is unresolved due to the lack of applicable data on component species. I repeated the same benthic transect (n=10, between 45-190 m depths) over eight years in a seasonally hypoxic fjord using remotely operated vehicles equipped with oxygen sensors to establish the lower oxygen levels at which 26 common epibenthic species can occur in the wild. By timing my surveys to shoaling hypoxia

events, I show that fish and crustacean populations persist even in severe hypoxia (<0.5 ml l^{-1}) with no mortality effects but that migration of mobile species occurs. Consequently, the immediate response to hypoxia expansion is the collapse of community structure; normally partitioned distributions of resident species coalesced and localized densities increased. After oxygen renewal and formation of steep oxygen gradients, former ranges re-established. High frequency data from the nearby VENUS subsea observatory show the average oxygen level at my site declined by ~0.05 ml l^{-1} $year^{-1}$ over the period of my study. The increased annual duration of the hypoxic (<1.4 ml l^{-1}) and severely hypoxic periods appears to reflect the oxygen dynamics demonstrated in offshore source waters and the adjacent Strait of Georgia. Should the current trajectory of oxygen loss continue, community homogenization and reduced suitable habitat may become the dominant state of epibenthic systems in the northeast Pacific. *In situ* oxygen occurrences were not congruent with lethal and sublethal hypoxia thresholds calculated across the literature for major taxonomic groups indicating that research biases towards laboratory studies on Atlantic species are not globally applicable. Region-specific hypoxia thresholds are necessary to predict future impacts of deoxygenation on marine biodiversity.

Introduction

Increased stratification of ocean surface waters and the decreasing strength of thermohaline circulation are causing a global shift in the concentration and distribution of oxygen in the ocean (Sarmiento *et al.*, 1998; Keeling *et al.*, 2010; IPCC, 2013). Oxygen enters into the ocean by diffusion at the air-sea interface and by photosynthesis in the

euphotic zone before being transported to depth. Because oxygen is less soluble in warmer water, a 1.5-4% net loss of oxygen will occur in conjunction with the projected sea surface temperature increase of 2-3°C for this century (Cocco *et al.*, 2013; IPCC, 2013). Global hot spots of oxygen loss are linked to the expansion of oxygen minimum zones (OMZs) which are naturally occurring, permanent mid-water oxygen-deficient layers (<10% of surface oxygen concentrations) that occur in upwelling zones along the continental margins of the Indian, eastern Pacific, and southeastern Atlantic Oceans (Helly & Levin, 2004; Gilly *et al.*, 2013). OMZs vary in depth, horizontal extent, and minimum oxygen concentration. Oxygen minima in the Pacific and Indian oceans are <0.1 ml l^{-l}, markedly lower than the oxygen minima of the South Atlantic (~0.4 ml l^{-1}) and the North Atlantic (~0.9 ml l^{-1}) ocean OMZs (Karstensen *et al.*, 2008). Compared to open ocean, coastal zones are losing oxygen at a faster rate because of the concomitant local effects of eutrophication (Diaz & Rosenberg, 2008; Levin *et al.*, 2009; Gilbert *et al.*, 2010). Although model consensus predicts a net global loss in overall oxygen content (Keeling *et al.*, 2010; Cocco *et al.*, 2013), oxygen loss will differ among regions because of the inter-ocean differences in oxygen distribution, rate of deoxygenation, and routes of supply (Hofmann *et al.*, 2011). In combination, the factors that create hypoxia and oxygen levels insufficient to support life in marine environments will inevitably induce both latitudinal and depth shifts in species distributions (Bijma *et al.*, 2013).

The major consequence of the expansion of oxygen-deficient, or hypoxic, waters is the reduction of available habitat for metazoan life (Whitney *et al.*, 2007; Stramma *et al.*, 2008, 2013). As hypoxia-intolerant metazoans migrate away from low-oxygen waters, their distributions are compressed into a reduced extent (Eby & Crowder, 2002;

Prince & Goodyear, 2006; Koslow *et al.*, 2011) thereby increasing foraging and competition for shelter among co-occurring species which leads to a net loss in species diversity and ecosystem function (Stramma *et al.*, 2010). The redistribution of some forage-fish species may facilitate the range expansion of hypoxia tolerant, top predators such as the Humboldt squid, *Dosidicus gigas* (Stewart *et al.*, 2014). Tolerance to hypoxia differs among species; therefore, 'winners' and 'losers' will emerge in future deoxygenation events. Although localized species replacement can occur, the general consequence of long-term deoxygenation is a community-wide shift to favour species with physiological adaptations to extreme hypoxia and/or hydrogen sulfide presence (Rosa & Seibel, 2010; Utne-Palm *et al.*, 2010; Seibel, 2011). Larval life-history stages are typically more sensitive to hypoxia but tolerance is often species-specific (Eerkes-Medrano *et al.*, 2013). Within adult populations, hypoxia can also select against larger, older individuals (Clark *et al.*, 2013). The well-established metabolic scaling laws would generally predict that less biomass will be found at lower oxygen levels due to the oxygen demands of larger body sizes (Ernest *et al.*, 2003). Overall, a marked shift in ecosystem energetics will occur with continued oxygen loss as the overall metabolism of the system decreases; alternative electron receptors that sequentially replace oxygen yield less energy at the base of the food web (Wright *et al.*, 2011). Sustained deoxygenation over multiple decades reduces overall success of commercial fisheries through the loss of demersal biomass (Kemp *et al.*, 2005). Such hypoxia-induced loss of carbon transfer to secondary production has already occurred in Chesapeake Bay, the Baltic Sea, and the Gulf of Mexico (Diaz & Schaffner, 1990; Karlson *et al.*, 2002; Rabalais *et al.*, 2002).

Given the ecological impacts of deoxygenation, several hypoxia thresholds have been derived to serve as general tools for assessing and managing the integrity of ecosystems. Large syntheses of the oceanographic literature have developed general thresholds for hypoxia (<1.4 ml l^{-1}, Rabalais *et al.*, 2010) and severe hypoxia (<0.5 ml l^{-1}, Diaz & Rosenberg, 2008; Chan *et al.*, 2008) for systems that are characterized by normoxia (>1.4 ml l^{-1}) and the lack of severe hypoxia over evolutionary time scales (Rabalais *et al.*, 2010). The applicability of these general thresholds is context-dependent because of the differences among major animal groups in hypoxia tolerances that interact with the often co-occurring and additive effects of sulfide exposure, ocean warming, and acidification (Pörtner, 2008; Vaquer-Sunyer & Duarte, 2008, 2010, 2011). As such, respiration indices calculated from oceanographic datasets (Brewer & Peltzer, 2009) have been criticized in their ecological applicability because they are not grounded in the physiology of organisms (Seibel & Childress, 2013). Several studies also point out the knowledge gaps in the current hypoxia literature (Vaquer-Sunyer & Duarte, 2008; Riedel *et al.*, 2012, 2014) in that the majority of studies (>90%) have used only laboratory experiments that do not reproduce the highly variable behaviour of oxygen *in situ*. Additionally, >70% of these studies use organisms that originate from the Atlantic Ocean (Diaz & Rosenberg, 1995; references in Vaquer-Sunyer & Duarte, 2008) where oxygen content has remained higher over much of the later Cenozoic. Although the Northeast Pacific is a current and future region of intensive oxygen loss (Helly & Levin, 2004; Stramma *et al.*, 2010; Hoffman *et al.*, 2011), there is a shortage of appropriate data, such as hypoxia tolerance, on resident species to determine how marine communities will

respond to expanding hypoxic waters. Thus, the applicability of current hypoxia thresholds remains unconfirmed in this region.

My study addresses the *in situ* hypoxia limits of species in the Northeast Pacific to determine how the expanding hypoxic waters can affect benthic community structure. A primary goal was to assess redistribution of mobile species in an open, field system as oxygen levels change. Observations occurred at key points during hypoxia expansion events and allowed us to concurrently map the distributions of numerous northeast Pacific epibenthic species relative to bottom oxygen concentration over eight years. High resolution records from the VENUS subsea observatory also revealed the long-term oxygen behaviour at the study site. My study is the first to use an open, naturally hypoxic system to (1) measure the *in situ* spatial and temporal variability in the hypoxia tolerances of benthic epifauna, (2) assess mobility and track species distribution changes during periods of hypoxia expansion and its consequence for community structure, and (3) test current hypoxia thresholds in a northeast Pacific benthic system to determine their applicability for this region. Empirical data on oxygen levels at which animals occur *in situ* and the physiological and behavioral responses of key species are required to model future population shifts. Ultimately, my results contribute to region-specific models of projected impact of deoxygenation on marine biodiversity.

Materials and methods

Study site

Saanich Inlet is a 24-km long reverse estuary with a maximum depth of 230 m (Fig. 2.1a) connected to the Strait of Georgia, which is a coastal sea with limited

exchange with the Pacific (Fig. 2.1a inset). Wind and tidal forces are relatively weak in Saanich Inlet with forces external to the inlet driving the primary circulation patterns (Gargett *et al.* 2003). Major freshwater input to Saanich Inlet comes from the Cowichan River, northwest of the inlet and has maximum flow during winter months, and from the Fraser River that can drive the greater estuarine circulation in the Salish Sea and stabilize

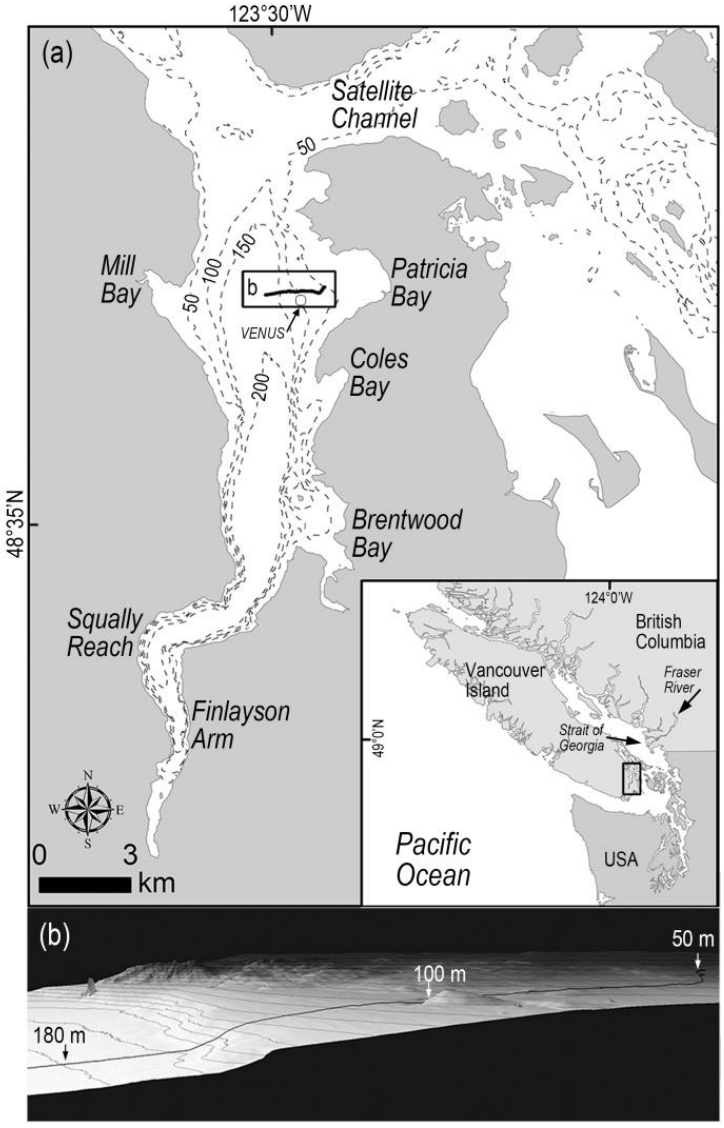

Figure 2.1. Overview of Saanich Inlet. (a) Saanich Inlet is adjacent to Strait of Georgia and connects to waters of the Northeast Pacific Ocean (inset) via restricted channels through the San Juan Islands. The VENUS instrumentation (white circle) is located approximately 200 m south of the transect line in Patricia Bay (solid black line). Bathymetry contours are in 50 m increments. (b) Transects were flown over a gradual soft bottom slope and transitioned from anoxic/hypoxic deep waters to normoxic shallow waters in Patricia Bay. Bathymetry contours overlaid onto 3D bottom topography are in 10 m increments. Total transect distance to 50 m is about 3 km

the upper water column in Saanich Inlet (Gargett *et al.*, 2003). A sill (75 m depth) at the mouth of Saanich Inlet permanently restricts deep water circulation and exchange with the Strait of Georgia. When water column stratification intensifies during the summer and, during poor ventilation, hypoxia develops from the high primary productivity in the inlet being consumed at depth by microbial respiration (Zaikova *et al.*, 2010). The primary productivity rate in Saanich Inlet is one of the highest among fjords in the northern hemisphere (Timothy & Soon, 2001; Grundle *et al.*, 2009). During winter months, phytoplankton can be light-limited rather than being nutrient-limited (Takahashi *et al.*, 1978). Annual oxygen renewal occurs when denser, oxygenated water flows over the sill and down into the deepest parts of the inlet (>200 m) in the fall (Anderson & Devol, 1973). Partial oxygen renewal of mid and deep waters (90-160 m) may occur in the spring (Manning *et al.*, 2010). This annual cycle of oxygen-depletion and recovery is predictable and well documented (Herlinveaux, 1962; Anderson & Devol, 1973; Tunnicliffe, 1981) although intensity and duration may vary (e.g. Matabos *et al*., 2012).

Benthic ROV transects

From 2006 to 2013, the same soft-bottom, benthic transect was repeated ten times (Fig. 2.1b, Table A.1) using remotely operated vehicles (ROV). This transect (~3 km length) begins in the middle of the inlet (~190 m depth) and is based on the one described in Yahel *et al.* (2008) and Katz *et al.* (2012) but with an extension into shallower depths (~45 m). This transect was repeated once every year until 2012 and, in 2013 it was repeated three times at different times of the hypoxia cycle: after spring renewal (May), after a full summer of deoxygenation (September), and during the onset of oxygen recovery in the fall (October).

During each transect, the ROV flew at 0.5 knots at <1 m above the bottom while recording the seafloor in high-definition 1080i video with water conductivity-temperature-depth (CTD) and oxygen with the CTD pump intake at 0.5 m above bottom of the ROV. From 2006 to 2010, a Sea-Bird SBE19plus CTD with an SBE43 oxygen sensor was used during transects while from 2010 to 2013, a Sea-Bird SBE 19plus V2 with SBE43 oxygen sensor was used. Manufacturer-calibrated accuracy, precision, and response time of the SBE43 oxygen sensor are ±2% of saturation which is 0.13 ml l^{-1} at 32 PSU and 10°C, 0.023 ml l^{-1} (1 μmol kg^{-1}) , and <1 sec respectively (http://www.seabird.com). CTD and oxygen data were recorded at 4 Hz and averaged to every second during dives. The first two transects (2006, 2007) were flown using a standard-definition camera system. One transect in May 2013 was flown with the work class ROV *Oceanic Explorer*, while all other transects were flown with the scientific ROV *ROPOS*. One-second interval navigation data were recorded with a high-precision ultra-short baseline system in all *ROPOS* transects. Because *Oceanic Explorer* lacked a similar system, navigation data were interpolated post-hoc; one-metre contours were created from multibeam bathymetry data (5 m grid cell) and x/y coordinates were interpolated along the line based on the bottom depth recorded from the calibrated CTD. Depending on the transect line, the average width of the field of view in the transect videos was between 1.3–4.2 m which was determined by paired horizontal scaling lasers (10 or 22 cm spaced).

Video analysis and data management

Individual animals were identified and counted for each second of video, georeferenced to the ROV navigation data and then aligned with the CTD and oxygen

data using synchronized timestamps. Videos were processed and data verified several times due to the high density of some species. Bacterial mats and sponges were recorded as presence-absence data at each second. To increase georeferencing accuracy, animals were only counted when they crossed the edge of the lower half of the screen during video playback. For each second of video, the ROV travelled ~0.2 m and would cover 0.26-0.84 m^2 in the field of view. To manage and analyze the data, matrices were compiled into a personal GIS geodatabase in ArcGIS© (ESRI) and analyzed in R (R Core Team, 2014).

In the biological literature, oxygen is most frequently reported in concentration units. To enable comparison, summary data is presented in units of oxygen concentration (ml l^{-1}). However, partial pressure units may better predict the effects of hypoxia stress at the organism level and enable comparisons across sites (Hoffman *et al.*, 2011). Therefore, in my multivariate analyses that test the effect of oxygen on community structure and species distributions, salinity, temperature, pressure, and density data were integrated with oxygen concentration and converted to partial pressure (kPa) using the R function pO2 (Hoffman *et al.*, 2011).

In situ oxygen limits for marine taxa

Under natural conditions animals will likely avoid hypoxia. However, the relative distance an organism lives from their critical oxygen levels will differ among species. Thus I apply the term "*in situ* oxygen occurrence" to the oxygen measurements recorded for every individual I observed.

To test the applicability of general hypoxia thresholds, I compare my *in situ* oxygen occurrence data against literature-derived sublethal and lethal hypoxia thresholds

as proposed by the meta-analysis presented in Vaquer-Sunyer & Duarte (2008); I use the original data from their supplementary tables in my analyses. Using the Student's-t distribution, I calculated the literature-derived sublethal thresholds (95% confidence intervals) to be: 2.53-3.64 ml l^{-1} for fish, 1.81-2.63 ml l^{-1} for crustaceans, 1.16-1.62 ml l^{-1} for molluscs, 0.50-1.21 ml l^{-1} for echinoderms, and 0.32-0.64 ml l^{-1} for cnidarians. Similarly, the 95% C.I. of the lethal thresholds are: 0.98-1.18 ml l^{-1} for fish and 1.53-1.91 ml l^{-1} for crustaceans.

Comparisons with the literature-derived thresholds were first done at the group level; *in situ* oxygen occurrences were pooled across transects into major taxonomic groups (fish, crustaceans, echinoderms, molluscs, and cnidarians) and then compared with the general hypoxia and severe hypoxia thresholds as well as the above group level literature-derived sublethal and lethal hypoxia. To assess the within-group variability of the *in situ* oxygen occurrence data, comparisons were also done between individual species and their respective group literature-derived-level. For species-level comparisons, only species with $n > 5$ occurrences across all transect lines were analyzed against their group thresholds (fish, crustaceans, echinoderms, and cnidarians). For a comparison, a bootstrap resampled distribution (n=1000 iterations) was generated by subtracting a randomly chosen value from the vector of individual *in situ* oxygen occurrences from a randomly chosen value from the vector of literature-derived hypoxia values for each group. This distribution of observed differences was then compared to a null distribution (centered on zero) to determine if a group- or species-level *in situ* oxygen occurrence was significantly different from the general hypoxia thresholds described in the literature. For comparisons where *in situ* oxygen occurrences were less than the sublethal hypoxia

threshold of their group, the same procedure was used to compare against the lower lethal hypoxia threshold. In comparisons where the null was rejected ($p<0.05$), inspection of the 95% C.I. of *in situ* oxygen occurrences for the species determined if they were greater or less than the literature-derived hypoxia threshold. In comparisons where the null was not rejected, the *in situ* oxygen occurrences were considered to fall within the range of the proposed sublethal hypoxia threshold. Dendrograms were generated for fish and crustaceans to cluster species with similar *in situ* oxygen occurrences using Gower's coefficient.

Community-level organization by oxygen gradients

To determine the response of the benthic community to the shifting oxygen profile, data from the three transects flown in 2013 were analyzed using canonical redundancy analyses (RDA, Legendre & Legendre, 2012). First, the sequential per second database entries for each transect were summarized into ~20 m^2 sections (for loop summation to a maximum of 20 m^2) which spaced the sections 12±8 m apart (mean±sd among all 3 transects). For each of these 20 m^2 sections, the mean depth, mean oxygen, median oxygen, standard deviation of oxygen, maximum oxygen, and minimum oxygen values were calculated and used as the predictor variables in the RDA analyses. Because *in situ* spatial variance is key to structuring species assemblages (Bates *et al.*, 2010), measurements of variability (maximum, minimum, standard deviation) were included along with measurements of central tendency (mean, median) as part of the predictor matrix. The animal counts for each 20 m^2 section were summed and standardized by the area covered in the video frames. A Hellinger-transformation (the square root of observed values divided by site sums; Legendre & Gallagher, 2001) was applied to the species data

for each transect line. RDA analyses were performed for each transect line using the *'vegan'* package in R (Oksanen *et al*., 2013). To prevent over fitting the model with too many predictor variables, model simplification was done using the *'packfor'* package (Dray *et al.*, 2011). A global $_{adj}R^2$ was first calculated using all predictor variables. Predictor variables were then retained based on maximum explained variance ($_{adj}R^2$) and predictors were excluded when they did not significantly explain additional variance in the species matrix or if they brought the model over the global $_{adj}R^2$. Significance of the retained predictor variables was calculated using permutation tests (n=999) (Borcard & Legendre, 2011).

To determine the community-wide response to hypoxia expansion and oxygen recovery, we analyzed the *in situ* oxygen occurrences for each species present at abundances over 10 individuals in all transects flown in 2013. Density plots were used to illustrate the species responses within the community to oxygen change. Within a species, bootstrap comparisons tested for significant changes in species' *in situ* oxygen occurrences between the three sampling periods (May, September, and October). To examine how the community structure was influenced by spatial redistribution of indicator species, I used bootstrap comparisons to assess significant changes in depth range during hypoxia expansion and oxygen recovery for the four most abundant mobile species (*Lyopsetta exilis*, *Munida quadrispina*, *Pandalus platyceros*, and *Pandalus jordani*).

Long-term oxygen profile from VENUS

VENUS is a cabled subsea observatory that was established in Saanich Inlet and, since 2006, has reported *in-situ* oxygen levels in the hypoxia transition zone (96 m

depth); it sits approximately 200 m south of my transect line (Fig. 2.1). This VENUS time series is globally unique in that the data resolves a seasonal hypoxia cycle in real-time and at high temporal resolution (data are collected every minute); VENUS data are open source and available through their web portal (www.oceannetworks.ca). VENUS data for the eight year period of Feb 2006 to Mar 2014 were examined to determine if long-term patterns of oxygen loss could be resolved. Because the annual hypoxia cycle appears as a sinusoidal pattern, the start (Mar.16, 2006) and end point (Mar. 11 2014) of the time-series were truncated to occur at the maximum oxygen concentrations of the year. Annual maintenance cruises to clean and recalibrate instruments, malfunctioning hardware, and infrastructure upgrades (July-Oct. 2011) created intermittent data gaps that cover approximately 8% of the oxygen time-series to date. Data gaps were linearly interpolated prior to analyzing the long-term trend using a one-year running mean. The cumulative annual duration at which the VENUS time-series was below the general and severe hypoxia thresholds was plotted and analyzed with linear regression.

Results

The deepest section of the transect (~190 m) is characterized by near-anoxic waters (<0.01 ml l^{-1}). From 190 m to about 100 m, the substratum is predominantly soft, soupy mud with no infauna and the water is almost permanently hypoxic. More consolidated muds appear at 90 m depth around outcropping bedrock while mixed sediments predominate in the upper reaches of the bay. The oxygen profiles transitioned from anoxia to severe hypoxia and hypoxia and into normoxic waters typical of the shallowest depths (~45 m) (Fig. 2.2).

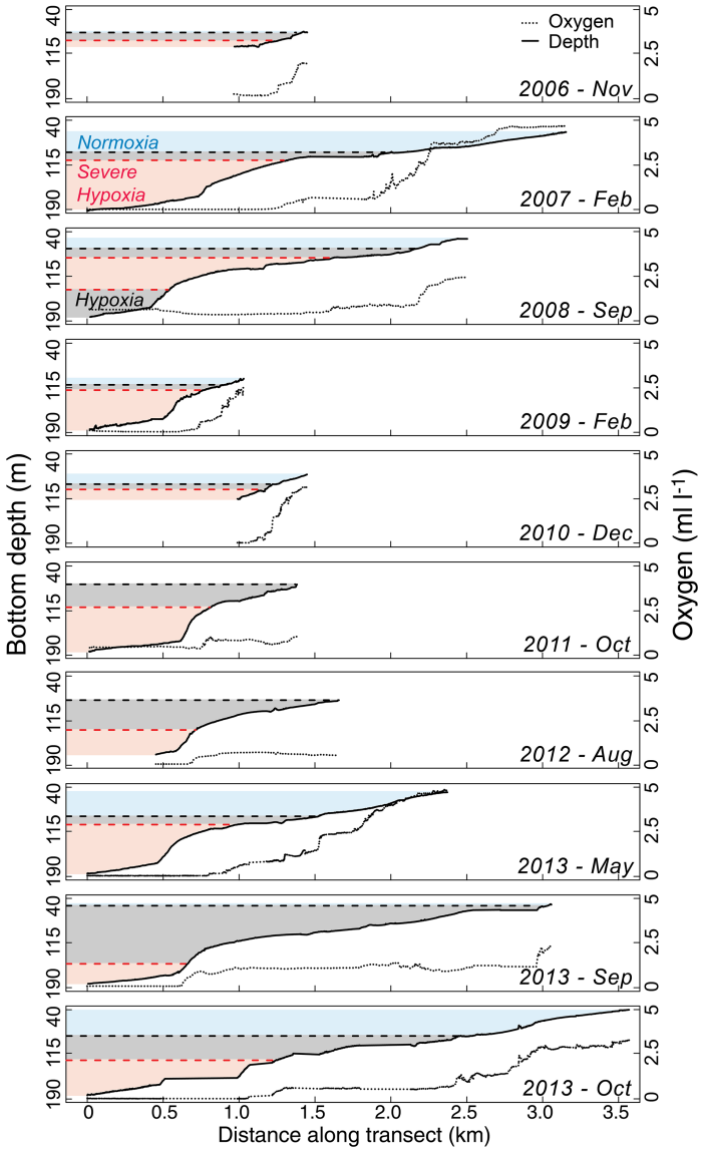

Figure 2.2. Horizontal oxygen profiles. Oxygen gradients occurred over short distances at the interface between the oxygenated upper layers and the hypoxic basin waters (e.g. May 2013). Gradients become less steep after summer deoxygenation and can result in hypoxic (<1.4 ml l^{-1} in grey) and severely hypoxic waters (<0.5 ml l^{-1} in red) expanding to cover > 96% of the transect area (e.g. Sep. 2013). Renewal processes re-establish oxygen gradients relatively rapidly as normoxic waters (>1.4 ml l^{-1} in blue) return (e.g. Oct. 2013) sometimes causing an intermediate layer of severely hypoxic water (Sep. 2008). Differences in the bottom profile were caused by slight deviations in the ROV heading during transects.

Generally, the epibenthos in the severe hypoxia zone (>120 m) consists of high densities of slender sole (*Lyopsetta exilis*) and squat lobster (*Munida quadrispina*) along with variably dense chemosynthetic bacterial mats (*Beggiatoa* spp.) that are absent in complete anoxia (Video A.1). Densities of slender sole and squat lobster in this zone were as high as 9 and 34 individuals m^{-2} respectively. Transition into the hypoxia zone (~100 m) coincides with a shift in megafauna as several other species of crustacean and

fish become common and bacterial mats disappear. Around 90 m depth, sessile species (sponges, anemones) colonize patches of outcropping bedrock and in the shallower depths the sediment is dominated by sea whips (~17 individuals m^{-2}). Visibility in the hypoxia transition zone would sometimes be poor due to dense clouds of zooplankton, herring, and resuspended sediments from flatfish activity. Despite the low oxygen levels measured in my study, no massive die-offs of fish or crustaceans were observed.

Seafloor oxygen profiles

The deeper portions of the basin (>100 m depth) never experienced normoxic conditions and zones of hypoxia and severe hypoxia were present every year. Where transects extended above the sill depth (~75 m), transition out of hypoxia was usual (Fig. 2.2). Steep oxygen gradients occurring over a relatively short distance were particularly evident in winter and spring (e.g. Feb. 2007, May 2013). These mid-depth gradients diminished as deoxygenation intensified in the basin during summer and fall months. In 2010, when the deep water renewal failed in the adjacent Strait of Georgia (Johannessen *et al.*, 2014), the fall renewal in Saanich Inlet was also weak (Fig. 2.2, Dec 2010). The volume of hypoxic waters (<1.4 ml l^{-1}) expanded and shifted the hypoxia boundary upwards (e.g. Fig. 2.2, Sep 2013) sometimes as deep water oxygen renewal occurred (e.g. Fig. 2.2, Sep 2008). In 2013, the percentage of transect area that was covered by hypoxia expanded from 67.3% (May) to 96.1% (Sep) during the summer but rapidly decreased back to 68.2% (Oct) when steep oxygen gradients recovered in the inlet. Within the same period, the percentage of seafloor area covered by severe hypoxia diminished from 51 % (May) to 19% (Sep) and expanded back to 31.5% (Oct) when steep oxygen gradients re-established.

The epibenthic animal community

Among all transects, 46 species from seven metazoan phyla were recorded totalling 55,573 sightings plus presence/absence records of two species of demosponges and *Beggiatoa* bacterial mats and all with *in situ* oxygen measurements (Table A.2). Because of the paucity of abundance data for marine species (Bates *et al.*, 2014) and the lack of *in situ* oxygen measurements for individual animal occurrences, I include my data for pelagic species (e.g. walleye pollock, shiner perch, dogfish) in Table A.2 but excluded them from my statistical analyses due to potential herding effects of the ROV. Although known as a mid-water feeder, I include Pacific hake because I commonly saw them with demersal behaviour in Saanich Inlet. Ten epibenthic species were present in every survey (except one truncated transect in 2009); these were four species of demersal fish: slender sole (*Lyopsetta exilis*), blue-barred prickleback (*Plectobranchus evides*), blackbelly eelpout (*Lycodes pacifica*), blacktip poacher (*Xeneretmus latifrons*); three species of crustaceans: squat lobster (*Munida quadrispina*), spot prawn (*Pandalus platyceros*), pink shrimp (*Pandalus jordani*); and two species of cnidarians: sea whip (*Halipteris willemoesi*), and giant anemone (*Metridium farcinem)*. Operational depth limits of the ROVs prevented me from surveying depths shallower than 30 m. Several species that were rarely sighted such as Dungeness crab (*Metacarcinus magister*), red rock crab (*Cancer productus*), spiny pink star (*Pisaster brevispinus*), sunflower star (*Pyncopodia helianthoides*), orange seapen (*Ptilosarcus gurneyi*) are common at shallower depths (<30 m) in Saanich Inlet and thus may have been avoiding the depth range of the hypoxia transition zone. Hereafter, I use common names to improve readability; Table A.2 lists species names.

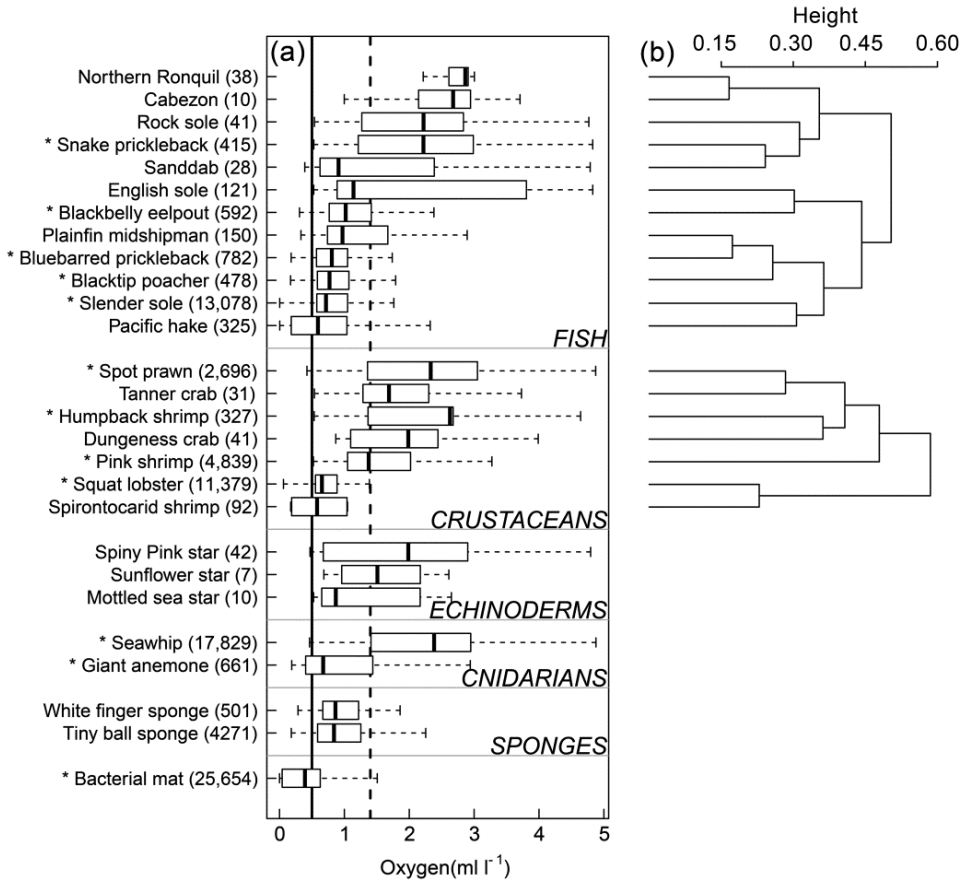

Figure 2.3. *In situ* oxygen measurements for individual occurrences of epibenthic species in Saanich Inlet. Only species with n>5 occurrences across all transect lines are summarized. (a) Centre line in each boxplot is median value. Edges of box indicate 1st and 3rd quartile ranges with whiskers indicating maximum and minimum oxygen occurrences of a species. Numbers of individuals are in parentheses. Asterisks highlight species that are also in Figure 4. Vertical lines indicate the hypoxia (dashed) and severe hypoxia (solid) thresholds. (b) Dendrograms generated from Gower's coefficient cluster species with similar *in situ* oxygen occurrences.

A large proportion of the individual animal observations occurred in hypoxic waters (Table 2.1). When individual counts for all the observed species (n=42) were pooled into major taxonomic groups, group-level *in situ* oxygen thresholds (95% C.I.) for fish, crustaceans, echinoderms, and sponges fell below the general hypoxia threshold but not the severe hypoxia threshold. Group-level *in situ* oxygen occurrences for fish, crustaceans, and molluscs were significantly lower than the literature-derived sublethal

hypoxia thresholds for their respective groups (all, $p<0.05$). The *in situ* oxygen occurrences for fish and crustaceans were also significantly lower than their literature-derived group thresholds for lethal hypoxia (both, $p<0.05$). However, *in situ* oxygen occurrences were highly variable within a group and driven by interspecific differences in hypoxia tolerance (Fig. 2.3a). Within my *in situ* observations for fish and crustaceans, two main subgroups were resolved (Fig. 2.3b). For fish, a high oxygen subgroup (northern ronquil, cabezon, rock sole, snake prickleback, sanddab) occurs in 2.11-2.28 ml l^{-1} (95% C.I.) and a low oxygen subgroup (english sole, blackbelly eelpout, plainfin midshipman, bluebarred prickleback, blacktip poacher, slender sole, Pacific hake) occurs in 0.97-1.00 ml l^{-1}. For crustaceans, a similar high oxygen subgroup (spot prawn, Tanner crab, humpback shrimp, Dungeness crab, pink shrimp) occurs in 1.89-1.94 ml l^{-1} and a low oxygen subgroup (squat lobster, spirontocarid shrimp) occurs in 0.71-0.72 ml l^{-1}.

Species-level *in situ* oxygen occurrences for twelve demersal fish species (Pacific hake, slender sole, blacktip poacher, bluebarred prickleback, plainfin midshipman, blackbelly eelpout, English sole, sanddab, snake prickleback, rock sole, cabezon, northern ronquil), six crustaceans (spirontocarid shrimp, squat lobster, pink shrimp, Dungeness crab, humpback shrimp, tanner crab), and one echinoderm (mottled sea star) were equal to, or lower than, the literature-derived sublethal hypoxia threshold of their respective group. The *in situ* oxygen occurrences of ten of these species (plainfin midshipman, blue-barred prickleback, blacktip poacher, slender sole, Pacific hake, Dungeness crab, Tanner crab, pink shrimp, spirontocarid shrimp, and squat lobster) were also below the literature-derived lethal hypoxia thresholds for their respective group (all $p<0.001$). The spironotocarid shrimp are quite small and may have not have been

detectable in most of the videos due to the low resolution of HD-video. Echinoderms and cnidarians were generally found in oxygen levels above their respective group's sublethal thresholds with only the one echinoderm species present in oxygen levels that were lower than the literature-derived sublethal hypoxia threshold.

Table 2.1. Summary of *in situ* oxygen limits for major animal groups in Saanich Inlet. The relative proportion of the individual counts that were observed below the general hypoxia (1.4 ml l^{-1}) and severe hypoxia thresholds (0.5 ml l^{-1}) are summarized. *In situ* oxygen limits are presented for each major taxonomic group. Superscript indicate that *in situ* oxygen occurrences for a group were significantly lower (α=0.05) than the literature derived lethal (^{L}) and/or sublethal (^{S}) hypoxia thresholds presented in Vaquer-Sunyer & Duarte (2008); we present our thresholds in concentration units (ml l^{-1}) for direct comparison and partial pressure for environment-adjusted values. NA indicates that there were no previous *in situ* hypoxia thresholds available for sponges (see methods for details). Sample sizes and the number of species are presented in Table S.2.

	Proportion below general thresholds		*In situ* oxygen limits (95% C.I)	
Group	< 1.4 ml l^{-1}	< 0.5ml l^{-1}	ml l^{-1}	kPa
Fish	0.85	0.18	^{L,S} 1.01 – 1.04	3.39 – 3.48
Crustaceans	0.73	0.07	^{L,S} 1.19 – 1.22	4.01 – 4.10
Molluscs	0.33	0.02	^{S} 1.61 – 2.29	5.44 – 7.65
Echinoderms	0.46	0	0.51 – 2.94	1.79 – 9.71
Cnidarians	0.26	0.02	2.42 – 2.45	8.10 – 8.22
Sponges	0.82	0.10	^{NA} 1.10 – 1.15	3.71 – 3.86

Community-level reorganization during the 2013 hypoxia cycle

The three transect lines established in May, September, and October of 2013 were the most complete in terms of surveying the entire depth range. The timing coincided with key transitions of the hypoxia cycle (Fig. 2.2) and illustrates the effect of shoaling hypoxia on the structure of the epibenthic species assemblage. In the presence of a steep oxygen gradient (Fig. 2.2: May 2013), *in situ* oxygen occurrences were well differentiated among species (Fig. 2.4: May) with distributions of some centred in normoxic waters (e.g. pink shrimp) and some in hypoxic waters (e.g. squat lobster,

slender sole). More than half the variance in the entire epibenthic species assemblage was explained by components of the oxygen regime (May 2013: RDA $_{adj}R^2$=0.58): maximum O_2, mean depth, minimum O_2 (all $p<0.001$), and standard deviation O_2 ($p<0.05$), were significant in predicting the distribution of the species assemblage in the late spring (Table 2.2).

After hypoxic waters expanded into shallower depths (Fig. 2.2: Sep 2013), nine out of eleven species that occurred in every 2013 transect showed significant decreases in their average oxygen occurrence (Fig. 2.4: Sep., all $p<0.05$). The mean depth, minimum O_2 and standard deviation O_2 (all $p<0.001$) still significantly predicted the species distributions, however, the explained variance in the entire species assemblage dropped by half (Sep. 2013: RDA $_{adj}R^2$=0.24) which corresponded to less differentiated oxygen occurrences among species. When normoxic waters reappeared and re-established the steep oxygen gradient (Fig. 2.2: Oct 2013), the explained variance in the species assemblage also increased (Oct. 2013: RDA $_{adj}R^2$=0.41) and the mean depth, O_2 maximum and standard deviation O_2 were significant predictors (all $p<0.001$). The increase in explained variance by the oxygen predictor variables corresponded with the reappearance of normoxic waters and six species undergoing spatial resorting to separate oxygen regimes; all had significant increases in their average *in situ* oxygen occurrence (Fig. 2.4: Oct, all $p<0.05$). In general, conversion of my data to oxygen partial pressures (kPa) slightly increased the amount of variance explained (1-2%) in the species assemblage compared to using just oxygen concentration units (ml l^{-1}). In general, including measurements of oxygen variability improved the best-fit model ($_{adj}R^2$) relative to using only measurements of central tendency.

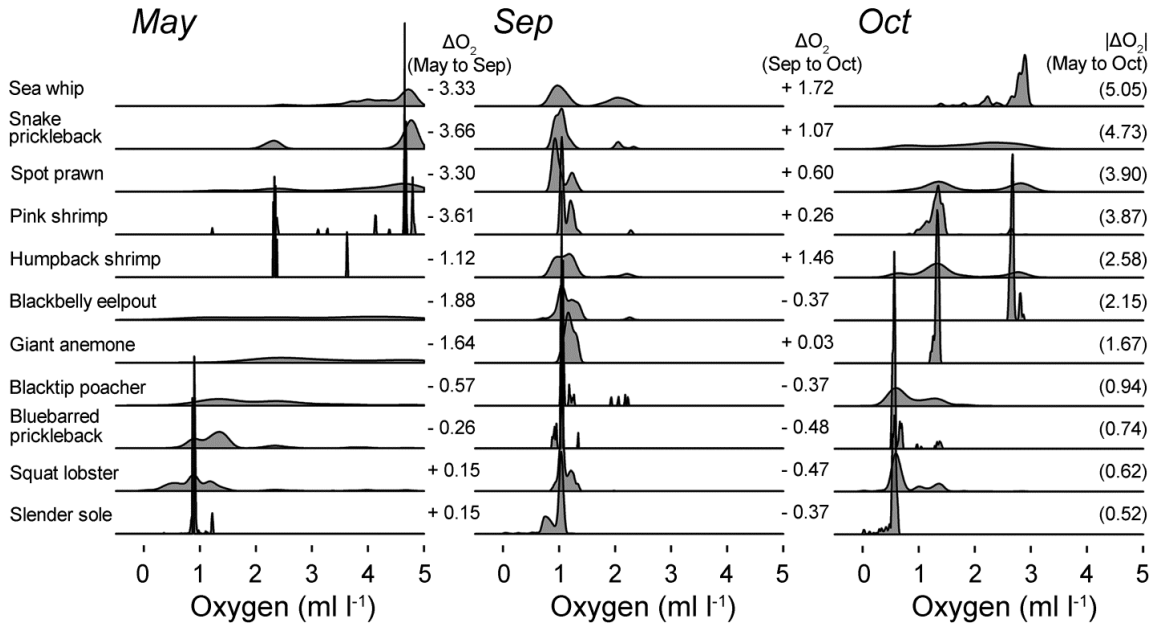

Figure 2.4. Shifts in species occurrences with respect to oxygen. The distributions of 11 species, common across the three 2013 transects, were partitioned to the oxygen gradient in May. With expansion of hypoxic waters, the differences among the species oxygen occurrences were lost by September. Partitioned distributions re-established with the return of normoxic waters in October. To visualize the species distributions at the same scale *in situ* oxygen occurrences are plotted as individual density plots (y-axis probability limits = (0, 1)) for each species and assembled into a waterfall plot for each time period. Numbers between time periods indicate the relative shift in the median oxygen occurrence for a species. Species are ranked in descending order by their absolute median shift in oxygen occurrence from May to October (far right in parentheses). All shifts in oxygen occurrence were significant ($p<0.05$) except the September to October shift for giant anemone.

Table 2.2. Canonical redundancy analyses (RDA) resolved how the entire epibenthic community was structured by depth and oxygen during the 2013 hypoxia cycle. In May, the community was highly structured (global $_{adj}R^2 = 0.59$); species abundances were partitioned across gradients of oxygen (Fig. 2.4: May) and depth (Fig. 2.6a). By September, and after deoxygenation, community structure was lost (global $_{adj}R^2 = 0.25$) which corresponded with a homogenization of the species occurrences across the oxygen gradient (Fig. 2.4: Sep.) and spatial overlap of their distributions (Fig. 2.6b). When oxygen renewal began in October community structure returned (global $_{adj}R^2 = 0.41$); species abundances resorted back along the gradients of oxygen (Fig. 2.4: Oct) and depth (Fig. 2.6c). Original predictor variables (mean depth, O_2 mean, O_2 median, O_2 max, O_2 min, O_2 sd) were calculated from summarizing database entries into 20 m^2 regions along each transect. Inclusion of predictor variables from model simplification was constrained to those that had maximum individual explained variance but did not exceed that of the global model (in bold). Permutation tests (n=1000 iterations) determined the significance of predictor variables. ** $p < 0.001$, * $p < 0.05$.

Before deoxygenation (May)		After deoxygenation (Sep)		Early stage recovery (Oct)	
	Variance		Variance		Variance
Global $_{adj}R^2$	**0.59**	**Global $_{adj}R^2$**	**0.25**	**Global $_{adj}R^2$**	**0.41**
O_2 max**	0.38	Mean depth**	0.13	Mean depth**	0.22
Mean depth**	0.19	O_2 min**	0.07	O_2 max**	0.17
O_2 min**	0.02	O_2 stdev**	0.05	O_2 stdev**	0.03
O_2 stdev*	0.01				

Change in the overall community structure was driven by the abundances of spot prawn, pink shrimp, and sea whip in high oxygen waters and of slender sole and squat lobsters in low-oxygen waters (Fig. 2.5a,b,c). Spot prawn, pink shrimp, and sea whip characterized normoxic waters and formed a community subgroup that had some of the highest seasonal shifts in their *in situ* oxygen occurrences (>3.5 ml l^{-1}). Because sea whips are sessile, they had the highest *in situ* oxygen occurrence shift (5.05 ml l^{-1}) as the oxygen concentration in the water changed around them. Slender sole and squat lobster form a different subgroup that characterized hypoxic waters with median shifts opposite to the normoxic subgroup (Fig. 2.4) and the lowest overall median shifts in *in situ* oxygen occurrence (<0.70 ml l^{-1}) as they migrated up- and down-slope.

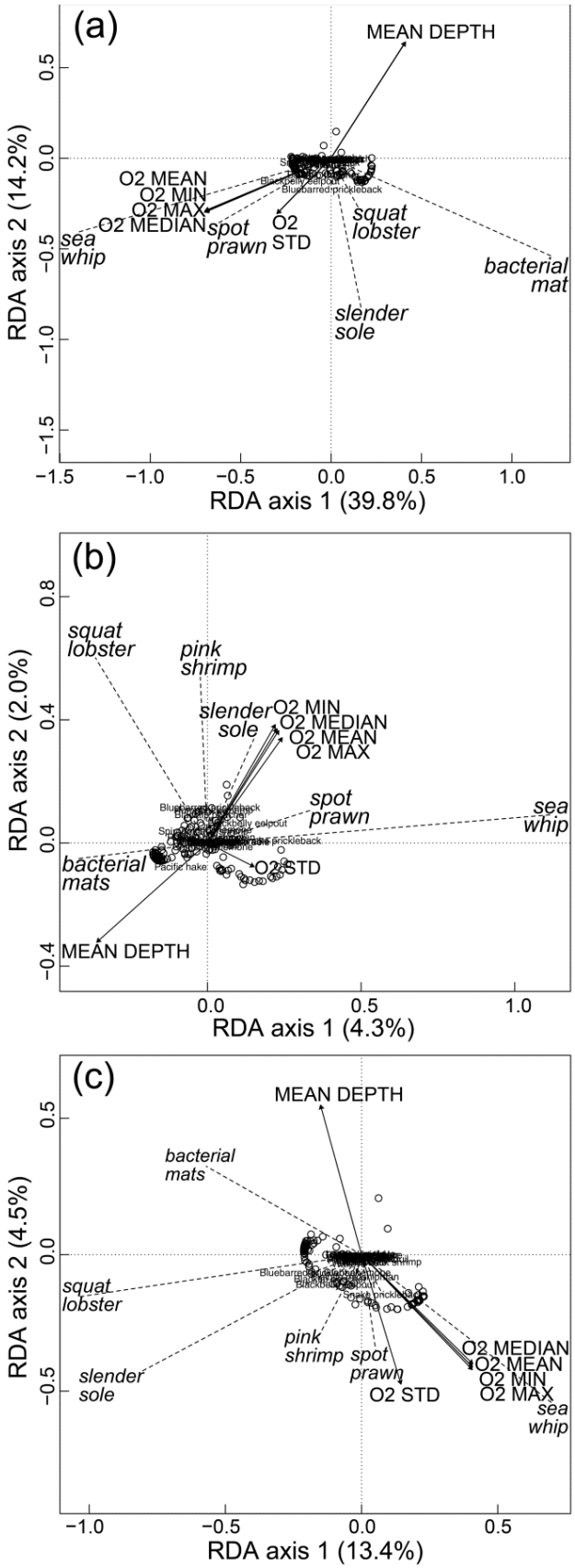

Figure 2.5. RDA correlation triplots for 2013 transect lines illustrate the relationship between species assemblage and oxygen regime. Bacterial mats and sea whips characterize the least and greatest oxygenated sites respectively. Change in structure of the entire community was driven by redistribution of the most abundant mobile species: slender sole, squat lobsters, spot prawns, and pink shrimp. Other species are clustered at the origin (0,0) and are not as strongly associated with the RDA axes. Black arrows indicate predictors (capitalized), black dashed lines indicate individual species (italicized), and circles indicate 20 m^2 sections along each transect. Percent of the variation explained by the first two canonical axes is shown in parentheses. (a) May (before deoxygenation). (b) September (after deoxygenation). (c) October (during early stage oxygen recovery).

In the presence of steep oxygen gradients, the two subgroups are spatially segregated with minimal habitat overlap (Fig. 2.6a, Fig. A.1). From 125 to 70 m depths, total animal density averaged 2±5 individuals m^{-2} (mean±sd) with a maximum of 35 individuals m^{-2} at 100 m depth. In the presence of expanding hypoxia, the spatial separation of the two subgroups collapsed (Fig. 2.6b, Fig. A.1) with significant depth shifts in the species distributions as slender sole migrated into shallower depths while squat lobsters, spot prawns, and pink shrimp descended into deeper depths (all $p<0.05$) with broader distributions establishing for all species. Animal distribution was also more homogenous: from 125 to 70 m depths, total animal density averaged 2±1 individuals m^{-2} with a maximum of 7 individuals m^{-2} at 95 m depth. When the oxygen gradient re-established, spatial resorting occurred (Fig. 2.6c, Fig. A1). From 125 to 70 m depths, total animal density averaged 4±3 with bimodal peaks of total animal density at 100 m depth (13 individuals m^{-2}) and 83 m depth (16 individuals m^{-2}). The distributions of squat lobster, spot prawn, and pink shrimp shifted back into shallower depths (all $p<0.05$). However, the average depth distribution of slender sole continued to decrease as more individuals shifted further into shallower depths ($p<0.05$). Transects flown prior to 2013 also captured the community structure at key stages during the hypoxia cycle. Spatially overlapping species distributions were evident in October 2011 when oxygen concentration was relatively constant throughout the transect area (Fig. 2.6d). Partitioned species distributions were also observed in September 2008, however the transition zone between hypoxia and normoxia occurred at a shallower depth (~70 m) and thus the divide between species distributions also occurred at this depth (Fig. 2.6e).

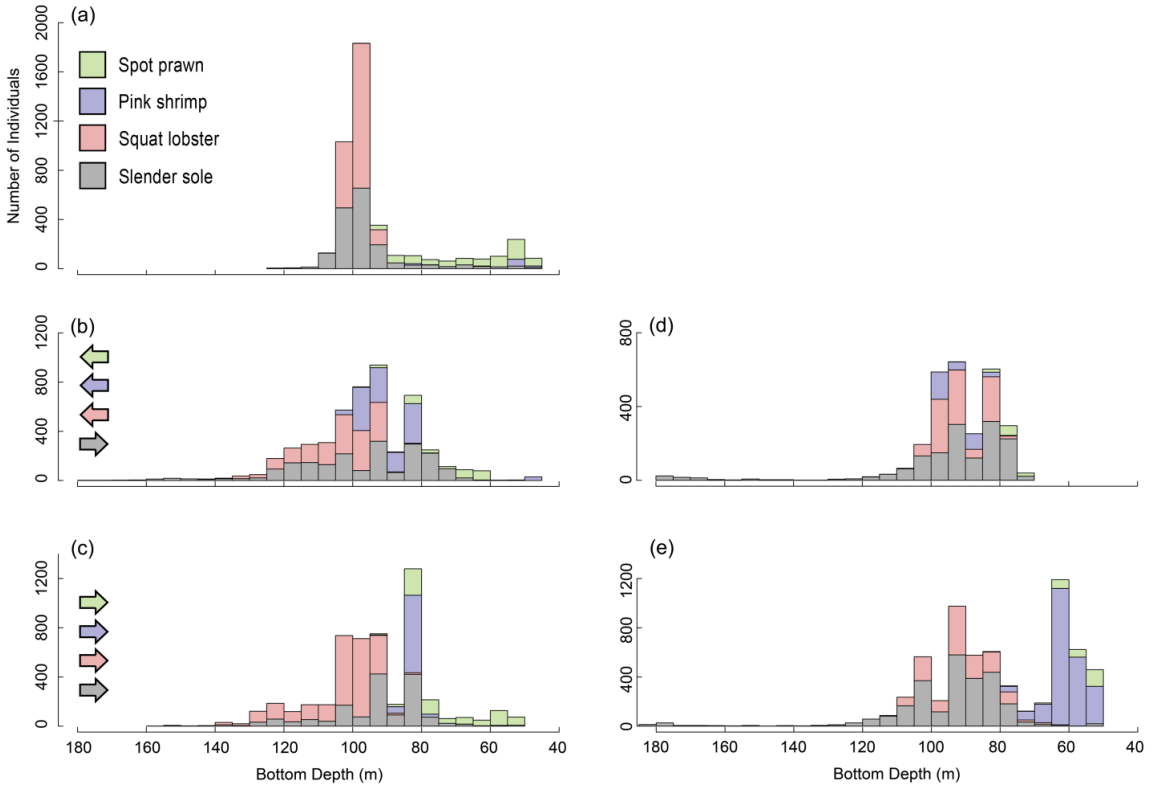

Figure 2.6. Spatial resorting of species. Counts of the four mobile species (slender sole, squat lobster, spot prawn, pink shrimp) driving community patterns (Fig. 5) are plotted as stacked bars. (a-c) Redistributions within 2013 hypoxia cycle. Arrows depict species movements shallower (→) or deeper (←) relative to the previous sampling period ($p<0.05$). (a) May: spatial segregation occurred with slender sole and squat lobster in deeper water when oxygen gradients were steep. (b) September: With shoaling hypoxia and near homogeneous oxygen, species overlapped spatially. (c) October: Spatial resorting re-established with onset of oxygen renewal. (d-e) The same species distribution patterns also occurred in prior years. (d) Similar to 2013, October 2011 showed spatially overlapping species in pervasive hypoxia along the transect. (e) September 2008 captured the deep-water renewal in progress as the severely hypoxic water encroached into shallower depths. The steep oxygen gradient was present in relatively shallower depths compared to 2013, but distinct spatial segregation was still present.

Long-term oxygen profile from VENUS

The eight year (2006-2014), oxygen data at the hypoxia transition zone (96 m) suggest the average oxygen concentration is declining at this depth in Saanich Inlet. A linear regression through these data depicts a significant decrease of ~0.05 ml $l^{-1}year^{-1}$ in the annual oxygen average over the eight year period of our study (Mar 2006-2014, Fig. 2.7a, $p<0.0001$). A one-year running mean (Fig. 2.7b) shows the drop in the long-term oxygen average coincides with the failure of the 2010 deep-water renewal in the Strait of Georgia (Johannssen *et al.*, 2014). Since 2010, the average annual oxygen concentration (<1.2 ml l^{-1}) has yet to completely recover to the higher oxygen levels (>1.4 ml l^{-1}) measured prior to 2010. The duration, as measured in cumulative days per year, at which the VENUS time-series is below the hypoxia and severe hypoxia thresholds appears to be annually increasing. Regression coefficients suggest the annual duration of hypoxia and severe hypoxia has increased by 7.1 and 8.6 days $year^{-1}$ respectively over the course of this study. However, this trend is not yet significant for either the hypoxia or severe hypoxia thresholds (linear regressions, both $p>0.05$; Fig. 2.7c).

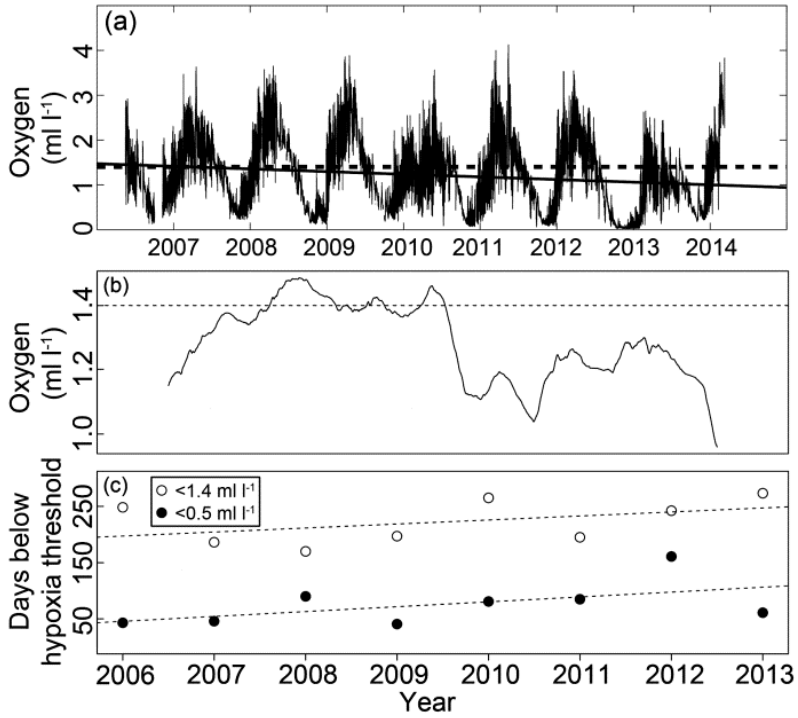

Figure 2.7. The VENUS oxygen time-series in Saanich Inlet at 96 m. (a) One minute interval data plotted from March 2006 to March 2014 illustrate the annual oxygen depletion and renewal of the hypoxia cycle. A linear regression (solid line) through this period shows a long-term trend of decreasing oxygen concentration (oxygen = 1.4 – 0.046*year, $p<0.001$). The horizontal dashed line marks the hypoxia threshold at 1.4 ml l^{-1}. (b) A one-year running mean shows that a weak renewal event in 2010 drives the majority of the decrease in the long-term oxygen average. Subsequent years have yet to re-establish an annual average oxygen level above 1.4 ml l^{-1}. (c) Points show the cumulative duration (in number of days) below the hypoxia and severe hypoxia threshold for each calendar year of the VENUS oxygen time-series for this period. Dashed regression lines show a trend of the increasing duration over time although the pattern is currently not significant ($p>0.05$). Note x-axis labels for (b,c) are different from (a).

Discussion

Repeated observations over several years established the lower oxygen concentrations at which 26 epibenthic metazoan species occur in the northeast Pacific Ocean. Additional species that occurred in low numbers (Table A.2) are otherwise common in the northeast Pacific, at least down to 150 m depth. As I encountered no dying or dead animals during the surveys, the absence of such species in some years was

likely caused by hypoxia avoidance. Overall, my detailed field records illustrate the differential tolerances that dictate the composition of natural assemblages that are usually studied by lower-resolution methods such as vertical oxygen profiles and bottom grabs. My approach reveals wide hypoxia tolerance in some mobile species. For example, lab studies have determined gadid fish (e.g. hake) to have relatively high oxygen requirements (Clarke & Johnston, 1999), yet my *in situ* observations show them to occur frequently in severe hypoxia where they may prey on slender sole and squat lobster. Pacific hake is also recorded in hypoxia in nearby Hood Canal, Puget Sound where it follows migrating zooplankton (Parker-Stetter *et al.*, 2009). Although spot prawn and pink shrimp are congeneric species, their mean oxygen occurrences, 2.5 ml l^{-1} and 1.6 ml l^{-1} respectively, were quite different. Critical oxygen tension, or the physiological threshold at which an organism switches from aerobic to anaerobic metabolism, is approximately 1.8 ml l^{-1} in the spot prawn (Whyte & Carswell, 1982) which explains their strong association with the higher range of oxygen concentrations measured in our study. Jamieson and Pikitch (1988) noted spot prawns, but not pink shrimp, dying in a hypoxic event in Saanich. During hypoxia in September 2013, pink shrimp and spot prawn may have sought higher oxygen by migrating; however, on a low slope bathed in low oxygen, the direction towards refuge may not have been obvious. Although sponges can dominate anoxic systems (Steckbauer e*t al.*, 2011; Riedel *et al.*, 2014), thresholds are not published. My *in situ* records for sponges highlight the hypoxia tolerance of this phylum. I can also expect the depth ranges of other sessile long-lived species to be pruned by episodic shoaling hypoxia; the sea whip experienced great shifts in ambient oxygen to as low as 0.5 ml l^{-1} despite its shallow range in Saanich Inlet.

Hypoxia thresholds in the northeast Pacific Ocean

My results fill a major knowledge gap on natural *in situ* hypoxia tolerances for marine biodiversity, specifically in the northeast Pacific. Species are naturally distributed across a wide range of oxygen concentrations because *in situ* oxygen is highly variable in time and space (Matabos *et al.*, 2012; this study). In general, the northeast Pacific is characterized by the natural occurrence of benthic species in hypoxic waters, the persistence of several populations in generally hypoxic conditions, and the dominance of extreme species in severe hypoxia. The most hypoxia sensitive species are likely underrepresented in my observations as I did not sample shallower than 30 m; thus my *in situ* oxygen occurrence values for these species are likely lower limits. The lack of consistency of my observations with hypoxia literature can be explained by the paucity of hypoxia tolerance studies in the northeast Pacific and the absence of *in situ* work that accounts for the natural mobility among species. Biases towards laboratory studies, Atlantic species, and to a lesser extent, commercially important (and thus larger) species have skewed general hypoxia thresholds towards higher, more conservative values. This supports the supposition that general thresholds are not applicable to all marine species (Levin *et al.*, 2009); regional context is necessary when describing the impacts of hypoxia for a system.

When calculating site-specific hypoxia thresholds, the practice of reporting oxygen data in concentration units needs to be reconsidered. Although oxygen partial pressure only slightly increased the variance explained in the community structure, this was a result of low variability in the other environmental variables at our site (temperature, salinity, density, pressure). A given oxygen concentration is not equivalent

at sites that differ widely in temperature and salinity because these parameters have a direct impact on oxygen solubility (Rabalais *et al.* 2009; Hofmann *et al.*, 2011). Oxygen partial pressure, not concentration, is also what drives the physiological delivery of oxygen within the organism (Seibel, 2011). In a system where populations are adapted to persist in low oxygen, physiological constraints rather than mortality effects may be the dominant driver of community structure. If this is the case, the loss of biomass and energy transfer in a hypoxic system will likely be more strongly coupled to the limits of aerobic metabolism. Thus, when defining group-specific thresholds, critical oxygen tensions may be a better predictor of species responses to hypoxia (Seibel, 2011; Seibel & Childress, 2013).

Hypoxia in the northeast Pacific Ocean

Multi-decadal oxygen records in the Northeast Pacific show persistent declines at Ocean Station Papa (Whitney *et al.*, 2007), in both offshore and inshore waters of California (Bograd *et al.*, 2008, 2014; McClatchie *et al.*, 2010; Koslow *et al.*, 2011; Booth *et al.*, 2014), Oregon (Pierce *et al.*, 2012), and British Columbia (Whitney, 2009; Crawford & Peña, 2013). Convergence of the oxygen-depleted North Pacific Current and the California Undercurrent occurs in this region (Whitney *et al.*, 2007). The oxygen minima of these water masses now appear in the summer as hypoxia and severe hypoxia in shallow depths (<70 m) on the inner continental shelf of Washington and Oregon (Grantham *et al.*, 2004; Connolly *et al.*, 2010) with increased frequency in the last decade (Chan *et al.*, 2008). Similarly, long-term oxygen decline and more frequent hypoxia are now recorded for the Strait of Georgia which is an inshore reflection of the offshore source waters (Johannessen *et al.*, 2014). While the inlets along the coast of British

Columbia and Alaska experience additional drivers, there is a strong connection to the Pacific in the oxygen renewal process. The oxygen decline recorded in the VENUS records in Saanich Inlet may, in part, be following the deoxygenation occurring in adjacent source waters and those of the Northeast Pacific. As the VENUS record extends over the 25 year observatory lifetime, the nature of this trend will be tested. However, as with most time series (see Bates *et al.*, 2014), data collection in this region is currently not designed to detect the concomitant community changes in species distributions in response to deoxygenation (although see Keller *et al.*, 2010).

Natural mesocosms like Saanich Inlet permit study of community patterns driven by deoxygenation and shoaling hypoxia in the Northeast Pacific. A long Holocene record of hypoxia in Saanich Inlet (O'Connell & Tunnicliffe, 2001) points towards some fauna adapted to chronic hypoxia exposure, especially the sessile invertebrates on fjord walls (Tunnicliffe, 1981). Indicator species that drive community patterns in Saanich Inlet are also common offshore from Alaska to California where they inhabit depths now affected by long-term oxygen loss and shoaling hypoxia (Helly & Levin, 2004; Hofmann *et al.*, 2011). Slender sole dominates the demersal fish biomass off California (Cross, 1987) and the ichthyoplankton off Oregon (Pearcy, 1978; Auth & Brodeur, 2006). Despite their abundance, slender sole are not commercially important because of their small size (Froese & Pauly, 2014). Squat lobster is distributed from Alaska to California (Benedict, 1902) and is physiologically adapted to living in extremely low oxygen concentrations (Burd, 1988). In general, squat lobsters (superfamilies Chirostyloidea and Galatheoidea) are common in low oxygen environments (Lovrich & Thiel, 2011).

Natural oxygen variability can drive the lower oxygen tolerances of a species assemblage. For example, estuaries, open coasts, and the upper depth boundaries of oxygen minimum zones are seasonally hypoxic; the benthic communities in these systems often have lower hypoxia thresholds compared to systems with temporally stable oxygen profiles (Diaz & Rosenberg, 1995; Brand & Griffiths, 2009). From my study, the generally low oxygen occurrences among species, the range of oxygen occurrences within species, and the significance of the oxygen predictors support the importance of oxygen variability as an important driver of community structure in some hypoxic systems (e.g. Matabos *et al.*, 2012). Thus, the minimal responses to hypoxia and unexpected tolerance to severe hypoxia observed in some species from the Northeast Pacific (Rankin *et al.*, 2013, Eerkes-Medrano *et al.*, 2013) may be explained by an adaptation to the oxygen dynamics characterizing this region. Over evolutionary time scales, the long-term oxygen dynamics of a system will determine the response of the community (Levin *et al.*, 2009) and predict the lower limits of community persistence.

Community responses to hypoxia expansion

Continuous oxygen and imagery acquisition by ROV yielded high-resolution datasets that revealed several important community responses during shoaling hypoxic events. Because of the high spatial-temporal variability of dissolved oxygen in the ocean, oxygen measurements must be made in parallel with *in situ* animal observations; such studies are required to accurately quantify the community-level response to oxygen loss.

The persistence of populations in low oxygen highlights the benefits of hypoxia tolerance and the functional role of species in hypoxic systems. With hypoxia tolerance, animals in low oxygen zones have refuge from predators (Altieri *et al.*, 2008; Utne-Palm

et al., 2010; Stewart *et al.*, 2013) and can exploit alternative food sources when infauna emerge during the onset of anoxia (Sturdivant *et al.*, 2012; Inagaki *et al.*, 2014). Thus, the lower threshold of aerobic energy transfer in metazoan food webs can be determined by the physiological limits of the component species. For example, squat lobsters are well adapted to flourish in low oxygen; they have plastic gill morphologies for enhanced respiration (Burd, 1988) and low critical oxygen tensions (~0.14 ml l^{-1}, Burd 1985). Also, high densities of squat lobster can occur well below the severe hypoxia threshold (~100 individuals m^{-2} in <0.2 ml l^{-1}, Burd & Brinkhurst, 1984). Thus, when microbial energetics have mostly switched to alternative electron receptors in such extreme hypoxia (Wright *et al.*, 2012), metazoan-based energy pathways can still be coupled to aerobic metabolism.

Migration of the hypoxia-tolerant slender sole into shallower depths during shoaling hypoxia events and the merging of formerly disjunct distributions point to mobility as a key determinant of community structure in hypoxic systems (Ekau *et al.*, 2010; Essington & Paulsen, 2010; Keller *et al.*, 2010). Competition during spatial co-occurrence happens only periodically in seasonally hypoxic systems because most species will move towards higher oxygen concentrations (e.g. Oct 2013). However, if the seasonal duration of hypoxia increases, the frequency of competition will also increase with the eventual net loss in biomass, food web complexity, and perhaps diminished provisioning of ecosystem services. Although I show several epibenthic species from the Northeast Pacific can occur in hypoxia, the largest species (such as the commercial species in our study) are mostly absent when hypoxia is severe.

The immediate consequence of increasing frequency of hypoxia shoaling events in the Northeast Pacific will be habitat loss and the collapse of community structure from

a system-wide shift towards homogenization. The first signs of such loss are indicated in catch records of groundfish that have moved shallower by 2 to 3 m each year over a decade (Whitney *et al.*, 2009) as hypoxia expanded on the British Columbia coast (Whitney, 2009). Community homogenization will be followed by the functional extinction of several local populations if the duration of hypoxia increases and the system drops toward severe hypoxia. Both oxygen concentrations and benthic communities can change quickly. As instrumentation tracks oxygen in key regions, monitoring strategies can use indicator species to determine biological responses. My study suggests that oxygen at 1.0-1.03 ml l^{-1} (95% C.I.) induces shoaling of slender sole and that oxygen at 1.03-1.14 ml l^{-1} and 1.13-1.15 ml l^{-1} induces movement of spot prawns and pink shrimp respectively. Similar values can now be derived for several other species (Table S2). While such guidelines require testing in other settings, combining rigorous laboratory measurements with field data is required to develop strategies for managing responses in ocean regions with expanding hypoxia.

Acknowledgements

I am grateful to R. Dewey, P. Macoun, and staff at Oceans Network Canada–VENUS for their devotion to supporting ecological research and making their data open-source. I thank the captains and crews of the CCGS Tully, CCGS, Vector, RV Thompson, RV Falkor and the associates of Canadian Scientific Submersible Facility and the Oceanic Explorer operators for their skill and field support. Comments from R. Hamme, F. Juanes, and three anonymous reviewers greatly improved an early version of this manuscript. Technical help came from R. Hamme, J. Rose, L. Teeter, J. Nephin, K.

Gale, and S.T. Bear. Supplementary support came from the Schmidt Ocean Institute cruise, "Open Ocean to Inner Sea". Primary funding came from an NSERC scholarship to J.W.F.C. and grants from NSERC Canada and the Canadian Healthy Oceans Network (CHONe) to V.T.

Literature cited

Altieri AH (2008) Dead zones enhance fisheries species by providing predation refuge. *Ecology*, **89**, 2808-2818.

Anderson JJ, Devol AH (1973) Deep water renewal in Saanich Inlet, an intermittently anoxic basin. *Estuarine & Coastal Marine Science*, **1**, 1-10.

Auth TD, Brodeur RD (2006) Distribution and community structure of ichthyoplankton off the coast of Oregon, USA, in 2000 and 2002. *Marine Ecology Progress Series*, **219**, 199-213.

Bates AE, Lee RW, Tunnicliffe V, Lamare MD (2010) Deep-sea hydrothermal vent animals seek cool fluids in a highly variable thermal environment. *Nature Communications*, **1**, 14.

Bates AE, Pecl GT, Frusher S *et al.* (2014) Defining and observing stages of climate-mediated range shifts in marine systems. *Global Environmental Change*, **26**, 27-38.

Benedict JE (1902) Description of a new genus and forty-six new species of Crustaceans of the family Galatheidae, with a list of the known marine species. *Proceedings of the United States National Museum*, **26**, 243-334.

Bijma J, Pörtner H, Yesson C, Rogers AD (2013) Climate change and the oceans – What does the future hold? *Marine Pollution Bulletin*, **74**, 495-505.

Bocard D, Gillet F, Legendre P (2011) Chapter 6 Canonical Ordination. In: Numerical ecology with R (eds Gentleman R, Hornik K, Parmigiani GG), pp. 154-197, Springer, New York.

Bograd SJ, Castro CG, Di Lorenzo E, Palacios DM, Bailey H, Gilly W, Chavez FP (2008) Oxygen declines and the shoaling of the hypoxic boundary in the California Current. *Geophysical Research Letters*, **35**, L12607.

Bograd SJ, Buil MP, Di Lorenzo E *et al.* (2015) Changes in source waters to the Southern California Bight. *Deep-Sea Research II: Topical Studies in Oceanogrphy*, **112**, 42-52.

Booth JAT, Woodson CB, Sutula M *et al.* (2014) Patterns and potential drivers of declining oxygen content along the southern California coast. *Limnology & Oceanography*, **59**, 1127-1138.

Brand T, Griffiths C (2009) Seasonality in the hydrography and biogeochemistry across the Pakistan margin of the NE Arabian Sea. *Deep Sea Research II: Topical Studies in Oceanography*, **56**, 283-295.

Brewer PG, Peltzer ET (2009) Limits to marine life. *Science*, **324**, 347-348.

Burd BJ (1985) Respiration of a low oxygen tolerant galatheid crab, *Munida quadrispina* (Benedict, 1902). *Canadian Journal of Zoology*, **63**, 2538-2542.

Burd BJ (1988) Comparative gill characteristics of *Munida quadrispina* (Decapoda, Galatheidae) from different habitat oxygen conditions. *Canadian Journal of Zoology*, **66**, 2320-2323.

Burd BJ, Brinkhurst RO (1984) The distribution of the galatheid crab *Munida quadrispina* (Benedict 1901) in relation to oxygen concentrations in British Columbia fjords. *Journal of Experimental Marine Biology & Ecology*, **81**, 1-20.

Chan F, Barth JA, Lubchenco J, Kirincich A, Weeks H, Peterson WT, Menge BA (2008) Emergence of anoxia in the California Current large marine ecosystems. *Science*, **319**, 5865.

Clark A, Johnston NM (1999) Scaling of metabolic rate with body mass and temperature in teleost fish. *Journal of Animal Ecology*, **68**, 893-905.

Clark MS, Husmann G, Thorne MAS, Burns G, Truebano M, Peck LS, Abele D, Philipp EER (2013) Hypoxia impacts large adults first: consequences in a warming world. *Global Change Biology*, **19**, 2251-2263.

Cocco V, Joos F, Steinacher M *et al.* (2013) Oxygen and indicators of stress for marine life in multi-model global warming projections. *Biogeosciences*, **10**, 1849-1868.

Connolly TP, Hickey BM, Geier SL, Cochlan WP (2010) Processes influencing seasonal hypoxia in the northern California Current System. *Journal of Geophysical Research*, **115**, C03021.

Crawford WR, Peña MA (2013) Declining oxygen on the British Columbia continental shelf. *Atmosphere-Ocean*, **51**, 88-103.

Cross JN (1987) Demersal fishes of the upper continental slope off southern California. *California cooperative oceanic fisheries investigations report*, **28**, 155-167.

Diaz RJ, Rosenberg R (2008) Spreading dead zones and consequences for marine ecosystems. *Science*, **321**, 926-929.

Diaz RJ, Rosenberg R (1995) Marine benthic hypoxia: A review of its ecological effects and the behavioural responses of benthic macrofauna. *Oceanography and Marine Biology: an Annual Review*, **33**, 245-303.

Diaz RJ, Schaffner LC (1990) The functional role of estuarine benthos, pp. 25-56. In: Perspectives on the Chesapeake Bay, 1990. Advances in Estuarine Science (eds Haire M, Krome, EC), pp. 25-56, Chesapeake Bay Program, Chesapeake Research Consortium Publication CBP/TRS41/90.

Dray S, Legendre P, Blanchet G (2011) Packfor: forward selection with permutation (Canoco p.46). R package version 0. 0-8/r100. <http://R-Forge.R-project/org/projects/sedar/>.

Eby LA, Crowder LB (2002) Hypoxia-based habitat compression in the Neuse River Estuary: context-dependent shifts in behavioral avoidance thresholds. *Canadian Journal of Fisheries & Aquatic Sciences*, **59**, 952-965.

Eerkes-Medrano D, Menge BA, Sislak C, Langdon CJ (2013) Contrasting effects of hypoxic conditions on survivorship of planktonic larvae of rocky intertidal invertebrates. *Marine Ecology Progress Series*, **478**, 139-151.

Ekau W, Auel H, Pörtner HO, Gilbert D (2009) Impacts of hypoxia on the structure and processes in pelagic communities (zooplankton, macro-invertebrates and fish). *Biogeosciences*, **7**, 1669-1699.

Ernest SKM, Enquist BJ, Brown JH *et al.* (2003) Thermodynamic and metabolic effects on the scaling of production and population energy use. *Ecology Letters*, **6**, 990-995.

Essington T, Paulsen C (2010) Quantifying hypoxia impacts on an estuarine demersal community using a hierarchical ensemble approach. *Ecosystems*, **13**, 1035-1048.

Froese R, Pauly D (2014) FishBase. World Wide Web electronic publication. www.fishbase.org (09/2014).

Gargett AE, Stucchi D, Whitney F (2003) Physical processes associated with high primary production in Saanich Inlet, British Columbia. *Estuarine & Coastal Shelf Science*, **56**, 1141-1156.

Gilbert D, Rabalais NN, Diaz RJ, Zhang J (2010) Evidence for greater oxygen decline rates in the coastal ocean than in the open ocean. *Biogeosciences*, **7**, 2283-2296.

Gilly WF, Beman JM, Litvin SY, Robison BH (2013) Oceanographic and biological effects of shoaling of the oxygen minimum zone. *Annual Reviews of Marine Science*, **5**, 393-420.

Grantham BA, Chan F, Nielsen KJ, Fox DS, Barth JA, Huyer A, Menge BA (2004) Upwelling-driven nearshore hypoxia signals ecosystem and oceanographic changes in the northeast Pacific. *Nature*, **429**, 749-754.

Grundle DS, Timothy DA, Varela DE (2009) Variations of phytoplankton productivity and biomass over an annual cycle in Saanich Inlet, a British Columbia fjord. *Continental Shelf Research*, **29**, 2257-2269.

Helly JJ, Levin LA (2004) Global distribution of naturally occurring marine hypoxia on continental margins. *Deep-Sea Research I: Oceanographic Research Papers*, **51**, 1159-1168.

Herlinveaux RH (1962) Oceanography of Saanich Inlet in Vancouver Island, British Columbia. *Journal of the Fisheries Research Board of Canada*, **19**, 1-37.

Hofmann A, Peltzer E, Walz P, Brewer P (2011) Hypoxia by degrees: establishing definitions for a changing oxygen. *Deep-Sea Research I: Oceanographic Research Papers*, **58**, 1212-1226.

Inagaki Y, Takatsu T, Kimura M, Kano Y, Takahashi T, Kamei Y, Kobayashi N, Maeda T (2014) Improved growth of flathead flounder *Hippoglossoides dubius* in hypoxic waters in Funka Bay, Japan. *Fisheries Science*, **80**, 725-734.

IPCC (2013). Carbon and other biogeochemical cycles. In: Climate Change 2013-The Physical Science basis. Contribution of Working Group I to the Fifth Assessment Report of the Intergovernmental Panel on Climate Change (edsStocker TF, Quin D, Plattner GK, Tignor M, Allen SK, Boschung J, Midgley PM), pp. 365-570. Cambridge University Press, Cambridge.

Jamieson GS, Pikitch EK (1988) Vertical distribution and mass mortality of prawns, *Pandalus platyceros*, in Saanich Inlet, British Columbia. *Fishery Bulletin*, **86**, 601-608.

Johannessen SC, Masson D, Macdonald RW (2014) Oxygen in the deep Strait of Georgia, 1951-2009: The roles of mixing, deep-water renewal, and remineralization of organic carbon. *Limnology & Oceanography*, **59**, 211-222.

Karlson K, Rosenberg R, Bonsdorff E (2002) Temporal and spatial large-scale effects of eutrophication and oxygen deficiency on benthic fauna in Scandinavian and Baltic

waters – A review. *Oceanography & Marine Biology, An Annual Review*, **40**, 427-489.

Karstensen J, Stramma L, Visbeck M (2008) Oxygen minimum zones in the eastern tropical Atlantic and Pacific oceans. *Progress in Oceanography*, **77**, 331-350.

Katz T, Yahel G, Reidenbach M *et al.* (2012). Resuspension of fish facilitates the transport and redistribution of coastal sediments. *Limnology & Oceanography*, **57**, 945-958.

Keeling RF, Körtzinger A, Gruber N (2010) Ocean deoxygenation in a warming world. *Annual Review of Marine Science*, **2**, 199-229.

Keller AA, Simon V, Chan F *et al.* (2010) Demersal fish and invertebrate biomass in relation to an offshore hypoxic zone along the US West Coast. *Fisheries Oceanography*, **19**, 76-87.

Kemp WM, Boynton WR, Adolf JE *et al.* (2005) Eutrophication of Chesapeake Bay: historical trends and ecological interactions. *Marine Ecology Progress Series* **303**, 1-29.

Koslow JA, Goericke R, Lara-Lopez A, Watson W (2011) Impact of declining intermediate-water oxygen on deepwater fishes in the California Current. *Marine Ecology Progress Series*, **436**, 207-218.

Legendre P, Gallagher ED (2001) Ecologically meaningful transformations for ordination of species data. *Oecologia*, **129**, 271-280.

Legendre P, Legendre L (2012) Redundancy analysis (RDA). In: Numerical Ecology 3rd edition, PP. 629–649, Elsevier, Amsterdam.

Levin LA, Ekau W, Gooday AJ *et al.* (2009) Effects of natural and human-induced hypoxia on coastal benthos. *Biogeosciences*, **6**, 2063-2098.

Lovrich GA & Thiel M (2011) Ecology, physiology, feeding, and trophic role of squat lobsters. In: Crustacean Issues. The Biology of Squat Lobsters (eds Poore GCB, Ahyong ST, Taylor J), pp.183-222, CSIRO Publishing.

Manning CC, Hamme RC, Bourbonais A (2010) Impact of deep-water renewal events on fixed nitrogen loss from seasonally-anoxic Saanich Inlet. *Marine Chemistry*, **122**, 1-10.

Matabos M, Tunnicliffe V, Juniper SK, Dean C (2012) A year in hypoxia: epibenthic community responses to severe oxygen deficit at a subsea observatory in a coastal inlet. *PLoS ONE*, **7**, e45626.

McClatchie S, Goericke R, Cosgrove R, Auad G, Vetter R (2010) Oxygen in the Southern California Bight: Multidecadal trends and implications for demersal fisheries. *Geophysical Research Letters*, **37**, L19602.

O'Connell JM, Tunnicliffe V (2001) The use of sedimentary fish remains for interpretation of long-term fish population fluctuations. *Marine Geology*, **174**, 177-195.

Oksanen J, Blanchet FG, Kindt R *et al.* (2013) Vegan: Community Ecology Package. -R package ver. 2.0-7, <http://CRAN.R-project.org/package=vegan/>.

Parker-Stetter SL, Horne JK, Langness MM (2009) The influence of midwater hypoxia on nekton vertical migration. *ICES Journal of Marine Science*, **66**, 1296-1302.

Pearcy WG (1978) Distribution and abundance of small flatfishes and other demersal fishes in a region of diverse sediments and bathymetry off Oregon. *Fishery Bulletin*, **76**, 629-640.

Pierce SD, Barth JA, Shearman RK, Erofeev AY (2012) Declining oxygen in the Northeast Pacific. *Journal of Physical Oceanography*, **42**, 495-501.

Pörtner HO (2008) Ecosystem effects of ocean acidification in times of ocean warming: a physiologist's view. *Marine Ecology Progress Series*, **373**, 203-217.

Prince ED, Goodyear CP (2006) Hypoxia-based habitat compression of tropical pelagic fishes. *Fisheries Oceanography*, **15**, 451-464.

R Core Team. 2014 *R: A language and environment for statistical computing.* R Foundation for Statistical Computing, Vienna, Austria. ISBN 3-900051-07-0, URL http://www.Rproject.org/.

Rabalais NN, Turner RE, Wiseman Jr WJ (2002) Gulf of Mexico hypoxia, A.K.A. "The Dead Zone". *Annual Review of Ecology & Systematics*, **33**, 235-263.

Rabalais NN, Diaz RJ, Levin LA, Turner RE, Gilbert D, Zhang J (2010) Dynamics and distribution of natural and human-caused hypoxia. *Biogeosciences*, **7**, 585-619.

Rankin PS, Hannah RW, Blume MTO (2013) Effect of hypoxia on rockfish movements: implications for understanding the roles of temperature, toxins and site fidelity. *Marine Ecology Progress Series*, **492**, 223-234.

Riedel B, Zuschin M, Stachowitsch M (2012) Tolerance of benthic macrofauna to hypoxia and anoxia in shallow coastal seas: a realistic scenario. *Marine Ecology Progress Series*, **458**, 39-52.

Riedel B, Pados T, Pretterebner K, Schiemer L, Steckbauer A, Haselmair A, Zuschin M, Stachowitsch M (2014) Effect of hypoxia and anoxia on invertebrate behaviour: ecological perspectives from species to community level. *Biogeosciences*, **11**, 1491-1518.

Rosa R, Seibel BA (2010) Metabolic physiology of the Humboldt squid *Dosidicus gigas:* implications for vertical migration in a pronounced oxygen minimum zone. *Progress in Oceanography*, **86**, 72-80.

Sarmiento JL, Hughes TMC, Stouffer RJ, Manabe S (1998) Simulated response of the ocean carbon cycle to anthropogenic climate warming. *Nature*, **393**, 245-249.

Seibel BA (2011) Critical oxygen levels and metabolic suppression in oceanic oxygen minimum zones. *Journal of Experimental Biology*, **214**, 326-336.

Seibel BA, Childress, JJ (2013) The real limits to marine life: a further critique of the Respiration Index. *Biogeosciences*, **10**, 2815-2819.

Steckbauer A, Duarte CM, Carstensen J, Vaquer-Sunyer R, Conley DJ (2011) Ecosystem impacts of hypoxia: thresholds of hypoxia and pathways to recovery. *Environmental Research Letters*, **6**, 025003.

Stewart JS, Field JC, Markaida U, Gilly WF (2013) Behavioral ecology of jumbo squid (*Dosidicus gigas*) in relation to oxygen minimum zones. *Deep-Sea Research II: Topical Studies in Oceanography*, **95**, 197-208.

Stewart JS, Hazen EL, Bograd SJ *et al.* (2014) Combined climate- and prey-mediated range expansion of Humboldt squid (*Dosidicus gigas*), a large marine predator in the California Current System. *Global Change Biology*, **20**, 1832-1843.

Stramma L, Johnson GC, Sprintall J, Mohrholz V (2008) Expanding oxygen-minimum zones in the tropical oceans. *Science*, **320**, 655-658.

Stramma L, Schmidtko S, Levin LA, Johnson GC (2010) Ocean oxygen minima expansions and their biological impacts. *Deep-Sea Research I: Oceanographic Research Papers*, **57**, 587-595.

Stramma L, Prince ED, Schmidtko S *et al.* (2013) Expansion of oxygen minimum zones may reduce available habitat for tropical pelagic fishes. *Nature Climate Change*, **2**, 33-37.

Sturdivant SK, Diaz RJ, Cutter GR (2012) Bioturbation in a declining oxygen environment, *in situ* observatiosn from a wormcam. *PloS ONE*, **7**, e34539.

Takahashi M, Barwell-Clarke J, Whitney F, Koeller P (1978) Winter condition of marine plankton populations in Saanich Inlet, B.C., Canada. I. Phytoplankton and its

surrounding environment. *Journal of Experimental Biology & Ecology*, **31**, 283-301.

Timothy DA, Soon MY (2001) Primary production and deep-water oxygen content of two British Columbian fjords. *Marine Chemistry*, **73**, 37-51.

Tunnicliffe V (1981) High species diversity and abundance of the epibenthic community in an oxygen-deficient basin. *Nature*, **294**, 354-356.

Utne-Palm AC, Salvanes AGV, Currie B *et al.* (2010) Trophic structure and community stability in an overfished ecosystem. *Nature*, **329**, 333-336.

Vaquer-Sunyer R, Duarte C (2008) Thresholds of hypoxia for marine biodiversity. *Proceedings of the National Academy of Science of the United States of America*, **105**, 15452-15457.

Vaquer-Sunyer R, Duarte C (2010) Sulfide exposure accelerates hypoxia-driven mortality. *Limnology & Oceanography*, **55**, 1075-1082.

Vaquer-Sunyer R, Duarte C (2011) Temperature effects on oxygen thresholds for hypoxia in marine benthic organisms. *Global Change Biology*, **17**, 1788-1797.

Whitney FA, Freeland HJ, Robert M (2007). Persistently declining oxygen levels in the interior waters of the eastern subarctic Pacific. *Progress in Oceanography*, **75**, 179-199.

Whitney FA (2009) Spreading hypoxia in deep waters along the west coast. In: State of the physical, biological, and selected fishery resources of Pacific Canadian marine ecosystems (eds Crawford WR, Irvine JR), Department of Fisheries and Oceans, Canadian Science Advisory Secretariat Research Document 2009/022.

Whitney F, Gilbert D, Sinclair A (2009) Impacts of spreading hypoxia on coastal biota of the subarctic Pacific. *Geochimica et cosmochimica acta*, **73**, 1435.

Whyte JNC, Carswell BL (1982) Determinants for live holding the spot prawn *Pandalus platyceros*, Brandt. *Canadian Technical Report of Fisheries Aquatic Sciences*, **1129**, 1-29.

Wright JJ, Konwar KM, Hallam SJ (2012) Microbial ecology of expanding oxygen minimum zones. *Nature Reviews Microbiology*, **10**, 381-394.

Yahel G, Yahel R, Katz T, Lazar B, Herut B, Tunnicliffe V (2008) Fish activity: a major mechanism for sediment resuspension and organic matter remineralization in coastal marine sediments. *Marine Ecology Progress Series*, **372**, 195-209.

Zaikova E, Walsh DA, Stilwell CP, Mohn WW, Tortel PD, Hallam SJ (2010) Microbial community dynamics in a seasonally anoxic fjord: Saanich Inlet, British Columbia. *Environmental Microbiology*, **12**, 172-191.

Chapter 3: Scale-dependent processes influence the temporal structure of epibenthic communities in a seasonally hypoxic system

Preface

Chapter 3 is a draft of a manuscript: Chu JWF, Curkan C, Tunnicliffe V. Scale-dependent processes influence the temporal structure of epibenthic communities in a seasonally hypoxic system.

Verena Tunnicliffe (dissertation supervisor, University of Victoria) contributed to the original survey design, camera deployment, provided resources for this study and writing of the paper. Curtis Curkan (B.Sc., University of Victoria) generated the animal abundance data under my supervision.

I designed the workflow for imagery analysis, analyzed the data, interpreted the results, and wrote the article.

Introduction

Rising atmospheric CO_2 is predicted to decrease the average oceanic oxygen content by 2-3% over the next century (Bopp *et al.*, 2013; Gattuso *et al.*, 2015). The long-term pattern of deoxygenation is superimposed onto natural cycles of variability (Whitney *et al.*, 2007; Frölicher *et al.*, 2009; Deutsch *et al.*, 2011), which are driven by multiple processes that control solubility, distribution, and total concentration of oxygen in the environment (Emerson & Bushinsky, 2014). At the decadal scale, oxygen oscillates because of natural climate cycles such as the Pacific Decadal Oscillation (PDO) and El Niño Southern Oscillation (ENSO) as well as the lunar tide cycle (Frölicher *et al.*, 2009;

Crawford & Peña, 2013). Annual and seasonal oxygen variability is induced by fluctuations in circulation, wind-driven upwelling, and primary production (Chan *et al.*, 2008; Booth *et al.*, 2012). Short-term oxygen variability (weeks to days) is associated with shifts in physical properties controlling oxygen solubility in surface waters such as temperature, salinity, and pressure as well as mixing and respiration (D'Avanzo & Kremer, 1994; Booth *et al.*, 2012; Frieder *et al.*, 2012). Additionally, diurnal and semidiurnal tidal components influence oxygen variability at subdaily scales (Frieder *et al.*, 2012; Sato *et al.*, 2014).

Regardless of the environmental driver of oxygen variability, biological communities have a similar response to oxygen deficiency (hypoxia). Along decreasing gradients of oxygen, benthic communities show a marked decrease in alpha diversity, abundance, and biomass (Levin, 2003; Quiroga *et al.*, 2005; Gooday *et al.*, 2010). In severe hypoxic conditions, communities become dominated by only a few hypoxia tolerant species (Levin & Gage, 1998; Levin *et al.*, 2009a) which are eventually excluded in the complete absence of oxygen (anoxia)Because of interspecific differences in hypoxia tolerance, community composition is also different (i.e., high beta diversity) across hypoxia gradients (Gooday *et al.*, 2010). While ecological studies have primarily examined community diversity along spatial gradients of hypoxia, they provide a framework for making similar predictions on how benthic communities will respond to oxygen variability over time.

Determining the processes responsible for structuring communities over time requires sampling the system before and after environmental perturbation (Underwood *et al.*, 2000). The response of the species composition to perturbation and the patterns of

recovery give insight into the processes that structure the community. If species abundances and composition are primarily influenced by changes in the environment (e.g. oxygen), community structure can potentially be explained by species-specific traits and species interactions (McGill *et al.*, 2006). However, random processes such as ecological drift and random dispersal can also create structure in biological communities (i.e., neutral theory; Hubbell, 1997; Bell, 2013), which predicts no relationship among species traits, abundances, community composition, and environmental conditions. Addressing the underlying processes that govern diversity relationships is important in the context of the effects of climate-driven change on marine communities; if neutral processes dominate, deoxygenation will not be a primary control on the identity, relative abundance, or spatial arrangement of species (i.e., compositional heterogeneity). Thus, our ability to link biological responses with changes in environmental oxygen over time will depend on the scale at which processes structure communities and testing if environment or neutral drivers influence species composition under various states of oxygen deficiency.

Temporal changes in biological communities also reflect an integrated response to multiple processes operating over long and short time scales (Barry *et al.*, 1995). Because of logistical challenges of benthic research, our ability to differentiate scale-dependent temporal changes in biological communities (short term versus long term responses) has been traditionally limited to annual and seasonal-scale time-series (Glover *et al.*, 2010), which cannot address the contribution of small-scale processes to structuring species composition. *In situ* high frequency data (measured at minute intervals) from the Victoria Experimental Network Under the Sea (VENUS) cabled observatory has revealed a highly

variable, but seasonally predictable hypoxia cycle that occurs in Saanich Inlet, British Columbia, Canada (Matabos *et al.*, 2012; Chu & Tunnicliffe, 2015). The natural *in situ* variability makes Saanich Inlet an ideal system to determine the time scales at which highly variable oxygen conditions can influence the structure of benthic communities.

Here, I address the temporal scales at which species composition and community structure are influenced by highly variable hypoxia. Data come from the 14-month deployment of a novel camera platform that collected images at <24 hr intervals, concomitant water column properties, measured at minute intervals, and span an entire hypoxia cycle in Saanich Inlet. Continuous observations during deoxygenation and reoxygenation phases of the hypoxia cycle allowed me to quantify the relative rates of community response and assess whether these differed among sessile and mobile species. Additionally, I combined several multivariate statistical methods designed to analyze the multiscale nature of ecological data-series (Legendre & Gauthier, 2014) with variance partitioning to assess whether temporal structure in the community- and species-level response were influenced by different processes at different scales.

Materials and methods

Saanich Inlet

Saanich Inlet (Fig. 3.1a) is a highly productive basin (Timothy & Soon, 2001; Grundle *et al.*, 2009) on Vancouver Island, British Columbia, Canada (Fig. 3.1a inset). The inlet has a maximum depth of 230 m and a shallow sill at 75 m that permanently restricts the deep water circulation and exchange with waters outside the inlet. An annual hypoxia cycle causes alternating phases of hypoxia expansion and oxygen recovery

(Anderson & Devol, 1973; Chu & Tunnicliffe, 2015). Hypoxia expansion results from increased stratification of the water column in the summer coupled with microbial

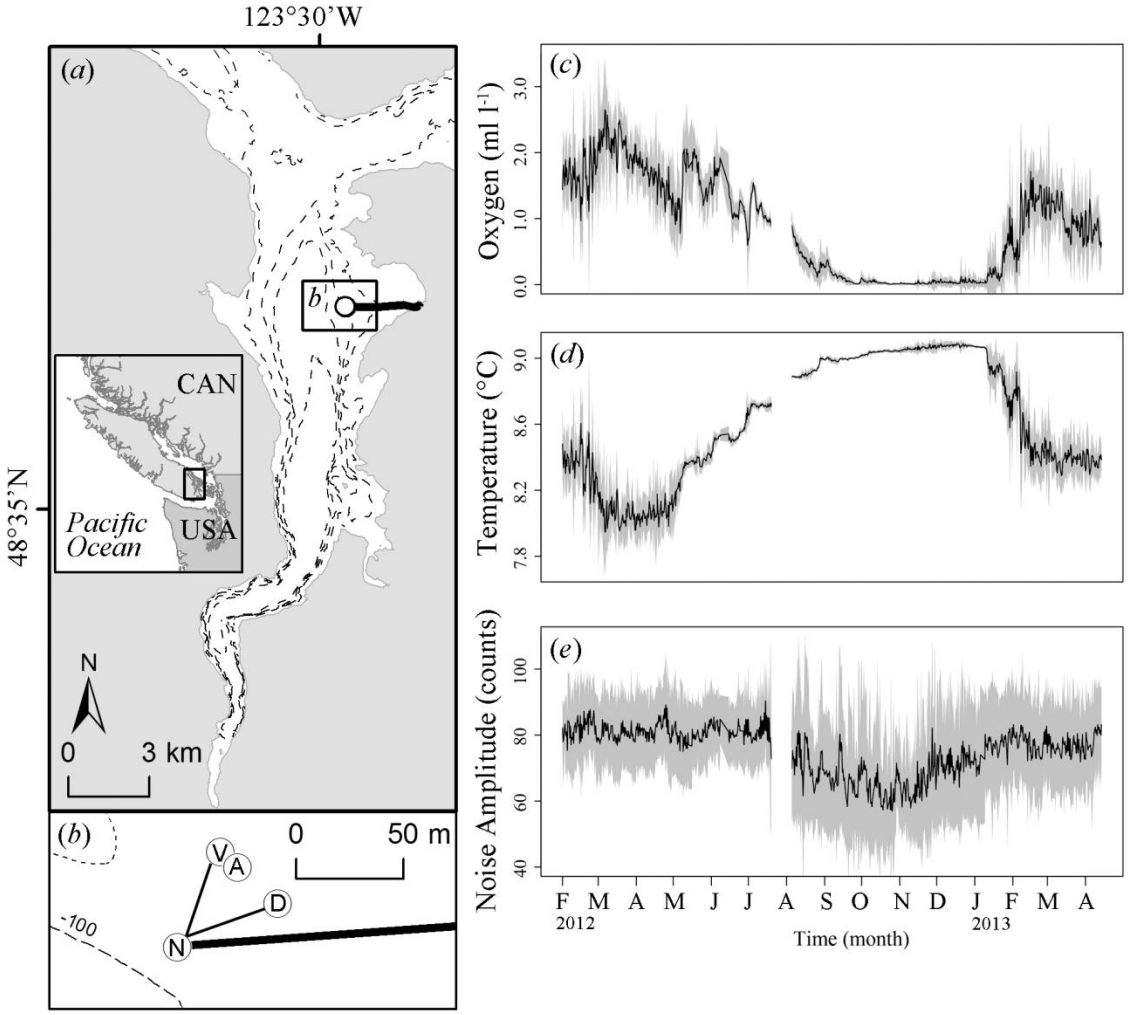

Figure 3.1. VENUS instrumentation in Saanich Inlet. (a) Saanich Inlet is located on Vancouver Island, British Columbia (inset). A surface to sea power cable (black line) connects to VENUS subsea instrumentation (white circle) at 96 m depth. Contours are in 50 m intervals. (b) The central node (site N) is the interface for power and communication to the main VENUS instrument platform (VIP; site V) and the DISCo camera array (site D). The Aquadopp current meter (site A) is tethered to the VIP. (c-f) *In situ* VENUS data highlights the magnitude of environmental variability over the duration of a hypoxia cycle. Environmental levels of (c) oxygen and (d) temperature were measured at 0.3 m above bottom at site D. (e) Suspended particulates and zooplankton were measured at 1 m above bottom using the return signal strength (noise amplitude) from beam 1 of the current meter at site A. Data are plotted as the mean (black line) with 2 S.D. (grey band) summarized into 12-hour intervals from original raw VENUS data which measures water column properties per minute.

consumption of primary production at depth. Oxygen is recovered into the system from deep-water renewal in the fall (Anderson & Devol, 1973) and partial renewal in the spring (Manning *et al.*, 2010). Intensity and duration of deoxygenation may vary between years (Matabos *et al.*, 2012; Chu & Tunnicliffe, 2015; Hamme *et al.*, 2015). The epibenthic community in Saanich Inlet is composed of dozens of fish and invertebrate species that are common to the continental shelf and slope waters of the northeast Pacific Ocean. Species distributions shift with the seasonal hypoxia cycle, with community-level changes primarily driven by abundant key species such as the hypoxia tolerant squat lobster *Munida quadrispina* and the slender sole *Lyopsetta exilis* (Chu & Tunnicliffe, 2015). Vertical diel migrations in zooplankton are also present throughout the year and are dominated by the euphausiid *Euphausia pacifica* (Sato *et al.*, 2013).

Ocean Networks Canada camera systems

Ocean Networks Canada (ONC, www.oceannetworks.ca) cabled observatory camera platforms are novel in that data are gathered in real time with scientist-controlled feedback, streamed and directly accessible through the internet with the potential to collect concomitant, high-frequency data from multiple instruments for an indeterminate period. Previous studies have either used high frequency data over short time intervals (data collected hourly over weeks to months: Aguzzi *et al.*, 2011; Matabos *et al.*, 2011, 2015; Robert *et al.*, 2012) or low frequency data over annual periods (data collected every few days: Matabos *et al.*, 2012; Juniper *et al.*, 2013) with manual capture.

The current study used new automated software developed to capture images at high frequency (hourly interval) over the course of a year. Additionally, an *in situ* camera

and sensor platform called DISCo (Digital Stills Camera System) was developed in-house by the VENUS observatory of ONC. The DISCo camera system consisted of a digital still camera with flash (modified 8MP CCD Olympus C8080 with an Ikelite 200W flash) and a pair of horizontal scaling lasers (7 cm) mounted to a Sidus pan and tilt unit (180° tilt range, 360° pan range). A Sea-bird SBE 16plus model 4996 CTD and an Aanderraa Optode model 4175 oxygen sensor were also mounted directly onto DISCo and measured water column properties 0.3 m above the seafloor at the location of the camera (Fig. 3.1b). Additional VENUS instrumentation used in this study includes near-bottom acoustic backscatter and water current sampled at 1 MHz from a Nortek Aquadopp profiling current meter which was mounted on a tripod-frame 8 m from the VIP and within 25 m of DISCo (Fig. 3.1b). The low-frequency wave amplitude of a single beam from the current meter was used as a proxy for near-bottom, suspended particles and zooplankton (e.g. Yahel *et al.*, 2008). This narrow beam was oriented parallel to the seafloor at 1 m above the bottom and resolved suspended particles >1 mm in size (Yahel *et al.*, 2005). Power to DISCo was supplied through a cable tethered to VENUS which also allowed remote operation of the camera and real-time acquisition and transfer of images and water column data to the internet

For this study, DISCo was deployed at 96 m at the bottom of Saanich Inlet, ~30 m from the main VENUS instrument platform (VIP), and at a location where the primary substratum is bedrock covered by a 10-20 cm deep layer of fine-silt with cobble (Anderson & Bell, 2014). This location is slightly upslope and shallower than past ONC still-camera deployments in Saanich Inlet (103 m, Matabos *et al.*, 2011, 2012) where the primary substratum consisted of poorly consolidated sediments dominated by *Beggiatoa*

spp. bacterial mats and minimal presence of infauna (Yahel *et al.*, 2008). DISCo was deployed from February 20, 2012 to May 6, 2013 (442 days), covering an entire hypoxia cycle in Saanich Inlet (Fig 3.1c). On Aug. 16, 2012, DISCo was recovered for maintenance and redeployed by the remotely operated vehicle (ROV) ROPOS. During redeployment, DISCo was carefully repositioned by ROPOS manipulators. After redeployment, the initial point of view prior to maintenance was recreated by remotely adjusting pan and tilt settings through ONC online software. The original DISCo automated protocol was programmed to collect images at a very high frequency: four images (two at 30° pan left, two at 30° pan right) every 30 minutes for 14 months over a full hypoxia cycle. However, 28% of the images from this initially proposed imagery time-series were lost or not captured due to VENUS power outages, DISCo malfunctioning, and a faulty flash unit. Missing imagery created irregular data gaps that ranged from 30 minutes to 15 days throughout the deployment. Thus, my protocols for imagery processing, imagery analysis, and statistical analyses were designed post-hoc to account for this irregular sampling design.

Images were analyzed in random order to reduce user-induced biases and only images captured at 00:00 and 12:00 local time were analyzed. At each 12 h mark, two images (the first captured from each pan position) were analyzed; if the first image of a pan position was missing, the second image was analyzed. If both images from a pan position were missing, both images from the other pan position were analyzed. If only one of the four images from a time point were present, only that image was analyzed. If all four images were missing, the images at the closest time point, within 30 minutes either side, were analyzed following the above steps. Using this protocol, a total of 1,573

images were analyzed which, due to data gaps, represents 85% of the 12-hour interval time-series. Additional steps used to accommodate remaining data-gaps are explained in the methods description for image and statistical analyses.

Imagery processing and data management

In each image, individual epibenthic animals were counted, identified to species when possible or classified to morphotype. Because the field of view was angled towards the seafloor, we used perspective grids that were calibrated with a temporary physical grid laid by the ROV to calculate the area covered in each image (Matabos *et al.*, 2011, 2012). Because sediment resuspension events caused by flatfish (Yahel *et al.*, 2008) and high zooplankton densities would sometimes affect visibility, a visibility rank was assigned to each image to assess overall image clarity where 1 = < 25% of the image was clearly visible, 2 = 25-50%, 3 = 50-75% and 4 = > 75 % (Matabos *et al.*, 2012). Presence/absence data were recorded for bacterial mat, euphausiid swarms, chaetognath swarms, amphipod swarms, copepod swarms, worm tubes, and settling phytoplankton blooms. Species abundances were standardized to densities (individuals m^{-2}) by pooling individual species counts from both images at a time point and dividing by the total area (2.7 m^2) covered in each field of view (1.3 m^2 pan left, 1.4 m^2 pan right). If only one photo was available at a time point (9% of the time series), species densities were calculated from a single image.

Water column data were collected at a one-minute interval (hereafter, raw data) by ONC instrumentation in Saanich Inlet (DISCo, Aquadopp, VIP) and accessed through the ONC website (www.oceannetworks.ca). The raw oxygen data had a slight offset

during the deployment which manifested as a minimum value peak in histograms of the measurements (~0.048 ml l^{-1}). I interpreted this as the occurrence of true anoxia as registered by the adjacent VIP oxygen sensor and confirmed through comparisons with multiple sensors and Winkler titrations (Hamme *et al.*, 2015). I therefore subtracted this value (~0.048 ml l^{-1}) from the entire oxygen time-series (e.g., Hamme *et al.*, 2015) before proceeding with analyses. Because oxygen partial pressure (pO_2) drives physiological acquisition, transport, and delivery of dissolved oxygen in water-breathing organisms (Dejours, 1975), pO_2 was calculated by integrating raw CTD data on salinity, temperature, pressure, and density with oxygen concentration values ('pO2', Hofmann *et al.*, 2011) and then used in all my statistical analyses. For comparability with past research, I present my results in the concentration unit ml l^{-1} which is most commonly used in biological studies. As temporal variability can affect how epibenthic organisms respond to environmental conditions (Bates *et al.*, 2010; Matabos *et al.*, 2012), raw data for oxygen, temperature, particulates were summarized into mean, maximum, minimum, and standard deviation for each 12 hour interval preceding the image timestamps and used as explanatory variables in the statistical analyses. All data processing and statistical analyses were done in R (v.2.15.; R Development Core Team 2013).

Statistical Analyses

Several multivariate methods were used to analyze diversity turnover and deconstruct the multiscale response at the level of community and key species (slender sole, squat lobster).

Temporal changes in diversity

Several community indices were calculated to assess community changes over the hypoxia cycle. Alpha diversity (Shannon-Weiner diversity index, H' $\log_2$) and species evenness (Pielou's Evenness Index, J) were calculated at each time point. Beta diversity was also calculated to assess the differences in diversity among time points (compositional heterogeneity). Although multiple definitions and indices exist to quantify beta diversity (Legendre, 2014), directional beta diversity was calculated following the variance partitioning framework of Legendre and De Cáceres (2013). In brief, total beta diversity (BD_{TOT}) among all time points is equal to the total sums of squares in the species composition matrix. BD_{TOT} can then be partitioned into the relative contributions from each time point (LCBD, local contribution to beta diversity) or by individual species (SCBD, species contribution to beta diversity) (Legendre & De Cáceres, 2013). The advantages of this method are that LCBD values can be mapped to the same dimensions of standard site by species data tables. Large LCBD values indicate time points where the composition of species is unique relative to the entire time-series because all sampling points are compared to a mean value. Beta diversity indices were calculated using the function 'beta.div' in R (Legendre & De Cáceres, 2013).

Redundancy analysis (RDA) was used to analyze the species relationships over the course of the time-series. Species count data were log(y + 1) transformed prior to RDA. Explanatory variables consisted of the sequential time stamp of each variable and a second-degree polynomial function applied to the time stamp (Borcard *et al.*, 2011); both were significant in explaining community variation within my time-series. An ordination plot of the first two RDA canonical axes was used to determine whether species

replacement or species recovery was occurring over the hypoxia cycle (Legendre & Salvat, 2015).

Piece-wise regression was used to calculate the rates of turnover in the species assemblage relative to the hypoxia cycle. Models were independently calculated for mean $[O_2]_{env}$, total abundance, abundance of mobile species, and abundance of sessile species. Model selection was determined using the Akaike Information Criterion (AIC) after sequential forward addition of break points to the model. The slope of each line in the final model was used to calculate relative rates of change in $[O_2]_{env}$, mobile species assemblage abundance, sessile species assemblage abundance, and total abundance during the hypoxia cycle. Piece-wise regression was done using the R package *'segmented'* (Muggeo, 2008).

Multiscale drivers of community structure

Distance-based Moran's eigenvector maps (dbMEMs) were used to analyze the multivariate (community-level) and univariate (key species-level) response. This family of analyses was originally developed under a spatial context to model autocorrelation and to determine the multiscale drivers of community variation (Borcard & Legendre, 2002; Legendre & Legendre, 2012; Legendre & Gauthier, 2014). Recently, dbMEM analyses were modified and applied to ecological time-series generated from ONC observatories (Matabos *et al.*, 2012, 2015; Cuvelier *et al.*, 2014). In brief, a dbMEM analysis first creates a truncated matrix of Euclidean distances from the observation points in a time series. In this respect, time-series data can be treated the same as sampling locations along a spatial transect in one dimension (Legendre & Legendre, 2012). A principal

coordinate analysis (PCoA) is applied to the truncated distance matrix; the resulting principle coordinates are orthogonal temporal eigenfunctions and describe all the temporal scales resolved in the sampling design. The eigenfunctions are then used as predictor variables in linear modeling to determine the temporal scales at which the species assemblage are structured (Legendre & Gauthier, 2014).

For all dbMEM analyses, data were first Hellinger transformed (the square root of observed values divided by sums at each timepoint) to prevent giving extra weight to the species that were rarely observed (Legendre & Gallagher, 2001). Before proceeding with analyses, linear trends in the data were assessed and detrended if significant because these would inflate the strength of any relationship resolved in subsequent community time-series analyses. To accommodate the maximum 15-day gap in my time-series, a staggered dbMEM matrix was created with separate blocks of MEM eigenvectors on either side of the 15-day interval (Declerck *et al.*, 2011; Legendre & Legendre, 2012). Excluding the 15-day gap, supplementary time points (n=19) were added to the time-series to reduce all other, smaller data-gaps to a maximum interval of 24 hours prior to generating the dbMEM (Borcard *et al.*, 2004). These steps were done so that the dbMEM analyses could resolve fine-scale temporal structures which would otherwise have been constrained to the size of our maximum data gap (15 days). Supplementary time points were removed prior to analytical steps involving species abundance data.

Although it is standard practice to focus on only dbMEMs that model positive correlation (Legendre & Legendre, 2012), dbMEM eigenfunctions with negative Moran's I, or negative temporal correlation, were also separately modeled in the present analyses. This was done because preliminary assessment of the data suggested negative correlation,

where values of close observations were less similar than those far apart (Legendre & Gauthier, 2014), occurred in the abundance of key species. From the full set of 816 dbMEMs, a forward selection protocol was used to retain only the subset of positive and negative correlation dbMEMs useful for modeling temporal variance in the species data (Legendre & Gauthier, 2014). The forward selection protocol first generates a global $_{adj}R^2$ value and uses a permutation procedure (n=999 iterations) to retain variables based on maximum explained variance and excluded those that did not explain additional variance or brought the model over the global $_{adj}R^2$ (Blanchet *et al.*, 2008). For the community-level analyses, forward-selection retained 109 dbMEM eigenfunctions (84 with positive Moran's I, 25 with negative Moran's I) which were used in the global model. Similarly, 166 (83 positive, 83 negative) and 212 (97 positive, 115 negative) dbMEM eigenfunctions were retained in the species-level analyses using only slender sole and squat lobster response data respectively. Because several timescales can be represented within a dbMEM eigenfunction, separate dbMEM scalograms were generated for each analysis in order to visually group eigenfunctions with positive Moran's I values into submodels (Borcard *et al.*, 2004). In general, these submodels represent temporal structure at very-broad scales (VBS) that span the whole hypoxia cycle, broad scales (BS) that span months to a year, medium scales (MS) that span weeks to months, and fine scales (FS) that span days to weeks. Retained dbMEM eigenfunctions with negative Moran's I values were not subdivided into submodels because of the relatively low $_{adj}R^2$ value resolved for the global model.

To determine the environmental variables driving temporal structure at the timescale represented by each submodel, species composition data were regressed against

a matrix of environmental explanatory variables (n=25). These variables included the dummy-coded visibility ranks (6), biological drivers as presence/absence data (7), mean values and measurements of variability (sd, max, min) for oxygen (4), temperature (4), suspended particulates (4). Model simplification was done by AIC stepwise regression which maximized explanatory power ($_{adj}R^2$) and parsimony (retaining only significant drivers of structural variance) while reducing collinearity among significant explanatory variables in the final retained set (Legendre & Gauthier, 2014). For the community-level analyses, dbMEM analyses were run twice. First, measurements of variability (sd, max, min) were excluded for oxygen, temperature, and noise amplitude. Second, the complete set of 25 explanatory variables was used. By including measurements of variability, the explanatory power ($_{adj}R^2$) of the global positive model and sub models improved by 11% and 3-7% respectively. Therefore, variability measurements were included in all explanatory matrices and only the results of those analyses are presented. Variance partitioning was used to illustrate the relative contribution of positive correlation, negative correlation, and environmental drivers matrices in explaining community variation in the time-series (Borcard *et al.*, 2011). Multivariate analyses, variance partitioning and Venn diagrams were done using the *'vegan'* (Oksanen *et al.*, 2015) and *'packfor'* R packages (Dray, 2013). dbMEM temporal eigenfunctions (formerly known as PCNM) were generated using the *'PCNM'* R package (Legendre *et al.*, 2013).

Oxygen trends from 10 years of VENUS data

Since 2006, *in situ* $[O_2]_{env}$ has been measured at the VENUS VIP at 96 m depth; data are measured every minute. Data from the 10-year period of March 2006 to January

2016 was analyzed for long-term trends of increasing periods of hypoxia as an update to the analysis from Chu and Tunnicliffe (2015). Because of the sinusoidal pattern of the hypoxia cycle, the start of the time series was truncated at the 2006 oxygen maximum (March 16, 2006). Intermittent data gaps were linearly interpolated prior to analyzing the long-term trend using a one-year running mean (Chu & Tunnicliffe, 2015). The cumulative, annual duration (from March to March) at which $[O_2]_{env}$ measured at VENUS was below the severe hypoxia threshold (0.5 ml l^{-1}, Chan *et al.*, 2008) and the 0.88 ml l^{-1} critical oxygen threshold presented for the eastern Pacific Ocean (Chu & Gale, submitted) was calculated. The latter threshold was determined with a global meta-analysis on crustaceans and falls within the range designated as the oxygen limiting zone for megafauna (Gilly *et al.*, 2013). Whereas the general hypoxia threshold (1.4 ml l^{-1}, Rabalais *et al.*, 2010) is too conservative to predict benthic fish and invertebrate abundance in this system (Chu & Tunnicliffe, 2015). Linear regressions were used to determine if the annual duration below each hypoxia threshold has increased over time.

Results

Community response in a highly variable environment

The *in situ* magnitude of environmental variability was resolved using the high-frequency VENUS data. Over the study period, the range of daily and hourly fluctuations in environmental oxygen concentration (hereafter $[O_2]_{env}$) reached ~2.7 ml l^{-1} (~9 kPa) and ~2.1 ml l^{-1} (7~ kPa) respectively (Fig. 3.1c). The range of maximum daily and hourly temperature fluctuations reached ~0.9°C and 0.7°C respectively (Fig. 3.1d). High variability coincided with high mean values in the water column properties; variability

and average values both diminished during the onset of deoxygenation in June 2012 before reaching minimum values during anoxia in October 2012. Brief pulses of higher variability reappeared in December 2012 although the mean $[O_2]_{env}$ did not markedly increase until January 2013. Near-bottom water temperature gradually increased from ~8.0°C to ~9.0°C in parallel with deoxygenation before decreasing again during reoxygenation. Noise amplitude in the Aquadopp beam markedly decreased during deoxygenation (Fig. 3.1e) indicating a decrease of near-bottom, suspended particles and zooplankton during severe hypoxia ($[O_2]_{env} < 0.5$ ml l^{-1}). The duration of severe hypoxia ($[O_2]_{env} < 0.5$ ml l^{-1}) lasted for 174 days which included 94 days when the average oxygen was near anoxia ($[O_2]_{env} < 0.05$ ml l^{-1}).

A total of 44,190 sightings of 41 species from eight metazoan phyla including presence/absence records of bacterial mats, zooplankton species, and worm tubes formed by emergent macroinfauna, were recorded. The sponges *Suberites simplex* and *Syringella amphispicula* contributed to over 50% of the total species abundance data. Despite the extensive period of anoxia, metazoan life was never entirely excluded from the epibenthic community (Video B.1). Composition of the species assemblage was characterized by a mixed assemblage of mobile and sessile species during the period of high $[O_2]_{env}$ at the start of the time series (Fig 3.2a). A large squat lobster migration event occurred in May 2012 when the density of squat lobster reached 123 ind. m^{-2} (Fig. 3.2b); this occurred before the onset of severe hypoxia in relatively high $[O_2]_{env}$ (mean±sd, 1.9±0.3 ml l^{-1}). When deoxygenation excluded most of the mobile species, slender sole and squat lobster remained although their overall density decreased in anoxia ($[O_2]_{env} \sim 0$ ml l^{-1}). Most other mobile megafauna were excluded in near-anoxia (0.05±0.01 ml l^{-1}).

During deoxygenation, community composition also shifted into a phase characterized by a mixed assemblage of sessile species and emergent macroinfauna when callianasid shrimp *Neotrypaea californiensis* and tubiculous polychaetes emerged from the sediment (Fig. 3.2c, Video B.1). Sessile species such as two giant anemones *Metridum farcimen*, finger sponge *Syringella amphispicula*, ball sponge *Suberites simplex*, and white ascidian *Ascidia* sp. survived throughout the anoxic period before mass mortality occurred after $[O_2]_{env}$ had already recovered to higher levels ($[O_2]_{env}$ = 0.6±0.3 ml l^{-1}). Habitat reoxygenation coincided with the disappearance of emergent macroinfauna and an increase in slender sole abundance (Fig. 3.2d).

Temporal turnover in diversity

Marked shifts in species diversity and composition corresponded to the shifting $[O_2]_{env}$ during the hypoxia cycle (Fig 3.3a). Periods of higher $[O_2]_{env}$ were associated with higher oxygen variability (Fig. 3.3a) which decreased with the onset of severe hypoxia and anoxia (Fig. 3.3a). Throughout periods of high $[O_2]_{env}$, alpha diversity (H') remained constant (Fig. 3.3b) but increased during the onset of severe hypoxia in September 2012 as a result of the emergence of macroinfauna. Maximum alpha diversity occurred in conjunction with the $[O_2]_{env}$ minimum in November and December 2012. Emergent infauna appear as epifauna because identity is equal among species present in a system and traits such as mode of life (e.g., infaunal or epifaunal) are not directly integrated into calculations of alpha diversity. In this regard, beta diversity is more useful in identifying the periods where marked changes in the community composition occurred. The

magnitude of change in species evenness (J) was minimal relative to marked shifts in the diversity indices throughout the seasonally shifting $[O_2]_{env}$ (Fig. 3.3c).

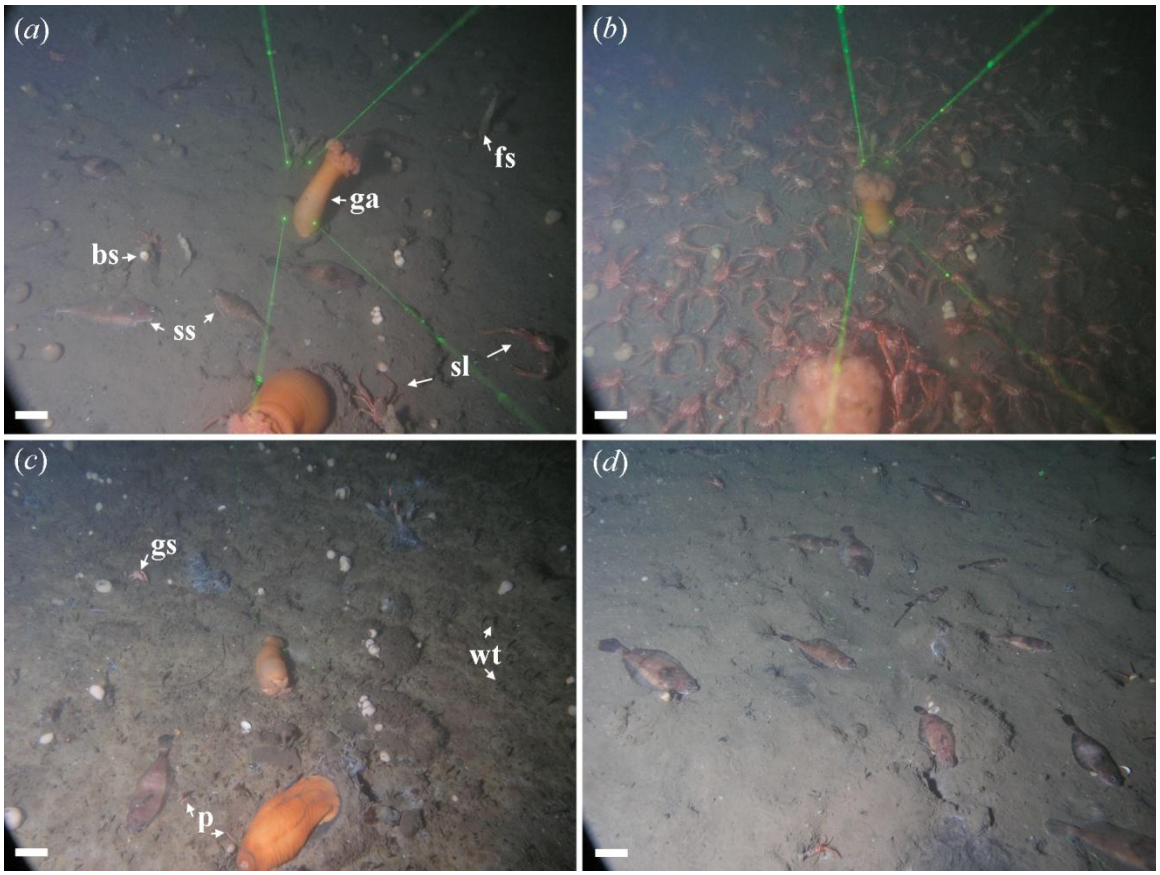

Figure 3.2. Epibenthic community phases in seasonal hypoxia. (a-d) Same field of view from DISCo. (a) At the beginning of the time-series (February 2012), environmental oxygen concentration ($[O_2]_{env}$) was 1.9±0.2 ml l^{-1} (mean±sd). The abundance of mobile species was dominated by slender sole (ss), squat lobster (sl). Sessile species included giant anemones (ga), ball sponges (bs), finger sponges (fs), and ascidians. (b) At the onset of deoxygenation in June 2012, a large squat lobster migration event was observed. Maximum density of adult squat lobster reached 123 ind. m^{-2} in $[O_2]_{env}$ = 1.9±0.3 ml l^{-1}. (c) By November 2012 alpha diversity increased in near-anoxia ($[O_2]_{env}$ = 0.05±0.01 ml l^{-1}) with the emergence of macroinfauna such as ghost shrimp (gs), mobile epifaunal polychaetes (p), and ones that built worm tubes (wt). Slender sole and sessile species were present in reduced numbers. (d) In February 2013 and after reoxygenation ($[O_2]_{env}$ = 0.6±0.3 ml l^{-1}), macroinfauna disappeared as slender sole abundance increased. However, the abundance of sessile species decreased after extended anoxia including mortality of the two giant anemones. Scale bars = 10 cm.

Low values of local contribution to beta diversity (LCBD) indicate similarity in the species composition at the beginning and end of the time-series. The increase in LCBD variability at the end of the time-series is a result of the deoxygenation-induced mortality of the sessile species assemblage, which contributed to the majority of the community abundance at the start of the time-series, and thus an increase in the proportion of mobile species during reoxygenation. Two different periods had an increase in beta diversity (LCBD, Fig. 3.3d) which indicate periods where the species assemblage was unique relative to the 'average' community composition, (represented by low values of LCBD). The first period occurred in May 2012 as a result of the squat lobster mass-migration event which corresponded to a decrease in alpha-diversity and species evenness (Fig. 3.3b,c). The second period occurred from October 2012 to February 2013 when deoxygenation induced the turnover in the composition of the species assemblage. This period was primarily driven by a phase shift in which the mobile species assemblage was replaced by emergent macroinfauna and the death of most sessile fauna by January 2013. The increase in alpha diversity over this period (Fig. 3.3b) also corresponded to an increase in beta diversity (LCBD) which reached a maximum in late November 2012, before returning to the mean, but more variable, level after the onset of reoxygenation (Fig. 3.3d). The two periods of high beta diversity can also be differentiated by their relative rates of compositional turnover: the deoxygenation-induced turnover in the community occurred gradually over four months compared to the rapid occurrence of the squat lobster migration event (< 1 month).

Values of species contribution to beta diversity (SCBD) for 11 species were well above the mean of the community assemblage: the spirontocarid shrimp *Spirontocaris*

sica, two demosponge species (*Syringella amphispicula*, *Suberites simplex*), four emergent macroinfauna species, white ascidian, slender sole *Lyopsetta exilis*, and both adult and post-recruit squat lobster *Munida quadrispina*. SCBD values for slender sole

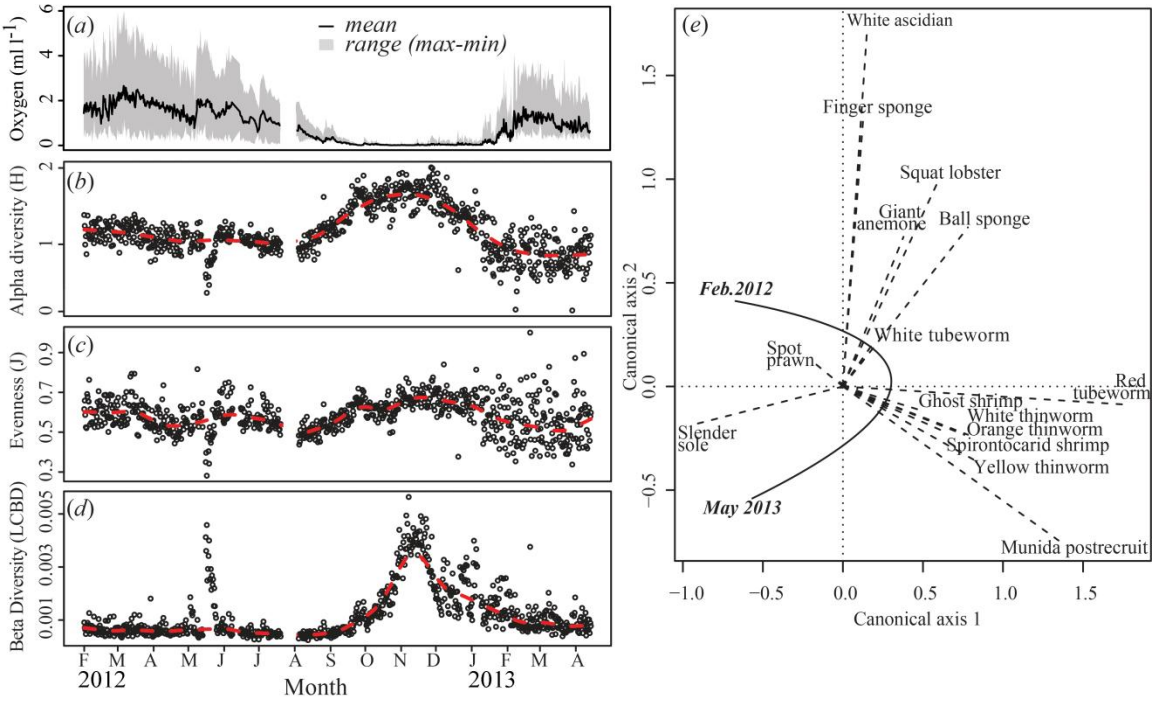

Figure 3.3. Turnover of species diversity in seasonal hypoxia. (a) Environmental oxygen data ($[O_2]_{env}$) from February 2012 to March 2013 are shown in 12 hour intervals summarized from per minute data. The annual hypoxia cycle is characterized by relatively higher average $[O_2]_{env}$ and variability before and after the onset of severe hypoxia ($[O_2]_{env}$ mean < 0.5 ml l^{-1}), anoxia ($[O_2]_{env}$ mean = 0 ml l^{-1}), and low variability as a result of deoxygenation. (b-d) Diversity indices plotted over time. Circles are sampling time-points. Red dashed lines are smoothing curves that illustrate general trends. (b) Alpha diversity (H'log_2) remained constant during periods of high $[O_2]_{env}$ and increased during anoxia because of emergent macroinfauna. (c) Magnitude of change in species evenness was small relative to the marked shifts in the diversity indices. (d) Beta diversity (LCBD) showed species turnover during anoxia; most mobile epifaunal species were replaced by emergent macroinfauna. (e) Ordination plot showing the species (dashed lines) relationships to time (curved line with start and end dates). Explanatory variables (not shown) were a second-degree polynomial function of the time vector. Species clustered near origin (0,0) were removed to improve clarity. Slender sole are strongly correlated to the beginning and end of the time-series which highlights their importance in driving community patterns in the hypoxia cycle. Sharp peaks in alpha diversity, evenness, beta diversity in May 2012 were a result of a mass migration of squat lobster appearing underneath the camera (Fig. 2b)

and both life stages of squat lobster were the highest among species and were an order of magnitude greater than the mean SCBD index value, highlighting their importance in driving temporal beta-diversity patterns in the hypoxia community. The contribution of slender sole to temporal diversity patterns can also be seen in the RDA ordination plot where the community composition before and after deoxygenation is primarily driven by the abundance of slender sole (Fig. 3.3e).

Relative rates of community decline and recovery in hypoxia

Piecewise regression revealed transition intervals among the species assemblage and allowed calculation of the relative rates of change in abundance relative to the hypoxia cycle. $[O_2]_{env}$ declined from a maximum in March 2012 until reaching anoxia in Oct 2012 before the onset of reoxygenation (Fig. 3.4a). The interval over which species abundance declined as a result of deoxygenation was different between sessile and mobile species. Despite deoxygenation occurring over seven months, a decline in the abundance of the mobile species assemblage occurred only for one-month at the end of the deoxygenation phase, centered on the $[O_2]_{env}$ minima, and began to immediately recover with the onset of reoxygenation (Fig. 3.4b). After the brief interval of decline (Nov. 2012), mobile species abundance increased because slender sole returned to the system with the onset of short-term variability (Fig. 3.4b-vi).

In contrast, the abundance of the sessile species began to decrease two-months before the $[O_2]_{env}$ minimum occurred and continued to decrease for four months after the onset of reoxygenation with a small increase at the end of the series (Fig. 3.4c). As a consequence, total animal abundance continued to decrease during reoxygenation and did

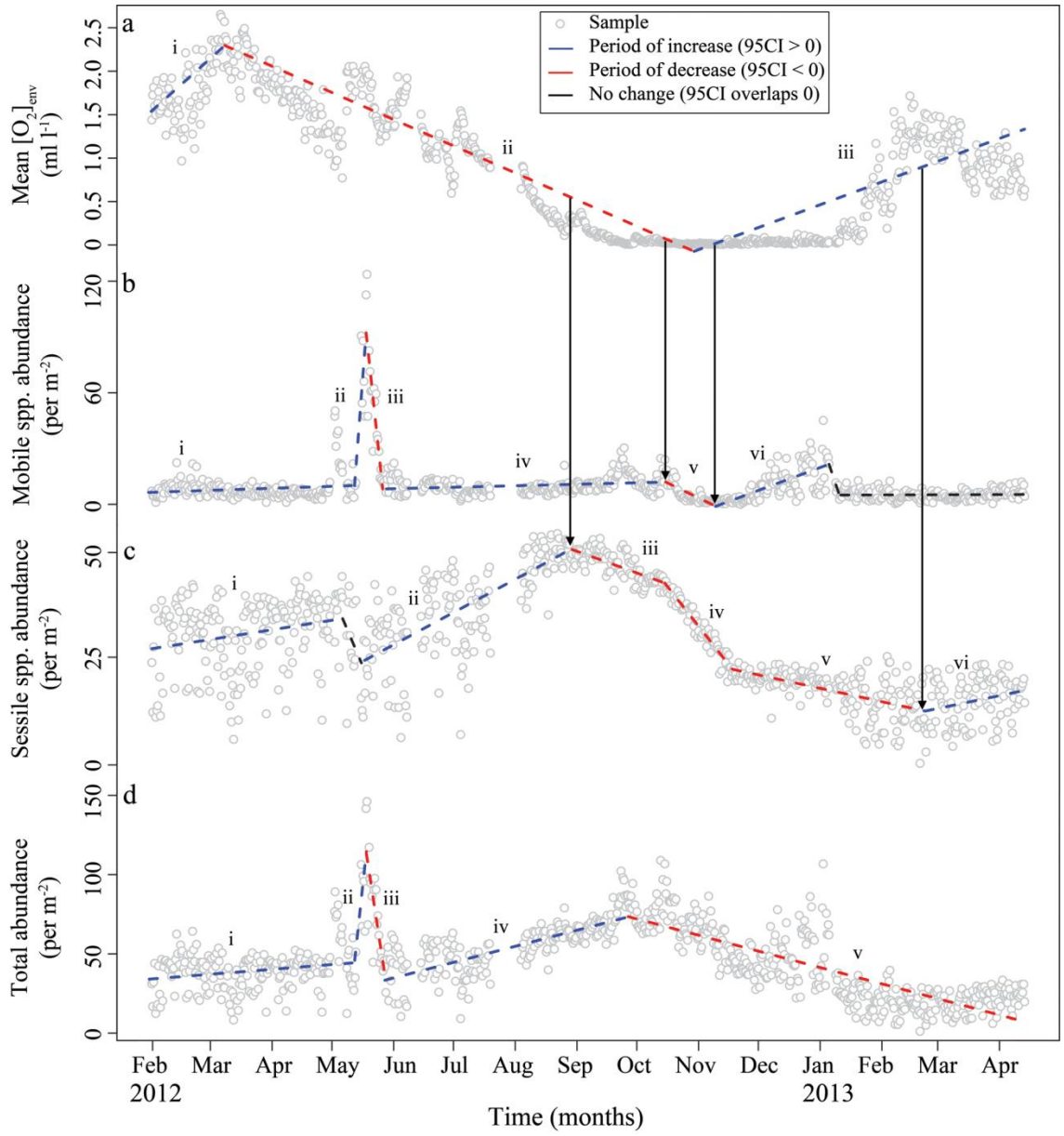

Figure 3.4. Rates of community response and recovery in seasonal hypoxia. Piecewise regression was used to determine temporal transition points in (a) mean $[O_2]_{env}$, (b) mobile species abundance, (c) sessile species abundance, and (d) total abundance. Segments indicate intervals when a variable significantly increased over time (95 CI > 0), decreased over time (95 CI < 0), or had no change (95 CI overlaps with 0). Intervals when the rate of change was significant (roman numerals) are summarized in Table 1. The interval over which mobile fauna decline (b, v) is notably shorter compared to the interval of decline for sessile fauna (intervals c, iii-v). A decrease in sessile species continued even during reoxygenation of the habitat. As a result, the total abundance of epibenthic animals continued to decrease until the end of the time-series (April 2013). Arrows highlight the relative interval when deoxygenation correlated with a decrease in abundance of mobile and sessile species.

not recover before the end of the time-series (Fig. 3.4d). In general, the rates at which species abundance decreased during deoxygenation were greater relative to periods where abundance increased during reoxygenation (Table 3.1). However, this may have been a result of the time-series not spanning more than one complete hypoxia cycle and thus the recovery rates at the start and end of the time-series were calculated from truncated periods of reoxygenation.

Table 3.1. Response rates in seasonal hypoxia. Negative rates indicate abundance declined over time. Roman numerals refer to line segments in Figure 3.4.

	Mean rate	95% CI lower	95% CI upper
Environmental oxygen		ml l^{-1} day^{-1}	
i	0.020	0.014	0.026
ii	- 0.010	- 0.010	- 0.010
iii	0.008	0.008	0.009
Mobile species abundance		Per m^{-2} day^{-1}	
i	0.039	0.011	0.067
ii	14.08	11.98	16.13
iii	- 10.11	- 11.34	- 8.88
iv	0.026	0.009	0.044
v	- 0.517	- 0.733	- 0.300
vi	0.385	0.321	0.450
Sessile species abundance		Per m^{-2} day^{-1}	
i	0.075	0.042	0.105
ii	0.253	0.224	0.281
iii	- 0.169	- 0.262	- 0.077
iv	- 0.601	- 0.749	- 0.452
v	- 0.102	- 0.132	- 0.071
vi	0.097	0.015	0.180
Total species abundance		Per m^{-2} day^{-1}	
i	0.100	0.038	0.161
ii	11.70	7.03	16.36
iii	- 8.26	- 10.36	- 6.15
iv	0.327	0.278	0.376
v	- 0.333	- 0.355	- 0.311

Multiscale temporal drivers of community structure

Species composition and the abundances of key-species were significantly structured at the multiple temporal scales of environmental variability resolved by sub-daily sampling over a 14-month hypoxia cycle. Within the 14-month observation window (broadest scale) of the time series, high oxygen phase occurs at the start and end of the time-series which is the largest environmental cycle resolved in the study. The smallest scale (shortest interval) resolved is limited to 24-hours because of the technological issues associated with the camera platform. Inclusion of measurements of short-term environmental variability (e.g., max, min, sd) improved overall explanatory power of my analyses (up to 3-11%).

In general, most of the variation in the biological response at both community and key-species levels was structured at the very broad and broad scales of temporal variability (5-30%, Table 3.2-3.4); this highlights the strong seasonal signal reflected in species composition. The global positive correlation model at the community level (n=42 species) explained half of the variation in species composition (84 dbMEMs, $_{adj}R^2 = 0.5$, $p<0.001$). 14 of the explanatory variables were significant in explaining community variation, including presence/absence of bacterial mats and several zooplankton groups, the average temperature and suspended particulates and zooplankton and several measurements of variability for oxygen, temperature, suspended particulates and zooplankton (Table 3.2). Explanatory variables that were never retained in either the global or any sub-model at the community-level were maximum and mean $[O_2]_{env}$. The

global dbMEM analysis modeling negative correlation at the community-level was also significant (25 dbMEMs, $p<0.05$) and indicated a small degree of oscillation within the biological community is correlated to suspended particulates and zooplankton, although the explanatory power of the global negative correlation model was low ($_{adj}R^2$ ~0.01). Small scale variance (days, weeks, months) explained additional variation in species composition (9-17%, Table 3.2). Although the significant explanatory variables were slightly different among the four sub-models compared to the global model, the final set of retained explanatory variables always included the presence/absence of certain zooplankton groups and measurements of variability (max, min, and/or sd) for the abiotic water column properties (oxygen, temperature, suspended particulates and zooplankton) in all dbMEM analyses.

dbMEM analyses on the abundance of slender sole and squat lobster revealed different responses in the abundances of key species. Similar to the community-level analyses, slender sole and squat lobster abundance was structured across the full spectrum of scales resolved in the time-series (Tables 3.3, 3.4). For slender sole, significant variance was explained by both the global positive correlation (n=83 dbMEMs, $_{adj}R^2$= 0.47, $p<0.01$) and negative correlation (n=83 dbMEMS, $_{adj}R^2$ = 0.03, $p<0.01$) models (Table 3.3). Explanatory variables of slender sole abundance that were retained as significant predictors at the global and sub-model level always included presence-absence of certain zooplankton groups and some measurement of variability for all three abiotic water column properties. In contrast, only the global positive correlation model was significant in explaining variation in squat lobster abundance (Table 3.4, n=97 dbMEMS, $_{adj}R^2$= 0.17, $p<0.0001$). Explanatory power of the global model for squat

lobster was also lower than that of the community and slender sole global models with no significant variance explained at fine-scales. In general, the significant partition of variance explained at small-scales, the significance of short-term variability as predictors of species composition, and the inclusion of multiple environmental factors such as temperature and surrogates of food all highlight how high-frequency observations can improve overall explanatory power in ecological analyses.

Table 3.2. Significant multiscale drivers of community structure. Response data included the entire species abundance matrix. Retained biological drivers were presence/absence of bacteria mats (BAC), amphipods (AMP), euphausiids (EUP), copepods (COP), worm tubes (WT), chaetognaths (CHA), and settling phytoplankton blooms (DIA). Explanatory variables never retained in any model were presence/absence of chaetognaths (CHA), oxygen mean, oxygen maxima, and temperature maxima.

				P-values of significant explanatory variables																
Model summary				Biological drivers (presence/absence)							Oxygen (kPa)		Temperature (ºC)			Aquadopp (counts)				
Global	MEMs	R^2	P-value	BAC	AMP	EUP	COP	WT	CHA	DIA	sd	min	mean	sd	min	mean	sd	min	max	
Negative	25	0.01	<0.01		<0.05		<0.05													
Positive	84	0.57	<0.001	<0.001	<0.001	<0.001	<0.01	<0.001		<0.01	<0.001	<0.01	<0.01	<0.001	<0.001	<0.001	<0.001	<0.001	<0.001	<0.01
Submodels																				
V.Broad	16	0.16	<0.001		<0.05			<0.001			<0.001			<0.05		<0.001	<0.001			
Broad	26	0.25	<0.001	<0.001		<0.05		<0.05	<0.05	<0.05	<0.001			<0.001			<0.05			
Medium	19	0.17	<0.001		<0.001		<0.01			<0.05		<0.05	<0.05	<0.05	<0.01	<0.05		<0.001		
Fine	23	0.09	<0.001	<0.001			<0.01	<0.05				<0.01			<0.05		<0.01			<0.05

Table 3.3. Significant multiscale drivers of slender sole abundance. Response data included only slender sole abundance. Retained biological drivers were presence/absence of amphipods (AMP), euphausiids (EUP), worm tubes (WT), chaetognaths (CHA), and settling phytoplankton blooms (DIA). Explanatory variables never retained in a model were bacterial mats (BAC), copepods (COP), and oxygen maxima.

				P-values of significant explanatory variables														
Model summary				Biological drivers (presence/absence)					Oxygen (kPa)			Temperature (ºC)				Aquadopp (counts)		
Global	MEMS	R^2	P-value	AMP	EUP	WT	CHA	DIA	mean	sd	min	mean	sd	min	max	mean	sd	min	max
Negative	83	0.03	<0.01	<0.01	<0.05		<0.001												<0.05
Positive	83	0.47	<0.01	<0.01	<0.05	<0.001	<0.001		<0.001			<0.001		<0.001	<0.001	<0.001	<0.001	<0.001	<0.001
Submodels																			
V. Broad	10	0.24	<0.001	<0.01		<0.001				<0.01			<0.001			<0.001			
Broad	24	0.3	<0.001				<0.001	<0.001			<0.001			<0.001		<0.01			
Medium	19	0.13	<0.001			<0.001					<0.01	<0.05	<0.001			<0.001	<0.001	<0.01	<0.05
Fine	30	0.01	<0.01				<0.05	<0.05								<0.05			

Table 3.4. Significant multiscale drivers of squat lobster abundance. Response data included only squat lobster abundance. Retained biological drivers were presence/absence of bacterial mats (BAC), euphausiids (EUP), settling phytoplankton blooms (DIA). Explanatory variables never retained in a model were amphipods (AMP), worm tubes (WT), copepods (COP), chaetognaths (CHA), mean temperature, and counts maxima of the Aquadopp.

				P-values of significant explanatory variables													
Model summary				Biological drivers (presence/absence)			Oxygen (kPa)				Temperature (ºC)			Aquadopp (counts)		
Global	MEMs	R^2	p-value	BAC	EUP	DIA	mean	sd	min	max	sd	min	max	mean	sd	min
Negative	115		n.s.													
Positive	97	0.17	<0.001			<0.001			<0.001	<0.001		<0.001	<0.001		<0.01	
Submodels																
V. Broad	10	0.11	<0.001	<0.05	<0.01	<0.001		<0.001			<0.001		<0.001			
Broad	21	0.05	<0.001					<0.001			<0.001			<0.001		<0.001
Medium	20	0.05	<0.001			<0.05	<0.001	<0.01			<0.01		<0.001	<0.01	<0.05	
Fine	46		n.s.													

Variance partitioning the responses of key-species

Total species abundance was primarily synchronized with the broad-scale pattern of the seasonal hypoxia cycle (Fig. 3.5a). Although environmental drivers were slightly different among temporal scales, ~40% of the community variation is constrained to the positive and negative autocorrelation modeled by the dbMEM eigenfunctions (Fig. 3.5b) with 30% of the community variation explained by the overlap between environment and positive temporal correlation. Negative correlation at the community-level is likely a result of the behavior of slender sole which dominate the mobile species assemblage. A diurnal pattern in slender sole abundance, in which more were observed at midnight compared to noon during oxygenated phases the hypoxia cycle (Fig. 3.5c), was associated with a large degree of negative correlation (28%, Fig. 3.5d). Although a large degree of periodicity characterizes the biological response for the general community and slender sole, squat lobster abundance remained relatively constant throughout the time-series. Aspects of the reproductive cycle of the squat lobster *Munida quadrispina* are represented in the migration event that occurred in May 2012 (Fig. 3.5e) and the influx of juvenile recruits in late 2012 (Fig. 3.5e). The rapid change in squat lobster abundance as a result of reproductive behavior is associated with a small degree of overlap between the environmental predictors and positive correlation (0.06, Fig. 3.5f). Thus, temporal structure in squat lobster abundance are either driven by the non-periodic components of the environment or generated by intraspecific interactions.

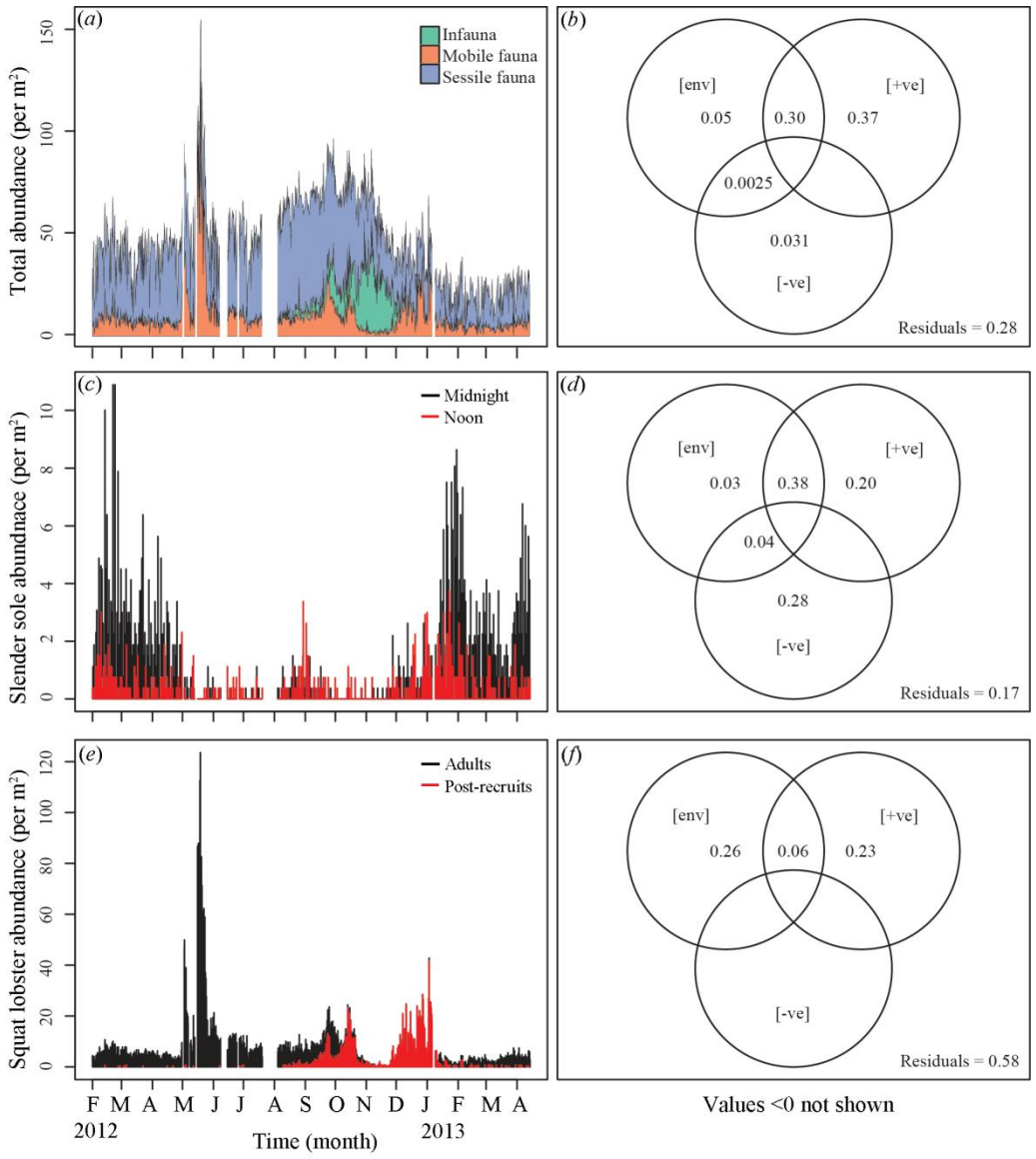

Figure 3.5. Patterns in temporal structure and variation partitioning. Venn diagram boxes represent total variance explained at the community or individual species-level. Overlapping circles represent variance explained by environmental variables ([env]), positive temporal correlation ([+ve], dbMEM eigenfunctions with positive Moran's I), and negative temporal correlation ([-ve], dbMEM eigenfunctions with negative Moran's I). Fractions of variance are computed from adjusted R^2 values. (a) A stacked area plot illustrates a substantial portion of temporal structure at the community level is explained by the (b) relationship between positive temporal correlation and environmental predictors ($_{adj}R^2$=0.30). (c) Overlapping high-density plots of daily slender sole abundance at noon and midnight illustrates a diurnal pattern and is associated with (d) a large proportion of variance explained by negative correlation. (e) Overlapping high-density plot illustrates temporal response in squat lobster is explained by reproductive behavior as density peaks in adults and recruitment occurs primarily in the low oxygen period. (f) A larger proportion of variance is explained by the environment that does not overlap with positive correlation.

10-year trends in the hypoxia cycle

The 10-year (March 2006 to January 2016) oxygen time-series shows the average $[O_2]_{env}$ has declined at the study site since the beginning of the VENUS. $[O_2]_{env}$ has significantly decreased by a rate of 0.063 ml l^{-1} $year^{-1}$ (Fig. 3.6a, $p<0.0001$) ,which is higher than the rate of 0.05 ml l^{-1} $year^{-1}$ previously calculated for the first 8 years of VENUS (Chu & Tunnicliffe, 2015). The negative long-term trend is a result of several years where the average $[O_2]_{env}$ for the year experienced a marked decline (2010, 2013, 2015) from either a weakened oxygen renewal (e.g., 2010, Chu & Tunnicliffe, 2015) or enhanced deoxygenation (Fig. 3.6b). The annual duration of severe hypoxia has significantly increased by 8.8 days $year^{-1}$ (Fig. 3.6c, $F_{1,8} = 6.99$, $p < 0.05$, $_{adj}R^2 = 0.4$). Similarly, the duration below the critical oxygen thresholds for the eastern Pacific Ocean has also significantly increased by 7.7 days $year^{-1}$ (Fig. 3.6c, $F_{1,8} = 6.04$, $p < 0.05$, $_{adj}R^2 = 0.36$).

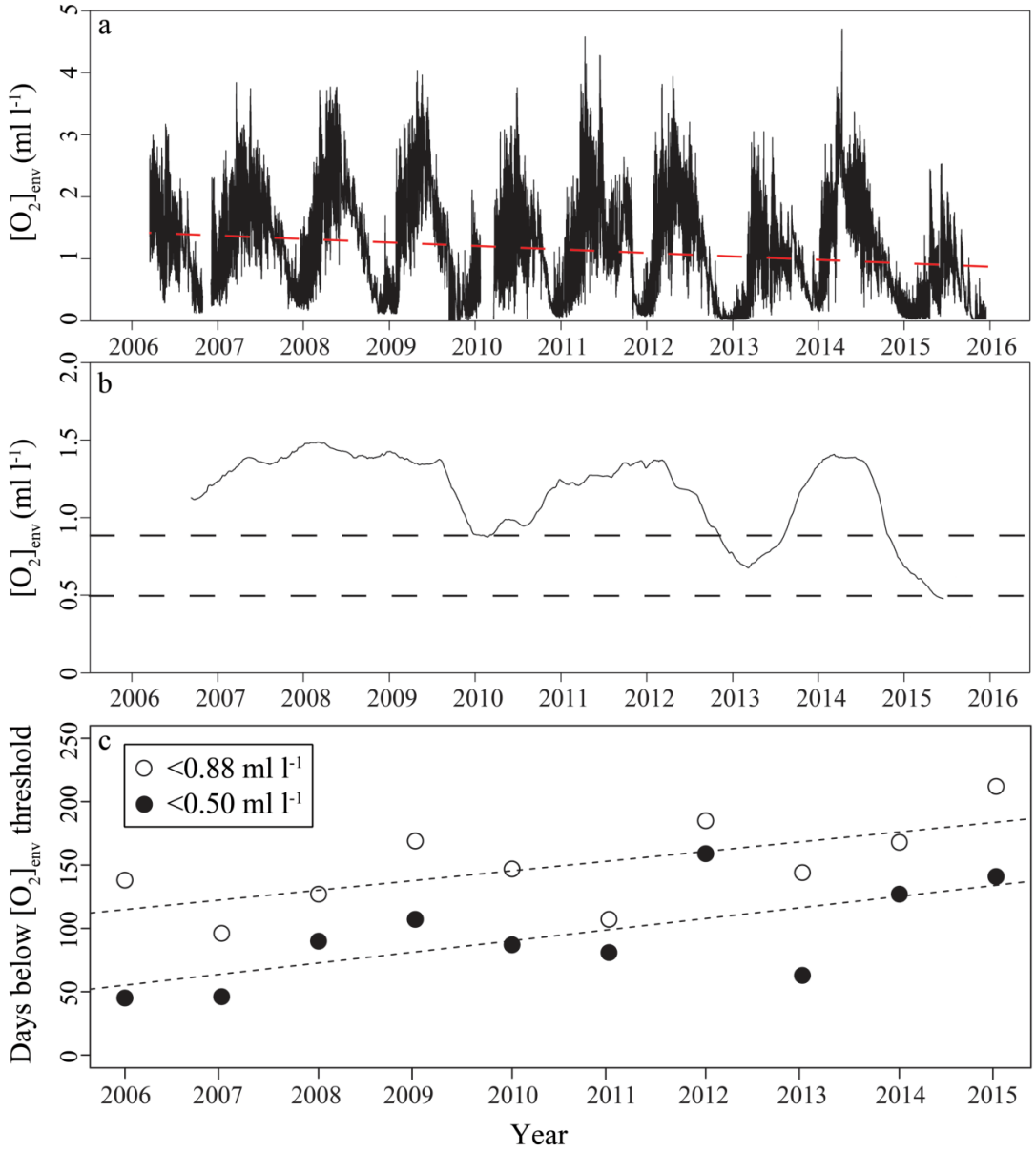

Figure 3.6. 10-year trends in the Saanich Inlet hypoxia cycle at 96 m. $[O_2]_{env}$ from VENUS was measured at minute intervals from March 2006 to January 2016. (a) A linear regression (dashed line) shows a long-term, significant trend of decreasing $[O_2]_{env}$ ($[O_2]_{env}$ = 1.4 – 0.063*year). (b) one-year running mean through the time-series shows the long-term trend is a result of years where there was weakened oxygen renewal or enhanced deoxygenation (2010, 2013, 2015). Dashed lines indicate the 0.5 ml l^{-1} severe hypoxia threshold and 0.88 ml l^{-1} critical oxygen threshold for the eastern Pacific Ocean. (c) The annual duration (cumulative number of days starting from March) at which the study site was below the severe hypoxia and critical oxygen thresholds. Dashed lines illustrate that the significant trend of increasing duration over time for both severe hypoxia (8.8 days $year^{-1}$) and critical oxygen thresholds (7.7 days $year^{-1}$)(both, $p<0.05$). Note the x-axis in a,b is different from c.

Discussion

Although the science of using cabled-observatory camera systems has advanced with every successive deployment, technological constraints continue to affect data quality. The final resolution of our time series (24 hr interval) was a result of the substantial amount of data (~28%) lost to technical issues which introduced large data gaps and irregular sampling that can limit ecological analyses (Matabos *et al.*, 2012, 2015; Cuvelier *et al.*, 2014; this study). Because of the nature of high-frequency data, temporal structure had a substantially autocorrelated component which can inflate type I error rates and cause inaccurate explanatory power when analyzed with classical inferential statistics (Fortin *et al.*, 1989; Legendre & Fortin, 1989). Nevertheless, irregular sampling intervals, data gaps, and autocorrelation are characteristic of most, if not all, observational studies in ecology. Despite technological limitations, a partial solution is the application of multivariate analyses and variance partitioning techniques that can provide insight into the scale-dependent processes structuring ecological communities over time.

Different rates of decline and recovery in hypoxic communities

At the broad scale, the epibenthic community in Saanich Inlet naturally oscillates between two phases that are synchronized to alternating periods of deoxygenation and reoxygenation (also seen in Matabos *et al.*, 2012). The timing and sequence of community turnover is primarily linked to the seasonal period of low oxygen. Deoxygenation deters most mobile species due to their ecophysiological constraints to aerobic metabolism and the inability to maintain constant oxygen uptake at low

environmental oxygen concentrations (Chu & Gale, submitted), resulting in the death of sessile species under extended exposure. Low critical oxygen thresholds allow slender sole and squat lobster to exploit low oxygen habitats (Chu & Gale, submitted), while hypoxia-sensitive species must migrate to shallower, more oxygenated waters (Chu & Tunnicliffe, 2015). The emergence of infauna is likely an escape response to the accumulation of hydrogen sulfide in the sediments which can reach lethal levels during anoxic periods (Sturdivant *et al.*, 2012). Shallowing in the depth of the sediment layer inhabited by bioturbators is typical of systems with variable states of oxygen deficiency (Long *et al.*, 2008; Levin *et al.*, 2009b). In addition to oxygen, species composition is influenced by factors such as temperature and food sources such as settling phytoplankton blooms and zooplankton. Organic matter content of sediments in addition to oxygen limitation has also been shown to explain macrofaunal community variation in oxygen minimum zones (Levin & Gage, 1998; Gooday *et al.*, 2010). As noted by Levin and Gage (1998), no single explanatory variable can readily predict community variation in oxygen deficient systems.

Differences in body form and life history between sessile and motile species influence the relative rates of response to deoxygenation and recovery in reoxygenation within the epibenthic community. Mortality of sessile species during anoxia contributed to a lagged progression in total abundance, in which the recovery rate of the community was slower than the rate of decline during deoxygenation. As a result, full recovery of the community did not occur by the end of my observation period. Basal metazoans such as cnidarians and sponges are the most common, and sometimes the most abundant, sessile species at this site and are generally hypoxia tolerant (Chu & Tunnicliffe, 2015).

Sassaman and Mangum (1972; 1973) noted the extreme hypoxia tolerance in epibenthic anemones and their potential to temporarily exploit anaerobic metabolism. Less is known about the hypoxia tolerance of sponges; however, the *in situ* oxygen range of occurrence of the sponge species at this site are among the lowest measured in the epibenthic community (Chu & Tunnicliffe, 2015). Their mortality during my study indicates that critical exposure times were exceeded and mortality as a response can naturally occur in seasonal deoxygenation events (Levin *et al.*, 2009b). Death as a stress response in sponges is a slow process and can occur months to years after the initial lethal exposure (Dunham *et al.*, 2015). Essington and Paulsen (2010) documented hypoxia-induced mortality in a similar sessile species assemblage in nearby Hood Canal, Washington over a period of three months. The re-establishment of community abundance to pre-deoxygenatoin levels will depend on recruitment and sustained growth of sessile species during the reoxygenation window between low oxygen phases.

Hypoxia-induced mortality of sessile species also indicates that benthic systems experience functional losses of reduced carbon sequestration and nutrient cycling as a result of the absence of filter feeders (Riedel *et al.*, 2012). The emergence of macro-infauna suggests that a further decline in ecosystem function may have resulted from a decrease in bioturbation (Witte *et al.*, 2003; Danovaro *et al.*, 2008); callianassid shrimp *Neotrypaea californiensis* were consistently observed above the sediment throughout the low oxygen phase which would have greatly reduced the amount of subsurface sediment transported by burrowing activity (Gagnon *et al.*, 2013). Although functional losses from detrimental shifts in mean environmental values (e.g., temperature) may be mediated by the positive influence of high temporal variability (Benedetti-Cecchi *et al.*, 2013), this

will not occur in systems influenced by deoxygenation because oxygen variability also decreases with the mean.

Drivers of temporal structure in epibenthic communities

The epibenthic community in Saanich Inlet is structured at multiple temporal scales of environmental variability resolved by sub-daily sampling over a 14-month hypoxia cycle. Most of the variation in the community is explained at broad scales indicating the strong influence of the seasonal signal. The proportion of variation explained by positive autocorrelation among models (20-37%) highlights the importance of accounting for temporal structures in ecological time-series and the strong influence of environmental oscillation on benthic communities (Menge *et al.*, 2011). Inclusion of short-term environmental fluctuations can improve explanatory power of analyses and better predict the timing of biological events. For example, the average $[O_2]_{env}$ did not increase above the critical oxygen threshold for slender sole (~0.36 ml l^{-1}, Chu & Gale, submitted) until the beginning of February 2013. The abundance of slender sole, however, increased at the beginning of January 2013, coinciding with an increase in short-term $[O_2]_{env}$ variability ($[O_2]_{env}$ range ~0.4 ml l^{-1}). The magnitude, duration, and frequency of the intermittent exposure to elevated $[O_2]_{env}$ likely allowed slender sole to recover into the system although the 'average' conditions were still extremely hypoxic (mean $[O_2]_{env}$ <0.1 ml l^{-1}). Wide range in magnitude and the high frequency of environmental oscillations can predict higher rates in ecological processes such as recruitment (i.e., "intermittency", Menge & Menge, 2013). In my study, the variation explained at small scales (1-17%) and the significance of short-term fluctuations as

explanatory variables highlight the improved understanding of community structure that can be gained using high frequency data.

Drivers of temporal structure in the abundance of key-species

As in the community-level analyses, most of the variance in slender sole abundance is explained at broad scales with a high degree of overlap (38%) among environmental predictors and positive correlation. However, 28% of the variance in slender sole abundance is explained by negative correlation, which can be indicative of temporal structure occurring at periods shorter than the 24 hour resolution of the analyses. A type II diurnal response, where fish migrate up to shallow depths during the day and down to deeper depths at night (Neilson & Perry, 1990), occurs in slender sole. This migration pattern is supported by replicate ROV surveys in the deeper depths of their distribution in Saanich Inlet (120-100 m) over a 24 hour period, where more slender sole were observed during evening hours compared to daylight hours (Table B.1). While, light can control diel movements in flatfish species found in shallow waters (<40 m, Kruuk, 1963), this is unlikely to directly contribute to the movement of slender sole. Slender sole are not found in the euphotic zone in Saanich Inlet (<30 m, De Robertis *et al.*, 2001), instead showing high fidelity to the severely hypoxic waters occurring in deeper depths (Chu & Tunnicliffe, 2015) where they occur in environmental oxygen levels that are close to their critical oxygen thresholds (Chu & Tunnicliffe, 2015; Chu & Gale, submitted). Most diel movements of fish in relation to prey distributions are type I responses (migrate up during night and down during day) with type II responses being less common and typically associated with predator avoidance (Neilson & Perry, 1990).

As planktivores, slender sole likely migrate to feed on the diel vertically migrating euphausiid *Euphausia pacifica* (Pearcy & Hancock, 1978) which are present in Saanich Inlet throughout the year (Sato *et al.*, 2013) and are limited by the depth of the hypoxic boundary (Beveridge, 2007). Slender sole likely migrate laterally upslope to mid-inlet depths during daylight hours to feed on descended zooplankton and return to the deep-waters at night as a refuge from piscovorous fish such as Pacific hake. Similar diurnal patterns have been reported in the hypoxia-tolerant bearded goby *Sufflogobius bibarbatus* that dominates demersal biomass in the eastern boundary region of the Benguella current (Utne-Palm *et al.*, 2010; Salvanes *et al.*, 2011). Diurnal behavior in slender sole may have gone undetected in past studies because of multi-day sampling intervals (Matabos *et al.*, 2012) or observations limited to only the low oxygen phase of the hypoxia cycle (Matabos *et al.*, 2015).

The seasonal hypoxia cycle also influences the temporal patterns of squat lobster abundance. In contrast to patterns observed in slender sole, minimal overlap among environmental predictors and positive correlation suggests that the temporal structure in squat lobster abundance reflects intraspecific interactions (Legendre & Gauthier, 2014). In a separate study, I monitored a captive population of squat lobster *Munida quadrispina* that underwent mass molting events during the spring (Fig. B.1), synchronized to the timing of the mass migration events observed in the field (Doya *et al.*, 2015; this study). Captive squat lobsters did not experience the influence of the seasonal hypoxia cycle (individuals were segregated and maintained in a perpetually dark, closed system, with recirculating sea water) thus molting appears to be endogenously controlled. Squat lobsters in general (Family Munididae) will migrate into shallow water at the beginning

of reproduction periods (Bahamonde *et al.*, 1986; Vinuesa, 2007) where copulation is preceded by molting events (Thiel & Lovrich, 2011). As squat lobster *M. quadrispina* occur close to their critical oxygen levels (0.2 ml l^{-1}, Chu and Gale submitted) in the deeper parts of Saanich Inlet (<100 m, Chu & Tunnicliffe, 2015), migration into shallower depths would allow access to the oxygen needed for the high energy requirements of reproduction and molting in crustaceans (Chang, 1995). Timing of juvenile recruitment as inferred by repeated observations (in 2008, 2009, and 2012) of post-recruitment juvenile squat lobster during the near-anoxia periods (Matabos *et al.*, 2012; Dinning & Metaxas, 2013; this study) also suggests that reproduction occurs during the low oxygen period. While environmental factors strongly influence species composition, underlying intraspecific interactions can contribute to community variation in hypoxic systems.

Temporal patterns of beta diversity

Time-series generated from cabled observatories now permits some ecological theory and predictions to be tested in logistically challenging environments. Within the sub-daily to 14-month time scales of my study, environmental variability explains more than half of the variation in community structure. Temporal patterns of community turnover also mirror the spatial turnover patterns established in gradients of low oxygen (Chu & Tunnicliffe, 2015) in that physiological tolerance to hypoxia determines species composition. The occurrence of similar species assemblages before and after the extended anoxic period, the recurrence of slender sole at the beginning and end of the time-series, and the dominance of squat lobster primarily during low oxygen all indicate

that species-specific traits are important in explaining community patterns under variable states of oxygen deficiency. If community structure was primarily influenced by neutral processes, then an equivalent assemblage comprised of different species would have established after environmental perturbation (Legendre & Salvat, 2015); this remains to be tested at broader scales.

However, the extent of autocorrelation in community variation would suggest that biological turnover and progression in variable states of oxygen deficiency is predictable over time. Short-term patterns of community decline and recovery in Saanich Inlet mirror the long-term (multiple years) comparisons of communities before and after severe and prolonged hypoxia in the Black Sea (Mee *et al.*, 2005; Mee, 2006). Ultimately, the severity, frequency, and duration, remains below critical oxygen levels will determine the recovery trajectory of the benthic communities (Mee, 2006) and the magnitude of the biological response in an ecosystem (Diaz & Rosenberg, 2008; Levin *et al.*, 2009b). Because oxygen deficiency selects towards communities dominated by few hypoxia tolerant species, continued deoxygenation below the critical thresholds of these key species will determine the critical tipping point (Scheffer *et al.*, 2001) at which complete exclusion of higher-level organisms will occur. For seasonally hypoxic systems, a permanent regime shift will occur when the frequency or duration at which the habitat remains below critical levels exceeds the time needed for the system to recover.

Acknowledgements

I thank the captains and crews of the CCGS Tully and the associates of the Canadian Scientific Submersible Facility and Ocean Networks Canada for field support. Thank you to A. Round, P. Macoun, K. Bartlett, and D. Hedji of VENUS and J. Vervynck for technical assistant with DISCo. M. Matabos provided advice on multivariate analysis. J. Rose and K. Gale provided additional technical help. Primary funding came from an NSERC PGS-D scholarship and Uvic graduate scholarships, and a MTS scholarship to J.W.F.C, an NSERC undergraduate student research award to C.C., and grants from NSERC Canada and the Canadian Healthy Oceans Network (CHONe) to V.T.

Literature cited

Aguzzi J, Costa C, Robert K, Matabos M, Antonucci F, Juniper SK, Menesatti P (2011) Automated image analysis for the detection of benthic crustaceans and bacterial mat coverage using the VENUS undersea cabled network. *Sensors*, **11**, 10534–10556.

Anderson GS, Bell LS (2014) Deep coastal marine taphonomy: investigation into carcass decomposition in the Saanich Inlet, British Columbia using a baited camera. *PloS ONE*, **9**, e110710.

Anderson JJ, Devol AH (1973) Deep Water Renewal in Saanich Inlet , an Intermittently Anoxic Basin. *Estuarine, Coastal & Shelf Science*, **16**, 1–10.

Bahamonde N, Henriquez G, Zuleta A, Bustos H, Bahamonde R (1986) Population Dynamics and Fisheries of Squat Lobsters, Family Galatheidae, in Chile. In: *North Pacific Workshop on stock assessment and management of invertebrates. Canadian special Publication of Fisheries Aquatic Science* (eds Jamieson GS, Bourne N), pp. 254–268.

Barry JP, Baxter CH, Sagarin RD, Gilman SE (1995) Climate-related, long-term faunal changes in a California Rocky Intertidal Community. *Science*, **267**, 672–675.

Bates AE, Lee RW, Tunnicliffe V, Lamare MD (2010) Deep-sea hydrothermal vent

animals seek cool fluids in a highly variable thermal environment. *Nature communications*, **1**, 14.

Bell G (2001) Neutral Macroecology. *Science*, **293**, 2413–2418.

Benedetti-Cecchi L, Bertocci I, Vaselli S, Maggi E (2013) Temporal Variance Reverses the Impact of High Mean Intensity of Stress in Climate Change Experiments. *Ecology*, **87**, 2489–2499.

Beveridge IA (2007) *Acoustic Observations of Zooplankton Distributions in Saanich Inlet, an intermittently anoxic fjord*. University of Victoria, 147 pp.

Blanchet FG, Legendre P, Borcard D (2008) Forward selection of explanatory variables. *Ecology*, **89**, 2623–2632.

Booth JAT, Mcphee-shaw EE, Chua P et al. (2012) Natural intrusions of hypoxic , low pH water into nearshore marine environments on the California coast. *Continental Shelf Research*, **45**, 108–115.

Bopp L, Resplandy L, Orr JC et al. (2013) Multiple stressors of ocean ecosystems in the 21st century: projections with CMIP5 models. *Biogeosciences*, **10**, 6225–6245.

Borcard D, Legendre P (2002) All-scale spatial analysis of ecological data by means of principal coordinates of neighbour matrices. *Ecological Modelling*, **153**, 51–68.

Borcard D, Legendre P, Avois-Jacquet C, Tuomisto H (2004) Dissecting the spatial structure of ecological data at multiple scales. *Ecology*, **85**, 1826–1832.

Borcard D, Gillet F, Legendre P (2011) *Numerical Ecology with R*. Springer New York, 227-292 pp., New York, NY.

Chan F, Barth JA, Lubchenco J, Kirincich A, Weeks H, Peterson WT, Menge BA (2008) Emergence of anoxia in the California current large marine ecosystem. *Science*, **319**, 920.

Chang S (1995) Physiological and biochemical changes during the molt cycle in decapod crustaceans : an overview. *Journal of Experimental Marine Biology & Ecology*, **193**, 1–14.

Chu JWF, Tunnicliffe V (2015) Oxygen limitations on marine animal distributions and the collapse of epibenthic community structure during shoaling hypoxia. *Global Change Biology*, **21**, 2989–3004.

Crawford WR, Peña MA (2013) Declining Oxygen on the British Columbia Continental Shelf Declining Oxygen on the British Columbia Continental Shelf. *Atmosphere-Ocean*, **51**, 88–103.

Cuvelier D, Legendre P, Laes A, Sarradin P (2014) Rhythms and Community Dynamics of a Hydrothermal Tubeworm Assemblage at Main Endeavour Field – A Multidisciplinary Deep-Sea Observatory Approach. *PLoS ONE*, **9**, e96924.

D'Avanzo C, Kremer JN (1994) Diel Oxygen Dynamics and Anoxic Events in an Eutrophic Estuary of Waquoit Bay, Massachusetts. *Estuaries*, **17**, 131–139.

Danovaro R, Gambi C, Dell'Anno A et al. (2008) Exponential Decline of Deep-Sea Ecosystem Functioning Linked to Benthic Biodiversity Loss. *Current Biology*, **18**, 1–8.

Declerck SAJ, Coronel JS, Legendre P, Brendonck L (2011) Scale dependency of processes structuring metacommunities of cladocerans in temporary pools of High-Andes wetlands. *Ecography*, **34**, 296–305.

Dejours P (1975) *Principles of comparative respiratory physiology*. American Elsevier, 254 pp.

Deutsch C, Brix H, Ito T, Thompson L (2011) Climate-Forced Variabilitiy of Ocean Hypoxia. *Science*, **333**, 336–339.

Diaz RJ, Rosenberg R (2008) Spreading dead zones and consequences for marine ecosystems. *Science*, **321**, 926–929.

Dinning KM, Metaxas A (2013) Patterns in the abundance of hyperbenthic zooplankton and colonization of marine benthic invertebrates on the seafloor of Saanich Inlet, a seasonally hypoxic fjord. *Marine Ecology*, **34**, 2–13.

Doya C, Aguzzi J, Chatzievangelou D, Costa C, Company JB, Tunnicliffe V (2016) The seasonal use of small-scale space by benthic species in a transiently hypoxic area. *Journal of Marine Systems*, **154**, 280–290.

Dray S (2013) Forward Selection with Permutation (Canoco p.46) v. 0.8.

Dunham A, Pegg JR, Carolsfeld W, Davies S, Murfitt I, Boutillier J (2015) Effects of submarine power transmission cables on a glass sponge reef and associated megafaunal community. *Marine Environmental Research*, **107**, 50-60.

Emerson S, Bushinsky S (2014) Oxygen Concentrations and Biological Fluxes in the Open Ocean. *Oceanography*, **27**, 168–171.

Essington TE, Paulsen CE (2010) Quantifying Hypoxia Impacts on an Estuarine Demersal Community Using a Hierarchical Ensemble Approach. *Ecosystems*, **13**, 1035–1048.

Fortin AM, Drapeau P, Legendre P (1989) Spatial Autocorrelation and Sampling Design in Plant Ecology. *Vegetatio*, **83**, 209–222.

Frieder CS, Nam SH, Martz TR, Levin LA (2012) High temporal and spatial variability of dissolved oxygen and pH in a nearshore California kelp forest. *Biogeosciences*, **9**, 3917–3930.

Frölicher TL, Joos F, Plattner G-K, Steinacher M, Doney SC (2009) Natural variability and anthropogenic trends in oceanic oxygen in a coupled carbon cycle-climate model ensemble. *Global Biogeochemical Cycles*, **23**, GB1003.

Gagnon J-M, Beaudin L, Silverberg N, Mauviel A (2013) Mesocosm and in situ observations of the burrowing shrimp Calocaris templemani (Decapoda: Thalassinidea) and its bioturbation activities in soft sediments of the Laurentian Trough. *Marine Biology*, **160**, 2687–2697.

Gattuso J-P, Magnan A, Bille R et al. (2015) Contrasting futures for ocean and society from different anthropogenic CO2 emissions scenarios. *Science*, **349**, aac4722–1–aac4722–10.

Gilly WF, Beman JM, Litvin SY, Robison BH (2013) Oceanographic and biological effects of shoaling of the oxygen minimum zone. *Annual Reviews of Marine Science*, **5**, 393-420.

Glover AG, Gooday AJ, Bailey DM et al. (2010) Temporal change in deep-sea benthic ecosystems: a review of the evidence from recent time-series studies. *Advances in Marine Biology*, **58**, 1–95.

Gooday AJ, Bett BJ, Escobar E et al. (2010) Habitat heterogeneity and its influence on benthic biodiversity in oxygen minimum zones. *Marine Ecology*, **31**, 125–147.

Grundle DS, Timothy DA, Varela DE (2009) Variations of phytoplankton productivity and biomass over an annual cycle in Saanich Inlet, a British Columbia fjord. *Continental Shelf Research*, **29**, 2257–2269.

Hamme RC, Berry JE, Klymak JM, Denman KL (2015) In situ O2 and N2 measurements detect deep-water renewal dynamics in seasonally-anoxic Saanich Inlet. *Continental Shelf Research*, **106**, 107–117.

Hofmann AF, Peltzer ET, Walz PM, Brewer PG (2011) Hypoxia by degrees: Establishing definitions for a changing ocean. *Deep Sea Research Part I: Oceanographic Research Papers*, **58**, 1212–1226.

Hubbell SP (1997) A unified theory of biogeography and relative species abundance and its application to tropical rain forests and coral reefs. *Coral Reefs*, **16**, S9–S21.

Juniper SK, Matabos M, Mihály S, Ajayamohan RS, Gervais F, Bui AOV (2013) A year in Barkley Canyon: A time-series observatory study of mid-slope benthos and habitat dynamics using the NEPTUNE Canada network. *Deep Sea Research Part II: Topical Studies in Oceanography*, **92**, 114–123.

Kruuk H (1963) Diurnal periodicity in the activity of the common sole, Solea vulgaris Quensel. *Netherlands Journal of Sea Research*, **2**, 1–28.

Legendre P (2014) Interpreting the replacement and richness difference components of beta diversity. *Global Ecology & Biogeography*, **23**, 1324–1334.

Legendre P, De Cáceres M (2013) Beta diversity as the variance of community data: dissimilarity coefficients and partitioning. *Ecology Letters*, **16**, 951–63.

Legendre P, Fortin M (1989) Spatial pattern and ecological analysis. *Vegetatio*, **80**, 107–138.

Legendre P, Gallagher ED (2001) Ecologically meaningful transformations for ordination of species data. *Oecologia*, **129**, 271–280.

Legendre P, Gauthier O (2014) Statistical methods for temporal and space − time analysis of community composition data Statistical methods for temporal and space – time analysis of community composition data. *Proceedings of the Royal Society of London. Series B. Biological Sciences*, **281**, 20132728.

Legendre P, Legendre L (2012) *Numerical ecology, 3rd edition*. Elsevier, 990 pp.

Legendre P, Salvat B (2015) Thirty-year recovery of mollusc communities after nuclear experimentations on Fangataufa atoll (Tuamotu, French Polynesia). *Proceedings of the Royal Society of London. Series B. Biological Sciences*, **282**, 20150750.

Legendre P, Dray S, Borcard D, Blanchet FG (2013) MEM spatial eigenfunction and principal coordinate analyses. R package PCNM, vers. 2.1-2.

Levin LA (2003) Oxygen Minimum Zone Benthos: Adaptation and Comunity Response to Hypoxia. *Oceanograpy and Marine Biology: an Annual Review*, **41**, 1–45.

Levin LA, Gage JD (1998) Relationships between oxygen, organic matter and the diversity of bathyal macrofauna. *Deep-Sea Research Part II: Topical Studies in Oceanography*, **34**, 129–163.

Levin LA, Whitcraft CR, Mendoza GF, Gonzalez JP, Cowie G (2009a) Oxygen and organic matter thresholds for benthic faunal activity on the Pakistan margin oxygen minimum zone (700–1100m). *Deep Sea Research Part II: Topical Studies in Oceanography*, **56**, 449–471.

Levin LA, Ekau W, Gooday AJ et al. (2009b) Effects of natural and human-induced hypoxia on coastal benthos. *Biogeosciences*, **6**, 2063–2098.

Long WC, Brylawski BJ, Seitz RD (2008) Behavioral effects of low dissolved oxygen on the bivalve Macoma balthica. *Journal of Experimental Marine Biology & Ecology*, **359**, 34–39.

Manning CC, Hamme RC, Bourbonnais A (2010) Impact of deep-water renewal events on fixed nitrogen loss from seasonally-anoxic Saanich Inlet. *Marine Chemistry*, **122**, 1–10.

Matabos M, Aguzzi J, Robert K, Costa C, Menesatti P, Company JB, Juniper SK (2011) Multi-parametric study of behavioural modulation in demersal decapods at the VENUS cabled observatory in Saanich Inlet, British Columbia, Canada. *Journal of Experimental Marine Biology & Ecology*, **401**, 89–96.

Matabos M, Tunnicliffe V, Juniper SK, Dean C (2012) A year in hypoxia: epibenthic community responses to severe oxygen deficit at a subsea observatory in a coastal inlet. *PloS ONE*, **7**, e45626.

Matabos M, Piechaud N, De Montigny F, Pierre-Marie S, Sarrazin J (2015) The VENUS cabled observatory as a method to observe fish behaviour and species assemblages in a hypoxic fjord , Saanich. *Canadian Journal of Fisheries & Aquatic Sciences*, **72**, 24–36.

McGill BJ, Enquist BJ, Weiher E, Westoby M (2006) Rebuilding community ecology from functional traits. *Trends in Ecology & Evolution*, **21**, 178–185.

Mee L (2006) Reviving Dead Zones. *Scientific American*, **295**, 78–85.

Mee L, Friedrich J, Gomoiu M (2005) Restoring the Black Sea in Times of Uncertainty. *Oceanography*, **18**, 100–111.

Menge BA, Menge DN. (2013) Dynamics of coastal meta-ecosystems: the intermittent upwelling hypothesis and a test in rocky intertidal regions. *Ecological Monographs*, **83**, 283–310.

Menge BA, Gouhier TC, Freidenburg T, Lubchenco J (2011) Linking long-term , large-scale climatic and environmental variability to patterns of marine invertebrate recruitment: Toward explaining " unexplained " variation. *Journal of Experimental Marine Biology & Ecology*, **400**, 236–249.

Muggeo VMR (2008) Segmented: an R package to fit regression models with broken-line relationships. *R news*, **8**, 20–25.

Neilson JD, Perry RI (1990) Diel Vertical Migrations of Marine Fishes: an Obligate or

Facultative Process? *Advances in Marine Biology*, **26**, 115–168.

Oksanen J, Blanchet FG, Kindt R et al. (2015) Vegan: Community Ecology Package.

Pearcy WG, Hancock D (1978) Feeding habits of Dover sole, Microstomus pacificus; rex sole, Glyptocephalus zachirus; slender sole, Lyopsetta exilis; and Pacific sanddab, Citharichthys sordidus, in a region of diverse sediments and bathymetry off Oregon. *Fishery Bulletin*, **76**, 641–651.

Quiroga E, Quiñones R, Palma M, Sellanes J, Gallardo VA, Gerdes D, Rowe G (2005) Biomass size-spectra of macrobenthic communities in the oxygen minimum zone off Chile. *Estuarine, Coastal & Shelf Science*, **62**, 217–231.

Rabalais NN, Díaz RJ, Levin L a., Turner RE, Gilbert D, Zhang J (2010) Dynamics and distribution of natural and human-caused hypoxia. *Biogeosciences*, **7**, 585–619.

Riedel B, Zuschin M, Stachowitsch M (2012) Tolerance of benthic macrofauna to hypoxia and anoxia in shallow coastal seas: A realistic scenario. *Marine Ecology Progress Series*, **458**, 39–52.

Robert K, Onthank KL, Juniper SK, Lee RW (2012) Small-scale thermal responses of hydrothermal vent polynoid polychaetes: Preliminary in situ experiments and methodological development. *Journal of Experimental Marine Biology & Ecology*, **420-421**, 69–76.

De Robertis A, Eiane K, Rau GH (2001) Eat and run: anoxic feeding and subsequent aerobic recovery by Orchomene obtusus in Saanich Inlet, British Columbia, Canada. *Marine Ecology Progress Series*, **219**, 221–227.

Salvanes A, Utne-Palm A, Currie B, Braithwaite V (2011) Behavioural and physiological adaptations of the bearded goby, a key fish species of the extreme environment of the northern Benguela upwelling. *Marine Ecology Progress Series*, **425**, 193–202.

Sassaman C, Mangum CP (1972) Adaptations to environmental oxygen levels in infaunal and epifaunal sea anemones. *Biological Bulletin*, **143**, 657–678.

Sassamant C, Mangum CP (1973) Relationship between aerobic and anaerobic metabolism in estuarine anemones. *Comparative Biochemistry and Physiology*, **44A**, 1313–1319.

Sato M, Dower JF, Kunze E, Dewey R (2013) Second-order seasonal variability in diel vertical migration timing of euphausiids in a coastal inlet. *Marine Ecology Progress Series*, **480**, 39–56.

Sato M, Klymak JM, Kunze E, Dewey R, Dower JF (2014) Turbulence and internal waves in Patricia Bay, Saanich Inlet, British Columbia. *Continental Shelf Research*,

85, 153-167.

Scheffer M, Carpenter S, Foley J a, Folke C, Walker B (2001) Catastrophic shifts in ecosystems. *Nature*, **413**, 591–596.

Sturdivant SK, Díaz RJ, Cutter GR (2012) Bioturbation in a declining oxygen environment, in situ observations from Wormcam. *PloS ONE*, **7**, e34539.

Thiel M, Lovrich GA (2011) Agonistic behaviour and reproductive biology of squat lobsters. In: *The Biology of Squat Lobster* (eds Poore GCB, Ahyong ST, Taylor J), p. 26. CSIRO Publishing, Collingwood.

Timothy DA, Soon MYS (2001) Primary production and deep-water oxygen content of two British Columbian fjords. *Marine Chemistry*, **73**, 37–51.

Underwood AJ, Chapman MG, Connell SD (2000) Observations in ecology: you can't make progress on processes without understanding the patterns. *Journal of Experimental Marine*, **250**, 97–115.

Utne-Palm AC, Salvanes AG V, Currie B et al. (2010) Trophic structure and community stability in an overfished ecosystem. *Science*, **329**, 333–6.

Vinuesa JH (2007) Reproduction Of Munida gregaria (Decapoda: Galatheidae) In San Jorge Gulf, Southwest Atlantic Ocean. *Journal of Crustacean Biology*, **27**, 437–444.

Whitney FA, Freeland HJ, Robert M (2007). Persistently declining oxygen levels in the interior waters of the eastern subarctic Pacific. *Progress in Oceanography*, **75**, 179-199.

Witte U, Wenzhöfer F, Sommer S et al. (2003) In situ experimental evidence of the fate of a phytodetritus pulse at the abyssal sea floor. *Nature*, **424**, 763–766.

Yahel R, Yahel G, Berman T, Jaffe JS, Genin A (2005) Diel pattern with abrupt crepuscular changes of zooplankton over a coral reef. *Limnology & Oceanography*, **50**, 930–944.

Yahel G, Yahel R, Katz T, Lazar B, Herut B, Tunnicliffe V (2008) Fish activity: a major mechanism for sediment resuspension and organic matter remineralization in coastal marine sediments. *Marine Ecology Progress Series*, **372**, 195–209.

Chapter 4: Ecophysiological limits to aerobic metabolism in hypoxia determines epibenthic distributions and energy sequestration in the northeast Pacific Ocean

Preface

Chapter 4 is a research article submitted to Limnology and Oceanography: Chu JWF, Gale KSP. Ecophysiological limits to aerobic metabolism in hypoxia determines epibenthic distributions and energy sequestration in the northeast Pacific.

Katie S.P. Gale (GIS Analyst, Fisheries and Oceans Canada) compiled the data for the global O_2^{crit} meta-analysis and provided input during the writing of the article. I conceived and designed the study, collected and maintained the live specimens, performed the experiments, analyzed the data, interpreted the results, and wrote the article.

Abstract

Expansion of oxygen deficient waters (hypoxia) in the northeast Pacific Ocean (NEP) will have marked impacts on marine life. The response of the resident communities will be a function of their ecophysiological constraints in low oxygen, although this remains untested in the NEP due to a lack of integrative studies. Here, I combine *in situ* surveys and lab-based respirometry experiments of three indicator species of hypoxic systems in the NEP (spot prawn *Pandalus platyceros*, slender sole *Lyopsetta exilis*, squat lobster *Munida quadrispina*) to test if metabolic constraints determine distributions and energy sequestration in a hypoxic setting. I integrate my

results with a global review of critical oxygen thresholds (O_2^{crit}; lower threshold of aerobic metabolism) for crustaceans to assess if regional differences exist based on physiologically-defined measures of hypoxia tolerance. I show that species-specific differences in O_2^{crit} and standard metabolic rates (1) determine the lowest environmental oxygen ($[O_2]_{env}$) at which *in situ* populations occur, (2) result in disproportionate shifts in distributions among co-occuring species during summer hypoxia expansion events, and (3) characterize seasonal shifts in megafaunal community respiration rates due to marked spatio-temporal variability in the $[O_2]_{env}$ profile. I show that the average O_2^{crit} in the NEP is significantly lower than other major ocean basins which suggest that the physiological response of local fauna will primarily be determined by the natural variability and oxygen exposure in a region. When developing management criteria for regions experiencing deoxygenation, I recommend integrating metabolism-based traits to calculate hypoxia thresholds for marine ecosystems.

Introduction

In the past 50 years, oxygen deficient waters of oxygen minimum zones (OMZs) (Stramma *et al.*, 2008; Keeling *et al.*, 2010) have expanded their global coverage by 4.5 million km^2 (Stramma *et al.*, 2010). Shoaling of the upper OMZ boundaries is linked to habitat compression, large-scale redistribution of fish communities, and the mass mortality of commercially valuable and other species (Grantham *et al.*, 2004; Koslow *et al.*, 2011; Stramma *et al.*, 2010; Deutsch *et al.*, 2015). Global models predict that a continued linear decrease in oceanic oxygen content will result in a 12-24% reduction in the biomass of global fish stocks by 2050 (Cheung *et al.*, 2013) and a 20% loss of viable

habitat by 2100 (Deutsch *et al.*, 2015). However, there is uncertainty in the magnitude of future oceanic oxygen loss. Furthermore, lack of field observations at the community level and insufficient integration of physiological principles reduces confidence in the predictions of the ecosystem-level response to deoxygenation (IPCC, 2013).

Consequences of multidecadal oxygen deficiency include a decline in local biomass through emigration, decreased growth, altered food-web dynamics, and death. This loss of ecosystem function is furthered by reductions in biologically-controlled nutrient cycling and energy transferred to higher trophic levels (Diaz & Schaffner, 1990; Ekau *et al.*, 2010; Koslow *et al.*, 2011). Cumulatively, these negative impacts translate into a net loss in ecosystem services (Diaz & Rosenberg, 2008) which is of global societal importance as almost all food provisions created by marine ecosystems require sufficient oxygen levels to sustain the growth and production of organisms (Diaz *et al.*, 2013). To support better projections regarding the magnitude of ecosystem function lost to oxygen deficiency, a standardized approach integrating metabolism based measurements made at higher trophic levels and grounded within a community-level framework is required.

The mechanism behind the response of marine ecosystems to decreases in environmental oxygen (hereafter, $[O_2]_{env}$) is directly linked to the physiology of the resident species (Pörtner & Farrell, 2008). In aquatic ectotherms, the metabolic relationship between oxygen consumption and $[O_2]_{env}$ is non-linear with an ecophysiological threshold occurring at species-specific critical oxygen levels (Dejours, 1975). In $[O_2]_{env}$ above species-specific critical oxygen levels (hereafter O_2^{crit}), organisms can regulate a constant rate of oxygen consumption that is independent of changes in

$[O_2]_{env}$. O_2^{crit} also marks the lowest $[O_2]_{env}$ at which a resting, unfed organism can maintain a constant rate of aerobic metabolism and marks the transition to anaerobic processes. In $[O_2]_{env}$ below O_2^{crit}, oxygen consumption shows a linear response to changes in $[O_2]_{env}$; metabolism is negatively affected through reduction in oxygen transport and delivery efficacy (Pörtner & Farrell, 2008). Because aquatic ectotherms naturally occur close to their lower limits of aerobic metabolism (Childress, 1975; Childress & Seibel, 1998; Seibel, 2011), O_2^{crit} values can: 1) be used as indicators of hypoxia tolerance (Portner and Farrell, 2008), 2) link changes in $[O_2]_{env}$ with higher-level energy transfer (Pörtner & Knust, 2007), and 3) be used to predict large-scale shifts in species distributions in response to deoxygenation (Deutsch *et al.,* 2015).

Current hypoxia thresholds that are generalized in the literature are biased towards Atlantic systems and fail to predict *in situ* species distributions in areas with historically lower oxygen levels such as the northeast Pacific Ocean (Chu & Tunnicliffe 2015a). Thus, *in situ* megafaunal populations in such regions occur in much lower oxygen concentrations than what general thresholds would predict. Although the metabolic relationship between oxygen demand and $[O_2]_{env}$ availability is well-established, only a handful of studies have applied O_2^{crit} as a tool for assessing ecological responses of *in situ* communities. O_2^{crit} values remain unknown for most marine species (Seibel & Childress, 2013) and are uncoupled from field abundance data which rarely have *in situ*, parallel measurements of $[O_2]_{env}$. Furthermore, no integrative datasets exist for the Pacific Ocean – areas of which are the most susceptible to aerobic habitat loss in the future (Deutsch *et al.,* 2011). Here, I present a study from the northeast Pacific Ocean in which I combine data on oceanographic oxygen profiles, field distributions of key

community species, and lab-based respirometry experiments. I determined if metabolic traits such as O_2^{crit} and metabolic rates could assess changes in distributions and aerobic energy sequestration among co-occuring species of megafauna under seasonally variable oxygen regimes. I factor in the well-established scaling relationships between metabolism and body size by measuring O_2^{crit} and standard metabolic rates across the full adult size class range of my three focal species (spot prawn *Pandalus platyceros*, slender sole *Lyopsetta exilis*, and squat lobster *Munida quadrispina*). I report on the first measurements of metabolic rate and O_2^{crit} for slender sole. Differences in hypoxia tolerance among major ocean basins would explain the inapplicability of general hypoxia thresholds in predicting *in situ* species distributions the northeast Pacific Ocean. Therefore, to empirically assess whether such regional differences in hypoxia tolerance exist, I complement my experimentally derived results with a global meta-analysis of O_2^{crit} values for crustaceans, the most common taxonomic group in hypoxia tolerance studies (Vaquer-Sunyer & Duarte, 2008).

Materials and methods

Field mapping animal distributions to $[O_2]_{env}$

Saanich Inlet (Fig. 4.1a) is a highly productive basin on Vancouver Island, British Columbia, Canada. A shallow sill (75 m depth) restricts deep water circulation and exchange with source waters outside the inlet. Near-anoxia (~0 ml l^{-1}) to severe hypoxia (<0.5 ml l^{-1}) characterizes the deepest parts (>200 m) of the inlet and normoxia (>1.4 ml l^{-1}) occurs in the shallower depths (<60 m). Deoxygenation expands the volume of

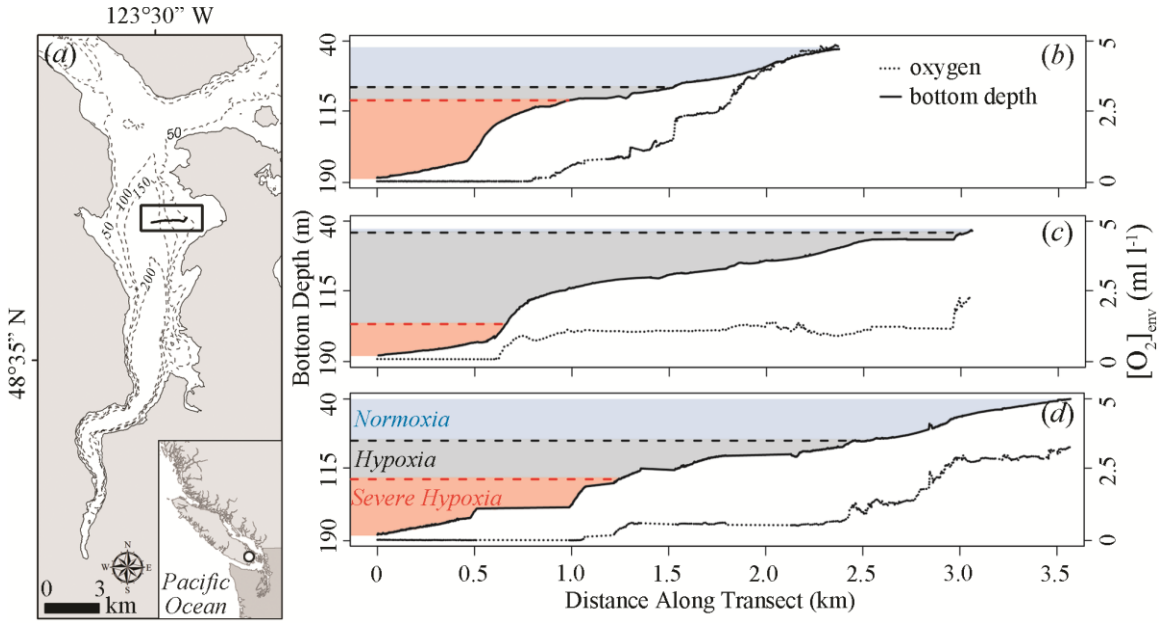

Figure 4.1. Study site and the seasonal hypoxia cycle. (a) *In situ* animal abundances relative to environmental oxygen ($[O_2]_{env}$) were measured along a benthic transect line in Saanich Inlet, Vancouver Island, British Columbia, Canada (inset circle). Seasonal deoxygenation events in the inlet creates zones of severe hypoxia (<0.5 ml l^{-1}), hypoxia (<1.4 ml l^{-1}), and normoxia (>1.4 ml l^{-1}) that expand and contract throughout the year. In 2013, remotely operated vehicles equipped with oxygen sensors and cameras repeated a bottom transect at three stages of the hypoxic cycle: (b) May, before summer deoxygenation and when steep oxygen gradients were evident, (c) September, after deoxygenation-induced expansion of hypoxic waters, and (d) October, during re-oxygenation and re-establishment of the steep oxygen gradient at the site. *In situ* oxygen data are from Chu & Tunnicliffe (2015a,b).

hypoxic and severely hypoxic deep waters into midwater depths over the course of the summer (Chu & Tunnicliffe, 2015a). Primarily in the fall, oxygenated water flows over the sill and down into the deepest parts of the inlet (Anderson & Devol, 1973). In 2013, remotely operated vehicle (ROV) imagery surveys repeated the same benthic transect line in Saanich Inlet at three times of the hypoxia cycle: before deoxygenation (May), after deoxygenation (September) and at the onset of oxygen recovery (October). This ~3km transect begins mid-inlet (~190 m bottom depth), transitions through the zones of severe hypoxia and hypoxia (<1.4 ml l^{-1}), and ends in the normoxic, shallow depths (~45 m).

Dozens of species common to the northeast Pacific Ocean occur in Saanich Inlet (Chu & Tunnicliffe, 2015a). Data on the distribution, density, and movement of the associated epibenthic species assemblage observed along transects are published in Chu & Tunnicliffe (2015a,b). Epibenthic animal distributions were mapped to their *in situ* environmental oxygen ($[O_2]_{env}$) which was measured within 1 m of the seafloor during transects. Concurrent with the seasonally-shifting oxycline, resident species show marked shifts in their density and spatial arrangement within the hypoxia transition zone. Structure of the whole community is primarily driven by the abundance of key mobile species and their fidelity to specific oxygen regimes. The commercially important spot prawn *Pandalus platyceros* (Fig. 4.2a) is strongly associated with normoxic conditions while squat lobster *Munida quadrispina* (Fig. 4.2b) and slender sole *Lyopsetta exilis* (Fig. 4.2c) are strongly associated with severely hypoxic conditions. The *in situ* oxygen occurrence data for these three species at each phase of the 2013 hypoxia cycle (Chu & Tunnicliffe, 2015b) were used to assess whether distribution patterns in the field were correlated to species-specific O_2^{crit}, which I experimentally determined in the laboratory. I report values of O_2^{crit} in both units of concentration ($[O_2]^{crit}$, ml l^{-1}) and the equivalent partial pressure (pO_2^{crit}, kPa).

Lab-based respirometry experiments

Adult spot prawn, squat lobster, and slender sole were captured from Saanich Inlet, British Columbia, Canada. Spot prawns (5-39 g) were caught at 70 m depth by shrimp traps in April 2014. Squat lobsters (wet weight, 2-20 g) and slender sole (6-68 g) were collected by a bottom otter trawl on the CCGS JP Tully at 100 m depth in

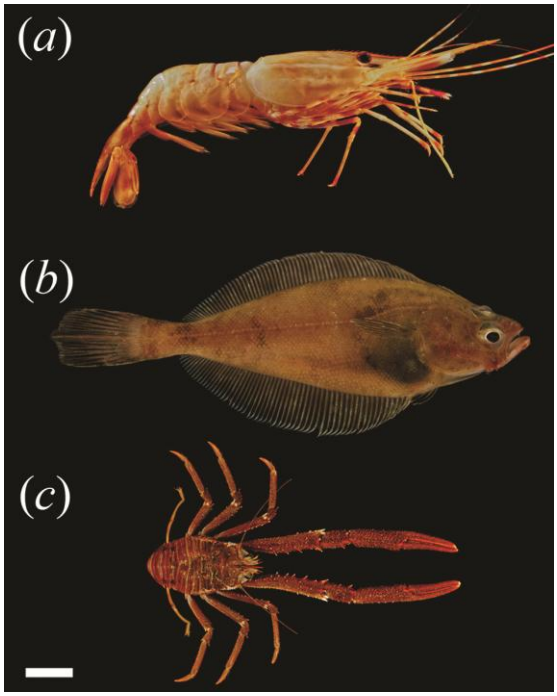

Figure 4.2. Focal species of this study. (a) spot prawn *Pandalus platyceros*, (b) slender sole *Lyopsetta exilis*, and (c) squat lobster *Munida quadrispina*. Scale bar = 2 cm.

October 2013 and September 2014. Animals were transported to holding tanks at the Outdoors Aquatics Unit at the University of Victoria within two hours of capture and acclimated to the recirculating sea water conditions for one month before experimentation. For the duration of this study, animals were kept in constant darkness, temperature (9±1°C), and salinity (31-32 ‰) under oxygen saturated conditions. Spot prawn and squat lobster were fed a weekly diet of frozen fish and cat food. Slender sole were fed a daily mixed diet of fish feed (Skretting GEMMA) supplemented with frozen krill and bloodworms. Animals were caught under a scientific license (XR 356 2013) issued by Fisheries and Oceans Canada. All experiments were conducted according to guidelines set out by the Canadian Council for Animal Care and protocols approved by the University of Victoria Animal Care Committee.

Standard respirometry protocols were used to measure mass-specific oxygen consumption rates (MO_2) and O_2^{crit} (Pörtner *et al.*, 2010). Data were collected per second

using a laptop running Autoresp software and dissolved oxygen was measured using a DAQ-PAC-G4 4-channel respirometry system and MINI-DO galvanic oxygen electrodes (Loligo Systems, Denmark). In all experiments, animals were first removed from the general population and isolated without food for 24 hours. Individuals were then weighed and moved into either a 1.7 L or 3.5 L respirometry chamber that was submerged in a 60 L aquarium. This larger aquarium functioned as both a water bath and the source of oxygen-saturated seawater for intermittent flushing of the respirometry chamber. Chambers were custom-built to have two pairs of input and output ports to accommodate both closed and flow-through respirometry methods. To prevent the buildup of oxygen gradients, a closed loop connected an external flow-through probe vessel to a submersible pump that continuously recirculated water inside the respirometry chamber during experiments. The entire volume of sea water in the system was exchanged weekly to prevent accumulation of metabolites. To mimic natural habitat conditions, darkness in the respirometry chambers was maintained with black plastic bags, salinity was kept constant at 35‰, and water temperature was kept constant at 9ºC using chillers. Following manufacturer protocols, oxygen electrodes were calibrated using a 2-point system: a saturated sodium sulphite solution for 0% oxygen saturation and 100% oxygen saturated sea water fully aerated with air stones. Electrodes were recalibrated every two weeks to prevent problems with long-term sensor drift.

Determining O_2^{crit} and standard metabolic rates (SMR)

Species-specific O_2^{crit} values were determined for spot prawn (n=19), slender sole (n=34), and squat lobster (n=25) using closed respirometry. In each O_2^{crit} experiment, an isolated individual was first acclimated to the respirometry chamber in flow-through

conditions for 12-24 hours. Flow-through was then stopped to begin the experiment. MO_2 (oxygen consumption rate) was calculated from the oxygen consumed over sequential 7 minute intervals for spot prawn and 10 minutes for slender sole and squat lobster. Experiments ended when MO_2 reached zero. Because the three focal species followed the general oxyregulation response curve, O_2^{crit} was calculated from the intersection between the linear regressions of the oxyregulation and oxyconformation phases on the plot of MO_2 versus $[O_2]_{env}$ for each individual animal (Yeager & Ultsch, 1989). O_2^{crit} and the slopes of the two linear regressions were calculated from each experiment using piece-wise regression analysis with the '*segmented'* package in R (Muggeo 2008).

Because MO_2 can quickly deplete oxygen and limit the duration of an experiment in closed conditions, mass-specific standard metabolic rates (SMR) for spot prawn (n=20), slender sole (n=34), squat lobster (n=32) were determined using intermittent flow-through respirometry. This method maintains $[O_2]_{env}$ above O_2^{crit} and can extend duration of metabolism-based experiments. In each SMR experiment, an isolated individual was first acclimated to the respirometry chamber under flow-through conditions for 12-24 hours before data collection began. Flush/wait/measure intervals were 300/120/420 seconds for spot prawn, 420/120/360 seconds for slender sole, and 300/120/600-900 seconds for squat lobster. Relatively longer measurement periods were required for squat lobster because of their lower MO_2. Experiments lasted for 24 hours for slender sole and 24-36 hours for spot prawn and squat lobster. Background respiration was measured using one hour blank controls which were subtracted from animal MO_2 measurements. To prevent brief periods of spontaneous activity from skewing calculations, the percentile method was used to calculate the SMR associated with each

individual experiment. This method takes the average of the lowest 10% of the MO_2 measurements in an experiment after exclusion of outliers. Outliers were defined as mean±2 sd of the lowest 10% of MO_2 values (Clark *et al.*, 2013).

To account for the variance associated with each individual trial (closed and intermittent), the variability associated with metabolism measurements, and the linear scaling relationship of body size with SMR, random-effects meta-analyses were used with body mass as a moderator to determine 'average' O_2^{crit}, oxyconformation slope, oxyregulation slope, mass-specific SMR, and mass-corrected SMR for each species. Restricted maximum-likelihood estimation was used in our mixed-effects models; mean and standard error for O_2^{crit}, slope of the oxyconformation phase, slope of the oxyregulation phase, and SMR were used as random effects and wet weight was used as a moderator. Meta-analyses were done using the *'metafor'* package in R (Viechtbauer, 2010). Two metabolic scaling relationships were calculated for each species using the formula $Y = aM^b$, where Y is either mass-specific (mg O_2 kg^{-1} hr^{-1}) or mass-corrected (mg O_2 hr^{-1}) oxygen consumption rates and M = wet body mass (kg). The constant *a* and scaling exponent *b* are calculated as the intercept and slope of a least squares linear regression after logarithmic transformation of both variables (Clarke & Johnston, 1999). Scaling exponents are typically -0.25 (mass-specific MO_2) and 0.75 (mass-corrected MO_2) for most animals (Schmidt-Nielsen, 1984).

Mapping aerobic habitat in the field

For each focal species, bootstrap resampling tests were used to test if field populations were constrained to $[O_2]_{env}$ above their species-specific O_2^{crit}. For a bootstrap test, a resampled distribution of differences (n=1000 samples) was generated by taking a

randomly chosen value from the vector of *in situ* oxygen occurrences in an ROV survey period (May, Sep, Oct) and subtracting it from the vector of lab-determined O_2^{crit} values for each focal species. The distribution of differences was then compared to a null distribution (centred on zero) to determine if *in situ* oxygen occurrences for each species at each phase of the hypoxia cycle were significantly different from its O_2^{crit}; that is whether the O_2^{crit} were lower than the $[O_2]_{env}$ at which field populations occurred. For each species, bootstrap tests were done at each survey period to determine if field populations were also redistributing according to the spatially shifting $[O_2]_{env}$ profile. In comparisons where the null was rejected ($p<0.05$), the mean-value of the distribution of differences was interpreted as the average 'oxygen distance' between the $[O_2]_{env}$ where populations occurred relative to their species-specific O_2^{crit}.

To illustrate the impact of expanding hypoxia on *in situ* aerobic energy sequestration in the field, metabolic parameters derived in the lab for each focal species were integrated with their *in situ* distributions at each phase of the 2013 hypoxia cycle. Species-specific, mass-corrected SMR calculated from the meta-analyses were converted to units of energy using 20.1 kJ of energy sequestered per litre of oxygen consumed during aerobic respiration (Schmidt-Nielsen, 1984). Energy values were used to represent the individual-based 'average aerobic energy sequestration' which were then multiplied by the *in situ* count data for each species. Individuals occurring in $[O_2]_{env}$ below their species-specific O_2^{crit} were considered functionally anaerobic and excluded from the aerobic energy budget. Calculations were done for each species at each ROV survey period (May, Sep, Oct) and then spatially mapped to the $[O_2]_{env}$ profile to determine the

relative energy contribution of each population to the total aerobic energy budget at each phase of the hypoxia cycle.

Regional hypoxia thresholds

I compiled a dataset of O_2^{crit} thresholds reported for crustaceans from major oceanographic regions that build upon the data and methods provided in similar meta-analysis (Vaquer-Sunyer & Duarte, 2008; Storch *et al.*, 2014; Deutsch *et al.*, 2015). However, unlike past studies that aimed to compare among taxa, the primary objective of this meta-analysis was to assess if differences in hypoxia tolerance exists among regions. Thus, only crustaceans were used because (1) large differences in hypoxia tolerance occur between major taxonomic groups and (2) a majority of metabolism studies has historically been performed on crustaceans (Vaquer-Sunyer & Duarte, 2008). Web of Science was searched with the Boolean parameters: (crustacea* or crab or lobster or shrimp) and (pcrit or "critical oxygen" or oxyconform* or oxyregulat* or o2crit or "o2 crit") OR [(LC50 or LD50 or "lethal dose" or "lethal concentration") AND (oxygen or o2 or anoxi* or hypoxi*)]}. Because O_2^{crit} values were often not linked to key-words in older literature, I supplemented key-word searches with manual methods that included searching through reference lists from metabolic scaling meta-analyses (Glazier 2005, Brey 2010) and respirometry equipment manufacturers (http://www.loligosystems.com). Temperature, salinity, animal weight, life stage, and location of animal collection were recorded with each associated O_2^{crit} record. Because targeted fish species are often exploited for their relatively larger sizes, biases may result if more exploited species are represented in an ocean region. Therefore, human exploitation status for each species was also classified. Species were classified as "exploited" or not if they supported

commercial, recreational, industrial, or subsistence fisheries. Exploitation status was confirmed by first querying Food and Agriculture Organization of the United Nations (FAO) capture fishery database which includes reported weights of all species caught annually by country or region. Species with any reported catch since 1950 were designed as a fishery species. For all species not in the FAO database, SeaLifeBase (http:www.sealifebase.org) was queried followed by a brief literature search. Reports where a species showed no regulatory ability were excluded. All O_2^{crit} values were converted into $pO2^{crit}$ (kPa) or $[O_2]^{crit}$ (ml l^{-1}) and in cases where salinity was not reported, a value of 32 PSU was adopted for unit conversions (mean from all reports ≥30 PSU, Storch *et al.*, 2014). O_2^{crit} values were spatially grouped into seven major ocean basins: East Pacific, West Pacific, East Atlantic, West Atlantic, South Pacific, Indian, and Southern (Antarctic); no values were available for the Arctic. All O_2^{crit} values extracted from the literature are reported (Table C.1); however, to compare O_2^{crit} between oceanographic regions, only one O_2^{crit} per species per study location was used. Comparisons among major ocean basins were also done with exploited species and non-exploited species to account for potential biases the proportion of exploited species represented in a regional pool of O_2^{crit} values. In cases where a study measured multiple O_2^{crit} for the same population, only the lowest reported O_2^{crit} was used (Storch *et al.*, 2014) because higher O_2^{crit} in a species were usually the result of cumulative stressor response in the studies I reviewed. 95% confidence intervals were generated for each region using bias-corrected and accelerated (BCa) bootstrap resampling. Pairwise permutation tests were used to assess if O_2^{crit} differed between ocean basins; p-values were adjusted for multiple comparisons using the false discovery rate method

(Mangiafico, 2015). This comparison was separately done with both $[O_2]^{crit}$ and pO_2^{crit} values to determine if results were dependent on choice of oxygen units.

Results

Species-specific hypoxia tolerance and oxygen requirements

Each species was able to regulate oxygen consumption (MO_2) within a range of $[O_2]_{env}$ and O_2^{crit} was resolved in each species (Fig. 4.3a). In general, mass-specific MO_2 linearly decreased with increasing body mass (Fig. 4.3b) and mass-corrected MO_2 increased with increasing body mass (Fig. 4.3c) for all three species. Linear relationships between mass-specific MO_2 and body mass were significant for spot prawn ($p<0.001$, $r^2 =0.57$) and slender sole ($p<0.001$, $r^2 = 0.52$) but not for squat lobster ($p>0.05$, $r^2 = 0.04$)(Table 1). Relationships between mass-corrected MO_2 and body mass were significant for spot prawn ($p<0.001$, $r^2 = 0.79$), slender sole ($p<0.001$, $r^2 = 0.66$), and squat lobster ($p <0.001$, $r^2 = 0.64$) (Table 4.1). Metabolic scaling exponents were summarized as 95% confidence intervals (95CI) to assess if metabolism of each focal species scaled to the general -0.25 (mass-specific MO_2) and 0.75 (mass-corrected MO_2) exponents known for most organisms. Of the three focal species, only spot prawn followed general scaling patterns. Exponents calculated for mass-specific MO_2 and mass-corrected MO_2 were generally lower in slender sole and higher in squat lobster (mean values in Table 4.1, 95CI in Table 4.2). No significant linear relationships were resolved between O_2^{crit} and MO_2 (Fig. 4.3d) or O_2^{crit} and body mass for any of the three species (all, $p > 0.05$).

Although oxyregulation occurred among species (Fig. 4.3a) and the metabolic scaling relationships were similar for the three species, hypoxia tolerance and aerobic

requirements differed. Mean O_2^{crit} for spot prawn was 1.01 ml l^{-1} or 3.2 kPa (n=19, 95CI = 0.79-1.23 ml l^{-1}) which was substantially higher than the mean O_2^{crit} of 0.36 ml l^{-1}or 1.1 kPa for slender sole (n=34, 95CI = 0.24-0.47 ml l^{-1}) and 0.21 ml l^{-1} or 0.7 kPa for squat lobster (n=25, 95CI = 0.04-0.39 ml l^{-1}). Because of differences in mean O_2^{crit}, the oxyconformation rate also differed among species. Mass-specific MO_2 declined by 83.94, 115.24, and 537.14 mg O_2 kg^{-1} hr^{-1} in spot prawn, slender sole, and squat lobster, respectively, for every ml l^{-1} decrease in $[O_2]_{env}$ until zero (Table 4.3). Because oxyconformation results in MO_2 decreasing towards zero, larger slope values are associated with low $[O_2]_{crit}$ and result in greater shifts in MO_2 per unit change in $[O_2]_{env}$. Similarly, SMR was substantially higher in spot prawn (mean effect = 74.7 mg kg^{-1} hr^{-1}) compared to slender sole (35.11 mg kg^{-1} hr^{-1}) and squat lobster (39.27 mg kg^{-1} hr^{-1}).

Metabolic suppression may have partially reduced the overall oxygen requirements of slender sole and squat lobster; both had positive oxyregulation slopes (decreasing MO_2 with decreasing O_2) (Table 4.3, both 95CI > 0) compared to spot prawn (95CI overlaps with zero). Further evidence of metabolic differences between spot prawn and squat lobster was in their potential to sustain anaerobiosis. All spot prawn died within a few hours when exposed to $[O_2]_{env} < O_2^{crit}$ compared to no mortality occurring in squat lobster even after individuals were exposed to anoxia ($[O_2]_{env}$ = zero), with no measureable MO_2, for up to 36 hours. Prolonged exposure to anoxia was not tested with slender sole.

Table 4.1. Linear scaling relationships between oxygen consumption rates and body mass. Linear scaling relationships were calculated for each species using the formula $Y = aM^b$, where Y is either mass specific (mg O_2 kg^{-1} hr^{-1}) or mass-corrected (mg O_2 hr^{-1}) oxygen consumption rates (MO_2) and M = wet body mass (kg). The constant *a* and scaling exponent *b* were calculated as the intercept and slope of a least squares linear regression after logarithmic transformation of both variables (Clarke & Johnston, 1999). Goodness of fit (R^2) for is in parentheses next to each formula. Asterisks denote a significant linear relationship between a response variable and body mass ($\alpha = 0.05$).

			Response variable (Y)	
Species	n	Body mass range (g)	Mass specific MO_2 (mg O_2 kg^{-1} hr^{-1})	Mass corrected MO_2 (mg O_2 hr^{-1})
Spot prawn	20	5.3 – 39.2	$1.17M^{-0.37}$ (0.57)*	$1.17M^{0.63}$ (0.79)*
Slender sole	34	6.4 – 67.8	$0.87M^{-0.41}$ (0.52)*	$0.87M^{0.59}$ (0.66)*
Squat lobster	32	2.3 – 20.0	$2.01M^{0.24}$ (0.04)	$1.68M^{1.1}$ (0.64)*

Table 4.2. Confidence limits of the **s**caling coefficients relating oxygen consumption rates to body mass. Sample sizes and body mass ranges are given in Table 4.1.

	Metabolic scaling exponents **(**95% C.I.)	
Species	Mass specific metabolic rate (mg O_2 kg^{-1} hr^{-1})	Mass corrected metabolic rate (mg O_2 hr^{-1})
Spot prawn	-0.53 to -0.21	0.47 to 0.79
Slender sole	-0.55 to -0.26	0.44 to 0.74
Squat lobster	-0.04 to 0.53	0.79 to 1.4

Table 4.3. Metabolic parameters measured for spot prawn, slender sole, and squat lobster. Mean (±95CI) of O_2^{crit}, oxyconformation slope, and oxyregulation slopes were determined with closed respirometry. Mass-specific and mass-corrected SMR were determined with intermittent respirometry. For each metabolic parameter, the average (mean-effect size) and species-specific confidence intervals were calculated following meta-analysis methodology to account for mean and standard error of each trial and scaling effect of body weight. Slopes for each phase of a species metabolism represent the per unit change of mass-specific metabolic rate (mg kg^{-1} hr^{-1}) for every unit of $[O_2]_{env}$ (ml l^{-1}).

	Metabolic slopes				SMR		
Species	n	O_2^{crit} (ml l^{-1})	conformation (mg kg^{-1} hr^{-1} per ml l^{-1})	regulation (mg kg^{-1} hr^{-1} per ml l^{-1})	n	mass-corrected (mg hr^{-1})	mass-specific (mg kg^{-1} hr^{-1})
Spot prawn	19	1.01 (0.20)	83.9 (13.9)	-1.5 (3.0)	20	0.41(0.2)	74.7(11.2)
Slender sole	34	0.36 (0.11)	115.2 (25.0)	0.9 (0.7)	34	0.23(0.2)	35.1(5.3)
Squat lobster	25	0.21 (0.17)	537.1 (313.2)	17.4(9.3)	32	0.09(0.1)	39.3(12.3)

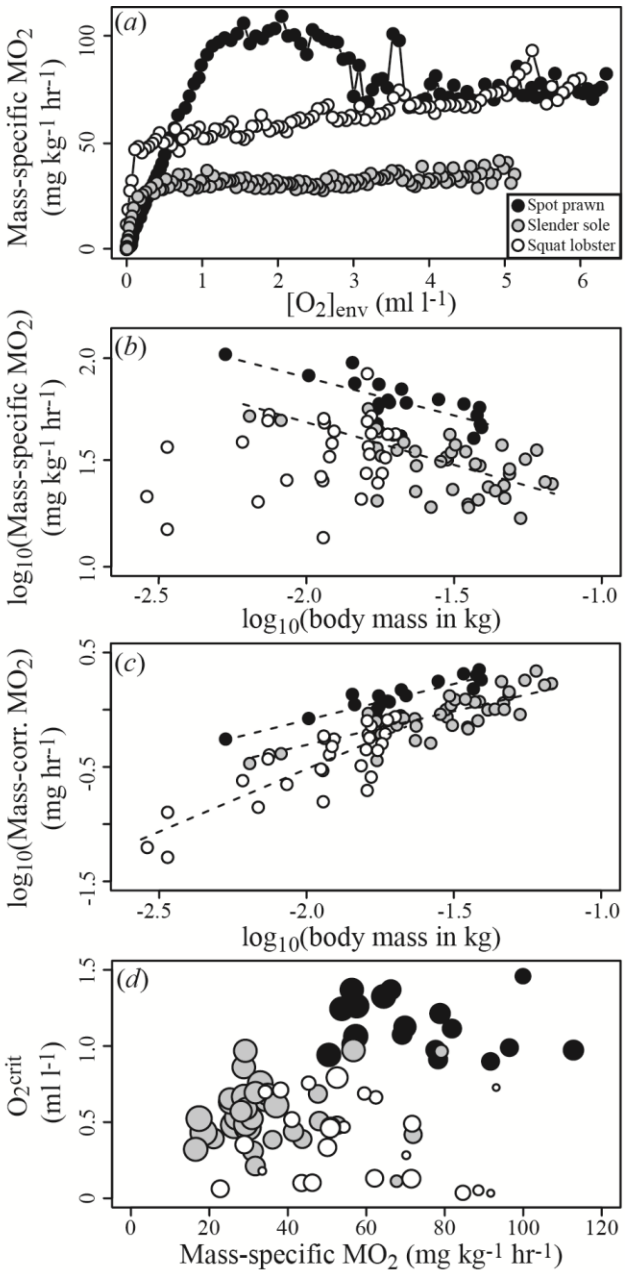

Figure 4.3. Lab-derived species-specific relationships between oxygen consumption and environmental oxygen ($[O_2]_{env}$). (a) Examples of a single oxyregulation response curve for spot prawn (14.3 g, wet weight), slender sole (20.3g), and squat lobster (14.8 g). Each focal species regulated oxygen consumption (mass-specific MO_2) independently of changes in ambient oxygen in the $[O_2]_{env}$ range above their species-specific O_2^{crit}. (b-c) Linear relationships between oxygen consumption and body mass. (b) Mass-specific MO_2 decreased with increasing body mass for spot prawn and slender sole ($p<0.05$) but not squat lobster. (c) Mass-corrected MO_2 increased with increasing body mass in all three species ($p<0.05$). Table 4.1 summarizes species-specific scaling formulas and Table 4.2 summarizes metabolic scaling coefficients. (d) Relationship between O_2^{crit}, mass-specific MO_2, and body mass. Regulated MO_2 was calculated as the mean of the regulated MO_2 measurements for each O_2^{crit} trial. Circle size scales to body mass. No significant relationships were resolved between O_2^{crit} and regulated (mass-specific) MO_2 or O_2^{crit} and body mass (plot not shown) for any of the three species (all $p > 0.05$).

Changes in field distributions and aerobic budgets

Relative physiological differences in hypoxia tolerance and oxygen requirements among species corresponded to the *in situ* response to changing $[O_2]_{env}$ (Fig. 4.4). Large shifts in the average *in situ* $[O_2]_{env}$ at which the spot prawn population occurred implies hypoxia avoidance and migration in response to the expanding and contracting hypoxic zone. In May, the lowest $[O_2]_{env}$ at which spot prawn occurred was marked by their O_2^{crit}. During this period, the average *in situ* $[O_2]_{env}$ of the spot prawn population (total abundance, n=670) was significantly greater than spot prawn O_2^{crit} (difference of +2.64 ml l^{-1}, $p<0.05$). This large 'oxygen distance' characterizes the distribution of the population prior to summer deoxygenation. After deoxygenation (September), total abundance of spot prawn decreased (n=281) and the remaining population occurred in $[O_2]_{env}$ that was significantly lower than their O_2^{crit} (difference of -0.10 ml l^{-1}, $p<0.05$). When re-oxygenation occurred in October, spot prawn abundance increased (n=684) and the average *in situ* $[O_2]_{env}$ of the population was again significantly higher than their species O_2^{crit} (difference of +0.81 ml l^{-1}, $p<0.05$). *In situ* populations of slender sole and squat lobster also occurred in $[O_2]_{env}$ that was significantly higher than their respective species O_2^{crit} (both species, $p<0.05$ for all periods). However, the abundances of slender sole (n=1712, 1952, 1553) and squat lobster (n=1553, 1559, 2183) were consistently high in all three phases of the hypoxia cycle (May, Sep, Oct) suggesting minimal migration or hypoxia avoidance occurred for these species. Furthermore, the relative change in the oxygen distance was minimal for slender sole (+0.48 to +0.75 ml l^{-1}) and squat lobster (+0.3 to +0.73 ml l^{-1}) compared to the marked shifts observed for spot prawn (-0.10 to +2.64 ml l^{-1}).

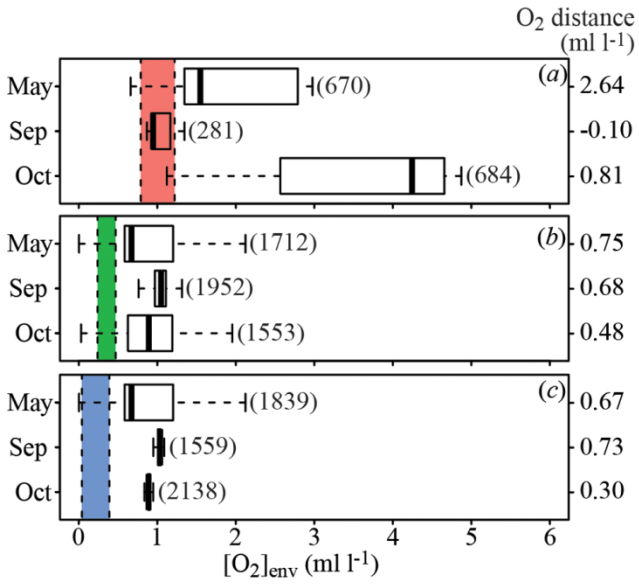

Figure 4.4. *In situ* distributions relative to species specific O_2^{crit}. *In situ* $[O_2]_{env}$ occurrence data for (a) spot prawn, (b) slender sole, and (c) squat lobster are plotted for each phase of the 2013 hypoxia cycle. Species abundances at each time period are in parentheses. Colored bars correspond to the lab-determined O_2^{crit} of each species (95% confidence interval). Individual bootstrap resampling tests were used to determine if the *in situ* $[O_2]_{env}$ occurrences for a species was greater than the species-specific O_2^{crit} at each phase of the hypoxia cycle (α= 0.05). O_2 distance is the mean-value of the distribution of differences from each bootstrap test and is interpreted as the difference in the $[O_2]_{env}$ at which the population occurred relative to its species-specific O_2^{crit}. In general, *in situ* populations occurred in higher $[O_2]_{env}$ relative to species-specific O_2^{crit}. For spot prawn, large fluctuations in abundance and O_2 distance implicates hypoxia avoidance in response to the expanding and contracting hypoxia zone. For slender sole and squat lobster, consistently high abundance and smaller O_2 distances with relatively little change between periods indicates a minimal response to the spatially shifting hypoxic interface.

Shifts in abundance and distribution also changed the amount of *in situ* aerobic energy sequestered through respiration with respect to location in the habitat (Fig. 4.5). Before deoxygenation occurred at our study site, a net respiration rate of 0.56 kJ m^{-2} hr^{-1} can be attributed to the three focal species which is approximately ~5% of the respiration rate measured for microbial community at this site (see Belley *et al.*, 2016 for microbial respiration rates). Despite representing only 17% of the combined abundance among the three species, spot prawn was responsible for 34% of the total aerobic budget because of their higher metabolic rates (Fig. 4.5a). Even in severe hypoxia ($[O_2]_{env}$ <0.5 ml l^{-1}),

aerobic metabolism was sustained because the O_2^{crit} of resident species (slender sole, squat lobster) are lower than the $[O_2]_{env}$ characterizing most of the study area. After hypoxia expansion, an overall decrease in $[O_2]_{env}$ coincided with the net respiration dropping to 0.43 kJ m^{-2} hr^{-1}, a ~23% decrease in the rate of energy sequestered. The lower net respiration rate was primarily attributed to a decrease in spot prawn abundance in the study area with the remaining population being functionally anaerobic (occurring below their species-specific O_2^{crit}). During the period of hypoxia expansion, the abundances of slender sole and squat lobster remained high, thus energy sequestered through respiration became almost entirely coupled to the populations of these two hypoxia-tolerant species (93%, Fig. 4.5b). A pre-deoxygenation state of community respiration returned (0.55 kJ m^{-2} hr^{-1}) when spot prawn migrated back into the system during early oxygen recovery which occurred in less than a month (Fig. 4.5c).

Differences in hypoxia tolerance among oceans

A total of 991 papers were identified and reviewed using my broad search criteria. Of these, 78 papers reported 309 O_2^{crit} values for marine crustaceans from collection sites that generally tracked regional coastlines (Fig. 4.6). O_2^{crit} values were found for 126 species, of which 55 had multiple O_2^{crit} values reported as some studies experimentally determined O_2^{crit} as a response to other environmental variables such as temperature (e.g. Vargo & Sastry, 1977). O_2^{crit} were significantly different among major oceanographic regions (Table 4.4, $p<0.001$). In comparison to the general 1.4 ml l^{-1} hypoxia threshold, only O_2^{crit} thresholds for crustaceans in the west and east Atlantic overlap with this value. In general, the lowest regional O_2^{crit}, or hypoxia threshold, values occurred in the east Pacific Ocean (0.91±0.68 ml l^{-1}, mean±sd) which was 33-39% lower than regions such as

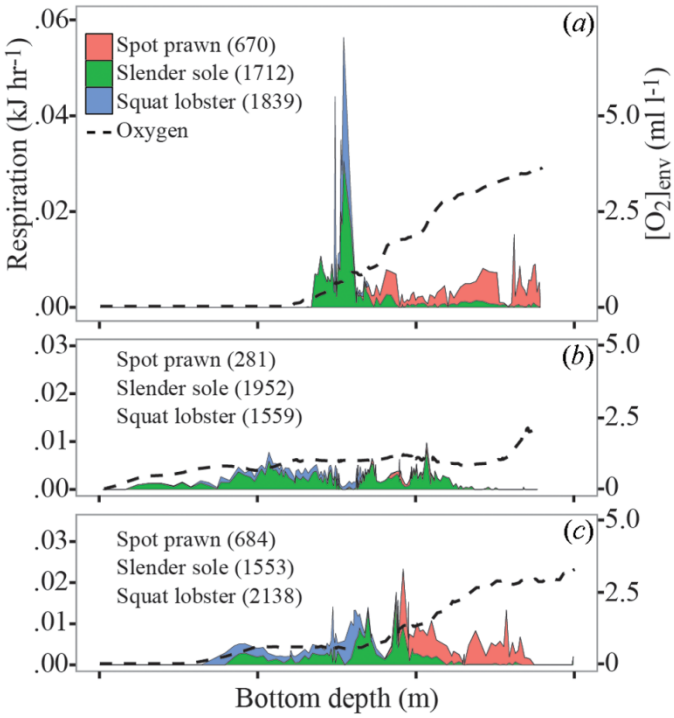

Figure 4.5. *In situ* changes in benthic respiration in response to seasonal hypoxia. Total aerobic respiration was calculated for each species relative to $[O_2]_{env}$ and spatially mapped to the seafloor at each phase of the 2013 hypoxia cycle. Species abundances are in parentheses. (a) In May 2013, before deoxygenation, a net respiration rate of 0.56 kJ m^{-2} hr^{-1} can be attributed to the three focal species. Spot prawn were responsible for 34% of the total aerobic budget. (b) In September 2013, after deoxygenation, total respiration rate decreases to 0.43 kJ m^{-2} hr^{-1}. A 23% decrease in aerobic energy sequestration is attributed to the hypoxia-induced exclusion of spot prawn from the study site and the remaining population becoming functionally anaerobic. (c) In October 2013, spot prawn returned to the system within 1 month of habitat reoxygenation which resulted in net respiration returning to pre-deoxygenation levels (0.55 kJ m^{-2} hr^{-1}).

the west Atlantic Ocean (1.36 ± 0.89 ml l^{-1}) and east Atlantic Ocean (1.44 ± 0.85 ml l^{-1}) where O_2^{crit} reports were also well represented. Despite the large area covered by polar seas, all O_2^{crit} reported from the Southern (Antarctic) Ocean (n=20) (1.67 ± 0.21 ml l^{-1}) came from a single study (Torres *et al.*, 1994) and O_2^{crit} have yet to be reported for populations originating from the Arctic Ocean. Regardless of the oxygen unit used in the regional comparison ($[O_2]^{crit}$ or pO_2^{crit}), a difference in hypoxia tolerance among regions was consistently resolved (Table 4.4).

More than 80% of O_2^{crit} values were for decapods (n=254) although O_2^{crit} values were also reported for amphipods (n=21), euphausids (n=10), lophogastrids (n=8), mysids (n=8), calanoids (n=4), isopods (n=3), and myodocopids (n=1). Because of the paucity of global coverage, only regions from the Atlantic and Pacific could be compared after further subdividing the dataset. In terms of exploitation status, there is a slight bias with more O_2^{crit} reported from exploited species in the Atlantic Ocean (44% of species-level O_2^{crit} values, West Atlantic: n= 14/36 species are exploited, East Atlantic n= 11/18 species) relative to the Pacific Ocean (25% of species-level O_2^{crit} values, West Pacific 3/5 species are exploited, East Pacific 11/50 species are exploited). Regardless of exploitation status, however, the O_2^{crit} threshold calculated for the East Pacific Ocean (95% C.I., exploited: 0.9-1.59 ml l^{-1}, non-exploited: 0.56-97 ml l^{-1}) was consistently lower than the West Atlantic (exploited: 1.72-2.43 ml l^{-1}, non-exploited: 0.96-1.22 ml l^{-1}) and East Atlantic (exploited: 1.72-2.43 ml l^{-1}, non-exploited: 0.74-1.83 ml l^{-1}).

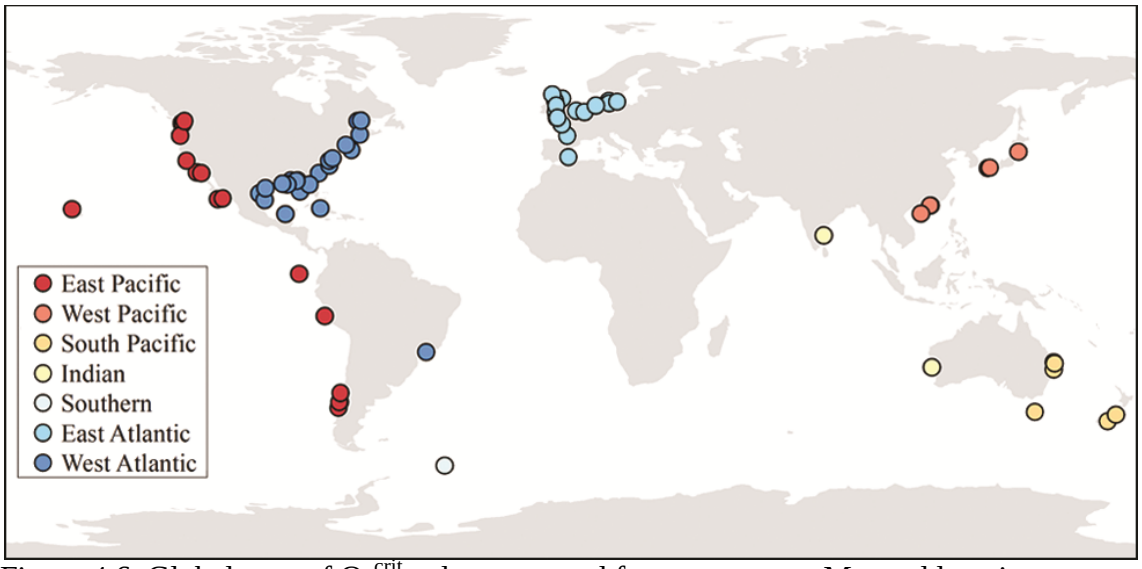

Figure 4.6. Global map of O_2^{crit} values reported for crustaceans. Mapped locations represent the collection site of a species that was used in studies where its O_2^{crit} was experimentally determined. General high spatial clustering of study sites prevent all point locations from being visible (n=309). Regional O_2^{crit} averages and confidence limits are presented in Table 4.4. Species names, locations, and associated references are reported in Table C.1.

Table 4.4. Mean (standard deviation) of hypoxia thresholds (O_2^{crit}) by oceanographic region. Thresholds were calculated using one O_2^{crit} reported per species in a study (n_{total} = 171). Comparisons between regions (permutation tests) were done separately for $[O_2]_{crit}$ (ml l^{-1}) and equivalent pO_2^{crit} (kPa). Letters indicate significant O_2^{crit} differences between oceanographic regions.

		ml l^{-1}		kPa	
Region	n	mean (sd)	95% C.I.	mean (sd)	95% C.I.
East Atlantic	28	1.44 (0.85) **a**	1.02 – 1.77	4.97 (3.06) **a**	3.50 – 6.24
West Atlantic	62	1.36 (0.89) **a**	0.99 – 1.37	4.95 (3.38) **a**	3.51 – 4.90
East Pacific	58	0.88 (0.66) **b**	0.58 – 0.96	2.74 (2.17) **b**	1.74 – 2.96
West Pacific	7	1.12 (0.74) **a,b**	0.56 – 1.79	4.15 (2.76) **a,b**	2.04 – 6.62
South Pacific	6	1.46 (0.97) **a,b**	0.68 – 2.36	5.02 (3.31) **a,b**	2.32 – 8.19
Indian	2	2.73 (1.94) **a**	1.35 – 2.73	9.90 (7.41) **a**	4.66 – 9.90
Antarctic	8	1.67 (0.21) **a**	1.57 – 1.82	4.33 (0.54) **a,b**	4.05 – 4.75

Discussion

My integration of seafloor imagery surveys with lab-based respirometry quantifies the *in situ* response of epibenthic species to expanding hypoxia in the northeast Pacific Ocean. Spatially shifting environmental oxygen ($[O_2]_{env}$) induces restructuring of species distributions with co-occurring species responding differently because of physiological differences in hypoxia tolerance and oxygen requirements. In general, species-specific critical oxygen tensions (O_2^{crit}) correlate to the lowest $[O_2]_{env}$ at which *in situ* populations occur (Seibel 2011). During periods of hypoxia expansion, the overall energy sequestered by respiration decreases; overall rates are determined by species-specific ability to regulate oxygen uptake at low $[O_2]_{env}$. However, significant differences in the average O_2^{crit} among oceans suggest that the evolutionary history of a region will influence the magnitude of aerobic habitat and energy sequestration lost to deoxygenation.

Species-specific traits drive community-level response

Species-specific metabolic traits determine the extent of community reorganization during periods of hypoxia expansion. Because the abundance and distributions of my focal species strongly influence compositional heterogeneity in the field, the loss of community structure as a result of hypoxia expansion (Chu & Tunnicliffe, 2015a) can be linked to the relative metabolic traits of these key species. For example, the lack of a clear scaling relationship between size and oxygen consumption in squat lobster suggests anaerobic processes may be important in their metabolism. Squat lobster are naturally found in $[O_2]_{env}$ below their species-specific O_2^{crit} (Chu &

Tunnicliffe, 2015a) where they aggregate at high densities (>100 individuals m^{-2}, Burd & Brinkhurst, 1984; Doya *et al.*, 2015). These dense clusters of squat lobster rapidly migrate into shallower depths to exploit food resources (Burd & Brinkhurst, 1984; Anderson & Bell, 2014) which is typical of the opportunistic species characterizing seasonally hypoxic systems (Pihl *et al.*, 1992; Diaz & Rosenberg, 1995). In general, squat lobsters (superfamilies Chirostyloidea and Galatheoidea) can be characterized with having low O_2^{crit} and metabolic rates, anoxia tolerance, and substantial anaerobic capacity (Childress, 1975; Quentin & Childress, 1976; Zainal *et al.*, 1992). Such physiological and behavioral adaptations likely facilitate rapid utilization of energy in highly variable oxygen conditions and may explain their general abundance in low oxygen systems.

Although slender sole dominate ichthyoplankton and demersal fish biomass throughout the northeast Pacific Ocean (Pearcy, 1978; Cross, 1987; Auth & Brodeur, 2006; Guan, 2015), my experiments are the first to highlight their metabolism and hypoxia tolerance. Among major teleost groups, flatfish (order Pleuronectiformes) are not generally considered to be hypoxia tolerant (Hochachka & Somero, 2002) which makes the low O_2^{crit} of slender sole (~0.36 ml l^{-1}) particularly unusual. Most pleuronectiforms have O_2^{crit} >1.0 ml l^{-1} (Table C.2); only hogchoker *Trinectes maculatus*, also known to be abundant in low oxygen systems, has similar hypoxia tolerance (0.28 ml l^{-1}, Pihl *et al.*, 1991). In terms of metabolic rates, meaningful comparisons must be made among species that occupy the same habitat niche. For example, metabolic rates of hogchoker reflect the thermal conditions of their surface water habitat (>20°C, Pihl *et al.*, 1991), conditions slender sole would never experience nor survive. Aerobic requirements and metabolic scaling coefficients reported for deep-sea fish are scant (Drazen & Seibel, 2007) so only

broad metabolism comparisons can be made. Slender sole have a functionally similar ecological role relative to the bearded goby *Sufflogobius bibarbatus,* which dominate hypoxic waters in the Benguela upwelling region of the East Atlantic. Although O_2^{crit} are similar between the two hypoxia-tolerant fish (bearded goby O_2^{crit} ~0.3 ml l^{-1}, Utne-Palm *et al.,* 2010), the goby has a higher metabolic rate (60-80 mg kg^{-1} hr^{-1}) which may reflect the energy requirements of its vertical migration behavior (Utne-Palm *et al.,* 2010; Salvanes *et al.,* 2011). Among fish of similar body mass and habitat temperature (adjusted to 9°C using a general Q_{10} of 2.5 for fish, Clarke & Johnston, 1999), the metabolic rate of slender sole is similar to that of other deep-sea fish such as fangtooth *Anoplogaster cornuta* (32-45 mg kg^{-1} hr^{-1}, Gordon *et al.,* 1976) and hagfish *Eptratretus deani* (~24 mg kg^{-1} hr^{-1}, Drazen & Yeh, 2012).

Although slender sole is not a commercially valuable species (due to their small size), they resuspend large amounts of bottom sediments which contribute to substantial fluxes in nutrient recycling and transport (Yahel *et al.,* 2008; Katz *et al.,* 2009; 2012). High abundance and fidelity to low $[O_2]_{env}$ (Chu & Tunnicliffe, 2015a) also suggest that they could be an important indicator species of hypoxic waters within their habitat range. Future deoxygenation of surface waters in the northeast Pacific Ocean may shift the distributions of larger, hypoxia-sensitive species pole ward (Deutsch *et al.,* 2015). This potential relaxation of pressure from predation and competition might also lead us to predict the expansion of the biogeographic range of slender sole and their functional contributions to benthic ecosystems.

Dexoxygenation-induced shifts in species distributions

A general consequence of hypoxia expansion is the compression of species distributions into shallower depths (Eby & Crowder, 2002; Prince & Goodyear, 2006; Koslow *et al.*, 2011; Stramma *et al.*, 2012). Among the overlapping species distributions at my study site, only spot prawn were compressed into shallower depths during hypoxia expansion, since lower tolerance and higher oxygen requirements restrict them to more oxygenated waters. Aerobic habitat is spatially constrained to areas where $[O_2]_{env}$ is above metabolic limits and the available extent of aerobic habitat will be smaller for species with relatively high hypoxia sensitivity (high O_2^{crit}) and high oxygen demand (SMR). However, in seasonally hypoxic systems, the realized extent of habitat use will be much smaller for hypoxia-sensitive species (Breitburg, 2002) because energy is allocated to migration in response to the spatio-temporal variability of the $[O_2]_{env}$ profile. This is consistent with the relatively large oxygen distance we observed for spot prawn which likely reflects an energetic balance of minimizing energy invested in hypoxia avoidance and resource exploitation. In contrast, slender sole and squat lobster consistently occurred much closer to their species-specific O_2^{crit} and persisted in severely hypoxic waters which are conditions that would also exclude predators (e.g. Altieri, 2008). For species adapted to persist in variable hypoxia, energy diverted from hypoxia and predator avoidance can instead be allocated towards growth and reproduction. Therefore, deoxygenation will disproportionately affect the component species of a habitat; net impact will be largely determined by species-specific metabolic constraints.

Low O_2^{crit}, low oxygen demand, and metabolic suppression underpin the success of many species in a variety of systems influenced by severe hypoxia (Childress & Seibel

1998; Levin 2003; Seibel, 2011). These traits are advantageous under deoxygenation because they facilitate the ability to regulate oxygen consumption across a wider range of $[O_2]_{env}$. A shift towards smaller individual- and assemblage-level fish sizes is also predicted (Cheung *et al.,* 2013) because of the direct relationship between mass-corrected oxygen demand and body size. However, this relationship was not observed in my study. Inter- and intra-speciifc measurements of oxygen consumption are typically variable (Clarke *et al.,* 2013) because of the compounding effects of life history strategy, phylogeny, and reproductive condition (Sibenaller et *al.,* 1982; Childress & Somero, 1990; Garenc *et al.,* 1999). These factors can mask linear relationships between body size, O_2^{crit}, and metabolism but can be accounted for by measuring oxygen consumption rates of conspecifics with body sizes ranging over four orders of magnitude (Rosa *et al.*, 2009). Thus, unresolved relationships between body size, metabolism, and O_2^{crit} may be due to the small, maximum adult sizes characteristic of my focal species.

Deoxygenation-induced shifts in ecosystem function

Species-specific adaptations and evolutionary history strongly reflect the oxygen characteristics of a region. Species from the northeast Pacific Ocean are adapted to much lower $[O_2]_{env}$ (Tunnicliffe, 1981; Chu & Tunnicliffe, 2015a) than those in the Atlantic Ocean. The marked difference in metabolic thresholds between the northeast Pacific and both sides of the Atlantic Ocean follows the $[O_2]_{env}$ minima characterizing these regions (Kamykowski & Zentara, 1990; Karstensen *et al.,* 2008). In terms of hypoxia tolerance, the extensive O_2^{crit} data I compiled can be considered baseline thresholds for the most prominently studied taxonomic groups among oceanographic regions. Limited global coverage of O_2^{crit} reflects the geographic bias of research effort (Richardson *et al.,* 2012)

but also shows that baselines have yet to be established for most taxa in the global ocean. Although common marine hypoxia thresholds (e.g. hypoxia <1.4 ml l^{-1}) are still used to describe regions perceived as oxygen deficient, they mostly apply to stable systems that lack seasonal variability and severe hypoxia as selective pressures (Rabalais *et al.*, 2010) and was originally conceived from observations centered on systems in the Atlantic Ocean (Chu & Tunnicliffe, 2015a). When applied to systems where $[O_2]_{env}$ in the Pacific Ocean, they fail to predict *in situ* distributions (i.e., animals are found in lower $[O_2]_{env}$ than expected, Keller *et al.*, 2010; 2015; Chu & Tunnicliffe, 2015a). A similar study on spatio-temporally variable hypoxia systems in the Atlantic (Lichtschlag *et al.*, 2015) also show thresholds responses occurring at the 1.4 ml l^{-1}; further evidence that the threshold response of communities in the northeast Pacific occur at lower environmental oxygen levels. As long-term deoxygenation progresses within a region, extirpation of the more sensitive species will likely lower the overall regional threshold. Empirical knowledge acquired now may not reflect historical conditions (Soulé 2005). Thus, an imperative first step for establishing realistic predictions on the biological consequences of deoxygenation will be to assess oxygen requirements and physiological constraints of the local species. This would explain the ocean scale differences already observed in species responses to deoxygenation (Prince *et al.*, 2010) and ground projections regarding future aerobic habitat loss and reduced ecosystem function.

Studies that make predictions on the biological consequences of marine deoxygenation have mostly projected large-scale shifts in species distributions (Stramma *et al.*, 2012; Deutsch *et al.*, 2015). However, the impacts of deoxygenation on ecosystem function are mostly driven by time-dependent, biological processes such as respiration,

which have threshold responses to changes in $[O_2]_{env}$ (Diaz & Rosenberg, 1995, 2008). In my system, the seasonal shifts in species distributions, community structure, and energy sequestration highlight the strong coupling of the biological response to the spatial and temporal variability of deoxygenation. The steep oxygen gradients (Chu & Tunnicliffe, 2015a) and short-term $[O_2]_{env}$ variability (Matabos *et al.*, 2012) that occur at my study site are typical of poorly-ventilated basins, the upper boundaries of oxygen minimum zones (Brand & Griffiths, 2008), and coastal upwelling regions (Booth *et al.,* 2012). In these systems, the depth at which the hypoxia interface occurs is highly variable because the hypoxic volume is controlled by seasonal and interannual variations in hydrography (Rabalais *et al.,* 2002; Astor *et al.,* 2003), wind-driven upwelling (Chan *et al.,* 2008), and primary production (Wang *et al.,* 2015). The amount of local energy displaced from higher trophic levels and diverted towards the microbial community is correlated to the timing and severity of seasonal low oxygen period, the duration at which a system stays below critical threshold levels, and the population dynamics of the components species (Baird *et al.,* 2004; Diaz & Rosenberg, 2008). If there is a long-term increase in the period during which a system remains below critical thresholds, deoxygenation-induced shifts in biological processes such as energy flow, biomass fixation, and nutrient cycling will follow. Because hypoxia sensitivity is not equal among species, the total energy shunted from megafauna communities, as a result of deoxygenation, will primarily be due to the long-term, exclusion of hypoxia-sensitive and large-bodied individuals because they contribute more to the aerobic capacity at higher trophic levels. However, any net loss of energy transfer may be partially compensated through an increase in population size of the hypoxia-tolerant, small-bodied individuals.

Cumulative impacts of multiple climate stressors on respiratory physiology

Deoxygenation of the ocean is one of the three main consequences of rising atmospheric CO_2, the others being ocean warming and acidification (Levin & Breitberg, 2015). Although the environmental drivers of these three climate-related stressors are different, their influence on biology can be unified by their effect on the aerobic performance and energy turnover of organisms (Pörtner & Farrell 2008; Pörtner, 2010; 2012). All three climate-related stressors affect respiratory physiology by influencing the overall efficiency and capacity of oxygen acquisition, transport, and storage in fish and invertebrates (Hochacka & Somero, 2009). Exposure to elevated temperature increases oxygen demand and O_2^{crit} in marine ecotherms (Pörtner & Knust, 2007; Pörtner, 2010), while exposure to increased pCO_2 can decrease overall aerobic capacity by reducing metabolic and energy turnover rates (Pörtner *et al.*, 2004; 2005; Pörtner, 2008). Cumulative exposure to multiple stressors will likely increase the overall magnitude of the response in aerobic capacity, energy allocation and turnover relative to a single climate-stressor like hypoxia. However, the relative contribution of each climate-related stressor to the overall reduction of aerobic metabolism and biomass fixation remains an open question because there is currently no experimental framework that can accommodate all three environmental variables with a single physiological response measurement. Therefore, unifying the effects of temperature, oxygen, and pH into an integrated, physiological framework (e.g., Del Raye & Weng, 2015) will become an important tool in predicting the cumulative impacts of climate-driven change on marine ecosystems and function.

Acknowledgements

I thank the chief scientists, captains and crews of the CCGS Tully, CCGS Vector, and RV Falkor and the associates of the Canadian Scientific Submersible Facility for field support. Early pilot experiments were supported by Ocean Networks Canada. Support came from staff at the UVIC Outdoor Aquatics Unit, F. Juanes, T. Nielsen, A. Preston, C. Secord, and J. Rose. Supplementary funding for field support came from the Schmidt Ocean Institute during the cruise, 'Open Ocean to Inner Sea'. Primary Funding came from NSERC PGS-D, Marine Technology Society, and UVIC donor award scholarships to J.W.F.C. and grants from NSERC Canada and the Canadian Healthy Oceans Network (CHONe) to V. Tunnicliffe.

Literature cited

Altieri AH (2008) Dead zones enhance key fisheries species by providing predation refuge. *Ecology*, **89**, 2808-2818.

Anderson GS, Bell LS (2014) Deep coastal marine taphonomy: Investigation into carcass decomposition in the Saanich Inlet, British Columbia using a baited camera. *PLoS ONE*, **9**, E110710.

Anderson JJ, Devol AH (1973) Deep water renewal in Saanich Inlet, an intermittently anoxic basin. *Estuaries & Coastal Marine Science*, **1**, 1-10.

Astor Y, Muller-Karger F, Scranton MI (2003) Seasonal and annual variation in the hydrography of the Cariaco Basin: implications for basin ventilation. *Continental Shelf Research, 23*, 125-144.

Auth TD, Brodeur RD (2006) Distribution and community structure of ichthyoplankton off the coast of Oregon, USA, in 2000 and 2002. *Marine Ecology Progress Series*, **219**, 199-213.

Baird D, Christian RR, Peterson CH, Johnson GA (2004) Consequences of hypoxia on estuarine ecosystem function: energy diversion from consumers to microbes. *Ecological Applications*, **14**, 805-822.

Belley R, Snelgrove PVR, Archambault P, Juniper SK (2016) Environmental drivers of benthic flux variation and ecosystem functioning in Salish Sea and Northeast Pacific Sediments. *PLoS ONE*, **11**, e0151110.

Booth JAT, McPhee-Shaw EE, Chua P, Kingsley E, Denny M, Phillips R, Bograd SJ, Zeidberg LD, Gilly WF (2012) Natural intrusions of hypoxic, low pH water into nearshore marine environments on the California coast. *Continental Shelf Research*, **45,** 108-115.

Brand TD, Griffiths C (2009) Seasonality in the hydrography and biogeochemistry across the Pakistan margin of the NE Arabian Sea. *Deep-Sea Research Part II: Topical Studies in Oceanography*, **56**, 283-295.

Breitburg D (2002) Effects of hypoxia, and the balance between hypoxia and enrichment, on coastal fishes and fisheries. *Estuaries*, **25**, 767-781.

Brey T (2010) An empirical model for estimating aquatic invertebrate respiration. *Methods in Ecology & Evolution*, **1**, 92-101.

Burd BJ, Brinkhurst RO (1984) The distribution of the galatheid crab *Munida quadrispina* (Benedict 1901) in relation to oxygen concentrations in British Columbia fjords. *Journal of Experimental Marine Biology & Ecology*, **81**, 1-20.

Chan F, Barth JA, Lubchenco J, Kirincich A, Weeks H, Peterson WT, Menge BA (2008) Emergence of anoxia in the California current large marine ecosystem. *Science*, **319**, 920.

Cheung WWL, Sarmiento JL, Dunne J, Frölicher TL, Lam VWY, Palomares MLD, Watson R, Pauly D (2013) Shrinking of fishes exacerbates impacts of global ocean changes on marine ecosystems. *Nature Climate Change*, **3**, 254-258.

Childress JJ (1975) The respiratory rates of midwater crustaceans as a function of depth of occurrence and relation to the oxygen minimum layer off southern California. *Comparative Biochemistry & Physiology Part A Physiology*, **50A**, 787-799.

Childress JJ, Seibel BA (1998) Life at stable low oxygen: adaptations of animals to oceanic oxygen minimum layers. *Journal of Experimental Biology*, **201,** 1223-1232.

Childress JJ, Somero GN (1990) Metabolic scaling: a new perspective based on scaling of glycolytic enzyme activities. *American Zoologist*, **30**, 161-173.

Chu, JWF, Tunnicliffe V (2015a) Oxygen limitations on marine animal distributions and the collapse of epibenthic community structure during shoaling hypoxia. *Global Change Biology*, **21**, 2989-3004.

Chu JWF, Tunnicliffe V (2015b) Data from: Oxygen limitations on marine animal distributions and the collapse of epibenthic community structure during shoaling hypoxia. *Dryad Data Repository*. doi:10.5061/dryad.1p55v.

Clarke A, Johnston NM (1999) Scaling of metabolic rate with body mass and temperature in teleost fish. *Journal of Animal Ecology*, **68**, 893-905.

Clark TD, Sandblom E, Jutfelt F (2013) Aerobic scope measurements of fishes in an era of climate change: Respirometry, relevance and recommendations. *Journal of Experimental Biology*, **216**, 2771-2782.

Cross JN (1987) Demersal fishes of the upper continental slope off southern California. *California Cooperative Oceanic Fisheries Investigations Report*, **28**, 155-167.

Dejours P (1975) Principles of Comparative Respiratory Physiology. New York, NY: American Elsevier.

Del Raye G, Weng KC (2015) An aerobic scope-based habitat suitability index for predicting the effects of multi-dimensional climate change stressors on marine teleosts. *Deep-Sea Research Part II:Topical Studies in Oceanography*, **113**, 280-290.

Deutsch C, Brix H, Ito T, Frenzel H, Thompson L (2011) Climate-forced variability of ocean hypoxia. *Science*, **333**, 336-339.

Deutsch C, Ferrel A, Seibel B, Pörtner H-O, Huey RB (2015) Climate change tightens a metabolic constraint on marine habitats. *Science*, **348**, 1132-1135.

Diaz RJ, Rosenberg R (1995) Marine benthic hypoxia: A review of its ecological effects and the behavioural responses of benthic macrofauna. *Oceanography and Marine Biology - An Annual Review*, **33**, 245-303.

Diaz RJ, Rosenberg R (2008) Spreading dead zones and consequences for marine ecosystems. *Science*, **321**, 926-929.

Diaz RJ, Schaffner LC (1990) The functional role of estuarine benthos. In Perspectives on the Chesapeake Bay, 1990 – Advances in Estuarine Sciences (eds M Haire, EC Krome), pp. 25-56. Gloucester Point, VA: Chesapeake Research Consortium.

Diaz RJ, Eriksson-Hagg H, Rosenberg R (2013) 4. Hypoxia. In Managing ocean environments in a changing climate: Sustainability and Economic Perspective (eds KJ Noone, UR Sumaila, RJ Diaz), pp. 67-96. San Diego, CA: Elsevier.

Doya C, Aguzzi J, Chatzievangelou D, Costa C, Company JB, Tunnicliffe V (2015) The seasonal use of small-scale space by benthic species in a transiently hypoxia area. *Journal of Marine Systems*, **154**, 280-290.

Drazen JC, Seibel BA (2007) Depth-related trends in metabolism of benthic and benthopelagic deep-sea fishes. *Limnology & Oceanography*, **52**, 2306-2316.

Drazen JC, Yeh J (2012) Respiration of four species of deep-sea demersal fishes measured *in situ* in the eastern North Pacific. *Deep-Sea Research Part I*, **60**, 1-6.

Eby LA, Crowder LB (2002) Hypoxia-based habitat compression in the Neuse River Estuary: context-dependent shifts in behavioral avoidance thresholds. *Canadian Journal of Fisheries & Aquatic Science*, **59**, 952-965.

Ekau W, Auel H, Pörtner H-O, Gilbert D (2010) Impacts of hypoxia on the structure and processes in pelagic communities (zooplankton, macro-invertebrates and fish). *Biogeosciences*, **7**, 1669-1699.

Garenc C, Couture P, Laflamme MA, Guderley H (1999) Metabolic correlates of burst swimming capacity of juvenile and adult threespine stickleback (*Gasterosteus aculeatus*). *Journal of Comparative Physiology B*, **169**, 113-122.

Glazier DS (2005) Beyond the '3/4-power law': variation in the intra- and interspecific scaling of metabolic rate in animals. *Biological Reviews*, **80**, 611-662.

Gordon MS, Belman BW, Chow PH (1976) Comparative studies on the metabolism of shallow-water and deep-sea fishes. IV. Patterns of aerobic metabolism in the mesopelagic fangtooth fish *Anoplogaster cornuta*. *Marine Biology*, **35**, 287-293.

Grantham, B.A. Chan F, Nielsen KJ, Fox DS, Barth JA, Huyer A, Lubchenco J, Menge BA (2004) Upwelling-driven nearshore hypoxia signals ecosystem and oceanographic changes in the northeast Pacific. *Nature*, **429**, 749-754.

Guan L (2015) Spatial and temporal dynamics of larval fish assemblages in the Strait of Georgia. PhD Thesis. University of Victoria, Victoria, BC.

Hochachka PW, Somero GN (2002) Biochemical adaptation: mechanism and process in physiological evolution. Oxford University Press.

IPCC (2013) Ocean Systems. In Climate Change 2014: Impacts, Adaptation, and Vulnerability. Contributions of Working Group II to the Fifth Assessment Report of the Intergovernmnetal Panel on Climate Change (eds Field CB *et al.*), pp. 411-484. Cambridge, UK: Cambridge University Press, Cambridge.

Kamykowski D, Zentara SJ (1990) Hypoxia in the world ocean as recorded in the historical data set. *Deep-Sea Research Part A: Oceanographic Research Papers*, **37**, 1861-1874.

Karstensen J, Stramma L, Visbeck M (2008) Oxygen minimum zones in the eastern tropical Atlantic and Pacific Oceans. *Progress in Oceanography*, **77**, 331-350.

Katz T, Yahel G, Yahel R, Tunnicliffe V, Herut B, Snelgrove P, Crusius J, Lazar B (2009) Groundfish overfishing, diatom decline, and the marine silica cycle: Lessons from Saanich Inlet, Canada, and the Baltic Sea cod crash. *Global Biogeochemical Cycles*, **23**, GB4032.

Katz T, Yahel G, Reidenbach M, Tunnicliffe V, Herut B, Crisius J, Whitney F, Snelgrove PVR, Lazar B (2012) Resuspension by fish facilitates the transport and redistribution of coastal sediments. *Limnology & Oceanography*, **57**, 945-958.

Keeling RF, Körtzinger A, Gruber N (2010) Ocean deoxygenation in a warming world. *Annual Review of Marine Science*, **2**, 199-229.

Keller AA, Simon V, Chan F, Wakefield WW, Clarke ME, Barth JA, Kamikawa D, Fruh EL (2010) Demersal fish and invertebrate biomass in relation to an offshore hypoxic zone along the US West Coast. *Fisheries Oceanography*, **19**, 76-87.

Keller AA, Ciannelli L, Wakefield WW, Simon V, Barth JA, Pierce SD (2015) Occurrence of demersal fishes in relation to near-bottom oxygen levels within the California Current large marine ecosystem. *Fisheries Oceanography*, **24**, 162-176.

Koslow JA, Goericke R, Lara-Lopez A, Watson W (2011) Impact of declining intermediate-water oxygen on deepwater fishes in the California Current. *Marine Ecology Progress Series.* **436**, 207-218.

Levin LA (2003) Oxygen minimum zone benthos: adaptation and community response to hypoxia. *Oceanography & Marine Biology: an Annual Review*, **41**, 1-45.

Levin LA, Breitburg DL (2015) Linking coasts and seas to address ocean deoxygenation. *Nature Climate Change*, **5**, 401-403.

Lichtschlag A, Donis D, Janssen F et al. (2015) Effects of fluctuating hypoxia on benthic oxygen consumption in the Black Sea (Crimean shelf). *Biogeosciences*, **12**, 5075-5092.

Mangiafico SS (2015) An R Companion for the Handbook of Biological Statistics v1.09. ‘rcompanion/org/rcompanion/

Matabos M, Tunnicliffe V, Juniper SK, Dean C (2012) A year in hypoxia: epibenthic community responses to severe oxygen deficit at a subsea observatory in a coastal inlet. *PLoS ONE*, **7**, e45626.

Muggeo VMR (2008) Segmented: an R package to fit regression models with broken-line relationships. *R news*, **8**, 20-25.

Pearcy WG (1978) Distribution and abundance of small flatfishes and other demersal fishes in a region of diverse sediments and bathymetry off Oregon. *Fishery Bulletin*, **76**, 629-640.

Pihl L, Baden SP, Diaz RJ (1991) Effects of periodic hypoxia on distribution of demersal fish and crustaceans. *Marine Biology*, **108**, 349-360.

Pihl L, Baden SP, Diaz RJ, Schaffner LC (1992) Hypoxia-induced structural changes in the diet of bottom-feeding fish and Crustacea. *Marine Biology*, **112**, 349-361.

Pörtner H-O (2008) Ecosystem effects of ocean acidification in times of ocean warming: a physiologist's view. *Marine Ecology Progress Series*, **373**, 203-217.

Pörtner H-O (2010) Oxygen- and capacity-limitation of thermal tolerance: a matrix for integrating climate-related stressor effects in marine ecosystems. *Journal of Experimental Biology*, **213**, 881-893.

Pörtner H-O (2012) Integrating climate-related stressors effects on marine organisms: unifying principles linking molecule to ecosystem-level changes. *Marine Ecology Progress Series*, **470**, 273-290.

Pörtner H-O, Dupont S, Melzner F, Storch D, Thorndyke M (2010) Chapter 10: Studies of metabolic rate and other characters across life stages. In Guide to best practices for ocean acidification research and data reporting. (eds U Riebesell, VJ Fabry, L Hansson, J-P Gattuso), pp. 167-180. Luxemburg: Publications Office of the European Union.

Pörtner H-O, Farrell AP (2008) Physiology and climate change. *Science*, **322**, 690-692.

Pörtner H-O, Knust R (2007) Climate change affects marine fishes through the oxygen limitation of thermal tolerance. *Science*, **315**, 95-97.

Pörtner H-O, Langenbuch M, Reipschläger A (2004) Biological impact of elevated ocean CO_2 concentrations: lessons from animal physiology and earth history. *Journal of Oceanography*, **60**, 705-718.

Pörtner H-O, Langenbuch M (2005) Synergistic effects of temperature extremes, hypoxia, and increases in CO_2 on marine animals: from earth history to global change. *Journal of Geophysical Research*, **110**, C09S10

Prince ED, Goodyear CP (2006) Hypoxia-based habitat compression of tropical pelagic fishes. *Fisheries Oceanography*, **15**, 451-464.

Prince ED, Luo J, Goodyear CP, Hoolihan HP, Snodgrass D, Orbesen ES, Serafy JE, Ortiz M, Schirripa MJ (2010) Ocean scale hypoxia-based habitat compression of Atlantic istiophorid billfishes. *Fisheries Oceanography*, **19**, 448-462.

Quentin LB, Childress JJ (1976) Respiratory adaptations of Pleuroncodes planipes to its environment off Baja, California. *Marine Biology*, **38**, 327-334.

Rabalais NN, Turner RE, Wiseman Jr WJ (2002) Gulf of Mexico hypoxia, A.K.A. "The Dead Zone". *Annual Review of Ecology & Systematics*, **33**, 235-263.

Rabalais NN, Diaz RJ, Levin LA, Turner RE, Gilbert D, Zhang J (2010) Dynamics and distribution of natural and human-caused hypoxia. *Biogeosciences*, **7**, 585-619.

Richardson AJ et al. (2012) Climate change and marine life. *Biology Letters*, **8**, 907-909.

Rosa R, Trueblood L, Seibel BA (2009) Ecophysiological influence on scaling of aerobic and anaerobic metabolism of pelagic gonatid squids. *Physiological & Biochemical Zoology*, **82**, 419-429.

Salvanes AGV, Utne-Palm AC, Currie B, Braithwaite VA (2011) Behavioural and physiological adaptations of the bearded goby, a key fish species of the extreme environment of the northern Benguela upwelling. *Marine Ecology Progress Series*, **425**, 193-202.

Schmidt-Nielsen K (1984) Scaling: why is animal size so important? New York, NY: Cambridge University Press.

Seibel BA (2011) Critical oxygen levels and metabolic suppression in oceanic oxygen minimum zones. *Journal of Experimental Biology*, **214**, 326-336.

Seibel BA, Childress JJ (2013) The real limits to marine life: a further critique of the Respiration Index. *Biogeosciences*, **10**, 2815-2819.

Siebenaller JF, Somero GN, Haedrich RL (1982) Biochemical characteristics of macrourid fishes differeing in their depths of distribution. *Biological Bulletin*, **163**, 240-249.

Soulé ME (2005) Marine conservation biology: the science of maintaining the sea's biodiversity. Washington, DC: Island Press.

Storch D, Menzel L, Frickenhaus S, Pörtner H-O (2014) Climate sensitivity across marine domains of life: limits to evolutionary adaptation shape species interactions. *Global Change Biology*, **20**, 3059-3067.

Stramma L, Johnson GC, Spirntall J, Mohrholz V (2008) Expanding oxygen-minimum zones in the tropical oceans. *Science*, **320**, 655-658.

Stramma L, Schmidtko S, Levin LA, Johnson GC (2010) Ocean oxygen minima expansions and their biological impacts. *Deep-Sea Research Part I: Oceanographic Research Papers*, **57**, 587-595.

Stramma L, Prince ED, Schmidtko S, Luo J, Hoolihan JP, Visbeck M, Wallace DWR, Brandt P, Körtzinger A (2012) Expansion of oxygen minimum zones may reduce available habitat for tropical pelagic fishes. *Nature Climate Change*, **2**, 33-37.

Torres JJ, Aarset AV, Donnelly J, Hopkins TL, Lancraft TM, Ainley DG (1994) Metabolism of Antarctic micronektonic Crustacea as a function of depth of occurrence and season. *Marine Ecology Progress Series*, **113**, 207-219.

Tunnicliffe V (1981) High species diversity and abundance of the epibenthic community in an oxygen-deficient basin. *Nature*, **294**, 354-356.

Utne-Palm AC et al. (2010) Trophic structure and community stability in an overfished ecosystem. *Nature*, **329**, 333-336.

Vargo SL, Sastry AN (1977) Acute temperature and low dissolved oxygen tolerances of Brachyuran crab (*Cancer irroratus*) larvae. *Marine Biology*, **40**, 165-171.

Vaquer-Sunyer R, Duarte C (2008) Thresholds of hypoxia for marine biodiversity. *Proceedings of the National Academy of Sciences of the United States of America*, **105**, 15452-15457.

Viechtbauer W (2010) Conducting meta-analyses in R with the metafor package. *Journal of Statistical Software*, **36**, 1-48.

Yahel G, Yahel R, Katz T, Lazar B, Herut B, Tunnicliffe V (2008) Fish activity: a major mechanism for sediment resuspension and organic matter remineralization in coastal marine sediments. *Marine Ecology Progress Series*, **372**, 195-209.

Yeager DP, Ultsch GR (1989) Physiological regulation and conformation: a basic program for the determination of critical-points. *Physiological Zoology*, **62**, 888-907.

Wang D, Gouhier TC, Menge BA, Ganguly AR (2015) Intensification and spatial homogenization of coastal upwelling under climate change. *Nature*, **518**, 390-394.

Zainal KAY, Taylor AC, Atkinson RJA (1992) The effect of temperature and hypoxia on the respiratory physiology of the squat lobster *Munida rugosa* and *Munida sarsi* (Anomura, Galatheidae). *Comparative Biochemistry & Physiology Part A: Physiology*, **101A**, 557-567.

Chapter 5: General Discussion

Dissertation summary

For over a century, studies have addressed the role oxygen has played in shaping the ecology and evolution of life (Ege & Krogh, 1914; Semenza, 2007; Thannickal, 2009). Since the middle of the 20th century, growing awareness of climate-driven changes in the ocean has focused related research on the future consequences of oxygen deficiency to marine biodiversity. Episodic or seasonal occurrence of hypoxia now occurs in estuaries, continental shelves, and margins (Rabalais *et al.*, 2014; Altieri & Gedan, 2015; Levin & Breitburg, 2015). Partitioning out the influence of environmental oxygen ($[O_2]_{env}$) variability on biological communities requires concomitant measurements of environmental oxygen and biological responses. The coarse resolution of traditional methods has obscured identification of the small-scale patterns and processes alongside the more well-defined broad-scale patterns of hypoxia. However, we can now experimentally test some ecological theory and predictions in logistically challenging environments because of advances in subsea technology.

My dissertation presents a novel integrative framework that focused on epibenthic, hypoxic communities from the northeast Pacific, combining *in situ* surveys in space and time with manipulative lab experiments. I used ecophysiological traits to mechanistically explain community-level patterns on the seafloor, applied advanced subsea vehicle and cabled observatory technology to generate high-resolution data, tested ecological theory over multiple scales, developed several biologically relevant oxygen

thresholds, and highlighted the extreme adaptations of several species that persist in oxygen conditions previously considered 'lethal'. My continuous observations plus live experiments, the first reported for several of my focal species, gave insight into their natural oxygen limits (Chapter 2), reproductive life history (Chapter 3, Appendix D), and migratory behavior (Chapter 4). My results emphasize the importance of Saanich Inlet as a model system for studying the ecology of oxygen deficient systems. The quantitative framework I developed to process and analyze the large spatial and temporal data series of Chapter 2 and 3 can be applied across multiple aquatic and terrestrial systems. Below, I synthesize the results of my spatial surveys, time-series, and manipulative experiments to link changes in biological community structure to variable states of oxygen deficiency in benthic systems, and suggest directions for future research.

Generalized model of spatio-temporal succession in hypoxic communities

Figure 5.1 illustrates a synthesis of my combined results and draws a picture of the general patterns of community structure, progression, and tipping points under variable states of oxygen deficiency. My general model of spatio-temporal community progression in variable states of oxygen deficiency integrates niche-based theory with the concepts of how hypoxia alters ecosystem energy flow, as outlined by Diaz and Rosenberg (2008). Benthic communities are impacted by variable states of oxygen deficiency (hypoxia) because of both naturally occurring cycles of environmental variability and long-term trends of oxygen loss. Within communities, species-specific differences in oxyregulatory ability determine the co-existence of species along gradients of $[O_2]_{env}$ (Chapter 2; Chu & Tunnicliffe, 2015). Natural *in situ* oxygen occurrence (Chu

& Tunnicliffe, 2015), mode of life, (Chapter 3), hypoxia tolerance (Chapter 4; Chu & Gale, submitted), and species interactions (Anderson & Bell, 2014; Chapter 3) determine the co-occurrence, spatial arrangement, and relative abundance of benthic species along $[O_2]_{env}$ gradients. In temporally variable systems where critical oxygen boundaries expand and contract (Fig. 5.1a; Chapter 4; Chu & Gale, submitted), hypoxia-sensitive species (i.e., those having high O_2^{crit}) occur at a greater distance from their lower oxygen limits than do hypoxia-tolerance species (i.e., those having low O_2^{crit}); this creates disjunct distributions among coexisting species in a habitat (Chapter 2; Chu & Tunnicliffe, 2015). The total energy transferred to higher trophic levels in a system is determined by combined metabolism among individuals. Species with high oxygen demand (i.e., high standard metabolic rates) contribute more per capita to the total energy budget (Chapter 4; Chu & Gale, submitted). Systems with variable periods of oxygen deficiency will influence the spatial arrangement of biological communities. Loss of oxygen gradients in the system results in a loss of community structure; distributions of coexisting species are compressed to overlap in a reduced aerobic habitat space (Fig. 5.1b; Chapter 2; Chu & Tunnicliffe, 2015). A lowered state of overall energy transfer to higher trophic levels results from the absence of hypoxia-sensitive species, which will migrate in search of higher oxygen levels (Chapter 4; Chu & Gale, submitted).

In systems influenced by variable states of oxygen deficiency, species-specific traits determine critical thresholds within the community (Chapter 4; Chu & Gale, submitted). The timing and duration of the occurrence of $[O_2]_{env}$ below critical oxygen thresholds determines the timing and magnitude of the community response. Once a system is below critical thresholds, migration in all but a few hypoxia-tolerant species

reduces overall community abundance (Fig. 5.1c, Chapter 3). In the absence of most species interactions, dominant species remain but in reduced numbers. Extended duration below critical thresholds results in the mortality of sessile species (Chapter 3). Since sessile species can dominate total abundance, community recovery is slower than decline because, unlike for mobile species, the rate of recovery of sessile species is dependent on recruitment (Chapter 3). Long-term patterns of deoxygenation result in increased duration below hypoxia thresholds. A permanent regime shift in the community will occur when the duration below critical thresholds exceeds the time needed for the community to recover (Fig. 5.1, 'tipping point').

My general framework of community progression model fits the spatio-temporal patterns documented for a number of systems with variable states of hypoxia on both sides of the Atlantic Ocean. For example, hypoxia gradients structure seasonal distribution patterns of fish and invertebrate assemblages in the eastern United States (Pihl *et al.*, 1991; Altieri, 2012). Similar community turnover patterns over progressively worsening hypoxia are characteristic of the northern Gulf of Mexico (Rabalais *et al.*, 2002), and hypoxia-induced mortality followed by recruitment has been documented for the Patuxent estuary in Chesapeake Bay (Holland & Mountford, 1977; Holland *et al.*, 1987) where diel-vertical migrations also occur within the zooplankton and fish communities (Cuker & Watson, 2002; Ludsin *et al.*, 2009). Delayed community recovery, where the time to complete recovery takes far longer than the initial period over which hypoxia-induced exclusion of species occurred (i.e., hysteresis-like response trajectory, Diaz & Rosenberg, 2008), has been documented in the Gullmarsfjord, Sweden (Rosenberg *et al.*, 2002) and in the Black Sea (Mee *et al.*, 2005; Mee, 2006). At the small

scale, these Atlantic systems are influenced by anthropogenic eutrophication, however, ocean wide changes in open water circulation, ventilation, oxygen solubility further influence deoxygenation in the Atlantic (Stendardo & Gruber, 2012). This is exemplified by the long-term deoxygenation of the Laurentian Channel where the weakening of the Labrador Current has also been linked as the primary driver of reduced oxygen supply to inshore regions of Atlantic Canada (Gilbert *et al.*, 2005). Studies on Northern shrimp *Pandalus borealis* (Dupont-Prinet *et al.*, 2013) and Atlantic cod *Gadus morhua* (Chabot & Claireaux, 2008) also suggest metabolic constraints in hypoxia are analogous in Atlantic and Pacific Canada with differences being driven by environmental hypoxia threshold levels.

In the northeast Pacific Ocean, changes in oxygen-variability is primarily driven by the upwelling-dominated hypoxic systems in this region (Chan *et al.*, 2008; Roegner *et al.*, 2011; Booth *et al.*, 2012). Such regional-scale processes in the northeast Pacific are likely to have influenced the deoxygenation in Saanich Inlet, which is connected to the Pacific through the Salish Sea. Saanich Inlet has a long Holocene record of high productivity and seasonal hypoxia (O'Connell & Tunnicliffe, 2001), which does not align with the recent timeframe of hypoxic systems characterized by anthropogenic eutrophication (Rabalais *et al.*, 2014; Altieri & Gedan, 2015). The years when $[O_2]_{env}$ was depressed in Saanich Inlet (2010, 2013, 2015; Chapter 3, Fig.3.6b) correlate with El Niño conditions and temperature anomalies that were present offshore (Fisheries and Oceans Canada 2011; 2014; 2015). While the driver of the 10-year trend of deoxygenation in Saanich Inlet remains to be confirmed, there is congruence among oceans in the general

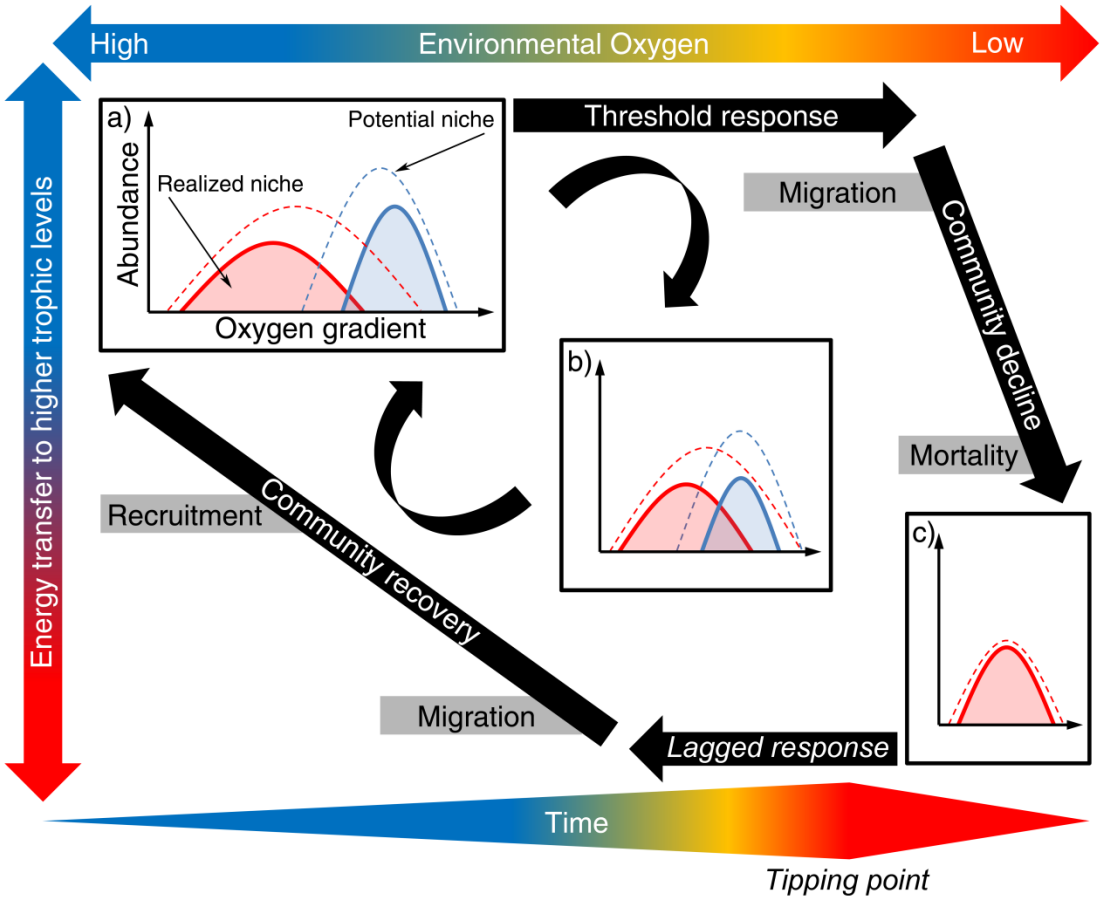

Figure 5.1. Species-specific traits determine community structure, progression, and tipping points in hypoxia-variable systems. Blue and red abundance curves represent two coexisting species that are differentiated by metabolic traits. Hypoxia-tolerant species occur closer to their lower hypoxia limits while hypoxia-sensitive species stay further away from their limits, leading to minimal spatial overlap among species. (b) Species-distributions naturally oscillate which dictate the amount of energy transferred to higher trophic levels. Hypoxia expansion reduces the oxygen gradient in the system; spatial overlap in distributions occurs when species are compressed into a smaller aerobic space. Less energy is transferred to higher trophic levels because hypoxia-sensitive species leave or become functionally anaerobic. (c) System gets pushed past a threshold. Migration and mortality exclude hypoxia-sensitive species; hypoxia-tolerant species remain but in reduced numbers. Rates of community decline are faster than rates of recovery because of mortality, which requires recruitment to increase energetic state back up to higher levels of energy transfer. Under long-term deoxygenation, the system progresses past the tipping point when the duration below threshold points exceeds the time needed for the community to recover to its higher energy-level state.

response and successional patterns in benthic communities exposed to variable states of oxygen deficiency.

Ecophysiology of multiple climate stressors

Rising atmospheric CO_2 is projected to shift the global average of temperature, pH, and oxygen detrimentally for marine ecosystems by the year 2100 (Bopp *et al.*, 2013; Mora *et al.*, 2013 Gattuso *et al.*, 2015). There is an urgent need to assess the cumulative effects of multiple climate stressors on biological communities because they naturally co-occur in most marine systems (e.g., upwelled deep waters along eastern boundary current regions are both hypoxic and acidic, Paulmier *et al.*, 2011). Future studies on climate change impacts need to address the effects of detrimental shifts in temperature, pCO_2/pH, and pO_2, as well as their combined contributions to the overall biological response. Together, detrimental shifts in temperature and pH directly reduce the capacity for aerobic ecotherms to physiologically acquire, transport, and deliver oxygen which ultimately limits the total aerobic energy transfer to higher trophic levels.

I apply the theoretical concept of oxygen- and capacity-limitation of thermal tolerance (OCLTT) outlined by Pörtner & Farrell (2008) and further developed by Pörtner (2010, 2012) to highlight how experimental respiratory physiology can serve as the tool that unites the effects of multiple climate stressors (Fig 5.2). The theory of OCLTT posits that the temperature-dependent performance of an individual is constrained by the capacity to supply oxygen to maintain physiological processes and detrimental shifts in temperature, pH/pCO_2, and pO_2 will limit the ability of organisms to acquire and deliver oxygen in relation to the change in oxygen demand. For water-

breathing ectotherms, aerobic performance (metabolism) is optimized over a narrow environmental temperature range (Pörtner & Farrell, 2008), where metabolic rates are highest at thermal optima and are species-specific. Physiological mechanisms act to regulate internal levels of pH and oxygen delivery, which is determined by the binding affinity of respiratory pigments (Hochachka & Somero, 2002). Projected increase in environmental temperature will reduce the functional temperature range for a species (Pörtner, 2010). Detrimental shifts in pH (ocean acidification) and pO_2 (hypoxia) reduces the binding affinity of respiratory pigments, resulting in a decrease in the overall efficiency in oxygen acquisition and delivery (Pörtner, 2008). Future detrimental shifts in these environmental variables will reduce the aerobic niche space of most marine ectotherms in the ocean (Pörtner & Knust, 2007; Deutsch *et al.*, 2015). The overall magnitude of aerobic potential lost as a result of multiple climate stressors will be partially offset by the acclimatization capacity for species in the short term (Stillman, 2003), adaptive capacity in the long-term (Hoffmann & Sgro, 2011), and the rate of change in the environment.

This general framework excludes indirect effects of climate-induced shifts in species interactions and phenology (Pörtner *et al.*, 2014) and assumes that the potential offset by compensatory processes (Crain *et al.*, 2008) are far exceeded by the unfavorable net effect of multiple climate stressors. Another caveat is that different mechanisms of oxygen acquisition and transport occur in lower-level animals such as sponges and cnidarians, as basal metazoans lack specialized structures and respiratory pigments for oxygen uptake and circulation found in higher level ectotherms. Although oxyregulation has evolved in some medusae (Thuesen *et al.*, 2005), basal metazoans have body plans

designed to maximize exposure of respiring cells to sea water for diffusion (Schmidt-Nielsen 1997) and most have only a partial ability to regulate oxygen uptake. Sponges and cnidarians are certainly not immune to detrimental shifts in their habitat (e.g., Chapter 3); however, the generality of the theory of OCLTT remains to be tested in these basal groups.

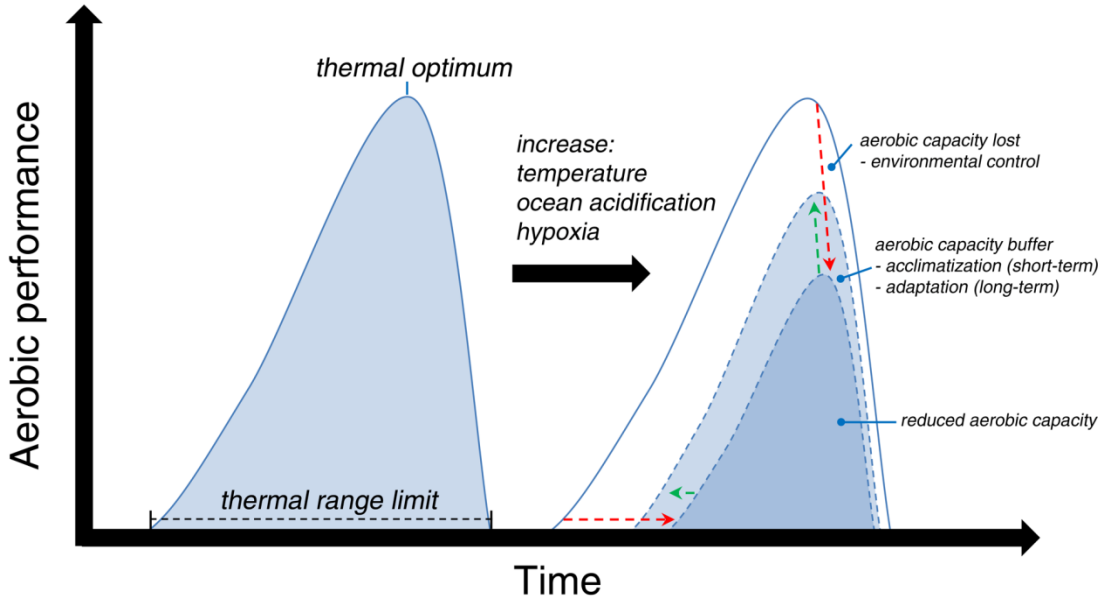

Figure 5.2. Physiological reduction in aerobic performance will result from the cumulative effects of multiple climate stressors. Over time, detrimental shifts in temperature, pCO_2, and hypoxia will result in an overall reduction in aerobic performance of individual species (red arrows). The potential to buffer reductions in aerobic performance (green arrows) and offset the potential loss in aerobic performance is determined by the capacity of a species to acclimatize in the short term or adapt in the long term, as well as the rate of change in the environment.

Predicting climate-change impacts on marine communities in the northeast Pacific

A possible extension of OCLTT is to integrate spatio-temporal projections of environmental change in temperature, pH, and oxygen to predict large-scale changes in

species distributions and functional losses incurred from reduced metabolism. This integrated approach has successfully been applied to Atlantic systems and species (Pörtner & Knust, 2007; Deutsch *et al.*, 2015) but may not be globally applicable until oceanographic and evolutionary history are also addressed (Chapter 4). In the northeast Pacific Ocean, multi-decadal, multi-species trawl surveys have been carried out by Fisheries and Oceans Canada, National Ocean and Atmospheric Administration (NOAA), the Southern California Coastal Water Research Project (SCCWRP), and the California Cooperative Oceanic Fisheries Investigations (CalCOFI) group (Orsi *et al.*, 2007; McClatchie *et al.*, 2014). The results of these surveys, through a concerted effort to combine data with different sampling methods, could realistically be used to address biogeographic shifts in community structure due to the climate-driven change in this region (e.g., Keller *et al.*, 2015). Other required biological data, such as regional-envelope data on ecophysiological limits and long-term ecological time-series, remain a constraint for making accurate forecasts on community-level responses under the current trajectory of climate change in the environment.

Species in my study occur throughout the continental shelf and slope of the northeast Pacific Ocean. Parameterization of their aerobic niche space is feasible because of their accessibility in Saanich Inlet. Although my results resolved short-term and seasonal patterns in hypoxic communities, extrapolating to broader scales (e.g., multi-decadal) would require scale-dependent structure to be assessed in both the environment and the biological response (Chapter 3). Resolving time-dependent shifts in community structure is more difficult because there are currently no ongoing programs generating high frequency datasets that have concomitant $[O_2]_{env}$ and biological measurements.

Because autocorrelation and multi-scale processes structure both the environmental and the community patterns, neutral processes may still dominate at the decadal scale; testing this would require extending biological observations over multiple years to match environmental records in this region.

Since VENUS launched in 2006, several permanent cabled observatories have been deployed throughout the northeast Pacific Ocean. Permanent infrastructure now exists at multiple stations in the Salish Sea (VENUS), on the continental shelf and slope of Canada (NEPTUNE) and Washington (OOI), at abyssal depths in Hawaii (ALOHA), in California (MARS), and in shallow-waters off Panama (PLUTO). With the multiple cabled observatory platforms located throughout this region comes optimism that their extensive oceanographic and geological monitoring programs will expand to include an equivalent emphasis on biological monitoring. This would provide a globally unique opportunity to look at spatio-temporal shifts at the regional and decadal scale for the entire biogeographic region of the northeast Pacific Ocean.

Literature cited

Altieri AH (2012) Dead Zones Enhance Key Fisheries Species by Providing Predation Refuge. *Ecology*, **89**, 2808–2818.

Altieri AH, Gedan KB (2015) Climate change and dead zones. *Global Change Biology*, **21**, 1395–1406.

Anderson GS, Bell LS (2014) Deep coastal marine taphonomy: investigation into carcass decomposition in the Saanich Inlet, British Columbia using a baited camera. *PloS ONE*, **9**, e110710.

Booth JAT, Mcphee-shaw EE, Chua P et al. (2012) Natural intrusions of hypoxic , low pH water into nearshore marine environments on the California coast. *Continental Shelf Research*, **45**, 108–115.

Bopp L, Resplandy L, Orr JC et al. (2013) Multiple stressors of ocean ecosystems in the 21st century: projections with CMIP5 models. *Biogeosciences*, **10**, 6225–6245.

Chabot D, Claireaux G (2008) Environmental hypoxia as a metabolic constraint on fish: The case of Atlantic cod, *Gadus morhua*. *Marine Pollution Bulletin*, **57**, 6-12.

Chan F, Barth JA, Lubchenco J, Kirincich A, Weeks H, Peterson WT, Menge BA (2008) Emergence of anoxia in the California current large marine ecosystem. *Science*, **319**, 920.

Chu JWF, Tunnicliffe V (2015) Oxygen limitations on marine animal distributions and the collapse of epibenthic community structure during shoaling hypoxia. *Global Change Biology*, **21**, 2989–3004.

Crain C, Kroeker K, Halpern B (2008) Interactive and cumulative effects of multiple human stressors in marine systems. *Ecology Letters*, **11**, 1304–1315.

Cuker BE, Watson MA (2002) Diel vertical migration of zooplankton in contrasting habitats of the Chesapeake Bay. *Estuaries*, **25**, 296-307.

Deutsch C, Farrel A, Seibel B, Portner H-O, Huey RB (2015) Climate change tightens a metabolic constraint on marine habitats. *Science*, **348**, 1132–1136.

Diaz RJ, Rosenberg R (2008) Spreading dead zones and consequences for marine ecosystems. *Science*, **321**, 926–929.

Dupont-Prinet A, Pillet M, Chabot D, Hansen T, Tremblay R, Audet C (2013) Northern shrimp (*Pandalus borealis*) oxygen consumption and metabolic enzyme activities are severely constrained by hypoxia in the Estuary and Gulf of St. Lawrence. *Journal of Experimental Marine Biology & Ecology*, **448**, 298-307.

Ege R, Krogh A (1914) On the Relation between the Temperature and the Respiratory Exchange in Fishes. *Internationale Revue der gesamten Hydrobiologie und Hydrographie*, **7**, 48–55.

Gattuso J-P, Magnan A, Bille R et al. (2015) Contrasting futures for ocean and society from different anthropogenic CO2 emissions scenarios. *Science*, **349**, aac4722–1–aac4722–10.

Hochachka PW, Somero GN (2002) *Biochemical adaptation, Mechanism and Process in Physiological Evolution*. Oxford University Press, Oxford, 478 pp.

Hoffmann AA, Sgro CM (2011) Climate change and evolutionary adaptation. *Nature*, **470**, 479–485.

Holland AF, Mountford NK (1977) Temporal Variation in Upper Bay Mesihaline Benthic Communities:I. The 9-m Mud Habitat. *Chesapeake Science*, **18**, 370–378.

Holland AF, Shaughnessy AT, Hiegel MH (1987) Long-term variation in mesohaline Chesapeake Bay macrobenthos: Spatial and temporal patterns. *Estuaries*, **10**, 227–245.

Keller AA, Ciannelli L, Wakefield WW, Simon V, Barth JA, Pierce SD (2015) Occurrence of demersal fishes in relation to near-bottom oxygen levels within the California Current large marine ecosystem. *Fisheries Oceanography*, **24**, 162-176.

Levin LA, Breitburg DL (2015) Linking coasts and seas to address ocean deoxygenation. *Nature Climate Change*, **5**, 401–403.

Ludsin SA, Zhang X, Brandt SB, Roman MR, Boicourt WC, Mason DM, Costantini M (2009) Hypoxia-avoidance by planktivorous fish in Chesapeake Bay: Implications for food web interactions and fish recruitment. *Journal of Experimental Marine Biology and Ecology*, **381**, S121-131.

McClatchie S, Duffy-Anderson J, Field JC et al. (2014) Long time series in US fisheries Oceanography. *Oceanography*, **27**, 48–68.

Mee LD, Friedrich J, Gomoiu MT (2005) Restoring in the Black Sea in Times of Uncertainty. *Oceanography*, **18**, 100–111.

Mora C, Wei CL, Rollo A et al. (2013) Biotic and human vulnerability to projected changes in ocean biogeochemistry over the 21st century. *PLoS Biology*, **11**, e1001682.

O'Connell JM, Tunnicliffe V (2001) The use of sedimentary fish remains for interpretation of long-term fish population fluctuations. *Marine Geology*, **174**, 177–

195.

Orsi JA, Harding JA, Pool SS et al. (2007) Epipelagic fish assemblages associated with juvenile Pacific salmon in neritic waters of the California current and the Alaska Current. *American Fisheries Society Symposium*, **57**, 105–155.

Paulmier A, Ruin-Pino D, Garçon V (2011) CO_2 maximum in the oxygen minimum zone (OMZ). *Biogeosciences*, **8**, 239-252.

Pihl L, Baden SP, Diaz RJ (1991) Effects of periodic hypoxia on distribution of demersal fish and crustaceans. *Marine Biology*, **108**, 349–360.

Pörtner H (2008) Ecosystem effects of ocean acidification in times of ocean warming: a physiologist's view. *Marine Ecology Progress Series*, **373**, 203–217.

Pörtner H (2010) Oxygen- and capacity-limitation of thermal tolerance: a matrix for integrating climate-related stressor effects in marine ecosystems. *Journal of Experimental Biology*, **213**, 881–893.

Pörtner HO (2012) Integrating climate-related stressor effects on marine organisms: Unifying principles linking molecule to ecosystem-level changes. *Marine Ecology Progress Series*, **470**, 273–290.

Pörtner HO, Farrell AP (2008) Physiology and Climate Change. *Science*, **322**, 690–692.

Pörtner HO, Knust R (2007) Climate change affects marine fishes through the oxygen limitation of thermal tolerance. *Science*, **315**, 95–97.

Pörtner H-O, Schmidt DN, Roberts JM, Rost B (2014) Ocean Systems. In Climate Change 2014: Impacts, Adaptation, and Vulnerability. Part A: Global and Sectoral Aspects. Contribution of Working Group II to the Fifth Assessment Report of the Intergovernmental Panel on Climate Change, pp. 411–484.

Rabalais NN, Turner RE, Wiseman WJ (2002) Gulf of Mexico Hypoxia, a.k.a. "the Dead Zone." *Annual Review of Ecology and Systematics*, **33**, 235–263.

Rabalais NN, Cai W-J, Carstensen J et al. (2014) Eutrophication-driven deoxygenation in the coastal ocean. *Oceanography*, **27**, 172–183.

Roegner GC, Needoba JA, Baptista AM (2011) Coastal upwelling supplies oxygen-depleted water to the Columbia River Estuary. *PLoS ONE*, **6**, e18672.

Rosenberg R, Agrenius S, Hellman B, Nilsson H, Norling K (2002) Recovery of marine benthic habitats and fauna in a Swedish fjord following improved oxygen conditions. *Marine Ecology Progress Series*, **234**, 43–53.

Semenza GL (2007) Life with oxygen. *Science*, **318**, 62–64.

Stillman JH (2003) Acclimation capacity underlies susceptibility to climate change. *Science*, **301**, 65.

Thannickal VJ (2009) Oxygen in the Evolution of Complex Life and the Price We Pay. *American Journal of Respiratory Cell and Molecular Biology*, **40**, 507–510.

Thuesen E V, Rutherford LD, Brommer PL, Garrison K, Gutowska MA, Towanda T (2005) Intragel oxygen promotes hypoxia tolerance of scyphomedusae. *The Journal of Experimental Biology*, **208**, 2475–2482.

Appendix A: Supporting material for Chapter 2

Table A.1. Metadata of transect lines. R - ROPOS; OE - Oceanic Explorer; water data collected using CTD+O_2 mounted to the remotely operated vehicle.

		Depth (m)		Oxygen (ml l^{-1})		Temperature (°C)		Salinity (PSU)		Density (kg m^{-3})	
Date	Transect	deep	shallow	mean	stdev	mean	stdev	mean	stdev	mean	stdev
2006/Nov/10	R1027	103.0	77.2	0.8	0.7	9.9	0.03	31.3	0.1	1024.5	0.1
2007/Feb/03	R1034-35	192.2	59.7	1.7	1.9	9.3	0.6	30.9	0.5	1024.5	0.4
2008/Sep/28	R1176	188.3	55.7	0.7	0.5	9.3	0.2	31.2	0.2	1024.6	0.3
2009/Feb/15	R1197	187.7	104.7	0.4	0.6	9.1	0.3	31.2	0.2	1024.8	0.2
2010/Dec/10	R1396	119.2	77.3	1.2	1.1	9.3	0.2	30.8	0.2	1024.2	0.2
2011/Oct/02	R1491	187.1	75.7	0.6	0.2	9.1	0.03	30.4	0.1	1024.1	0.3
2012/Aug/12	R1588	173.0	82.9	0.5	0.2	8.8	0.1	30.9	0.1	1024.5	0.2
2013/May/07	OE0045	185.1	48.5	1.4	1.5	8.6	0.3	30.8	0.5	1024.4	0.5
2013/Sep/07	R1645	185.5	50.8	0.8	0.5	9.2	0.2	31.0	0.3	1024.5	0.4
2013/Oct/14	R1677	187.1	43.1	1.1	1.1	9.6	0.6	30.8	0.5	1024.2	0.7

Table A.2. Animal count data by transect date and summary of *in situ* oxygen occurrence by species. Oxygen data are presented in both units of concentration (ml l^{-1}) and partial pressure (kPa).

	METADATA		
Common name	***Scientific Name***	***Major Group***	***Data Type***
Bacterial mat	*Beggiatoa spp.*	**Bacteria**	*presence/absence*
Ball sponge	*Suberities sp.*	sponge	*presence/absence*
Finger sponge	*Syringella sp.*	sponge	*presence/absence*
Slender sole	*Lyopsetta exilis*	fish	*count*
Pollock	*Theragra chalcogramma*	fish	*count*
Bluebarred prickleback	*Plectobranchus evides*	fish	*count*
Blackbelly eelpout	*Lycodopsis pacifica*	fish	*count*
Snake prickleback	*Lumpenus sagitta*	fish	*count*
Blacktip poacher	*Xeneretmus latifrons*	fish	*count*
Pacific hake	*Merluccius productus*	fish	*count*
Plainfin midshipman	*Porichthys notatus*	fish	*count*
English sole	*Parophrys vetulus*	fish	*count*
Shiner perch	*Cymatogaster aggregata*	fish	*count*
Rock sole	*Lepidopsetta bilieneata*	fish	*count*
Northern Ronquil	*Ronquilus jordani*	fish	*count*
Pacific Sanddab	*Citharichthys sp.*	fish	*count*
Cabezon	*Scorpaenichthys marmoratus*	fish	*count*
Dover sole	*Microstomus pacificus*	fish	*count*
Longnose Skate	*Raja rhina*	fish	*count*
Sculpin	*unknown teleost*	fish	*count*
Greenstripe Rockfish	*Sebastes elongatus*	fish	*count*
Pacific Dogfish	*Squalus acanthias*	fish	*count*
Longspine Combfish	*Zaniolepis latipinnis*	fish	*count*
Red Rockfish	*Sebastes sp.*	fish	*count*
Squat lobster	*Munida quadrispina*	crustaceans	*count*
Pink shrimp	*Pandalus jordani*	crustaceans	*count*
Spot prawn	*Pandalus platyceros*	crustaceans	*count*
Humpback shrimp	*Pandalus hypsinotus*	crustaceans	*count*
Spirontocarid shrimp	*Spirontocaris sp.*	crustaceans	*count*
Dungeness crab	*Metacarcinus magister*	crustaceans	*count*
Tanner crab	*Chionoectes bairdi*	crustaceans	*count*
Red rock crab	*Cancer productus*	crustaceans	*count*
Decorator crab	*Chorilia longipes*	crustaceans	*count*
Red Octopus	*Octopus rubescens*	mollusc	*count*
Tritonia nudibranch	*Tritonia sp.*	mollusc	*count*
Spiny pink seastar	*Pisaster brevispinus*	echinoderm	*count*
Mottled star	*Evasterias troschelli*	echinoderm	*count*
Sunflower star	*Pycnopodia helianthoides*	echinoderm	*count*
Mudstar	*Luidia foliolata*	echinoderm	*count*
Rainbow star	*Orthasterias koehleri*	echinoderm	*count*
Sunstar	*Solaster sp.*	echinoderm	*count*
Seawhip	*Halipteris willemoesi*	cnidarian	*count*
Giant anemone	*Metridium farcinem*	cnidarian	*count*
Crimson anemone	*Cribinopsis fernaldi*	cnidarian	*count*
Orange seapen	*Ptilosarcus gurneyi*	cnidarian	*count*

	COUNTS										
Common name	***R1027, 2006-11-10***	***R10345, 2007-02-04***	***R1176, 2008-09-28***	***R1197, 2009-02-15***	***R1396, 2010-12-10***	***R1491, 2011-10-02***	***R1588, 2012-08-12***	***OE0045, 2013-05-07***	***R1645, 2013-09-07***	***R1677, 2013-10-14***	***TOTAL BY SP.***
Bacterial mat	910	3117	3825	2074	2059	3965	2238	2727	2050	2688	
Ball sponge	29	531	639		275	661	562	407	580	584	
Finger sponge	1	10	5		21	172	54	3	156	78	
Slender sole	513	269	2562	123	1100	1484	1810	1712	1952	1553	***13078***
Pollock	22	894	24	4	67	12	8	6	3	21	***1061***
Bluebarred prickleback	31	26	83	1	41	89	63	130	123	195	***782***
Blackbelly eelpout	14	11	89		26	84	55	100	99	114	***592***
Snake prickleback	2		24		132	22	3	21	92	123	***419***
Blacktip poacher	66	14	52	1	17	74	86	46	58	65	***479***
Pacific hake	40	121		87	35	8		4	18	12	***325***
Plainfin midshipman	7		60			34			8	41	***150***
English sole	1	26	8		7	18	4	15	34	8	***121***
Shiner perch	21	4	13		30			2		9	***79***
Rock sole	3	4	2		2		5	5	6	14	***41***
Northern Ronquil					3				5	27	***35***
Pacific Sanddab	1		6		4	2	6	3	3	3	***28***
Cabezon					1			2	3	4	***10***
Dover sole					1				2	1	***4***
Longnose Skate			2							1	***3***
Sculpin			1							1	***2***
Greenstripe Rockfish						1	1				***2***
Pacific Dogfish							1				***1***
Longspine Combfish					1						***1***
Red Rockfish										1	***1***
Squat lobster	935	662	1240	62	887	955	1102	1839	1559	2138	***11379***
Pink shrimp	16	35	2242		40	303	220	88	1183	712	***4839***
Spot prawn	75	186	286		419	88	7	670	281	684	***2696***
Humpback shrimp	18	11	17		6		11	25	71	168	***327***
Spirontocarid shrimp	49								43		***92***
Dungeness crab		3	8		3			5	17	5	***41***
Tanner crab		1	1		3		1	3	7	15	***31***
Red rock crab						4					***4***
Decorator crab							1				***1***
Red Octopus	3				1				1		***5***
Tritonia nudibranch								2			***2***
Spiny pink seastar		2	1			10		6	12	11	***42***
Mottled star			2			4	1			3	***10***
Sunflower star			4		1				1	1	***7***
Mudstar			1				1		2		***4***
Rainbow star										1	***1***
Sunstar								1			***1***
Seawhip	338	1604	6065		707	370	209	2527	2509	3875	***18204***
Giant anemone	19	109	262		63	85	48	18	30	30	***664***
Crimson anemone									3	1	***4***
Orange seapen										3	***3***
TOTAL BY TRANSECT	***2174***	***3982***	***13055***	***278***	***3597***	***3647***	***3643***	***7230***	***8125***	***9840***	***55571***

	In situ Oxygen occurrence summary (ml/L)						*In situ Oxygen occurrence summary (kPa)*					
Common name	*Mean*	*median*	*min*	*max*	*sd*	*range*	*Mean*	*median*	*min*	*max*	*sd*	*range*
Bacterial mat	0.39	0.39	0.00	1.83	0.32	1.8	1.33	1.33	0.00	6.08	1.06	6.1
Ball sponge	1.14	0.84	0.18	3.77	0.85	3.6	3.82	2.84	0.62	12.52	2.80	11.9
Finger sponge	1.02	0.86	0.29	3.73	0.45	3.4	3.44	2.90	0.98	12.40	1.50	11.4
Slender sole	0.96	0.72	0.00	4.84	0.75	4.8	3.21	2.42	0.01	15.85	2.48	15.8
Pollock	0.57	0.52	0.00	4.64	0.59	4.6	1.94	1.78	0.01	15.23	1.98	15.2
Bluebarred prickleback	0.98	0.81	0.18	4.70	0.66	4.5	3.27	2.71	0.62	15.38	2.20	14.8
Blackbelly eelpout	1.43	1.02	0.31	4.88	1.06	4.6	4.76	3.45	1.06	15.96	3.46	14.9
Snake prickleback	2.19	2.22	0.53	4.83	0.98	4.3	7.36	7.54	1.76	15.80	3.24	14.0
Blacktip poacher	1.00	0.77	0.17	4.76	0.77	4.6	3.35	2.59	0.59	15.57	2.53	15.0
Pacific hake	0.68	0.59	0.00	2.90	0.58	2.9	2.28	2.02	0.01	9.94	1.94	9.9
Plainfin midshipman	1.20	0.97	0.33	2.89	0.61	2.6	4.07	3.27	1.14	9.93	2.10	8.8
English sole	2.26	3.81	0.53	1.14	1.60	0.6	7.51	3.86	1.76	15.80	5.22	14.0
Shiner perch	2.17	1.98	0.52	4.77	0.70	4.3	7.34	6.79	1.75	15.62	2.28	13.9
Rock sole	2.19	2.22	0.54	4.77	1.20	4.2	7.34	7.58	1.79	15.60	3.96	13.8
Northern Ronquil	2.67	2.86	1.81	3.00	0.36	1.2	9.12	6.15	6.15	10.30	1.26	4.2
Pacific Sanddab	1.58	0.91	0.39	4.79	1.24	4.4	5.28	3.08	1.34	15.66	4.09	14.3
Cabezon	2.48	2.68	1.00	3.71	0.85	2.7	8.37	9.16	3.37	12.17	2.81	8.8
Dover sole	2.02	2.00	0.95	3.13	1.17	2.2	6.83	6.83	3.21	10.46	3.95	7.3
Longnose Skate	0.68	0.69	0.54	0.82	0.14	0.3	2.31	2.35	1.83	2.76	0.46	0.9
Sculpin	1.92	1.92	1.42	2.42	0.71	1.0	6.55	6.55	4.83	8.27	2.43	3.4
Greenstripe Rockfish	0.63	0.63	0.60	0.65	0.03	0.0	2.10	2.10	2.02	2.17	0.11	0.1
Pacific Dogfish	0.59	0.59	0.59	0.59	NA	NA	1.97	1.97	1.97	1.97	NA	NA
Longspine Combfish	3.16	3.16	3.16	3.16	NA	NA	10.54	10.54	10.54	10.54	NA	NA
Red Rockfish	0.56	0.56	0.56	0.56	NA	NA	1.89	1.89	1.89	1.89	NA	NA
Squat lobster	0.72	0.65	0.01	3.15	0.31	3.1	2.41	2.21	0.02	10.52	1.04	10.5
Pink shrimp	1.59	1.38	0.52	4.83	0.71	4.3	5.37	4.67	1.74	15.79	2.37	14.0
Spot prawn	2.47	2.33	0.42	4.87	1.23	4.5	8.23	7.82	1.45	15.95	4.00	14.5
Humpback shrimp	2.21	2.63	0.53	4.65	0.77	4.1	7.52	8.96	1.78	15.27	2.61	13.5
Spirontocarid shrimp	0.61	0.58	0.17	1.05	0.42	0.9	2.09	1.99	0.59	3.56	1.40	3.0
Dungeness crab	2.01	1.99	0.87	4.66	1.02	3.8	6.75	6.76	2.93	15.28	3.35	12.3
Tanner crab	1.83	1.69	0.54	3.97	0.82	3.4	6.17	5.74	1.79	13.02	2.72	11.2
Red rock crab	0.75	0.69	0.67	0.93	0.12	0.3	2.50	2.32	2.26	3.11	0.41	0.9
Decorator crab	0.60	0.60	0.60	0.60	NA	NA	2.00	2.00	2.00	2.00	NA	NA
Red Octopus	1.02	0.83	0.18	2.24	0.76	2.1	3.46	2.85	0.63	7.55	2.53	6.9
Tritonia nudibranch	3.50	3.50	3.49	3.50	0.01	0.0	11.48	11.48	11.46	11.51	0.03	0.0
Spiny pink seastar	2.17	1.99	0.47	4.80	1.45	4.3	7.26	6.74	1.59	15.69	4.75	14.1
Mottled star	1.29	0.87	0.53	2.65	0.85	2.1	4.39	2.91	1.75	9.07	2.93	7.3
Sunflower star	1.58	1.51	0.68	2.61	0.75	1.9	5.35	5.12	2.31	8.75	2.55	6.4
Mudstar	1.21	1.01	0.54	2.28	0.79	1.7	4.12	3.42	1.78	7.83	2.73	6.0
Rainbow star	2.66	2.66	2.66	2.66	NA	NA	9.10	9.10	9.10	9.10	NA	NA
Sunstar	4.63	4.63	4.63	4.63	NA	NA	15.11	15.11	15.11	15.11	NA	NA
Seawhip	2.48	2.38	0.46	4.88	1.28	4.4	8.32	8.12	1.56	15.96	4.18	14.4
Giant anemone	1.11	0.67	0.19	4.79	0.97	4.6	3.75	2.25	0.64	15.65	3.22	15.0
Crimson anemone	1.84	1.83	1.05	2.65	0.65	1.6	6.25	6.20	3.53	9.06	2.25	5.5
Orange seapen	2.88	2.88	2.88	2.88	0.00	0.0	9.89	9.89	9.88	9.90	0.01	0.0

Video A.1. Epibenthic community structure along the hypoxia gradient in Saanich Inlet. Deeper waters (>120 m) in Saanich Inlet are characterized by low dissolved oxygen concentrations (<0.1 ml l^{-1}) and variably dense H_2S bacterial mats (*Beggiatoa* spp.). High densities of slender sole (*Lyopsetta exilis*) and squat lobster (*Munida quadrispina*) can occur here. Slender sole bury themselves in the bacterial mat; intense flatfish activity resuspends substantial amounts of the sediment creating pits. Changes in the community composition and structure occurs concurrently with the oxygen profile as it transitions from near anoxia (<0.01 ml l^{-1}) to severe hypoxia (<0.5 ml l^{-1}) and hypoxia (<1.4 ml l^{-1}) and into oxygenated waters (>2 ml l^{-1}) that are typical of the shallowest depths (~45 m).

Please refer to data in the supporting document ***gcb12898-sup-0003-VideoS2.avi***

access at: http://onlinelibrary.wiley.com/wol1/doi/10.1111/gcb.12898/suppinfo

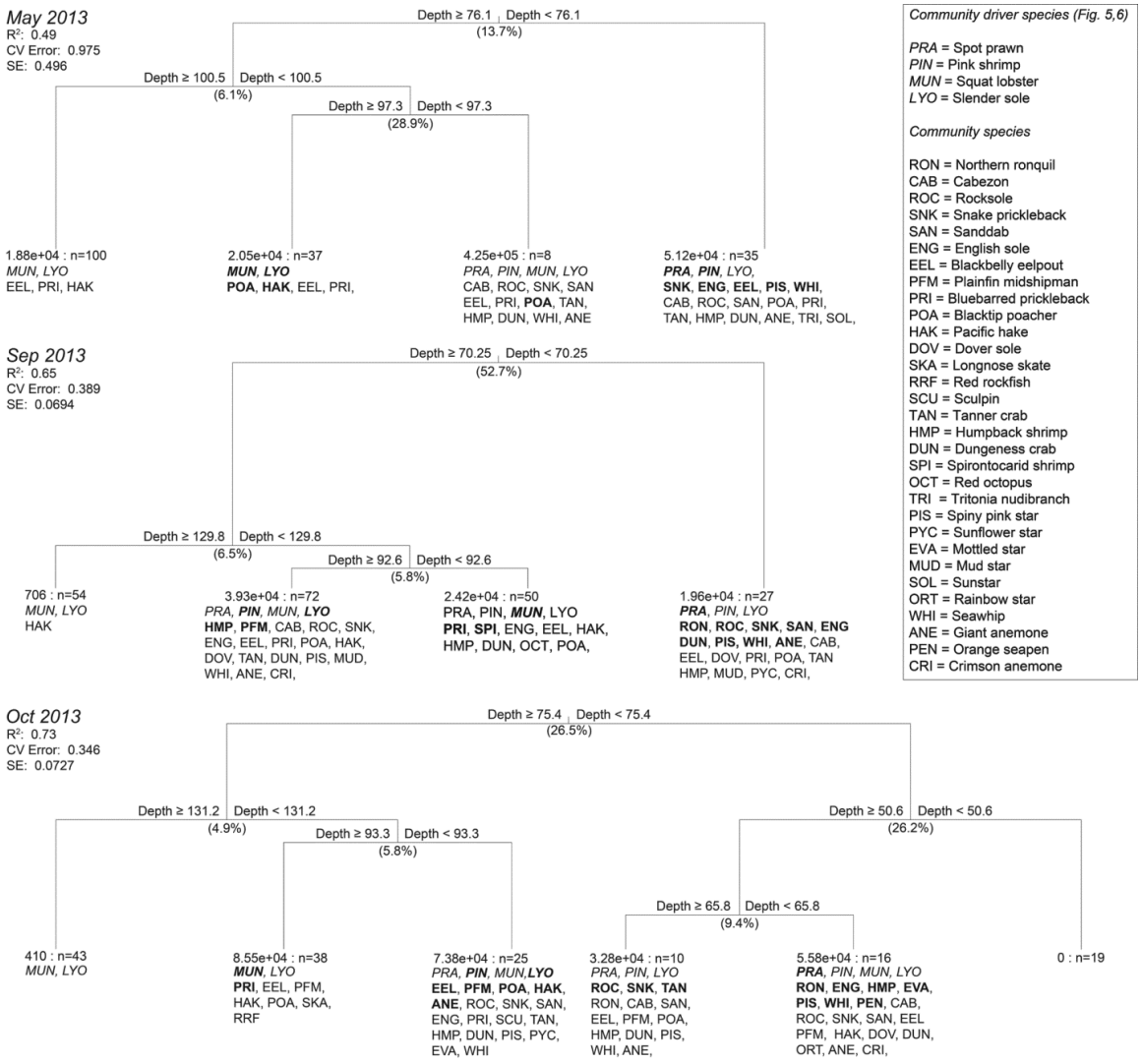

Figure A.1. Constrained clustering of 2013 transect data using multivariate regression tree (MRT) analysis illustrates spatial partitioning and coalescence of species distributions in hypoxia. *May*: Partitioned species distributions correlated to the well-defined oxygen gradient (Fig. 2.1 May 2013). Slender sole and squat lobster were indicator species of the deeper, less oxygenated waters; rest of species assemblage and most commercially important species were partitioned to shallower depths. *Sep:* Because the oxygen gradient was homogeneous (Fig.2.1 Sep 2013), distribution of the hypoxia-tolerant species coalesced with rest of the community assemblage. Slender sole and squat

lobsters became indicator species of shallower depths compared to May; pink shrimp became indicator species of deeper depths relative to squat lobster. *Oct*: During oxygen renewal, species distributions repartitioned. A community subgroup defined the shallowest depths where high oxygen concentrations reappeared (Fig. 2.1 Oct 2013). Squat lobsters returned to indicator species status for deeper depths.

MRT analysis (De'ath, 2002) clustered sites (20 m^2 sections along transect, see Methods) based on the composition of species; tree creation was constrained by bottom depth for each transect. Multiple trees were generated (n=100) and cross-validated to generate the most parsimonious and best predictive tree. The variance explained by each split is summarized at the node in parentheses. The relative error and number of sites is given at each leaf. Species occurrences are summarized for each leaf; the four mobile species identified as the drivers of community structure (Fig. 2.5, Fig. 2.6) are listed first (in italics) followed by the rest of the species assemblage. Indicator species (in bold) were determined for each leaf (*'IndVal'*, Dufrene & Legendre, 1997) which represents a species that has high specificity (large mean abundance in a leaf relative to other leaves) and fidelity (present in most sites within a leaf).

Literature cited

De'ath G (2002) Multivariate regression trees: A new technique for modeling species-environment relationships. *Ecology*, **83**, 1105–1117.

Dufrene M, Legendre P (1997) Species Assemblages and Indicator Species: the Need for a Flexible Asymmetrical Approach. *Ecological Monographs*, **67**, 345–366.

Appendix B: Supporting material for Chapter 3

Video B.1. Transitional phases of the epibenthic community in seasonal hypoxia, Saanich Inlet. Please refer to video at https://vimeo.com/57821838. Video is from August 22, 2012 to December 31, 2012 and shows the broad-scale transition of the epibenthic community as environmental oxygen declines towards zero. Species composition is characterized by a mixed assemblage of mobile and sessile species during the period of high $[O_2]_{env}$ at the start of the imagery series macroinfauna such as the callianasid shrimp *Neotrypaea californiensis* and tubiculous polychaetes emerged from the sediment during deoxygenation. Sessile species such as two giant anemones *Metridum farcimen*, ball sponge *Suberites simplex*, and finger sponge *Syringella amphispicula*, survived throughout the anoxic period before mass mortality occured at the end of the imagery time series.

Table B.1. Slender sole *Lyopsetta exilis* were counted from ROV surveys flown along the same section of a benthic transect line at 100 to 120 m depth in Saanich Inlet (see Chapter 2) during night and day (local time). The total abundance is the sum of unburied, partially buried, and buried counts of slender sole. Unburied individuals were observed to be 100% above the sediment. Partially buried individuals were observed to have 50% of body surface above sediments. Buried individuals were observed to have <10% body surface above sediments.

	Night	Day (dawn)
ROV transect	R1645 – Sep.7, 2013	R1647 – Sep. 8, 2013
Time (local time zone)	21:35 to 22:07	4:01 to 4:36
Total abundance	**518**	**807**
Unburied	297	568
Partially buried	50	56
Buried	171	183

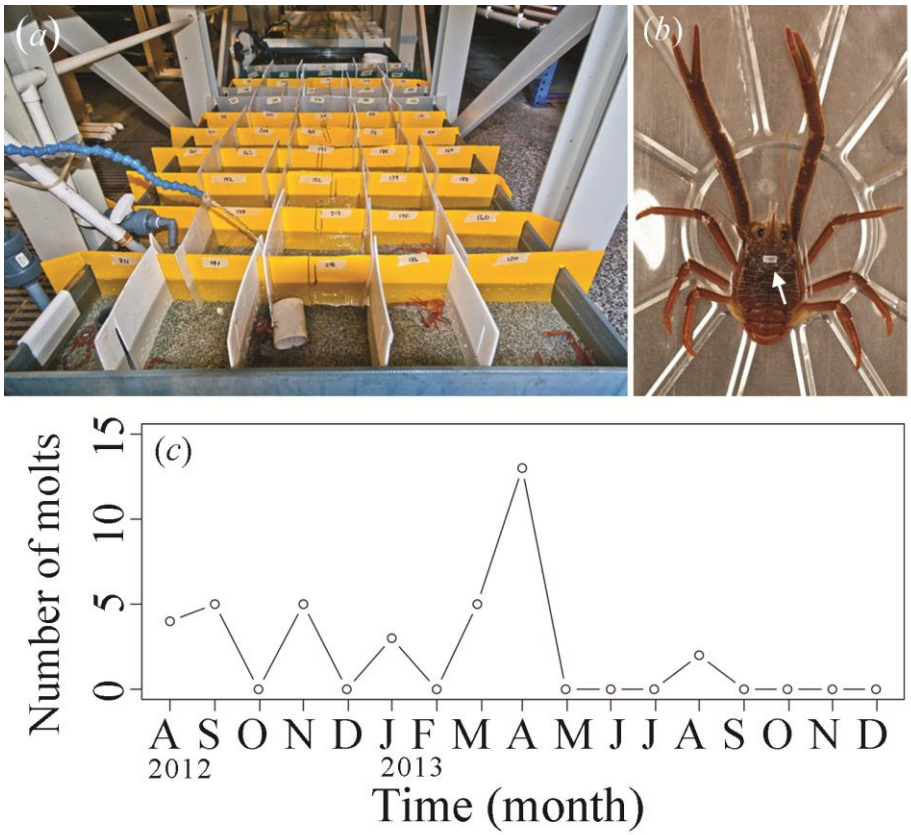

Figure B.1. A population of squat lobster *Munida quadrispina* was maintained for lab experiments (see Chapter 4). (a) Individual squat lobsters (n=100) were kept in oxygen saturated, recirculating sea water tables at the University of Victoria from August 2012 – December 2013 and isolated from each other because of cannibalism. Sea water tables were kept under black plastic for the duration of captivity (removed for this image). (b) Individual squat lobsters were tagged with unique identifiers (arrow) which were superglued onto their carapace and retagged after molting. (c) A marked increase in the number of molted squat lobsters occurred in April 2013.

Appendix C: Supporting material for Chapter 4

Table C.1. Global meta-analysis of O_2^{crit} values for crustaceans. *Physiology and geographic data*.

Species	o2crit_mlL	o2crit_kpa	Temperature	Salinity	Ocean	latitude_dd	longitude_dd	Exploitation
Gammarus duebeni	0.36	1.34	20	34	East Atlantic	50.350	-4.450	No
Gammarus duebeni	0.72	2.67	20	34	East Atlantic	50.350	-4.450	No
Echinogammarus pirloti	0.65	2.20	15	32	East Atlantic	55.733	-4.952	No
Echinogammarus obtusatus	0.67	2.20	13	32	East Atlantic	55.733	-4.952	No
Penaeus monodon	0.35	1.41	27.1	32	South Pacific	-29.379	153.289	Yes
Lithodes santolla	1.48	4.70	11	32	East Pacific	-39.805	-73.271	Yes
Petrolisthes laevigatus	1.64	5.20	11	32	East Pacific	-41.700	-73.700	No
Petrolisthes laevigatus	1.64	5.20	11	32	East Pacific	-41.700	-73.700	No
Calocaris macandreae	0.30	0.93	10	32	East Atlantic	55.533	-4.837	No
Cancer pagurus	2.57	8.00	10	32	East Atlantic	55.765	-4.926	Yes
Corystes cassivelaunus	1.06	3.33	10	34	East Atlantic	52.086	-4.756	No
Galathea strigosa	1.90	6.00	10	34	East Atlantic	52.086	-4.756	No
Galathea strigosa	2.33	7.33	10	34	East Atlantic	52.086	-4.756	No
Galathea strigosa	2.33	7.33	10	34	East Atlantic	52.086	-4.756	No
Corystes cassivelaunus	2.45	7.73	10	34	East Atlantic	52.086	-4.756	No
Munida quadrispina	0.14	0.43	10	30	East Pacific	48.547	-123.525	No
Homarus gammarus	0.79	2.67	15	32	East Atlantic	56.333	-2.772	Yes
Maja brachydactyla	2.24	8.51	20.55	37	East Atlantic	37.833	-0.767	Yes
Maja brachydactyla	2.26	8.81	22.61	37	East Atlantic	37.833	-0.767	Yes
Boreomysis californica	0.14	0.41	5.5	32	East Pacific	33.000	-118.700	No
Pleuroncodes planipes	0.16	0.53	15	32	East Pacific	33.000	-118.700	Yes
Pasiphaea emarginata	0.20	0.57	5.5	32	East Pacific	33.000	-118.700	No
Plesionika sp.	0.26	0.80	5.5	32	East Pacific	33.000	-118.700	No
Neognathophausia ingens	0.28	0.80	5.5	32	East Pacific	33.000	-118.700	No
Gnathophausia zoea	0.33	0.93	5.5	32	East Pacific	33.000	-118.700	No
Sergia phorca	0.33	0.93	5.5	32	East Pacific	33.000	-118.700	No
Bathycalanus princeps	0.34	0.97	5.5	32	East Pacific	33.000	-118.700	No
Systellaspis cristata	0.34	0.97	5.5	32	East Pacific	33.000	-118.700	No
Hymenodora frontalis	0.36	1.03	5.5	32	East Pacific	33.000	-118.700	No
Gennadas propinquus	0.37	1.07	5.5	32	East Pacific	33.000	-118.700	No
Pseudocallisoma coecum	0.37	1.07	5.5	32	East Pacific	33.000	-118.700	No

Acanthephyra curtirostris	0.39	1.11	5.5	32	East Pacific	33.000	-118.700	No
Bathycalanus richardi	0.43	1.20	4	32	East Pacific	33.000	-118.700	No
Gaussia princeps	0.45	1.33	7	32	East Pacific	33.000	-118.700	No
Neognathophausia gigas	0.48	1.33	4	32	East Pacific	33.000	-118.700	No
Fagegnathophausia gracilis	0.49	1.36	4	32	East Pacific	33.000	-118.700	No
Gigantocypris agassizii	0.50	1.40	4	32	East Pacific	33.000	-118.700	No
Neognathophausia ingens	0.53	1.47	4	32	East Pacific	33.000	-118.700	No
Pasiphaea pacifica	0.54	1.60	7.5	32	East Pacific	33.000	-118.700	No
Anuropus bathypelagicus	0.65	1.87	5.5	32	East Pacific	33.000	-118.700	No
Notostomus sp.	0.67	1.87	4	32	East Pacific	33.000	-118.700	No
Phronima sedentaria	0.69	2.13	10	32	East Pacific	33.000	-118.700	No
Euphausia pacifica	0.77	2.40	10	32	East Pacific	33.000	-118.700	Yes
Hyperia galba	0.79	2.47	10	32	East Pacific	33.000	-118.700	No
Pasiphaea chacei	0.81	2.40	7.5	32	East Pacific	33.000	-118.700	No
Eusergestes similis	0.88	2.73	10	32	East Pacific	33.000	-118.700	No
Palaemonetes pugio	1.18	5.20	30	25	West Atlantic	32.744	-79.938	No
Gnathophausia zoea	0.66	2.05	10	32	East Pacific	21.333	-158.333	No
Oplophorus spinosus	0.78	2.43	10	32	East Pacific	21.333	-158.333	No
Neognathophausia gigas	0.81	2.29	5	32	East Pacific	21.333	-158.333	No
Thysanopoda cornuta	0.85	2.64	5	32	East Pacific	21.333	-158.333	No
Notostomus elegans	0.98	3.04	10	32	East Pacific	21.333	-158.333	No
Acanthephyra smithi	1.17	3.64	10	32	East Pacific	21.333	-158.333	No
Notostomus elegans	1.20	3.73	10	32	East Pacific	21.333	-158.333	No
Acanthephyra acutifrons	1.24	3.85	10	32	East Pacific	21.333	-158.333	No
Acanthephyra curtirostris	1.24	3.85	10	32	East Pacific	21.333	-158.333	No
Fagegnathophausia gracilis	1.26	3.57	5	32	East Pacific	21.333	-158.333	No
Sergia tenuiremis	1.37	4.25	10	32	East Pacific	21.333	-158.333	No
Systellaspis debilis	1.50	4.67	10	32	East Pacific	21.333	-158.333	No
Sergia bisulcata	1.68	5.23	10	32	East Pacific	21.333	-158.333	No
Sergia fulgens	1.70	5.31	10	32	East Pacific	21.333	-158.333	No
Oplophorus gracilirostris	1.73	5.40	10	32	East Pacific	21.333	-158.333	No
Jasus edwardsii	2.19	7.31	13	35	South Pacific	-42.949	147.363	Yes
Panulirus cygnus	1.35	4.66	15	35	Indian	-28.770	114.606	Yes
Panulirus cygnus	1.46	5.66	23	35	Indian	-28.770	114.606	Yes
Panulirus cygnus	1.56	6.69	31	35	Indian	-28.770	114.606	Yes
Munida quadrispina	0.21	0.64	9	31	East Pacific	48.664	-123.481	No
Pandalus platyceros	1.01	3.07	9	31	East Pacific	48.673	-123.528	Yes
Penaeus esculentus	1.23	3.74	25	35	South Pacific	-27.206	153.250	Yes
Callinectes similis	1.48	5.73	24	30	West Atlantic	29.112	-90.190	Yes
Callinectes sapidus	3.66	14.13	24	30	West Atlantic	30.407	-88.832	Yes
Rhithropanopeus harrisii	0.57	1.77	10	32	West Atlantic	35.131	-76.504	No

Funchalia villosa	0.90	2.67	7	32	West Atlantic	27.000	-86.000	No
Stylopandalus richardi	0.95	3.33	17	32	West Atlantic	27.000	-86.000	No
Sergia robusta	0.95	3.33	17	32	West Atlantic	27.000	-86.000	Yes
Gennadas valens	1.00	3.33	14	32	West Atlantic	27.000	-86.000	No
Parasergestes armatus	1.00	3.33	14	32	West Atlantic	27.000	-86.000	No
Funchalia villosa	1.09	4.00	20	32	West Atlantic	27.000	-86.000	No
Gennadas scutatus	1.09	4.00	20	32	West Atlantic	27.000	-86.000	No
Gennadas valens	1.09	4.00	20	32	West Atlantic	27.000	-86.000	No
Oplophorus gracilirostris	1.09	4.00	20	32	West Atlantic	27.000	-86.000	No
Acanthephyra purpurea	1.13	3.33	7	32	West Atlantic	27.000	-86.000	No
Oplophorus gracilirostris	1.13	3.33	7	32	West Atlantic	27.000	-86.000	No
Systellaspis debilis	1.13	3.33	7	32	West Atlantic	27.000	-86.000	No
Acanthephyra purpurea	1.20	4.00	14	32	West Atlantic	27.000	-86.000	No
Sergia grandis	1.20	4.00	14	32	West Atlantic	27.000	-86.000	No
Sergia robusta	1.20	4.00	14	32	West Atlantic	27.000	-86.000	Yes
Systellaspis debilis	1.20	4.00	14	32	West Atlantic	27.000	-86.000	No
Deosergestes corniculum	1.28	4.67	20	32	West Atlantic	27.000	-86.000	No
Sergia splendens	1.28	4.67	20	32	West Atlantic	27.000	-86.000	No
Sergia talismani	1.28	4.67	20	32	West Atlantic	27.000	-86.000	No
Systellaspis debilis	1.28	4.67	20	32	West Atlantic	27.000	-86.000	No
Sergia grandis	1.64	6.00	20	32	West Atlantic	27.000	-86.000	No
Pandalus borealis	0.69	1.89	5	28	West Atlantic	49.317	-67.600	Yes
Pandalus borealis	0.99	2.90	8	28	West Atlantic	49.317	-67.600	Yes
Pandalus borealis	1.18	3.26	5	28	West Atlantic	49.317	-67.600	Yes
Pandalus borealis	1.59	4.66	8	28	West Atlantic	49.317	-67.600	Yes
Lepidophthalmus jamaicense	0.37	1.33	25	20	West Atlantic	29.295	-89.908	No
Carcinus maenas	0.21	0.70	15	30	East Atlantic	44.652	-1.179	Yes
Eriocheir sinensis	0.21	0.70	15	30	East Atlantic	44.652	-1.179	Yes
Neohelice granulata	1.40	4.77	20	20	West Atlantic	26.380	-98.820	No
Penaeus duorarum	0.95	3.61	27.8	20	West Atlantic	30.402	-86.777	Yes
Americamysis bahia	1.06	3.86	25	20	West Atlantic	30.402	-86.777	No
Americamysis bahia	1.09	3.94	24	20	West Atlantic	30.402	-86.777	No
Crangon crangon	1.11	3.83	20	22	East Atlantic	55.642	12.088	Yes
Crangon crangon	2.83	10.00	18.5	30	East Atlantic	48.202	-2.933	Yes
Crangon crangon	3.40	12.00	18.5	32	East Atlantic	48.202	-2.933	Yes
Crangon crangon	3.96	14.00	18.5	32	East Atlantic	48.202	-2.933	Yes
Palaemon adspersus	3.15	8.95	10	17.5	East Atlantic	54.842	12.211	Yes
Archaeomysis grebnitzkii	2.17	6.67	10	30	East Pacific	48.541	-123.012	No
Neomysis awatschensis	2.17	6.67	10	30	East Pacific	48.541	-123.012	No
Metapenaeus monoceros	1.05	3.91	21.25	32	West Pacific	34.318	132.391	Yes
Metapenaeus monoceros	1.05	3.91	21.25	32	West Pacific	34.318	132.391	Yes

Metapenaeus monoceros	2.38	8.86	21.25	32	West Pacific	34.318	132.391	Yes
Portunus trituberculatus	1.82	6.77	21.25	32	West Pacific	34.414	133.029	Yes
Portunus trituberculatus	2.38	8.86	21.25	32	West Pacific	34.414	133.029	Yes
Pleuroncodes monodon	0.15	0.50	13	32	East Pacific	-12.443	-78.114	Yes
Tenagomysis novaezealandiae	0.77	2.62	20	20	South Pacific	-45.928	170.390	No
Menippe mercenaria	2.00	7.40	25	22	West Atlantic	29.139	-83.035	Yes
Panopeus herbstii	2.80	10.35	25	22	West Atlantic	29.139	-83.035	No
Calanus finmarchicus	2.04	6.91	15	32	East Atlantic	55.687	-4.980	Yes
Penaeus setiferus	0.81	3.07	30	15	West Atlantic	19.810	-90.606	Yes
Penaeus setiferus	0.89	3.36	30	15	West Atlantic	19.810	-90.606	Yes
Penaeus setiferus	1.30	5.62	30	38	West Atlantic	19.810	-90.606	Yes
Penaeus setiferus	1.47	6.34	30	38	West Atlantic	19.810	-90.606	Yes
Penaeus setiferus	1.53	6.58	30	38	West Atlantic	19.810	-90.606	Yes
Penaeus setiferus	1.66	6.28	30	15	West Atlantic	19.810	-90.606	Yes
Penaeus setiferus	1.68	6.36	30	15	West Atlantic	19.810	-90.606	Yes
Penaeus setiferus	1.73	7.46	30	38	West Atlantic	19.810	-90.606	Yes
Homarus americanus	0.58	1.97	15	32	West Atlantic	45.074	-67.053	Yes
Homarus americanus	1.19	3.38	5	32	West Atlantic	45.074	-67.053	Yes
Chionoecetes opilio	1.96	5.27	2.2	32	West Atlantic	49.373	-66.577	Yes
Metacarcinus magister	1.38	4.00	8	27	East Pacific	48.551	-123.078	Yes
Bythograea thermydron	0.45	1.20	2	32	East Pacific	0.810	-86.187	No
Bythograea thermydron	0.58	1.87	12	32	East Pacific	0.810	-86.187	No
Neotrypaea californiensis	0.64	2.00	10	32	East Pacific	44.617	-124.021	Yes
Neotrypaea californiensis	0.82	2.55	10	32	East Pacific	44.617	-124.021	Yes
Palaemonetes pugio	0.49	1.77	20	30	West Atlantic	30.343	-87.168	No
Crangon septemspinosa	0.70	2.53	20	30	West Atlantic	30.343	-87.168	No
Palaemonetes vulgaris	0.70	2.45	18	30	West Atlantic	30.343	-87.168	No
Palaemonetes vulgaris	0.70	2.67	24	30	West Atlantic	30.343	-87.168	No
Homarus americanus	0.70	2.53	20	30	West Atlantic	39.947	-69.608	Yes
Americamysis bahia	0.84	3.30	26	30	West Atlantic	30.343	-87.168	No
Homarus americanus	0.98	3.49	19	30	West Atlantic	39.947	-69.608	Yes
Palaemonetes pugio	1.12	4.34	25	30	West Atlantic	30.343	-87.168	No
Dyspanopeus sayi	1.33	5.01	23	30	West Atlantic	30.343	-87.168	No
Palaemonetes vulgaris	1.47	5.69	25	30	West Atlantic	30.343	-87.168	No
Cancer irroratus	1.54	5.56	20	30	West Atlantic	30.343	-87.168	Yes
Eurypanopeus depressus	1.54	5.60	20.5	30	West Atlantic	30.343	-87.168	No
Dyspanopeus sayi	1.75	6.32	20	30	West Atlantic	30.343	-87.168	No
Cancer irroratus	1.82	6.57	20	30	West Atlantic	30.343	-87.168	Yes
Libinia dubia	1.89	6.83	20	30	West Atlantic	30.343	-87.168	No
Homarus americanus	1.96	7.03	19.5	30	West Atlantic	39.947	-69.608	Yes
Cancer irroratus	2.10	7.59	20	30	West Atlantic	30.343	-87.168	Yes

Homarus americanus	2.17	7.72	19	30	West Atlantic	39.947	-69.608	Yes
Dyspanopeus sayi	2.59	10.03	25	30	West Atlantic	30.343	-87.168	No
Palaemon elegans	0.61	1.90	10	32	East Atlantic	55.765	-4.926	No
Nihonotrypaea japonica	0.56	2.07	20.5	32.6	West Pacific	39.468	141.985	No
Cancer pagurus	2.43	8.00	14	30	East Atlantic	52.458	1.743	Yes
Cancer pagurus	3.24	10.67	14	30	East Atlantic	52.458	1.743	Yes
Cancer pagurus	3.24	10.67	14	30	East Atlantic	52.458	1.743	Yes
Cancer pagurus	3.90	11.56	8	30	East Atlantic	52.458	1.743	Yes
Cancer pagurus	4.05	12.00	8	30	East Atlantic	52.458	1.743	Yes
Cancer pagurus	4.05	12.00	8	30	East Atlantic	52.458	1.743	Yes
Palaemon varians	1.73	11.56	24	14	East Atlantic	55.283	14.689	Yes
Palaemon adspersus	2.05	7.14	24	14	East Atlantic	55.283	14.689	Yes
Panulirus interruptus	1.77	6.58	20	35	East Pacific	24.583	-112.000	Yes
Panulirus interruptus	1.86	7.61	27	35	East Pacific	24.583	-112.000	Yes
Lithodes santolla	2.81	9.00	12	31	East Pacific	-39.803	-73.418	Yes
Trypaea australiensis	1.21	4.63	22	35	South Pacific	-27.583	153.467	No
Callinectes danae	3.25	12.93	25	35	West Atlantic	-24.000	-45.900	Yes
Carcinus maenas	0.96	2.85	7	33	East Atlantic	55.750	-4.927	Yes
Carcinus maenas	1.10	3.76	15	33	East Atlantic	55.750	-4.927	Yes
Carcinus maenas	2.12	8.03	22	33	East Atlantic	55.750	-4.927	Yes
Penaeus setiferus	2.80	9.55	28	1	West Atlantic	21.604	-79.581	Yes
Penaeus schmitti	3.15	11.85	25	25	West Atlantic	21.604	-79.581	Yes
Penaeus setiferus	3.15	11.19	25	15	West Atlantic	21.604	-79.581	Yes
Penaeus setiferus	3.15	10.56	25	5	West Atlantic	21.604	-79.581	Yes
Penaeus schmitti	3.50	14.19	25	38	West Atlantic	21.604	-79.581	Yes
Penaeus schmitti	3.50	13.55	25	30	West Atlantic	21.604	-79.581	Yes
Penaeus schmitti	3.50	12.79	25	20	West Atlantic	21.604	-79.581	Yes
Penaeus schmitti	3.50	12.43	25	15	West Atlantic	21.604	-79.581	Yes
Penaeus setiferus	3.50	13.55	25	30	West Atlantic	21.604	-79.581	Yes
Penaeus setiferus	3.50	13.17	25	25	West Atlantic	21.604	-79.581	Yes
Penaeus setiferus	3.50	12.79	25	20	West Atlantic	21.604	-79.581	Yes
Penaeus setiferus	3.50	12.08	25	10	West Atlantic	21.604	-79.581	Yes
Penaeus setiferus	3.64	14.67	25	37	West Atlantic	21.604	-79.581	Yes
Penaeus setiferus	3.15	11.49	27	15	West Atlantic	24.234	-97.229	Yes
Penaeus setiferus	3.15	12.88	27	35	West Atlantic	24.234	-97.229	Yes
Nephrops norvegicus	1.93	6.30	12	34	East Atlantic	57.633	-5.850	Yes
Penaeus vannamei	1.34	5.37	27.7	30.5	West Atlantic	27.967	-97.000	Yes
Penaeus monodon	1.55	6.30	28.3	30.6	West Atlantic	27.967	-97.000	Yes
Homarus gammarus	1.26	4.36	15	35.7	East Atlantic	52.176	4.333	Yes
Eurypanopeus depressus	1.38	5.07	30	10	West Atlantic	29.227	-89.995	No
Palaemonetes pugio	1.67	6.13	30	10	West Atlantic	29.227	-89.995	No

Rhithropanopeus harrisii	2.07	7.60	30	10	West Atlantic	29.227	-89.995	No
Penaeus aztecus	3.60	12.27	20	20	West Atlantic	29.227	-89.995	Yes
Callinectes sapidus	4.08	15.87	30	20	West Atlantic	29.227	-89.995	Yes
Penaeus aztecus	4.18	16.27	30	20	West Atlantic	29.227	-89.995	Yes
Callinectes sapidus	4.85	16.53	20	20	West Atlantic	29.227	-89.995	Yes
Penaeus indicus	4.10	15.14	28.2	14.5	Indian	13.001	80.256	Yes
Callinectes sapidus	2.27	8.88	25	32	West Atlantic	36.683	-76.667	Yes
Callinectes sapidus	4.70	18.40	25	32	West Atlantic	36.683	-76.667	Yes
Carcinus maenas	2.60	8.80	15	32	East Atlantic	54.236	-4.548	Yes
Carcinus maenas	1.71	5.33	10	32	East Atlantic	50.299	-4.162	Yes
Carcinus maenas	2.26	8.00	18	32	East Atlantic	50.299	-4.162	Yes
Carcinus maenas	2.48	8.00	18	16	East Atlantic	50.299	-4.162	Yes
Carcinus maenas	2.84	8.00	10	16	East Atlantic	50.299	-4.162	Yes
Carcinus maenas	1.15	4.00	17	32	East Atlantic	50.299	-4.162	Yes
Carcinus maenas	0.79	2.67	15	32	East Atlantic	50.299	-4.162	Yes
Neotrypaea californiensis	0.40	1.25	10	33	East Pacific	44.619	-124.028	Yes
Upogebia pugettensis	1.70	5.33	10	33	East Pacific	44.619	-124.028	Yes
Vibilia stebbingi	1.49	3.87	0.5	32	Antarctica	-60.000	-40.000	No
Euphausia superba	1.54	4.00	0.5	32	Antarctica	-60.000	-40.000	No
Cyllopus lucasii	1.59	4.13	0.5	32	Antarctica	-60.000	-40.000	No
Cyphocaris richardi	1.59	4.13	0.5	32	Antarctica	-60.000	-40.000	No
Cyphocaris richardi	1.59	4.13	0.5	32	Antarctica	-60.000	-40.000	No
Cyphocaris richardi	1.59	4.13	0.5	32	Antarctica	-60.000	-40.000	No
Primno macropa	1.64	4.27	0.5	32	Antarctica	-60.000	-40.000	No
Thysanoessa macrura	1.64	4.27	0.5	32	Antarctica	-60.000	-40.000	Yes
Cyphocaris faurei	1.70	4.40	0.5	32	Antarctica	-60.000	-40.000	No
Euphausia superba	1.80	4.67	0.5	32	Antarctica	-60.000	-40.000	No
Primno macropa	1.80	4.67	0.5	32	Antarctica	-60.000	-40.000	No
Vibilia stebbingi	1.80	4.67	0.5	32	Antarctica	-60.000	-40.000	No
Primno macropa	1.90	4.93	0.5	32	Antarctica	-60.000	-40.000	No
Thysanoessa macrura	2.06	5.33	0.5	32	Antarctica	-60.000	-40.000	Yes
Cyllopus lucasii	2.11	5.47	0.5	32	Antarctica	-60.000	-40.000	No
Euphausia superba	2.16	5.60	0.5	32	Antarctica	-60.000	-40.000	No
Euphausia superba	2.16	5.60	0.5	32	Antarctica	-60.000	-40.000	No
Eusirus antarcticus	2.16	5.60	0.5	32	Antarctica	-60.000	-40.000	No
Euphausia superba	2.26	5.87	0.5	32	Antarctica	-60.000	-40.000	No
Euphausia superba	2.67	6.93	0.5	32	Antarctica	-60.000	-40.000	No
Carcinus maenas	0.24	0.93	25	32	West Atlantic	37.373	-75.663	Yes
Rhithropanopeus harrisii	0.36	1.40	25	32	West Atlantic	37.373	-75.663	No
Eurypanopeus depressus	0.40	1.56	25	32	West Atlantic	37.373	-75.663	No
Palaemonetes pugio	0.50	1.97	25	32	West Atlantic	37.373	-75.663	No

Ampelisca abdita	0.63	2.47	25	32	West Atlantic	37.373	-75.663	No
Homarus americanus	0.64	2.49	25	32	West Atlantic	37.373	-75.663	Yes
Crangon septemspinosa	0.68	2.66	25	32	West Atlantic	37.373	-75.663	No
Callinectes sapidus	0.70	2.74	25	32	West Atlantic	37.373	-75.663	Yes
Palaemonetes vulgaris	0.71	2.80	25	32	West Atlantic	37.373	-75.663	No
Americamysis bahia	0.89	3.48	25	32	West Atlantic	37.373	-75.663	No
Cancer irroratus	0.45	1.51	15	30	West Atlantic	41.620	-71.350	Yes
Cancer irroratus	0.57	1.75	10	30	West Atlantic	41.620	-71.350	Yes
Cancer irroratus	0.57	1.75	10	30	West Atlantic	41.620	-71.350	Yes
Cancer irroratus	0.60	1.84	10	30	West Atlantic	41.620	-71.350	Yes
Cancer irroratus	0.61	2.04	15	30	West Atlantic	41.620	-71.350	Yes
Cancer irroratus	0.68	2.27	15	30	West Atlantic	41.620	-71.350	Yes
Cancer irroratus	0.93	2.86	10	30	West Atlantic	41.620	-71.350	Yes
Cancer irroratus	1.07	3.87	20	30	West Atlantic	41.620	-71.350	Yes
Cancer irroratus	1.08	3.61	15	30	West Atlantic	41.620	-71.350	Yes
Cancer irroratus	1.19	3.98	15	30	West Atlantic	41.620	-71.350	Yes
Cancer irroratus	1.30	4.00	10	30	West Atlantic	41.620	-71.350	Yes
Cancer irroratus	1.41	5.09	20	30	West Atlantic	41.620	-71.350	Yes
Cancer irroratus	1.58	5.29	15	30	West Atlantic	41.620	-71.350	Yes
Cancer irroratus	1.61	5.82	20	30	West Atlantic	41.620	-71.350	Yes
Cancer irroratus	1.70	5.23	10	30	West Atlantic	41.620	-71.350	Yes
Cancer irroratus	1.74	6.29	20	30	West Atlantic	41.620	-71.350	Yes
Cancer irroratus	2.09	8.09	25	30	West Atlantic	41.620	-71.350	Yes
Cancer irroratus	2.10	8.13	25	30	West Atlantic	41.620	-71.350	Yes
Cancer irroratus	2.20	7.95	20	30	West Atlantic	41.620	-71.350	Yes
Cancer irroratus	2.29	8.27	20	30	West Atlantic	41.620	-71.350	Yes
Cancer irroratus	2.40	9.29	25	30	West Atlantic	41.620	-71.350	Yes
Cancer irroratus	3.05	11.81	25	30	West Atlantic	41.620	-71.350	Yes
Cancer irroratus	3.35	12.97	25	30	West Atlantic	41.620	-71.350	Yes
Cancer irroratus	3.80	14.71	25	30	West Atlantic	41.620	-71.350	Yes
Cancer irroratus	4.20	17.31	30	30	West Atlantic	41.620	-71.350	Yes
Cancer irroratus	4.43	18.26	30	30	West Atlantic	41.620	-71.350	Yes
Cancer irroratus	4.50	18.55	30	30	West Atlantic	41.620	-71.350	Yes
Cancer irroratus	4.70	19.37	30	30	West Atlantic	41.620	-71.350	Yes
Cancer irroratus	5.06	20.85	30	30	West Atlantic	41.620	-71.350	Yes
Cancer irroratus	6.05	24.93	30	30	West Atlantic	41.620	-71.350	Yes
Idotea emarginata	1.48	5.00	15	32	East Atlantic	54.180	7.899	No
Idotea emarginata	1.61	5.00	10	32	East Atlantic	54.180	7.899	No
Penaeus californiensis	1.26	5.15	27	35	East Pacific	24.782	-110.479	Yes
Jasus edwardsii	3.00	10.40	15	36	South Pacific	-43.883	172.967	Yes
Pugettia producta	2.76	9.33	15	32	East Pacific	36.628	-121.917	No

Pandalus platyceros	2.45	7.53	10	30	East Pacific	49.309	-122.609	Yes
Pandalus platyceros	3.50	9.17	5	20	East Pacific	49.309	-122.609	Yes
Panulirus interruptus	0.10	0.33	16	32	East Pacific	32.720	-117.286	Yes
Panulirus interruptus	1.42	5.18	20	32	East Pacific	32.720	-117.286	Yes
Panulirus interruptus	1.51	5.21	16	32	East Pacific	32.720	-117.286	Yes
Panulirus interruptus	1.60	5.23	13	32	East Pacific	32.720	-117.286	Yes
Melita longidactyla	1.12	4.05	20	30	West Pacific	22.457	114.210	No
Metapenaeus ensis	0.54	1.85	22	16	West Pacific	22.495	114.034	Yes
Pleuroncodes monodon	1.00	3.19	11	33	East Pacific	-36.829	-73.034	Yes
Pleuroncodes monodon	1.00	3.19	11	33	East Pacific	-36.829	-73.034	Yes
Penaeus vannamei	0.37	1.52	28	31	West Pacific	19.815	111.096	Yes
Penaeus vannamei	0.40	1.65	29	31	West Pacific	19.815	111.096	Yes
Penaeus vannamei	0.42	1.57	23	31	West Pacific	19.815	111.096	Yes
Penaeus vannamei	0.42	1.55	22	31	West Pacific	19.815	111.096	Yes
Penaeus vannamei	0.44	1.79	29	31	West Pacific	19.815	111.096	Yes
Penaeus vannamei	0.45	1.77	26	31	West Pacific	19.815	111.096	Yes
Penaeus vannamei	0.46	1.77	25	31	West Pacific	19.815	111.096	Yes
Penaeus vannamei	0.75	3.10	30	30	West Pacific	19.815	111.096	Yes
Penaeus vannamei	0.79	3.24	29	30	West Pacific	19.815	111.096	Yes
Penaeus vannamei	0.90	3.67	29	30	West Pacific	19.815	111.096	Yes
Penaeus vannamei	0.91	3.70	29	30	West Pacific	19.815	111.096	Yes
Penaeus vannamei	0.93	3.85	30	30	West Pacific	19.815	111.096	Yes
Penaeus vannamei	0.94	3.89	30	30	West Pacific	19.815	111.096	Yes
Penaeus vannamei	0.97	3.98	29	31	West Pacific	19.815	111.096	Yes
Penaeus vannamei	0.98	4.05	30	30	West Pacific	19.815	111.096	Yes
Penaeus vannamei	1.04	4.30	30	30	West Pacific	19.815	111.096	Yes
Penaeus vannamei	1.05	4.39	31	30	West Pacific	19.815	111.096	Yes
Penaeus vannamei	1.21	4.94	29	31	West Pacific	19.815	111.096	Yes
Penaeus vannamei	1.21	4.97	30	30	West Pacific	19.815	111.096	Yes
Penaeus vannamei	1.23	5.08	30	30	West Pacific	19.815	111.096	Yes
Penaeus vannamei	1.48	6.10	30	30	West Pacific	19.815	111.096	Yes
Penaeus aztecus	1.77	5.86	20	15	West Atlantic	29.386	-91.538	Yes

Table C.1. Global meta-analysis of O_2^{crit} values for crustaceans. *Metadata*.

Species	**ORDER**	**FAMILY**	**Description of Geographic Location**	**Reference**
Gammarus duebeni	Amphipoda	Gammaridae	Looe, Cornwall, UK	Agnew and Jones 1986
Gammarus duebeni	Amphipoda	Gammaridae	Looe, Cornwall, UK	Agnew and Jones 1986
Echinogammarus pirloti	Amphipoda	Gammaridae	Cumbrae Island,Scotland, UK	Agnew and Taylor 1985

Echinogammarus obtusatus	Amphipoda	Gammaridae	Cumbrae Island,Scotland, UK	Agnew and Taylor 1985
Penaeus monodon	Decapoda	Penaeidae	Goodwood Island, New South Wales, Australia	Allan and Maguire 1991
Lithodes santolla	Decapoda	Lithodidae	Seno de Reloncavf, Puerto Monte, Chile	Alter et al 2015
Petrolisthes laevigatus	Decapoda	Porcellanidae	Seno de Reloncavf, Puerto Monte, Chile	Alter et al 2015
Petrolisthes laevigatus	Decapoda	Porcellanidae	Seno de Reloncavf, Puerto Monte, Chile	Alter et al 2015
Calocaris macandreae	Decapoda	Axiidae	Firth of Clyde, Scotland, UK	Anderson et al 1994
Cancer pagurus	Decapoda	Cancridae	Millport, Isle of Cumbrae, Scotland, UK	Bradford and Taylor 1982
Corystes cassivelaunus	Decapoda	Corystidae	Port Erin, Isle of Man, UK	Bridges and Brand 1980
Galathea strigosa	Decapoda	Galatheidae	Port Erin, Isle of Man, UK	Bridges and Brand 1980
Galathea strigosa	Decapoda	Galatheidae	Port Erin, Isle of Man, UK	Bridges and Brand 1980
Galathea strigosa	Decapoda	Galatheidae	Port Erin, Isle of Man, UK	Bridges and Brand 1980
Corystes cassivelaunus	Decapoda	Corystidae	Port Erin, Isle of Man, UK	Bridges and Brand 1980
Munida quadrispina	Decapoda	Munididae	Saanich Inlet, British Columbia, Canada	Burd 1985
Homarus gammarus	Decapoda	Nephropidae	St Andrews, England, UK	Butler et al 1978
Maja brachydactyla	Decapoda	Majidae	Galiciea, Spain	Cerezo Valverde et al 2012
Maja brachydactyla	Decapoda	Majidae	Galiciea, Spain	Cerezo Valverde et al 2012
Boreomysis californica	Mysida	Mysidae	basins off Southern California, USA	Childress 1975
Pleuroncodes planipes	Decapoda	Munididae	basins off Southern California, USA	Childress 1975
Pasiphaea emarginata	Decapoda	Pasiphaeidae	basins off Southern California, USA	Childress 1975
Plesionika sp.	Decapoda	Pandalidae	basins off Southern California, USA	Childress 1975
Neognathophausia ingens	Lophogastrida	Gnathophausiidae	basins off Southern California, USA	Childress 1975
Gnathophausia zoea	Lophogastrida	Gnathophausiidae	basins off Southern California, USA	Childress 1975
Sergia phorca	Decapoda	Sergestidae	basins off Southern California, USA	Childress 1975
Bathycalanus princeps	Calanoida	Megacalanidae	basins off Southern California, USA	Childress 1975
Systellaspis cristata	Decapoda	Oplophoridae	basins off Southern California, USA	Childress 1975
Hymenodora frontalis	Decapoda	Acanthephyridae	basins off Southern California, USA	Childress 1975
Gennadas propinquus	Decapoda	Benthesicymidae	basins off Southern California, USA	Childress 1975
Pseudocallisoma coecum	Amphipoda	Scopelocheiridae	basins off Southern California, USA	Childress 1975
Acanthephyra curtirostris	Decapoda	Acanthephyridae	basins off Southern California, USA	Childress 1975
Bathycalanus richardi	Calanoida	Megacalanidae	basins off Southern California, USA	Childress 1975
Gaussia princeps	Calanoida	Metridinidae	basins off Southern California, USA	Childress 1975
Gnathophausia gigas	Lophogastrida	Gnathophausiidae	basins off Southern California, USA	Childress 1975
Fagegnathophausia gracilis	Lophogastrida	Gnathophausiidae	basins off Southern California, USA	Childress 1975
Gigantocypris agassizii	Myodocopida	Cypridinidae	basins off Southern California, USA	Childress 1975
Neognathophausia ingens	Lophogastrida	Gnathophausiidae	basins off Southern California, USA	Childress 1975
Pasiphaea pacifica	Decapoda	Pasiphaeidae	basins off Southern California, USA	Childress 1975
Anuropus bathypelagicus	Isopoda	Anuropidae	basins off Southern California, USA	Childress 1975
Notostomus sp.	Decapoda	Acanthephyridae	basins off Southern California, USA	Childress 1975
Phronima sedentaria	Amphipoda	Phronimidae	basins off Southern California, USA	Childress 1975
Euphausia pacifica	Euphausiacea	Euphausiidae	basins off Southern California, USA	Childress 1975
Hyperia galba	Amphipoda	Hyperiidae	basins off Southern California, USA	Childress 1975

Pasiphaea chacei	Decapoda	Pasiphaeidae	basins off Southern California, USA	Childress 1975
Eusergestes similis	Decapoda	Sergestidae	basins off Southern California, USA	Childress 1975
Palaemonetes pugio	Decapoda	Palaemonidae	Charleston harbor, South Carolina, USA	Cochran and Burnett 1996
Gnathophausia zoea	Lophogastrida	Gnathophausiidae	Oahu, HI, USA	Cowles et al 1991
Oplophorus spinosus	Decapoda	Oplophoridae	Oahu, HI, USA	Cowles et al 1991
Neognathophausia gigas	Lophogastrida	Gnathophausiidae	Oahu, HI, USA	Cowles et al 1991
Thysanopoda cornuta	Euphausiacea	Euphausiidae	Oahu, HI, USA	Cowles et al 1991
Notostomus elegans	Decapoda	Acanthephyridae	Oahu, HI, USA	Cowles et al 1991
Acanthephyra smithi	Decapoda	Acanthephyridae	Oahu, HI, USA	Cowles et al 1991
Notostomus elegans	Decapoda	Acanthephyridae	Oahu, HI, USA	Cowles et al 1991
Acanthephyra acutifrons	Decapoda	Acanthephyridae	Oahu, HI, USA	Cowles et al 1991
Acanthephyra curtirostris	Decapoda	Acanthephyridae	Oahu, HI, USA	Cowles et al 1991
Gnathophausia gracilis	Lophogastrida	Gnathophausiidae	Oahu, HI, USA	Cowles et al 1991
Sergia tenuiremis	Decapoda	Sergestidae	Oahu, HI, USA	Cowles et al 1991
Systellaspis debilis	Decapoda	Oplophoridae	Oahu, HI, USA	Cowles et al 1991
Sergia bisulcata	Decapoda	Sergestidae	Oahu, HI, USA	Cowles et al 1991
Sergia fulgens	Decapoda	Sergestidae	Oahu, HI, USA	Cowles et al 1991
Oplophorus gracilirostris	Decapoda	Oplophoridae	Oahu, HI, USA	Cowles et al 1991
Jasus edwardsii	Decapoda	Palinuridae	Taroona, Tasmania, Australia	Crear and Forteath 2000
Panulirus cygnus	Decapoda	Palinuridae	Geraldton, Western Australia	Crear and Forteath 2001
Panulirus cygnus	Decapoda	Palinuridae	Geraldton, Western Australia	Crear and Forteath 2001
Panulirus cygnus	Decapoda	Palinuridae	Geraldton, Western Australia	Crear and Forteath 2001
Munida quadrispina	Decapoda	Munididae	Saanich Inlet, British Columbia, Canada	***Current Study***
Pandalus platyceros	Decapoda	Pandalidae	Saanich Inlet, British Columbia, Canada	***Current Study***
Penaeus esculentus	Decapoda	Penaeidae	Moreton Bay, Queensland, Australia	Dall 1986
Callinectes similis	Decapoda	Portunidae	Port Fourchon, Louisiana, USA	Das and Stickle 1993
Callinectes sapidus	Decapoda	Portunidae	Ocean Springs, Mississippi, USA	Das and Stickle 1993
Rhithropanopeus harrisii	Decapoda	Panopeidae	Neuse River, North Carolina, USA	Diamond et al 1989
Funchalia villosa	Decapoda	Penaeidae	Gulf of Mexico, Mexico, USA	Donnelly and Torres 1988
Stylopandalus richardi	Decapoda	Pandalidae	Gulf of Mexico, Mexico, USA	Donnelly and Torres 1988
Sergia robusta	Decapoda	Sergestidae	Gulf of Mexico, Mexico, USA	Donnelly and Torres 1988
Gennadas valens	Decapoda	Benthesicymidae	Gulf of Mexico, Mexico, USA	Donnelly and Torres 1988
Parasergestes armatus	Decapoda	Sergestidae	Gulf of Mexico, Mexico, USA	Donnelly and Torres 1988
Funchalia villosa	Decapoda	Penaeidae	Gulf of Mexico, Mexico, USA	Donnelly and Torres 1988
Gennadas scutatus	Decapoda	Benthesicymidae	Gulf of Mexico, Mexico, USA	Donnelly and Torres 1988
Gennadas valens	Decapoda	Benthesicymidae	Gulf of Mexico, Mexico, USA	Donnelly and Torres 1988
Oplophorus gracilirostris	Decapoda	Oplophoridae	Gulf of Mexico, Mexico, USA	Donnelly and Torres 1988
Acanthephyra purpurea	Decapoda	Acanthephyridae	Gulf of Mexico, Mexico, USA	Donnelly and Torres 1988
Oplophorus gracilirostris	Decapoda	Oplophoridae	Gulf of Mexico, Mexico, USA	Donnelly and Torres 1988
Systellaspis debilis	Decapoda	Oplophoridae	Gulf of Mexico, Mexico, USA	Donnelly and Torres 1988
Acanthephyra purpurea	Decapoda	Acanthephyridae	Gulf of Mexico, Mexico, USA	Donnelly and Torres 1988

Sergia grandis	Decapoda	Sergestidae	Gulf of Mexico, Mexico, USA	Donnelly and Torres 1988
Sergia robusta	Decapoda	Sergestidae	Gulf of Mexico, Mexico, USA	Donnelly and Torres 1988
Systellaspis debilis	Decapoda	Oplophoridae	Gulf of Mexico, Mexico, USA	Donnelly and Torres 1988
Deosergestes corniculum	Decapoda	Sergestidae	Gulf of Mexico, Mexico, USA	Donnelly and Torres 1988
Sergia splendens	Decapoda	Sergestidae	Gulf of Mexico, Mexico, USA	Donnelly and Torres 1988
Sergia talismani	Decapoda	Sergestidae	Gulf of Mexico, Mexico, USA	Donnelly and Torres 1988
Systellaspis debilis	Decapoda	Oplophoridae	Gulf of Mexico, Mexico, USA	Donnelly and Torres 1988
Sergia grandis	Decapoda	Sergestidae	Gulf of Mexico, Mexico, USA	Donnelly and Torres 1988
Pandalus borealis	Decapoda	Pandalidae	St Lawrence River, Quebec, Canada	Dupont-Prinet et al 2013
Pandalus borealis	Decapoda	Pandalidae	St Lawrence River, Quebec, Canada	Dupont-Prinet et al 2013
Pandalus borealis	Decapoda	Pandalidae	St Lawrence River, Quebec, Canada	Dupont-Prinet et al 2013
Pandalus borealis	Decapoda	Pandalidae	St Lawrence River, Quebec, Canada	Dupont-Prinet et al 2013
Lepidophthalmus jamaicense	Decapoda	Callianassidae	Grand Terre Island, Lousiana, USA	Felder 1979
Carcinus maenas	Decapoda	Portunidae	Arcachon, France	Forgue et al 1992
Eriocheir sinensis	Decapoda	Varunidae	Arcachon, France	Forgue et al 1992
Neohelice granulata	Decapoda	Varunidae	Rio Grande City, Brazil	Geihs et al 2013
Penaeus duorarum	Decapoda	Penaeidae	Santa Rosa Sound, FL, USA	Goodman and Campbell 2007
Americamysis bahia	Mysida	Mysidae	Santa Rosa Sound, FL, USA	Goodman and Campbell 2007
Americamysis bahia	Mysida	Mysidae	Santa Rosa Sound, FL, USA	Goodman and Campbell 2007
Crangon crangon	Decapoda	Crangonidae	Roskilde-Isefjord, Denmark	Hagerman and Szaniawska 1986
Crangon crangon	Decapoda	Crangonidae	Penza estuary, Bretagne, France	Hagerman and Vismann 1995
Crangon crangon	Decapoda	Crangonidae	Penza estuary, Bretagne, France	Hagerman and Vismann 1995
Crangon crangon	Decapoda	Crangonidae	Penza estuary, Bretagne, France	Hagerman and Vismann 1995
Palaemon adspersus	Decapoda	Palaemonidae	Auno Fjord, South Sealand, Denmark	Hagerman and Weber 1981
Archaeomysis grebnitzkii	Mysida	Mysidae	Eagle Cove, San Juan Island, WA, USA	Jawed 1973
Neomysis awatschensis	Mysida	Mysidae	Eagle Cove, San Juan Island, WA, USA	Jawed 1973
Metapenaeus monoceros	Decapoda	Penaeidae	Hiroshima, Japan	Kang and Matsuda 1994
Metapenaeus monoceros	Decapoda	Penaeidae	Hiroshima, Japan	Kang and Matsuda 1994
Metapenaeus monoceros	Decapoda	Penaeidae	Hiroshima, Japan	Kang and Matsuda 1994
Portunus trituberculatus	Decapoda	Portunidae	Hiroshima, Japan	Kang et al 1993
Portunus trituberculatus	Decapoda	Portunidae	Hiroshima, Japan	Kang et al 1993
Pleuroncodes monodon	Decapoda	Munididae	Peruvian coast	Kiko et al 2015
Tenagomysis novaezealandiae	Mysida	Mysidae	Kaikorai estuary, New Zealand	Larkin et al 2007
Menippe mercenaria	Decapoda	Menippidae	Cedar Key, Florida, USA	Leffler 1973
Panopeus herbstii	Decapoda	Panopeidae	Cedar Key, Florida, USA	Leffler 1973
Calanus finmarchicus	Calanoida	Calanidae	Garoch Head, Scotland, UK	Marshall and Nicholls 1935
Penaeus setiferus	Decapoda	Penaeidae	Lerma, Campeche, Mexico	Martinez et al 1998
Penaeus setiferus	Decapoda	Penaeidae	Lerma, Campeche, Mexico	Martinez et al 1998
Penaeus setiferus	Decapoda	Penaeidae	Lerma, Campeche, Mexico	Martinez et al 1998
Penaeus setiferus	Decapoda	Penaeidae	Lerma, Campeche, Mexico	Martinez et al 1998
Penaeus setiferus	Decapoda	Penaeidae	Lerma, Campeche, Mexico	Martinez et al 1998

Penaeus setiferus	Decapoda	Penaeidae	Lerma, Campeche, Mexico	Martinez et al 1998
Penaeus setiferus	Decapoda	Penaeidae	Lerma, Campeche, Mexico	Martinez et al 1998
Penaeus setiferus	Decapoda	Penaeidae	Lerma, Campeche, Mexico	Martinez et al 1998
Homarus americanus	Decapoda	Nephropidae	New Brunswick, Canada	McLeese 1956
Homarus americanus	Decapoda	Nephropidae	New Brunswick, Canada	McLeese and Watson 1968
Chionoecetes opilio	Decapoda	Oregoniidae	Gulf of St Lawrence, New Brunswick, Canada	McLeese and Watson 1968
Metacarcinus magister	Decapoda	Cancridae	San Juan Island, WA, USA	McMahon et al 1979
Bythograea thermydron	Decapoda	Bythograeidae	Rose Garden, Galapagos Rift	Mickel and Childress 1982
Bythograea thermydron	Decapoda	Bythograeidae	Mussel Bed, Galapagos Rift	Mickel and Childress 1982
Neotrypaea californiensis	Decapoda	Callianassidae	Yaquina Bay, Oregon, USA	Miller et al 1976
Neotrypaea californiensis	Decapoda	Callianassidae	Yaquina Bay, Oregon, USA	Miller et al 1976
Palaemonetes pugio	Decapoda	Palaemonidae	Gulf Breeze, Florida, USA	Miller et al 2002
Crangon septemspinosa	Decapoda	Crangonidae	Gulf Breeze, Florida, USA	Miller et al 2002
Palaemonetes vulgaris	Decapoda	Palaemonidae	Gulf Breeze, Florida, USA	Miller et al 2002
Palaemonetes vulgaris	Decapoda	Palaemonidae	Gulf Breeze, Florida, USA	Miller et al 2002
Homarus americanus	Decapoda	Nephropidae	Veatch and Oceanographer Canyon, USA	Miller et al 2002
Americamysis bahia	Mysida	Mysidae	Gulf Breeze, Florida, USA	Miller et al 2002
Homarus americanus	Decapoda	Nephropidae	Veatch and Oceanographer Canyon, USA	Miller et al 2002
Palaemonetes pugio	Decapoda	Palaemonidae	Gulf Breeze, Florida, USA	Miller et al 2002
Dyspanopeus sayi	Decapoda	Panopeidae	Gulf Breeze, Florida, USA	Miller et al 2002
Palaemonetes vulgaris	Decapoda	Palaemonidae	Gulf Breeze, Florida, USA	Miller et al 2002
Cancer irroratus	Decapoda	Cancridae	Gulf Breeze, Florida, USA	Miller et al 2002
Eurypanopeus depressus	Decapoda	Panopeidae	Gulf Breeze, Florida, USA	Miller et al 2002
Dyspanopeus sayi	Decapoda	Panopeidae	Gulf Breeze, Florida, USA	Miller et al 2002
Cancer irroratus	Decapoda	Cancridae	Gulf Breeze, Florida, USA	Miller et al 2002
Libinia dubia	Decapoda	Epialtidae	Gulf Breeze, Florida, USA	Miller et al 2002
Homarus americanus	Decapoda	Nephropidae	Veatch and Oceanographer Canyon, USA	Miller et al 2002
Cancer irroratus	Decapoda	Cancridae	Gulf Breeze, Florida, USA	Miller et al 2002
Homarus americanus	Decapoda	Nephropidae	Veatch and Oceanographer Canyon, USA	Miller et al 2002
Dyspanopeus sayi	Decapoda	Panopeidae	Gulf Breeze, Florida, USA	Miller et al 2002
Palaemon elegans	Decapoda	Palaemonidae	Isle of Cumbrae, Firth of Clyde, Scotland, UK	Morris and Taylor 1985
Nihonotrypaea japonica	Decapoda	Callianassidae	Yamada Bay, Orikasa River, Japan	Mukai and Koike 1984
Cancer pagurus	Decapoda	Cancridae	Norfolk, S, Lowestoft	Naylor et al 1999
Cancer pagurus	Decapoda	Cancridae	Norfolk, UK	Naylor et al 1999
Cancer pagurus	Decapoda	Cancridae	Norfolk, UK	Naylor et al 1999
Cancer pagurus	Decapoda	Cancridae	Norfolk, UK	Naylor et al 1999
Cancer pagurus	Decapoda	Cancridae	Norfolk, UK	Naylor et al 1999
Cancer pagurus	Decapoda	Cancridae	Norfolk, UK	Naylor et al 1999
Palaemon varians	Decapoda	Palaemonidae	Roskilde Fjord, Denmark	Nielsen and Hagerman 1998
Palaemon adspersus	Decapoda	Palaemonidae	Roskilde Fjord, Denmark	Nielsen and Hagerman 1998
Panulirus interruptus	Decapoda	Palinuridae	Bahia, Magdalena, Califronia, USA	Ocampo et al 2003

Panulirus interruptus	Decapoda	Palinuridae	Bahia, Magdalena, Califronia, USA	Ocampo et al 2003
Lithodes santolla	Decapoda	Lithodidae	Puerto Montt, Chile	Paschke et al 2010
Trypaea australiensis	Decapoda	Callianassidae	North Stradbroke Island, Queensland, Australia	Paterson and Thorne 1995
Callinectes danae	Decapoda	Portunidae	Sao Paulo, Brazil	Rantin et al 1996
Carcinus maenas	Decapoda	Portunidae	Millport, Scotland, UK	Robertson et al 2002
Carcinus maenas	Decapoda	Portunidae	Millport, Scotland, UK	Robertson et al 2002
Carcinus maenas	Decapoda	Portunidae	Millport, Scotland, UK	Robertson et al 2002
Penaeus setiferus	Decapoda	Penaeidae	Zaza, Cuba	Rosas et al 1997
Penaeus schmitti	Decapoda	Penaeidae	Zaza, Cuba	Rosas et al 1997
Penaeus setiferus	Decapoda	Penaeidae	Zaza, Cuba	Rosas et al 1997
Penaeus setiferus	Decapoda	Penaeidae	Zaza, Cuba	Rosas et al 1997
Penaeus schmitti	Decapoda	Penaeidae	Zaza, Cuba	Rosas et al 1997
Penaeus schmitti	Decapoda	Penaeidae	Zaza, Cuba	Rosas et al 1997
Penaeus schmitti	Decapoda	Penaeidae	Zaza, Cuba	Rosas et al 1997
Penaeus schmitti	Decapoda	Penaeidae	Zaza, Cuba	Rosas et al 1997
Penaeus setiferus	Decapoda	Penaeidae	Zaza, Cuba	Rosas et al 1997
Penaeus setiferus	Decapoda	Penaeidae	Zaza, Cuba	Rosas et al 1997
Penaeus setiferus	Decapoda	Penaeidae	Zaza, Cuba	Rosas et al 1997
Penaeus setiferus	Decapoda	Penaeidae	Zaza, Cuba	Rosas et al 1997
Penaeus setiferus	Decapoda	Penaeidae	Zaza, Cuba	Rosas et al 1997
Penaeus setiferus	Decapoda	Penaeidae	Gulf of Mexico, Mexico	Rosas et al 1999
Penaeus setiferus	Decapoda	Penaeidae	Gulf of Mexico, Mexico	Rosas et al 1999
Nephrops norvegicus	Decapoda	Nephropidae	Scottish coast, Scotland, UK	Schmitt and Uglow 1998
Penaeus vannamei	Decapoda	Penaeidae	Corpus Christi, TX, USA	Seidman and Lawrence 1985
Penaeus monodon	Decapoda	Penaeidae	Galveston, TX, USA	Seidman and Lawrence 1985
Homarus gammarus	Decapoda	Nephropidae	Leiden, Netherlands	Spoek 1974
Eurypanopeus depressus	Decapoda	Panopeidae	Grand Isle, LA, USA	Stickle et al 1989
Palaemonetes pugio	Decapoda	Palaemonidae	Grand Isle, LA, USA	Stickle et al 1989
Rhithropanopeus harrisii	Decapoda	Panopeidae	Grand Isle, LA, USA	Stickle et al 1989
Penaeus aztecus	Decapoda	Penaeidae	Grand Isle, LA, USA	Stickle et al 1989
Callinectes sapidus	Decapoda	Portunidae	Grand Isle, LA, USA	Stickle et al 1989
Penaeus aztecus	Decapoda	Penaeidae	Grand Isle, LA, USA	Stickle et al 1989
Callinectes sapidus	Decapoda	Portunidae	Grand Isle, LA, USA	Stickle et al 1989
Penaeus indicus	Decapoda	Penaeidae	Adyar estuary, Bay of Bengal, India	Subrahmanyam 1962
Callinectes sapidus	Decapoda	Portunidae	Newport river estuary, Beaufort, NC, USA	Tankersley and Wieber 2000
Callinectes sapidus	Decapoda	Portunidae	Newport river estuary, Beaufort, NC, USA	Tankersley and Wieber 2000
Carcinus maenas	Decapoda	Portunidae	Isle of Man, UK	Taylor 1976
Carcinus maenas	Decapoda	Portunidae	Birmingham, England, UK	Taylor 1981
Carcinus maenas	Decapoda	Portunidae	Birmingham, England, UK	Taylor 1981
Carcinus maenas	Decapoda	Portunidae	Birmingham, England, UK	Taylor 1981
Carcinus maenas	Decapoda	Portunidae	Birmingham, England, UK	Taylor 1981

Carcinus maenas	Decapoda	Portunidae	Plymouth, England, UK	Taylor and Butler 1973
Carcinus maenas	Decapoda	Portunidae	Plymouth, England, UK	Taylor and Butler 1978
Neotrypaea californiensis	Decapoda	Callianassidae	Coquille Point, Yaquina Bay, OR, USA	Thompson and Pritchard 1969
Upogebia pugettensis	Decapoda	Upogebiidae	Coquille Point, Yaquina Bay, OR, USA	Thompson and Pritchard 1969
Vibilia stebbingi	Amphipoda	Vibiliidae	Scotia Sea, Antarctica	Torres et al 1994
Euphausia superba	Euphausiacea	Euphausiidae	Scotia Sea, Antarctica	Torres et al 1994
Cyllopus lucasii	Amphipoda	Cyllopodidae	Scotia Sea, Antarctica	Torres et al 1994
Cyphocaris richardi	Amphipoda	Cyphocarididae	Scotia Sea, Antarctica	Torres et al 1994
Cyphocaris richardi	Amphipoda	Cyphocarididae	Scotia Sea, Antarctica	Torres et al 1994
Cyphocaris richardi	Amphipoda	Cyphocarididae	Scotia Sea, Antarctica	Torres et al 1994
Primno macropa	Amphipoda	Phrosinidae	Scotia Sea, Antarctica	Torres et al 1994
Thysanoessa macrura	Euphausiacea	Euphausiidae	Scotia Sea, Antarctica	Torres et al 1994
Cyphocaris faurei	Amphipoda	Cyphocarididae	Scotia Sea, Antarctica	Torres et al 1994
Euphausia superba	Euphausiacea	Euphausiidae	Scotia Sea, Antarctica	Torres et al 1994
Primno macropa	Amphipoda	Phrosinidae	Scotia Sea, Antarctica	Torres et al 1994
Vibilia stebbingi	Amphipoda	Vibiliidae	Scotia Sea, Antarctica	Torres et al 1994
Primno macropa	Amphipoda	Phrosinidae	Scotia Sea, Antarctica	Torres et al 1994
Thysanoessa macrura	Euphausiacea	Euphausiidae	Scotia Sea, Antarctica	Torres et al 1994
Cyllopus lucasii	Amphipoda	Cyllopodidae	Scotia Sea, Antarctica	Torres et al 1994
Euphausia superba	Euphausiacea	Euphausiidae	Scotia Sea, Antarctica	Torres et al 1994
Euphausia superba	Euphausiacea	Euphausiidae	Scotia Sea, Antarctica	Torres et al 1994
Eusirus antarcticus	Amphipoda	Eusiridae	Scotia Sea, Antarctica	Torres et al 1994
Euphausia superba	Euphausiacea	Euphausiidae	Scotia Sea, Antarctica	Torres et al 1994
Euphausia superba	Euphausiacea	Euphausiidae	Scotia Sea, Antarctica	Torres et al 1994
Carcinus maenas	Decapoda	Portunidae	Coastal Virginia, USA	US EPA 2000a
Rhithropanopeus harrisii	Decapoda	Panopeidae	Coastal Virginia, USA	US EPA 2000a
Eurypanopeus depressus	Decapoda	Panopeidae	Coastal Virginia, USA	US EPA 2000a
Palaemonetes pugio	Decapoda	Palaemonidae	Coastal Virginia, USA	US EPA 2000a
Ampelisca abdita	Amphipoda	Ampeliscidae	Coastal Virginia, USA	US EPA 2000a
Homarus americanus	Decapoda	Nephropidae	Coastal Virginia, USA	US EPA 2000a
Crangon septemspinosa	Decapoda	Crangonidae	Coastal Virginia, USA	US EPA 2000a
Callinectes sapidus	Decapoda	Portunidae	Coastal Virginia, USA	US EPA 2000a
Palaemonetes vulgaris	Decapoda	Palaemonidae	Coastal Virginia, USA	US EPA 2000a
Americamysis bahia	Mysida	Mysidae	Coastal Virginia, USA	US EPA 2000a
Cancer irroratus	Decapoda	Cancridae	Narragansett Bay, RI, USA	Vargo and Sastry 1977
Cancer irroratus	Decapoda	Cancridae	Narragansett Bay, RI, USA	Vargo and Sastry 1977
Cancer irroratus	Decapoda	Cancridae	Narragansett Bay, RI, USA	Vargo and Sastry 1977
Cancer irroratus	Decapoda	Cancridae	Narragansett Bay, RI, USA	Vargo and Sastry 1977
Cancer irroratus	Decapoda	Cancridae	Narragansett Bay, RI, USA	Vargo and Sastry 1977
Cancer irroratus	Decapoda	Cancridae	Narragansett Bay, RI, USA	Vargo and Sastry 1977
Cancer irroratus	Decapoda	Cancridae	Narragansett Bay, RI, USA	Vargo and Sastry 1977

Cancer irroratus	Decapoda	Cancridae	Narragansett Bay, RI, USA	Vargo and Sastry 1977
Cancer irroratus	Decapoda	Cancridae	Narragansett Bay, RI, USA	Vargo and Sastry 1977
Cancer irroratus	Decapoda	Cancridae	Narragansett Bay, RI, USA	Vargo and Sastry 1977
Cancer irroratus	Decapoda	Cancridae	Narragansett Bay, RI, USA	Vargo and Sastry 1977
Cancer irroratus	Decapoda	Cancridae	Narragansett Bay, RI, USA	Vargo and Sastry 1977
Cancer irroratus	Decapoda	Cancridae	Narragansett Bay, RI, USA	Vargo and Sastry 1977
Cancer irroratus	Decapoda	Cancridae	Narragansett Bay, RI, USA	Vargo and Sastry 1977
Cancer irroratus	Decapoda	Cancridae	Narragansett Bay, RI, USA	Vargo and Sastry 1977
Cancer irroratus	Decapoda	Cancridae	Narragansett Bay, RI, USA	Vargo and Sastry 1977
Cancer irroratus	Decapoda	Cancridae	Narragansett Bay, RI, USA	Vargo and Sastry 1977
Cancer irroratus	Decapoda	Cancridae	Narragansett Bay, RI, USA	Vargo and Sastry 1977
Cancer irroratus	Decapoda	Cancridae	Narragansett Bay, RI, USA	Vargo and Sastry 1977
Cancer irroratus	Decapoda	Cancridae	Narragansett Bay, RI, USA	Vargo and Sastry 1977
Cancer irroratus	Decapoda	Cancridae	Narragansett Bay, RI, USA	Vargo and Sastry 1977
Cancer irroratus	Decapoda	Cancridae	Narragansett Bay, RI, USA	Vargo and Sastry 1977
Cancer irroratus	Decapoda	Cancridae	Narragansett Bay, RI, USA	Vargo and Sastry 1977
Cancer irroratus	Decapoda	Cancridae	Narragansett Bay, RI, USA	Vargo and Sastry 1977
Cancer irroratus	Decapoda	Cancridae	Narragansett Bay, RI, USA	Vargo and Sastry 1977
Cancer irroratus	Decapoda	Cancridae	Narragansett Bay, RI, USA	Vargo and Sastry 1977
Cancer irroratus	Decapoda	Cancridae	Narragansett Bay, RI, USA	Vargo and Sastry 1977
Cancer irroratus	Decapoda	Cancridae	Narragansett Bay, RI, USA	Vargo and Sastry 1977
Cancer irroratus	Decapoda	Cancridae	Narragansett Bay, RI, USA	Vargo and Sastry 1977
Idotea emarginata	Isopoda	Idoteidae	Helgoland, Germany	Vetter et al 1999
Idotea emarginata	Isopoda	Idoteidae	Helgoland, Germany	Vetter et al 1999
Penaeus californiensis	Decapoda	Penaeidae	Baja California Sur, Mexico	Villarreal and Ocampo 1993
Jasus edwardsii	Decapoda	Palinuridae	Canterbury coast, New Zealand	Waldron 1991
Pugettia producta	Decapoda	Epialtidae	Pacific Grove, CA, USA	Weymouth et al 1944
Pandalus platyceros	Decapoda	Pandalidae	Howe Sound, Canada	Whyte and Carswell 1982
Pandalus platyceros	Decapoda	Pandalidae	Howe Sound, Canada	Whyte and Carswell 1982
Panulirus interruptus	Decapoda	Palinuridae	San Diego, USA	Winget 1969
Panulirus interruptus	Decapoda	Palinuridae	San Diego, USA	Winget 1969
Panulirus interruptus	Decapoda	Palinuridae	San Diego, USA	Winget 1969
Panulirus interruptus	Decapoda	Palinuridae	San Diego, USA	Winget 1969
Melita longidactyla	Amphipoda	Melitidae	Sam Mun Tsai, Hong Kong, China	Wu and Or 2005
Metapenaeus ensis	Decapoda	Penaeidae	Mai Po Nature Reserve, Hong Kong, China	Wu et al 2002
Pleuroncodes monodon	Decapoda	Munididae	Continental shelf of south-central Chile	Yannicelli et al 2013
Pleuroncodes monodon	Decapoda	Munididae	Continental shelf of south-central Chile	Yannicelli et al 2013
Penaeus vannamei	Decapoda	Penaeidae	Wenchang, Hainan, China	Zhou et al 2014
Penaeus vannamei	Decapoda	Penaeidae	Wenchang, Hainan, China	Zhou et al 2014
Penaeus vannamei	Decapoda	Penaeidae	Wenchang, Hainan, China	Zhou et al 2014

Penaeus vannamei	Decapoda	Penaeidae	Wenchang, Hainan, China	Zhou et al 2014
Penaeus vannamei	Decapoda	Penaeidae	Wenchang, Hainan, China	Zhou et al 2014
Penaeus vannamei	Decapoda	Penaeidae	Wenchang, Hainan, China	Zhou et al 2014
Penaeus vannamei	Decapoda	Penaeidae	Wenchang, Hainan, China	Zhou et al 2014
Penaeus vannamei	Decapoda	Penaeidae	Wenchang, Hainan, China	Zhou et al 2014
Penaeus vannamei	Decapoda	Penaeidae	Wenchang, Hainan, China	Zhou et al 2014
Penaeus vannamei	Decapoda	Penaeidae	Wenchang, Hainan, China	Zhou et al 2014
Penaeus vannamei	Decapoda	Penaeidae	Wenchang, Hainan, China	Zhou et al 2014
Penaeus vannamei	Decapoda	Penaeidae	Wenchang, Hainan, China	Zhou et al 2014
Penaeus vannamei	Decapoda	Penaeidae	Wenchang, Hainan, China	Zhou et al 2014
Penaeus vannamei	Decapoda	Penaeidae	Wenchang, Hainan, China	Zhou et al 2014
Penaeus vannamei	Decapoda	Penaeidae	Wenchang, Hainan, China	Zhou et al 2014
Penaeus vannamei	Decapoda	Penaeidae	Wenchang, Hainan, China	Zhou et al 2014
Penaeus vannamei	Decapoda	Penaeidae	Wenchang, Hainan, China	Zhou et al 2014
Penaeus vannamei	Decapoda	Penaeidae	Wenchang, Hainan, China	Zhou et al 2014
Penaeus vannamei	Decapoda	Penaeidae	Wenchang, Hainan, China	Zhou et al 2014
Penaeus vannamei	Decapoda	Penaeidae	Wenchang, Hainan, China	Zhou et al 2014
Penaeus vannamei	Decapoda	Penaeidae	Wenchang, Hainan, China	Zhou et al 2014
Penaeus aztecus	Decapoda	Penaeidae	Louisiana, USA	Zou and Stueben 2006

Literature cited in Table C.1

Agnew DJ, Jones MB (1986) Metabolic adaptations of *Gammarus duebeni* Liljeborg (Crustacea, Amphipoda) to hypoxia in a sewage treatment plant. *Comparative Biochemistry and Physiology Part A: Physiology*, **84**, 475–478.

Agnew DJ, Taylor AC (1985) The effect of oxygen tension on the physiology and distribution of *Echinogammarus pirloti* (Sexton & Spooner) and *E. obtusatus* (Dahl) (Crustacea: Amphipoda). *Journal of Experimental Marine Biology & Ecology*, **87**, 169–190.

Allan GL, Maguire GB (1991) Lethal levels of low dissolved oxygen and effects of short-term oxygen stress on subsequent growth of juvenile *Penaeus monodon*. *Aquaculture*, **94**, 27–37.

Alter K, Paschke K, Gebauer P, Cumillaf J-P, Pörtner H-O (2015) Differential physiological responses to oxygen availability in early life stages of decapods developing in distinct environments. *Marine Biology*, **162**, 1111–1124.

Anderson SJ, Taylor AC, Atkinson RJA (1994) Anaerobic metabolism during anoxia in the burrowing shrimp *Calocaris macandreae* Bell (Crustacea: Thalassinidea). *Comparative Biochemistry and Physiology Part A: Physiology*, **108**, 515–522.

Bradford SM, Taylor AC (1982) The respiration of *Cancer pagurus* under normoxic and hypoxic conditions. *Journal of Experimental Biology*, **97**, 273–288.

Bridges CR, Brand AR (1980) Oxygen consumption and oxygen-independence in marine crustaceans. *Marine Ecology Progress Series*, **2**, 133–141.

Burd BJ (1985) Respiration of a low oxygen tolerant galatheid crab, *Munida quadrispina*. *Canadian Journal of Zoology*, **63**, 2538–2542.

Butler PJ, Taylor EW, McMahon BR (1978) Respiratory and circulatory changes in the lobster (*Homarus vulgaris*) during long-term exposure to moderate hypoxia. *Journal of Experimental Biology*, **73**, 131–146.

Cerezo Valverde J, Aguado-Giménez F, Dolores Hernández M, García García B (2012) Oxygen consumption response to gradual hypoxia in spider crab, *Maja brachydactyla*: critical and lethal oxygen saturations and recovery ability. *Journal of the World Aquaculture Society*, **43**, 433–441.

Childress JJ (1975) The respiratory rates of midwater crustaceans as a function of depth of occurrence and relation to the oxygen minimum layer off Southern California. *Comparative Biochemistry and Physiology Part A: Physiology*, **50**, 787–799.

Cochran RE, Burnet LE (1996) Respiratory responses of the salt marsh animals, *Fundulus heteroclitus, Leiostomus xanthurus*, and *Palaemonetes pugio* to environmental hypoxia and hypercapnia and to the organophosphate pesticide, azinphosmethyl. *Journal of Experimental Marine Biology & Ecology*, **195**, 125–144.

Cowles DL, Childress JJ, Wells ME (1991) Metabolic rates of midwater crustaceans as a function of depth of occurrence off the Hawaii Islands: food availability as a selective factor? *Marine Biology*, **110**, 75–83.

Crear BJ, Forteath GNR (2000) The effect of extrinsic and intrinsic factors on oxugen consumption by the southern rock lobster, *Jasus edwardsii*. *Journal of Experimental Marine Biology & Ecology*, **252**, 129–147.

Crear BJ, Forteath GNR (2001) Flow-rate requirements for captive western rock lobsters (*Panulirus cygnus*): effects of body weight, temperature, activity, emersion, daily rhythm, feeding and oxygen tension on oxygen consumption. *Marine & Freshwater Research*, **52**, 763–771.

Dall W (1986) Estimation of routine metabolic rate in a penaeid prawn, *Penaeus esculentus* Haswell. *Journal of Experimental Marine Biology & Ecology*, **96**, 57–74.

Das T, Stickle WB (1993) Sensitivity of crabs *Callinectes sapidus* and *C. similis* and the gastropod *Stramonita haemastoma* to hypoxia and anoxia. *Marine Ecology Progress Series*, **98**, 263–274.

Diamond DW, Scott LK, Forward RB, Kirby-Smith W (1989) Respiration and osmoregulation of the estuarine crab, *Rhithropanopeus harrisii* (Gould): Effects of the herbicide, alachlor. *Comparative Biochemistry and Physiology Part A: Physiology*, **93**, 313–318.

Donnelly J, Torres JJ (1988) Oxygen consumption of midwater fishes and crustaceans from the eastern Gulf of Mexico. *Marine Biology*, **97**, 483–494.

Dupont-Prinet A, Pillet M, Chabot D, Hansen T, Tremblay R, Audet C (2013) Northern shrimp (*Pandalus borealis*) oxygen consumption and metabolic enzyme activities are severely constrained by hypoxia in the Estuary and Gulf of St. Lawrence. *Journal of Experimental Marine Biology & Ecology*, **448**, 298–307.

Felder DL (1979) Respiratory adaptations of the estuarine mud shrimp, *Callianassa jamaicense* (Schmitt, 1935) (Crustacea, Decapoda, Thalassinidea). *Biological Bulletin*, **157**, 125–137.

Forgue J, Massabuau J-C, Truchot J-P (1992) When are resting water-breathers lacking O2? Arterial PO2 at the anaerobic threshold in crab. *Respiration Physiology*, **88**, 247–256.

Geihs MA, Maciel FE, Vargas MA, Cruz BP, Nery LEM. 2013 Effects of hypoxia and reoxygenation on the energetic metabolism of the crab *Neohelice granulata* (Decapoda, Varunidae). *Journal of Experimental Marine Biology & Ecology*, **445**, 69–78.

Goodman LR, Campbell JG (2007) Lethal levels of hypoxia for gulf coast estuarine animals. *Marine Biology*, **152**, 37–42.

Hagerman L, Szaniawska A (1986) Behaviour, tolerance and anaerobic metabolism under hypoxia in the brackish-water shrimp *Crangon crangon*. *Marine Ecology Progress Series*, **34**, 125–132.

Hagerman L, Vismann B (1995) Anaerobic metabolism in the shrimp *Crangon crangon* exposed to hypoxia, anoxia and hydrogen sulfide. *Marine Biology*, **123**, 235–240.

Hagerman L, Weber RE (1981) Respiratory rate, haemolymph oxygen tension and haemocyanin level in the shrimp *Palaemon adspersus*: Rathke. *Journal of Experimental Marine Biology & Ecology*, **54**, 13–20.

Jawed M (1973) Effects of environmental factors and body size on rates of oxygen consumption in *Archaeomysis grebnitzkii* and *Neomysis awatschensis* (Crustacea: Mysidae). *Marine Biology*, **21**, 173–179.

Kang JC, Matsuda O (1994) Combined effects of hypoxia and hydrogen sulfide on early developmental stages of white shrimp *Metapenaeus monoceros*. *Journal of the Faculty of Applied Biological Science Hiroshima University*, **33**, 21–27.

Kang JC, Matsuda O, Yamamoto T (1993) Effects of low dissolved oxygen and hydrogen sulfide on early developmental stages of blue crab *Portunus trituberculatus* in Hiroshima bay, Japan. *Journal of the Faculty of Applied Biological Science Hiroshima University*, **33**, 21-27.

Kiko R, Hauss H, Dengler M, Sommer S, Melzner F (2015) The squat lobster *Pleuroncodes monodon* tolerates anoxic 'dead zone' conditions off Peru. *Marine Biology*, **162**, 1913–1921.

Larkin G, Closs GP, Peake B (2007) Tolerance and behaviour of the mysid shrimp *Tenagomysis novae-• zealandiae* to low dissolved oxygen. *New Zealand Journal of Marine & Freshwater Research*, **41**, 317–323.

Leffler CW (1973) Metabolic rate in relation to body size and environmental oxygen concentration in two species of xanthid crabs. *Comparative Biochemistry and Physiology Part A: Physiology*, **44**, 1047–1052.

Marshall SM, Nicholls AG, Orr AP (1935) On the biology of *Calanus finmarchicus*. Part VI. Oxygen consumption in relation to environmental conditions. *Journal of the Marine Biological Association of the United Kingdom*, **20**, 1–27.

Martínez E, Aguilar M, Trejo L, Hernández I, Díaz-Iglesia E, Soto, LA., Sanchez A, Rosas C (1998) Lethal low dissolved oxygen concentrations for postlarvae and early juvenile *Penaeus setiferus* at different salinities and pH. *Journal of the World Aquaculture Society*, **29**, 221–229.

McLeese DW (1956) Effects of temperature, salinity and oxygen on the survival of the American lobster. *Journal of the Fisheries Board of Canada*, **13**, 247–272.

McLeese DW, Watson J (1968) Oxygen consumption of the spider crab (*Chionoecctes opilio*) and the American lobster (*Homarus americanus*) at a low temperature. *Journal of the Fisheries Research Board of Canada*, **25**, 1729–1732.

McMahon BR, McDonald DG, Wood CM (1979) Ventilation, oxygen uptake and haemolymph oxygen transport, following enforced exhausting activity in the Dungeness crab, *Cancer magister*. *Journal of Experimental Biology*, **80**, 271–285.

Mickel TJ, Childress JJ (1982) Effects of temperature, pressure and oxygen concentration on the oxygen consumption rate of the hydrothermal vent crab *Bythograea thermydron* (Brachyura). *Physiological Zoology*, **55**, 199–207.

Miller KI, Pritchard AW, Rutledge PS (1976) Respiratory regulation and the role of the blood in the burrowing shrimp *Callianassa californiensis* (Decapoda: Thalassinidea). *Marine Biology*, **36**, 233–242.

Miller DC, Poucher SL, Coiro L (2002) Determination of lethal dissolved oxygen levels for selected marine and estuarine fishes, crustaceans, and a bivalve. *Marine Biology*, **140**, 287–296.

Morris S, Taylor AC (1985) The respiratory response of the intertidal prawn *Palaemon elegans* (Rathke) to hypoxia and hyperoxia. *Comparative Biochemistry and Physiology Part A: Physiology*, **81**, 633–639.

Mukai H, Koike I (1984) Behavior and respiration of the burrowing shrimps *Upogebia major* (de Haan) and *Callianassa japonica* (de Haan). *Journal of Crustacean Biology*, **4**, 191–200.

Naylor JK, Taylor EW, Bennett DB (1999) Oxygen uptake of developing eggs of *Cancer pagurus* (Crustacea: Decapoda: Cancridae) and consequent behaviour of the ovigerous females. *Journal of the Marine Biological Association of the United Kingdom*, **79**, 305–315.

Nielsen A, Hagerman L (1998) Effects of short-term hypoxia on metabolism and haemocyanin oxygen transport in the prawns *Palaemon adspersus* and *Palaemonetes varians*. *Marine Ecology Progress Series*, **167**, 177–183.

Ocampo L, Patiño D, Ramírez C (2003) Effect of temperature on hemolymph lactate and glucose concentrations in spiny lobster *Panulirus interruptus* during progressive hypoxia. *Journal of Experimental Marine Biology & Ecology*, **296**, 71–77.

Paschke K, Cumillaf JP, Loyola S, Gebauer P, Urbina M, Chimal ME, Pascual C, Rosas C (2010) Effect of dissolved oxygen level on respiratory metabolism, nutritional physiology, and immune condition of southern king crab *Lithodes santolla* (Molina, 1782) (Decapoda, Lithodidae). *Marine Biology*, **157**, 7–18.

Paterson BD, Thorne MJ (1995) Measurements of oxygen uptake, heart and gill bailer rates of the callianassid burrowing shrimp *Trypaea australiensis* Dana and its responses to low oxygen tensions. *Journal of Experimental Marine Biology & Ecology*, **194**, 39–52.

Rantin FT, Kalinin AL, de Freitas JC (1996) Cardio-respiratory function of swimming blue crab *Callinectes danae* Smith, during normoxia and graded hypoxia. *Journal of Experimental Marine Biology & Ecology*, **198**, 1–10.

Robertson RF, Meagor J, Taylor, EW (2002) Specific dynamic action in the shore crab, *Carcinus maenas* (L.), in relation to acclimation temperature and to the onset of the emersion response. *Physiological & Biochemical Zoology*, **75**, 350–359.

Rosas C, Sánchez A, Díaz-Iglesia E, Brito R, Martinez E, Soto LA (1997) Critical dissolved oxygen level to *Penaeus setiferus* and *Penaeus schmitti* postlarvae (PL10-18) exposed to salinity changes. *Aquaculture*, **152**, 259–272.

Rosas C, Martinez E, Gaxiola G, Brito R, Sánchez A, Soto LA (1999) The effect of dissolved oxygen and salinity on oxygen consumption, ammonia excretion and osmotic pressure of *Penaeus setiferus* (Linnaeus) juveniles. *Journal of Experimental Marine Biology & Ecology*, **234**, 41–57.

Schmitt ASC, Uglow RF (1998) Metabolic responses of *Nephrops norvegicus* to progressive hypoxia. *Aquatic Living Resources*, **11**, 87–92.

Seidman ER, Lawrence AL (1985) Growth. Feed digestibility, and proximate body composition of juvenile *Penaeus vannamei* and *Penaeus monodon* grown at different dissolved oxygen levels. *Journal of the World Mariculture Society*, **16**, 333–346.

Spoek GL (1974) The relationship between blood haemocyanin level, oxygen uptake, and the heart-beat and scaphognathite-beat frequencies in the lobster *Homarus gammarus*. *Netherlands Journal of Sea Research*, **8**, 1–26.

Stickle WB, Kapper MA, Liu L-L, Gnaiger E, Wang SY (1989) Metabolic adaptations of several species of crustaceans and molluscs to hypoxia: tolerance and microcalorimetric studies. *Biological Bulletin*, **177**, 303–312.

Subrahmanyam CB (1962) Oxygen consumption in relation to body weight and oxygen tension in the prawn *Penaeus indicus* (Milne Edwards). *Proceedings of the Indian Academy of Sciences-Section B*, **55**, 152–161.

Tankersley RA, Wieber MG (2000) Physiological responses of postlarval and juvenile blue crabs *Callinectes sapidus* to hypoxia and anoxia. *Marine Ecology Progress Series*, **194**, 179–191.

Taylor AC (1976) The respiratory responses of *Carcinus maenas* to declining oxygen tension. *Journal of Experimental Biology*, **65**, 309–322.

Taylor EW (1981) Some effects of temperature on respiration in decapodan crustaceans. *Journal of Thermal Biology*, **6**, 239–248.

Taylor EW, Butler PJ (1973) The behaviour and physiological responses of the shore crab *Carcinus maenas* during changes in environmental oxygen tension. *Netherlands Journal of Sea Research*, **7**, 496–505.

Taylor EW, Butler PJ (1978) Aquatic and aerial respiration in the shore crab, *Carcinus maenas* (L.), acclimated to 15 °C. *Journal of Comparative Physiology*, **127**, 315–323.

Thompson RK, Pritchard AW (1969) Respiratory adaptations of two burrowing crustaceans, *Callianassa californiensis* and *Upogebia pugettensis* (Decapoda, Thalassinidea). *Biological Bulletin*, **136**, 274–287.

Torres JJ, Aarset AV, Donnelly J, Hopkins TL, Lancraft TM., Ainley DG (1994) Metabolism of Antarctic micronektonic Crustacea as a function of depth of occurrence and season. *Marine Ecology Progress Series*, **113**, 207–220.

U.S. EPA (2000) Ambient Aquatic Life Water Quality Criteria for Dissolved Oxygen (Saltwater): Cape Cod to Cape Hatteras.

Vargo SL, Sastry AN (1977) Acute temperature and low dissolved oxygen tolerances of brachyuran crab (*Cancer irroratus*) Larvae. *Marine Biology*, **40**, 165–171.

Vetter R-AH, Franke H-D, Buchholz F (1999) Habitat-related differences in the responses to oxygen deficiencies in *Idotea baltica* and *Idotea emarginata* (Isopoda, Crustacea). *Journal of Experimental Marine Biology & Ecology*, **239**, 259–272.

Villarreal H, Ocampo L (1993) Effect of size and temperature on the oxygen consumption of the brown shrimp *Penaeus californiensis* (Holmes, 1900). *Comparative Biochemistry and Physiology Part A: Physiology*, **106**, 97–101.

Waldron FM (1991) Respiratory and acid-base physiology of the New Zealand rock lobster, *Janus edwardsii* (Hutton). PhD Thesis, University of Canterbury

Weymouth FW, Crimson JM, Hall VE, Belding HS, Field J (1944) Total and tissue respiration in relation to body weight a comparison of the kelp crab with other crustaceans and with mammals. *Physiological Zoology*, **17**, 50–71.

Whyte JNC, Carswell BL (1982) Determinants for live holding the spot prawn *Pandalus platyceros*, Brandt. *Canadian Technical Report of Fisheries Aquatic Sciences*, **1129**, 1-29

Winget RR (1969) Oxygen consumption and respiratory energetics in the spiny lobster, *Panulirus interruptus* (Randall). *Biological Bulletin*, **136**, 301–312.

Wu RSS, Or YY (2005) Bioenergetics, growth and reproduction of amphipods are affected by moderately low oxygen regimes. *Marine Ecology Progress Series*, **297**, 215–223.

Wu RSS, Lam PKS, Wan KL (2002) Tolerance to, and avoidance of, hypoxia by the penaeid shrimp (*Metapenaeus ensis*). *Environmental Pollution*, **118**, 351–355.

Yannicelli B, Paschke K, González RR, Castro LR (2013) Metabolic responses of the squat lobster (*Pleuroncodes monodon*) larvae to low oxygen concentration. *Marine Biology*, **160**, 961–976.

Zhou H, Li Y, Wei L, Zhang Z, Huang H, Diao X, Xiang J (2014) Sensitivity of larvae and adult and the immunologic characteristics of *Litopenaeus vannamei* under the acute hypoxia. *Journal of Chemistry*, **2014**, 1–6.

Zou E, Stueben B (2006) Acute exposure to naphthalene reduces oxyregulating capacity of the brown shrimp, *Penaeus aztecus*, subjected to progressive hypoxia. *Marine Biology*, **149**, 1411–1415.

Table C.2. O_2^{crit} values reported for flatfish (order Pleuronectiformes). O_2^{crit} in $[O_2]$ and equivalent pO_2 units are reported with each species along with common names, family, and location of population from the associated reference (Ref.)

Common Name	Species	Family	Location	$[O_2]^{crit}$ (ml l^{-1})	pO_2^{crit} (kPa)	Ref.
Slender sole	*Lyopsetta exilis*	Pleuronectidae	East Pacific	0.36	1.1	1
Hogchoker	*Trinectes maculates*	Achiridae	West Atlantic	0.36	3.9	2
Windowpane flounder	*Scophthalmus aquosus*	Scophthalmidae	West Atlantic	0.64	3.5	3
Winter Flounder	*Pseudopleuronectes americanus*	Pleuronectidae	West Atlantic	0.90	3.0	3
Summer Flounder	*Paralichthys dentatus*	Paralichthyidae	West Atlantic	0.77	3.8	3
Summer Flounder	*P. dentatus*	Paralichthyidae	West Atlantic	1.12	5.2	3
Summer Flounder	*P. dentatus*	Paralichthyidae	West Atlantic	1.40	4.0	4
Turbot	*Scophthalmus maximus*	Scophthalmidae	East Atlantic	1.13	4.0	5
Starry Flounder	*Platichthys stellatus*	Pleuronectidae	East Pacific	2.00	6.7	6
European Flounder	*Platichthys flesus*	Pleuronectidae	East Atlantic	2.80	8.0	7

Literature cited in Table C.2

[1] *This study*

[2] Pihl L, Baden SP, Diaz RJ (1991) Effects of periodic hypoxia on distribution of demersal fish and crustaceans. *Marine Biology*, **108**, 349-360.

[3] Miller DC, Poucher SL, Coiro L (2002) Determination of lethal dissolved oxygen levels for selected marine and estuarine fishes, crustaceans, and a bivalve. *Marine Biology*, **140**, 287–296.

[4] Capossela KM, Brill RW, Fabrizio MC, Bushnell PG (2012) Metabolic and cardiorespiratory responses of summer flounder *Paralichthys dentatus* to hypoxia at two temperatures. *Journal of Fish Biology*, **8**, 1043-1058.

[5] Maxime V, Pichavant K, Goeuf G, Nonnotte G (2000) Effects of hypoxia on respiratory physiology of turbot, *Scophthalmus maximus. Fish Physiology & Biochemistry*, **22**, 51-59.

[6] Watters KW, Smith LS (1973) Respiratory dynamics of the starry flounder *Platichthys stellatus* in response to low oxygen and high temperature. *Marine Biology*, **19**, 133-148.

[7] Steffensen JF, Lomholt JP, Johansen K (1982) Gill ventilation and O2 extraction during graded hypoxia in two ecologically distinct species of flatfish, the flounder (*Platichthys flesus*) and the plaice (*Pleuronectes platessa*). *Environmental Biology of Fishes*, **2**, 157-163.

Appendix D: Mechanisms of propagule release in the carnivorous sponge *Asbestopluma occidentalis*

Preface

Appendix D is a research article in Invertebrate Biology: Chu JWF, Reiswig HM (2014) Mechanisms of propagule release in the carnivorous sponge *Asbestopluma occidentalis*. Invertebrate Biology, 133, 109-120.

This article was a product of coursework I took for my PhD dissertation requirements. Dr. Henry M. Reiswig (*retired* Adjunct Professor, University of Victoria) supervised the coursework (BIOL 550B – Advanced Invertebrate Biology), re-examined and measured spicules from the original type specimen of *A. occidentalis*, and provided input during the writing of the article.

I conceived and designed the study, did the field work, performed the experiments, generated and analyzed the data, interpreted the results, and wrote the article.

Abstract

Carnivorous sponges characteristically inhabit the deep sea, so extensive observations of the biology of living specimens are rare. I report on newly discovered shallow water (<30 m depth) populations of the carnivorous sponge *Asbestopluma occidentalis* and on observations of living adults and larvae from this unique group of sponges. In the Salish Sea, British Columbia, Canada, populations of *A. occidentalis* exist at depths as shallow as 18 m, where they co-occur with hexactinellid sponges. Adults

with and without embryos (n=127) were collected and easily maintained in the laboratory for several months, allowing continuous examination of live specimens. Parent sponges naturally disassociated their tissue, facilitating larval release and dispersal. Dispersed larvae had actively beating cilia, but no swimming was observed. Larvae settled and attached from several hours to several days post-release. After larval release, parent sponges reaggregated their disassociated bodies into spherical balls of apparently undifferentiated tissue, which could also disperse and settle. Sexually mature adults were sampled in the field from August to November, with a high proportion of adults containing mature embryos in late November. High-resolution photography and electron microscopy verified that adults were covered with anisochelae spicules, and used these to capture nauplii of *Artemia* sp. under experimental conditions; however, time-lapse photography showed that some captured prey could free themselves with vigorous swimming. The occurrence of abundant shallow-water populations of *A. occidentalis* in the Salish Sea provides a rare opportunity to study the evolution and ecology of carnivory in the Porifera.

Introduction

Carnivorous sponges (Demospongiae, Poecilosclerida) have drastically deviated from the typical body plan known in all other members of the phylum Porifera. Non-carnivorous sponges have an aquiferous system that functions to create an internal, unidirectional flow of water for suspension feeding, waste removal, and dispersal of gametes and larvae (Simpson, 1984). Carnivorous sponges, however, have lost or markedly modified the function of the aquiferous system and employ surface spicules to

prey on tiny crustaceans (Kübler & Barthel, 1999; Vacelet, 2007) as an adaptation to living in the food-impoverished deep sea (Vacelet & Boury-Esnault, 1995). The evolutionary significance of predation in this gutless phylum has been thoroughly described (Vacelet & Boury-Esnault, 1995). However, the loss of the aquiferous system also means that carnivorous sponges lack the internal plumbing used to capture sperm and release offspring. Modification of the sponge body plan has also resulted in reproductive strategies and larvae that are atypical in the Porifera (Vacelet, 2007; Riesgo, 2010; Lee *et al.*, 2012). Our knowledge of the reproductive ecology of carnivorous sponges has been limited due to their preferred deep-sea habitat.

Prior to my study, populations of carnivorous sponges accessible by SCUBA had been reported at only six locations: the 3PP cave on La Ciotat (Vacelet & Boury-Esnault, 1995; Vacelet, 1996) and Jarre Island Cave (Bakran-Petricioli *et al.*, 2007) in the French Mediterranean, Veli Garmenjak Island cave off of Croatia in the Adriatic Sea (Bakran-Petricioli *et al.*, 2007), McMurdo Sound in Antarctica (Van Soest & Baker, 2011), and along the coasts of the Ria de Arousa, Galicia, Spain and the Island of Groix, Britanny, France (P. Chevaldonné pers. comm.). At the first four sites, shallow-water carnivorous sponge can be found with or near shallow-water populations of glass sponges (Hexactinellida), including *Oopsacas minuta* TOPSENT 1927 in the Mediterranean (Vacelet *et al.*, 1994) and Adriatic (Bakran-Petricioli *et al.*, 2007) and *Rossella nuda* TOPSENT 1901, *R. racovitzae* TOPSENT 1901, and *Anoxycalyx joubini* (TOPSENT 1916) in McMurdo Sound (Dayton *et al.*, 1974; Dayton, 1979). Coastal British Columbia, Canada (BC) is also well-documented to have hexactinellids at SCUBA depths (Leys *et al.*, 2004); the potential for shared habitat requirements between glass sponges and

carnivorous sponges suggested that British Columbia could also be harboring populations of carnivorous sponges accessible by SCUBA.

While surveying five shallow water (<30 m) locations in the Salish Sea, British Columbia, known to have the glass sponges *Rhabdocalyptus dawsoni* (LAMBE 1893) and *Aphrocallistes vastus* SCHULZE 1886, I discovered large populations of the carnivorous sponge *Asbestopluma (Asbestopluma) occidentalis* (LAMBE 1893) at all locations. The abundance of shallow-water populations of *A. occidentalis* enabled me to access a large sample of adult sponges and to continuously monitor their life history in the laboratory. Sexually immature and mature specimens were sampled and kept alive in the laboratory for several months, enabling me to make the first observations of larval release, behavior, and settlement in carnivorous sponges that lack choanocyte chambers and an aquiferous system. Such descriptions are unknown for carnivorous sponges due in part to their usual restriction to deep-sea habitats.

Materials and methods

Field sites and sponge sampling

Populations of *Asbestopluma occidentalis* were found throughout the Salish Sea at all five sites surveyed by SCUBA (Fig. D.1, Table D.1). Each dive site was accessible from the shoreline, and the sponges were collected within recreational SCUBA depths (18-35 m) and normal no-decompression diving limits. The sponges were nearly always found attached to hard bedrock on vertical walls with slightly overhanging areas and dark conditions (Fig. D.2A). Although the population density of sponges was not quantified, 30-40 individuals could easily be observed within a 5 min inspection of the rock walls at

Table D.1. Dive site locations and depths of shallow-water populations of *Asbestopluma occidentalis.* "Date" indicates when *A. occidentalis* were first discovered at each site. "Depth" only refers to shallowest occurrence of sponges because divers were unable to survey the deepest depth of the habitat range. Dive site numbers in parentheses are the same as those in Figure D.1.

Date	Dive Site	Latitude	Longitude	Depth (m)
2010-Nov-05	(2) Whytecliff Park, Howe Sound	49.372	-123.294	27.4
2011-Jul-26	(1) Kelvin Grove, Howe Sound	49.45	-123.242	18.0
2011-Sep-24	(5) Mckenzie Bight, Saanich Inlet	48.564	-123.479	27.4
2011-Sep-25	(3) Madrona Point, Strait of Georgia	49.317	-124.239	28.7
2011-Nov-11	(4) Willis Point, Saanich Inlet	48.564	-123.499	27.4

each site. The invertebrate community found with the sponges was diverse, and included orange cup corals (*Balanophyllia elegans* VERRILL 1864), calcareous tubeworms (*Serpula* sp.), encrusting bryozoans, hydroids, anemones, and several crustacean species (Fig. D.2B). Individuals of the glass sponges *Rhabdocalyptus dawsoni* and *Aphrocallistes vastus* were found growing on the same hard bedrock in close proximity to *A. occidentalis* or several meters deeper. From 2011 to 2012 (Table D.2), adults of *A. occidentalis* with body lengths >1 cm (Fig. D.2C) were carefully collected by dislodging them from the bedrock using the tip of a dive knife, and placing them into plastic Ziploc bags (Video D.1). Sponges collected from one of the locations, Saanich Inlet (Fig. D.1, Table D.1), were transported to the laboratory at the University of Victoria and were the primary specimens used in my observations.

Table D.2. Sampling dates, effort, and proportion of sexually reproductive sponges.

Sampling date	Dive site	Sponges sampled	Proportion with embryos (n)
2011-Jul-26	Kelvin Grove	4	0.00 (0)
2011-Aug-02	Kelvin Grove	15	0.07 (1)
2011-Oct-16	Mckenzie Bight	17	0.35 (6)
2011-Nov-13	Willis Point	21	0.48 (10)
2012-Sep-08	Willis Point	50	0.34 (17)
2012-Nov-24	Willis Point	20	1.00 (20)

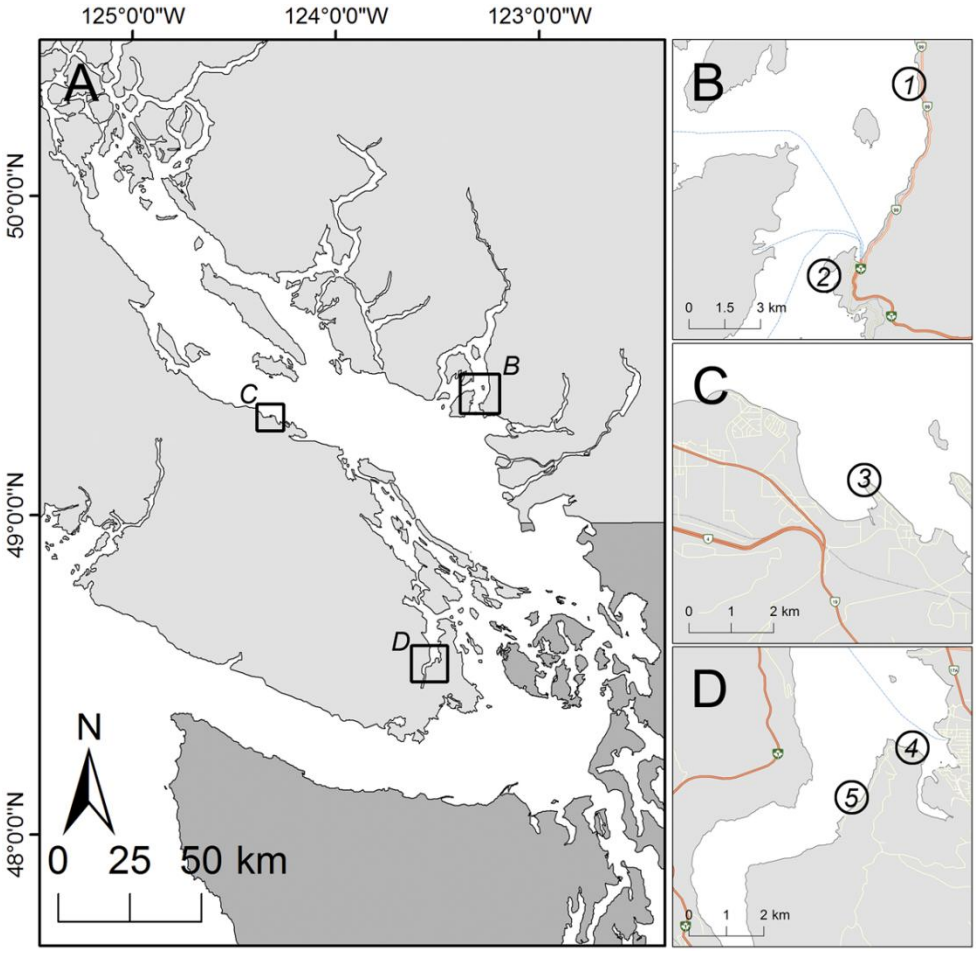

Figure D.1. Locations of shallow-water populations of *Asbestopluma occidentalis*. Inset letters in overall map of Salish Sea (A) correspond to maps of Howe Sound (B), Strait of Georgia (C), and Saanich Inlet (D). Public highways are used as identifying local landmarks. Numbers correspond to the dive sites listed in Table D.1.

Maintenance of sponges in the laboratory

Sponges were maintained individually in separate containers because they would stick together after being dislodged during sampling. Sponges were placed in 9 cm diameter Petri dishes with 15 ml of 0.45µm-filtered sea water that was replaced every 2-3 weeks. All adults were examined with an Olympus SZX12 dissecting microscope

(Olympus Corporation, Tokyo Japan) within 24 h of collection for signs that they were brooding embryos, which were visible through the transparent outer tissue layer (Riesgo

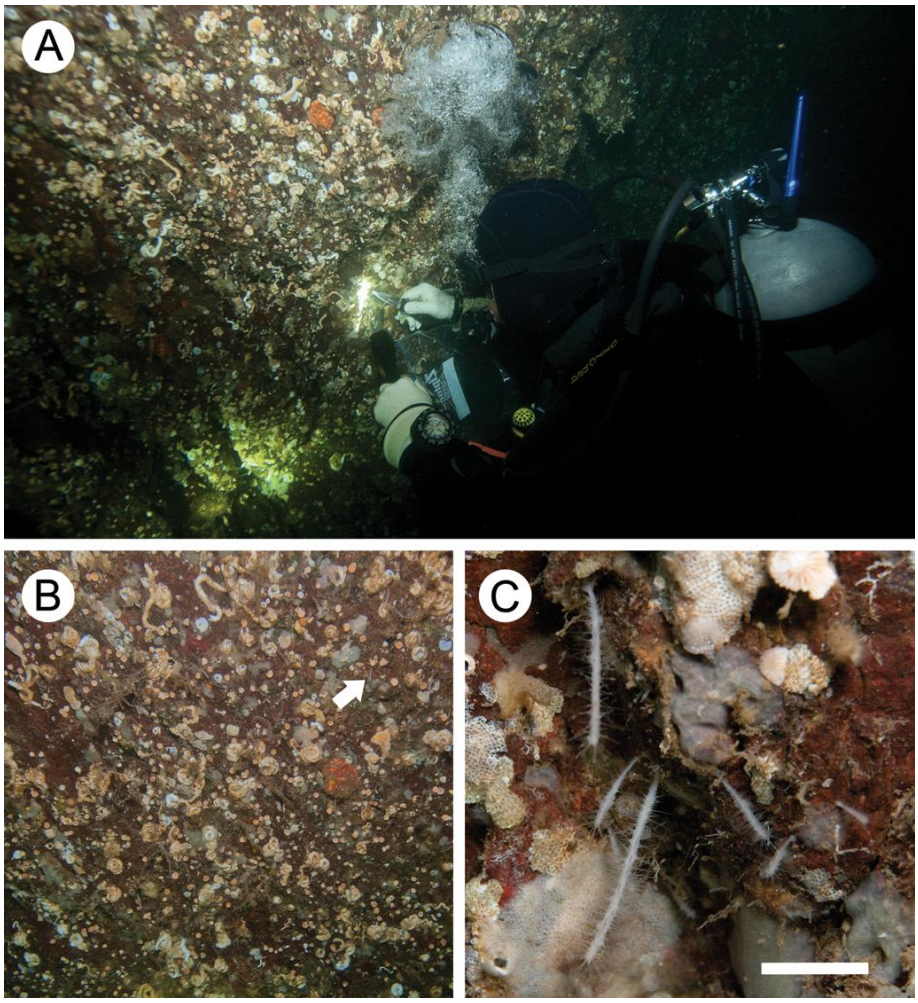

Figure D.2. Hard substratum habitat of the carnivorous sponge *Asbestopluma occidentalis*. (A) Adult sponges were found on near vertical rock walls within a diverse associated invertebrate community of sessile epifauna. (B) A typical area of hard substratum with adult sponges (arrow; there are more than 20 individuals in this image). (C) Adult individuals of *A. occidentalis*. Scale bar in C=1 cm; no scale bars are available for A and B. Images courtesy of Ian Redan.

et al., 2007). Sponges were segregated into three groups: sexually mature for observation of larval release, sexually immature for monitoring of condition (starved), and sexually

immature for feeding experiments. All sponges were kept at 4°C, and sexually mature specimens were frequently examined (2-3 times a week) with a dissecting microscope for released larvae. All adult sponges except the feeding group were starved throughout the duration of observations (2-3 months); those segregated for feeding experiments were supplied with live 24-36 h-old nauplii of *Artemia* sp. (San Francisco Bay Brand) during feeding experiments.

Released larvae were collected with glass Pasteur pipettes and transferred to 3.5 cm diameter Petri dishes filled with filtered sea water; a glass cover slip was laid on the bottom of the Petri dish as a settlement substrate. Settled larvae were viewed with an Olympus IX71 inverted microscope (Olympus Corporation, Tokyo Japan) and imaged with a Qimaging CCD camera (Qimaging Corporation, Surrey, British Columbia, Canada) and the free open-source software Micro-Manager 1.4 (University of California, San Francisco, California, USA).

Still and time-lapse photography

Adult sponges were placed in clean 9 cm diameter Petri dishes filled with filtered sea water on top of a black surface. Images were taken with a Pentax K-7 14 megapixel DSLR camera (Pentax Ricoh Imaging Company Inc., Tokyo, Japan) with a reverse mounted Pentax SMC-M 28 mm F3.5 lens on top of extension tubes of varying lengths (9, 16, or 30 mm) or a Vivitar 2x macro focusing teleconverter lens (Sakar International Inc., Edison, New Jersey, USA). Lighting was provided by an external Pentax AF-360FGZ flash connected by a hotshoe sync cable. Sponges were photographed in thirds (top, middle, base) and the sections were processed and stitched together in Adobe

Photoshop (Adobe Systems Inc., San Jose, California, USA) to yield high-resolution images of each whole individual.

Prey capture and feeding experiments were recorded using time-lapse photography using a Pentax K-10D 10 megapixel DSLR camera with the same lenses as above, with a fiber-optic light source (Fisher Scientific International Inc., Hampton, New Hampshire, USA) instead of a flash. The camera was tethered to and controlled by a laptop running the software PK_tether (Kos 2011) which enabled the high-resolution images to be captured directly to the hard drive every 30 s. Images were combined into movie clips (1080p, 25 fps, h264 video codec) using free Avidemux software (Avidemux 2012) and processed in Adobe Premiere Pro (Adobe Systems Inc., San Jose, California, USA).

Scanning electron microscopy

Sponges were prepared for fixation in three different ways. Adults brooding larvae were cut into transverse sections and placed into Eppendorf tubes with filtered sea water, and live larvae were either pipetted into Eppendorf tubes in filtered sea water or placed on poly-L-lysine coated (Sigma-Aldrich Canada Co., Oakville, Ontario, Canada), 10 mm diameter, round glass cover slips in a Petri dish with filtered sea water. Excess sea water was pipetted out from each container and specimens were fixed by addition of a cocktail of 2% glutaraldehyde and 1% osmium tetroxide in 0.45 M sodium acetate buffer (pH 6.4) with 10% sucrose in the final volume, at 4°C (Leys *et al.*, 2006). The fixative was changed after 30 min and the specimens were left at 4°C for 2 h or overnight. Specimens were then rinsed 3x in filtered sea water, 2x in distilled water, followed by sequential rinses of 30%, 50%, and 70% ethanol (10 min each rinse) before a final

immersion in 100% ethanol. Specimens were then critical-point dried, mounted onto aluminum stubs with nail polish or double-sided tape, sputter coated with gold, and viewed using a Hitachi S-3500N scanning electron microscope at the University of Victoria (Hitachi High-Technologies Corp., Tokyo, Japan). The poly-L-lysine coated cover slips proved to be unreliable as larvae were lost during the critical-point drying stage, therefore all images presented are from the first two preparation protocols.

Results

Observations of adult sponges

I sampled 127 adults of *Asbestopluma occidentalis* and maintained them alive for several months in the laboratory. The dominant morphotype of this species conformed to the original description (Lambe, 1893) and the 45 specimens described in Riesgo *et al.* (2007). Adults had a central, creamy white stalk 1-2 cm long and 0.8-1 mm wide (Fig. D.3A) with an endoskeleton made of styles (886±254 µm long, n=100 [mean ± sd] and 9.3±2.6 µm wide, n=26). Several of the sampled sponges (n=12), however, had signs of bipartioning (Fig. D.3B) or what appeared to be conjoined individuals connected by an umbilicus of tissue (Fig. D.3C). None of these specimens split to form two asexually-produced individuals for the duration of my observations. Lateral body extensions (filaments) supported by bundled tylostyle spicules projected outwards along the sponge body except near the basal region, which narrowed slightly before forming a holdfast to anchor onto hard substratum. A smaller size class of (sub)tylostyles (204±65 µm long, n=25 and 4.1±1.2 µm wide, n=25) occurred primarily in the holdfast but was also strewn throughout the main body of the sponge. Small forcep spicules (40.1±2.3 µm long, n=25)

were distributed throughout the sponge body. Interestingly, the smaller size class of subtylostyles was not mentioned in the original description by Lambe (1893), and on reinspection of the type specimen (Canadian Museum of Nature catalog number 1900-2887) I failed to detect these spicules. Palmate anisochelae (11.9±0.9 µm long, n=25)

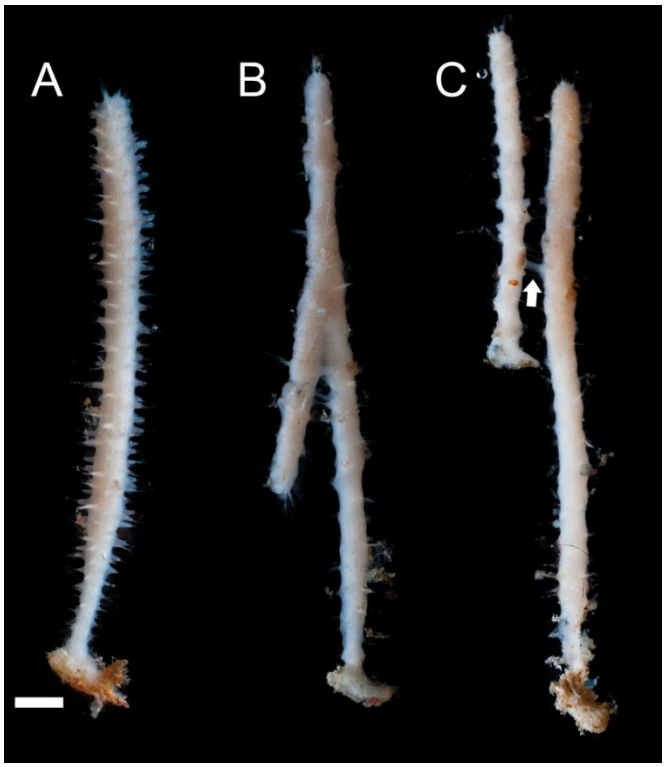

Figure D.3. Morphotypes of adults of *Asbestopluma occidentalis*. (A) The typical adult morphotype consisted of a slender,white central stalk with lateral projections and a basal holdfast. Atypical morphotypes (B,C) occurred in ~10 % of the samples in this study. (B) Bipartitioning morphotype where the central stalk appeared to split in half. (C) Conjoined sponges connected by an umbilicus of tissue (arrow). Scale bar=1 mm.

coated the entire external surface of the adult body in areas with tissue (Fig. D.4A) except the distal tips of the filaments, which were often bare in adults without visible reproductive structures (Fig. D.4B). Tissue was able to migrate outwards along these bundles of tylostyles, functionally increasing the surface area of the individual and the

probability of prey capture (Fig. D.4B,C). When freshly sampled in the field, sponges always had many tiny crustaceans (amphipods, isopods, ostracods) already captured in their Velcro-like anisochelae, or were in the process of digestion (visible in all figures showing adult sponges). Feeding experiments verified that *A. occidentalis*, like *A. hypogea* Vacelet & Boury-Esnault 1996, could passively capture nauplii of *Artemia* sp. (Video D.2). Time-lapse video sequences indicate that not all ensnared prey were subsequently digested. Some nauplii of *Artemia* sp. were able to escape when vigorously swimming and only slightly hooked onto the anisochelae (Video D.3).

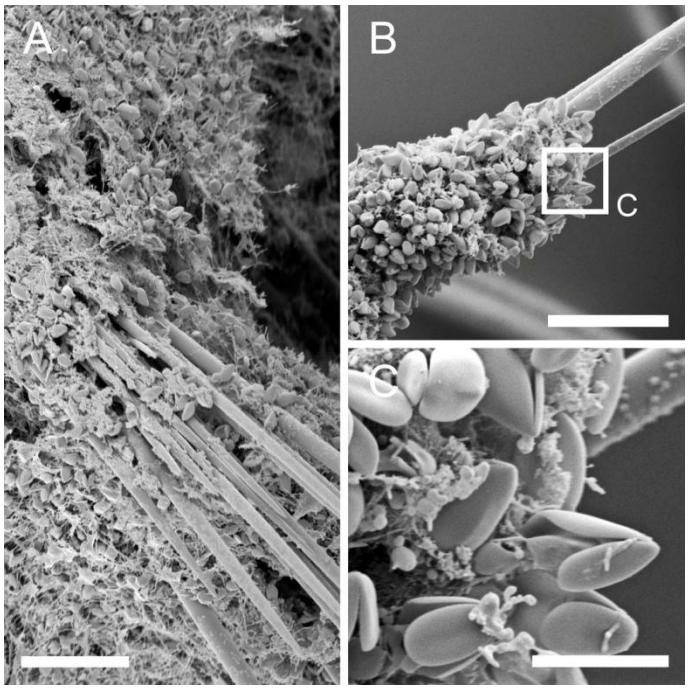

Figure D.4. Locations of external anisochelae spicules in adults of *Asbestopluma occidentalis*. (A) The external surface of the main body trunk of the adult sponge was completely covered in anisochelae spicules anchored with collagen. Scale bar= 50 μm. (B) Tissue that migrated outwards along the lateral projections of bundled tylostyles served as extended capture point areas for prey. Scale bar= 50 μm. (C) Anisochelae acted as "fish hooks" for capturing prey. Scale bar=10 μm.

Reproductive biology

Adult sponges with embryos were sampled from August to November, with the highest proportion of sampled specimens having embryos in late November (Table D.2). I also found individuals with spermatic cyst development throughout my sampling periods. Clusters of spermatic cysts were most noticeable in the bulbous protrusion found at the distal points of the filaments, which were most apparent at the apical end of the sponge body (Fig. D.5A). Mature spermatic cysts were transported away from the central stalk towards the bulbous protrusions of filaments, where concentrations of up to 20-30 spermatic cysts were observed (Fig. D.5B,C). Despite their presence in my sampled sponges, I did not attempt to monitor the release and capture of the spermatic cysts in this study, focusing instead on the embryos and larvae.

Developing embryos were readily visible underneath the transparent outer tissue layers of the parent's main body trunk. Adults with brooding embryos were easily reared in the laboratory through larval release. Within weeks of the initial stage of larval release and while embryos continually matured, most of the tissue in the parent sponges retracted away from the lateral projections and concentrated around the main body trunk (Fig. D.6A). In adults where release of larvae was imminent, the adult trunk tissue began to naturally disassociate (Fig. D.6B), a phenomenon that was not observed in adults without embryos that were sampled at the same time (Table D.2). Within the first 24 h of a period of larval release, anywhere from 1-221 larvae detached from their parent sponge. The process of larval release occurred over several days in the laboratory. After larval release, the parent sponges lost over 50% of their tissue mass, which exposed the inner core of longitudinal tylostyles that make up the primary endoskeleton of the body trunk (Fig.

D.6C). Each larva was encapsulated in an envelope of follicle cells and anchored inside the parent body by collagen strands (Fig. D.6D,E). Disassociation of the parent tissue coinciding with larval release freed the larvae from the follicle cell envelope (Fig. D.6F), enabling the ciliated larvae to individually disperse from the parent.

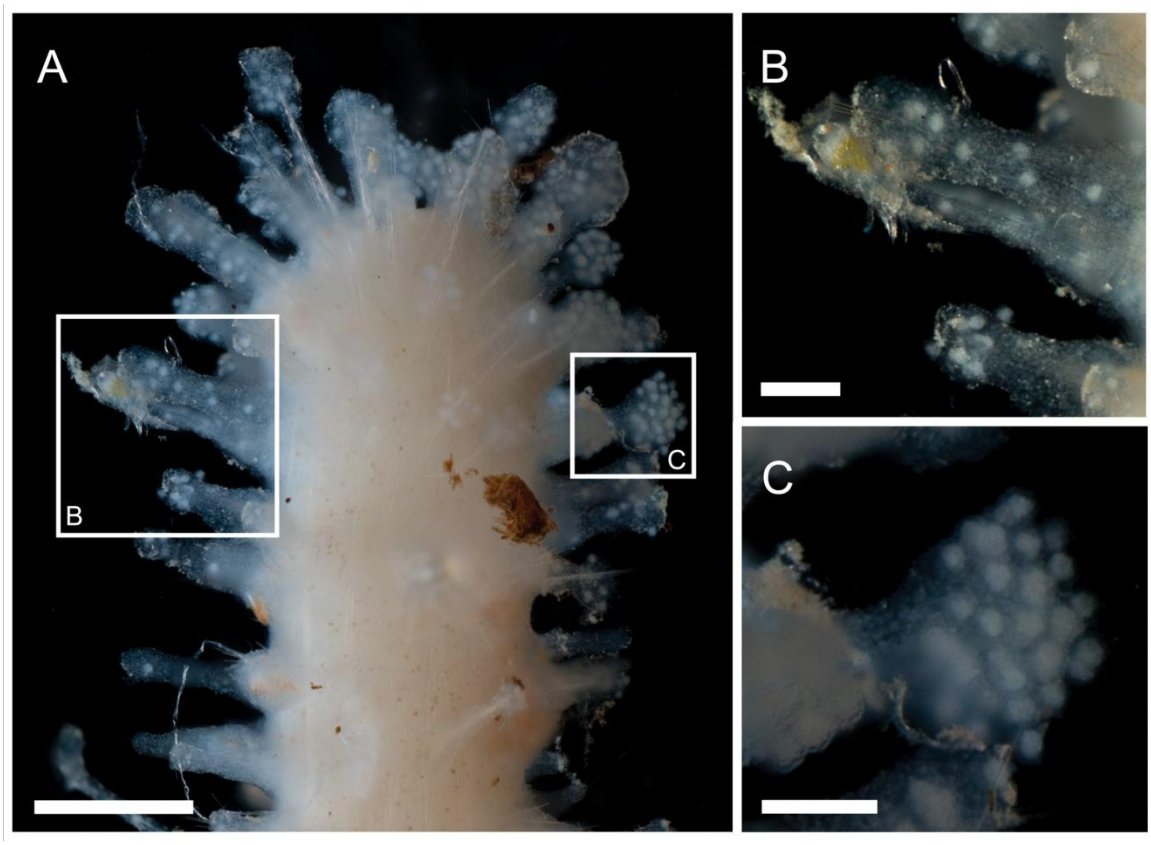

Figure D.5. Spermatic cyst development in *Asbestopluma occidentalis*. (A) Bulbous protrusions of tissue occurred at the distal tips of the filaments and were most abundant at the distal end of the sponge. Scale bar=0.5 mm. (B) Spermatic cysts migrated from the central stalk outwards towards the bulbs along the filaments. Scale bar=100 μm. (C) Twenty to thirty spermatic cysts could occur in a single bulbuous protrusion. Scale bar=100 μm.

At the end of larval release, the remaining disassociated tissue on the parent sponges reaggregated into spherical balls of apparently undifferentiated tissue (Fig. D.7A). Tissue aggregates detached from the parent body which, at this late life cycle stage, consisted mainly of bare spicules (Fig. D.7B). Aggregates varied in size from

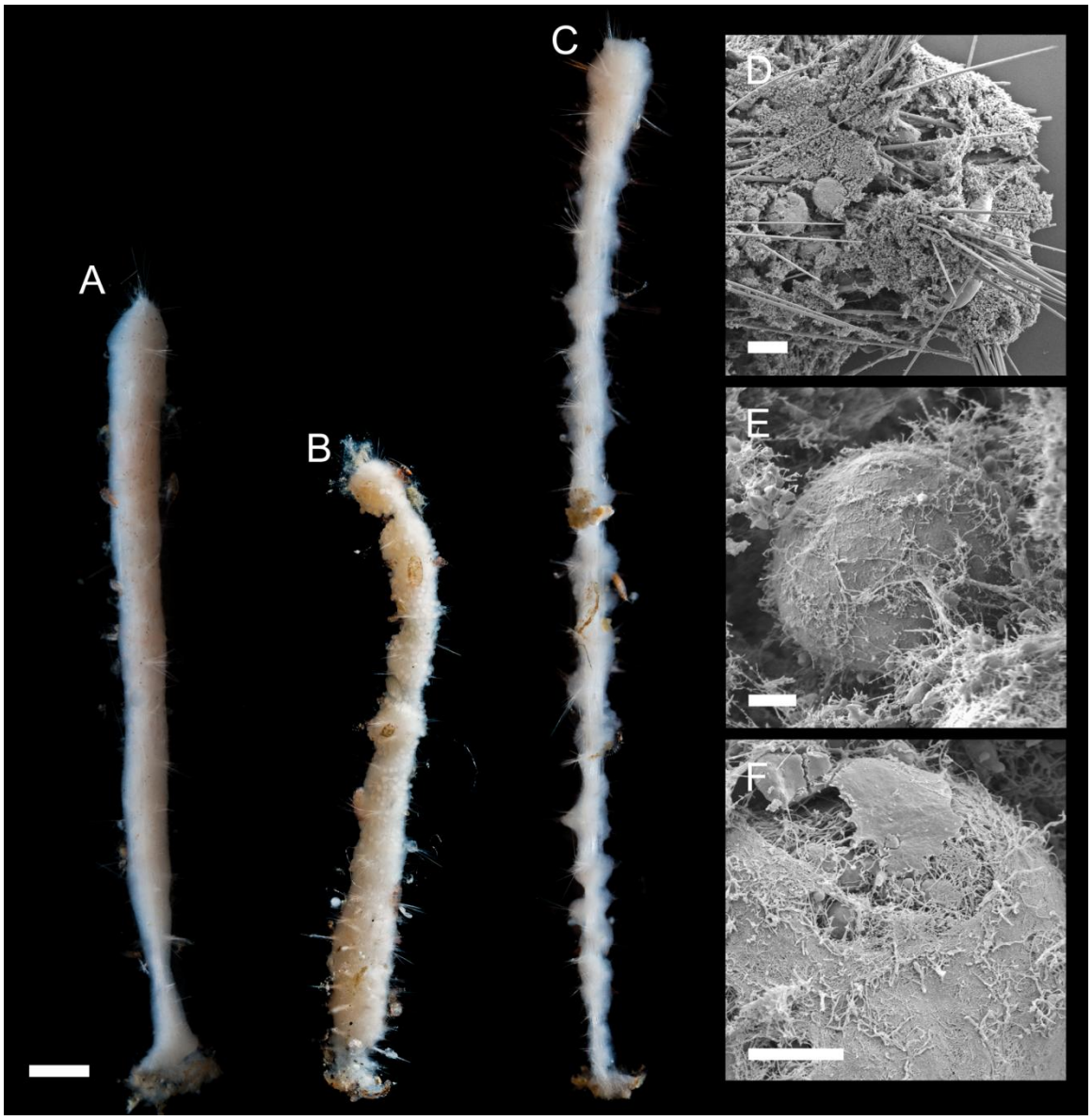

Figure D.6. Larval release in *Asbestopluma occidentalis*. (A) Adult tissue retracted from filament spicule bundles and concentrated around the main body trunk days to weeks before release of larvae. Scale bar=1 mm. (B) Natural disassociation of tissue in the adult coincided with larval release. Scale bar=1 mm. (C) After larval release >50% of the parent sponges' initial organic mass was lost. This individual released 221 larvae within 24 h and was photographed immediately afterwards. Scale bar=1 mm. (D) Larvae were encapsulated in the parent's body in an envelope of follicle cells. Scale bar=20 µm. (E) Larvae were anchored in the parent's body by collagen strands. (F) Disassocation of the parent tissue freed the larvae from the follicle cell envelope. Scale bar=20 µm. Sponges in A-C were different individuals.

1 mm (Fig. D.7C) to 70 µm (Fig. D.7D) in diameter. Dispersed tissue aggregates were similar in size to larvae, but when inspected under magnification appeared as non-ciliated spheres of tissue (Fig. D.7E). Tissue aggregates were collected and, when gathered into Petri dishes, fused to become larger spheres that settled on glass cover slips or on the bottom of Petri dishes. In adults that were sampled without embryos, senescence occurred after several months and appeared as the loss of the typical creamy-white color of a healthy-looking sponge, an increase in translucence over time, and an absence of tissue disassociation and reaggregation.

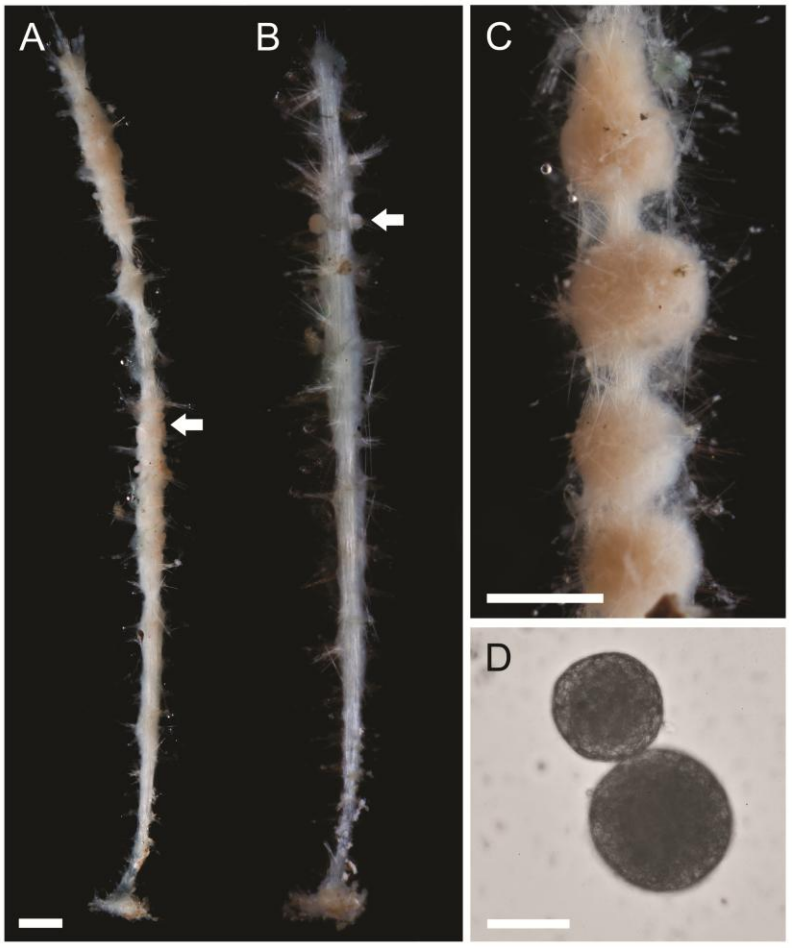

Figure D.7. Reaggreation of disassociated tissue in adults of *Asbestopluma occidentalis* after larval release. (A) After releasing their larvae, parent sponges reaggregated their disassociated tissue into spherical balls (arrow). Scale bar=1 mm. (B) End stage parent sponge with only a few remaining tissue aggregates (arrow) on the now exposed spicule skeleton. Scale bar=1 mm. (C) Tissue aggregate formation around body trunk. Scale bar=1 mm. (D) Dispersed tissue aggregates. Scale bar=20 µm.

Larvae of Asbestopluma occidentalis

The dispersed larvae were typical non-tufted parenchymella (Maldonado 2006) known for other poecelosclerids and identical to those described in detail by Riesgo et al. (2007). They were covered by multiciliated cells over two-thirds of the body except for their posterior pole and lacked external spicules when examined by scanning electron microscopy (SEM: Fig. D.8A). Internal anisochelae spicules were visible in larvae compressed by a glass coverslip and viewed under brightfield illumination (Fig. D.8B). In uncompressed larvae, no obvious swimming was seen after several minutes of observation under magnification despite continuous beating of their cilia. Larvae released within one week from the adults collected in early September were smaller and wider than those released from adults collected in late November (Fig. D.8C). September larvae were slightly more spherical (Fig. D.8D) compared to the elongated larvae from November (Fig. D.8E).

Larvae successfully settled, attached, and spread onto glass cover slips at the bottom of the Petri dishes from several hours to several days after dispersal (Fig. D8F). Although we did not keep track of time to settlement for individual larvae, those released from September sponges typically took days to settle and spread, compared to larvae released from November sponges, which settled overnight. During settlement, larvae would stick to the glass cover slips and no longer roll when the Petri dish was jostled. Numerous pseudopodia were seen at the leading edge of the spreading tissue in settled larvae (Fig. D8G). I did not attempt to monitor settled larvae beyond this time point in their life history.

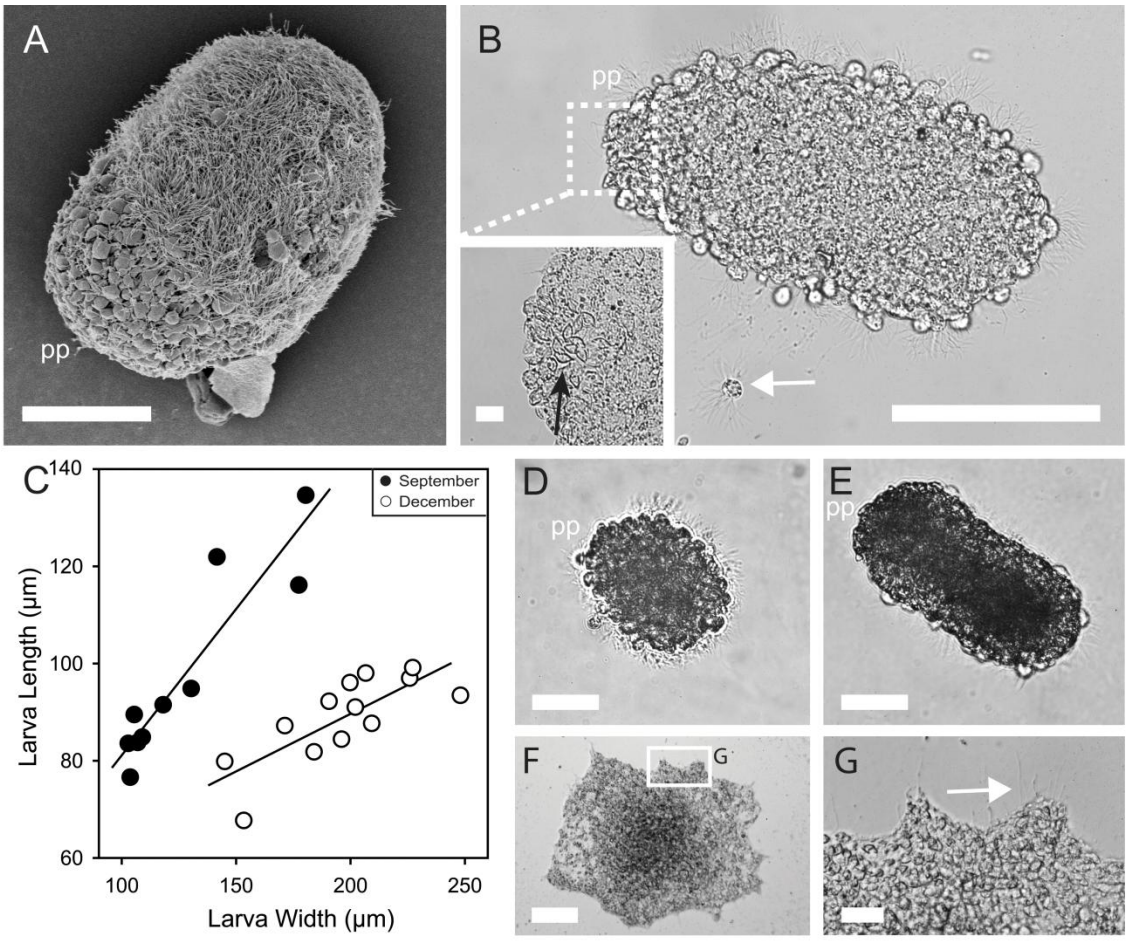

Figure D.8. Larvae of *Asbestopluma occidentalis*. (A) Dispersed parenchymella larvae covered in multiciliated cells except for the posterior pole (pp). Scale bar=50 µm. (B) Compression of larvae showed anisochelae spicules located internally (inset arrow). Note a detached multiciliated cell (arrow). Scale bar=100 µm; inset scale bar=10 µm. Size differences of dispersed larvae are shown in panels C-E. (C) Larvae (n=9) released from adults sampled in September were on average smaller than larvae (n=13) released from adults sampled in November. Scale bar=50 µm. (D) A larva released from a sponge sampled in September. These were shorter and slightly wider than larvae released from sponges sampled in November (see E). Scale bar=50 µm. (E) A larva released from a sponge sampled in November. Scale bar=50 µm. Note that only a small subsample of all larvae released during these two periods were measured. (F) Larvae settled in the lab from from several hours to several days after dispersal from the parent. Scale bar=50 µm. (G) Settled larvae spread across the substratum using pseudopodia (arrow). Scale bar=20 µm.

Discussion

I report on several shallow-water (<30 m) populations of *Asbestopluma occidentalis* in the Salish Sea and provide the first descriptions of larval behavior, settlement, and post-settlement behavior in a carnivorous sponge. I also describe a novel mechanism of larval release and post-release behavior in a sponge that lacks an aquiferous system. Prior to my study, the shallow water population of *A. (Asbestopluma) hypogea* from the 3PP cave was the only carnivorous sponge where repetitive sampling enabled live specimens to be continuously monitored in a laboratory (Vacelet & Boury-Esnault, 1995; Vacelet & Duport, 2004; Martinand-Mari *et al.*, 2012). Although geographically distant, *A. occidentalis* and *A. hypogea* are likely phylogenetically close. My discovery of shallow-water *A. occidentalis* creates the future opportunity to use a comparative approach to address the ecology of carnivory in sponges.

Observations of adult sponges

Asbestopluma occidentalis holds the record for the deepest occurrence of a sponge species, at 8840 m (Koltun, 1970). With my discovery of their shallow limit of 18 m, and if the original identification of *A. occidentalis* in hadal depths was accurate, then *A. occidentalis* to my knowledge has the widest occurring depth range of all known sponges, if not all metazoans. The distinct upper depth limit at the site of each sponge population is likely due to the photic zone being limited to the upper 30 m of the water column in the Strait of Georgia (Johannessen *et al.*, 2006). In Saanich Inlet, light attenuation drops off after 30 m which coincides with the photic zone's lower depth limit

(De Robertis *et al.*, 2001). The temperature at these depths was ~11°C across all the locations, and remains relatively constant throughout the year (Johannessen *et al.*, 2006; Beveridge, 2007). Lack of light and stable low temperatures are characteristic deep-sea habitat requirements for *A. hypogea* (Vacelet & Boury-Esnault, 1995; 1996) that also appear to be necessary for *A. occidentalis*. I was able to predict the presence of *A. occidentalis a priori* based entirely on the presence of glass sponges at each dive site, which indicates shared environmental conditions required by both deep-sea sponge groups. Interestingly, whereas glass sponges can exclude other suspension-feeding sponges (Chu *et al.*, 2010), *A. occidentalis* can co-exist with glass sponges because they can use the dead skeletons of glass sponges as a recruitment substratum (Riesgo *et al.*, 2007) and they lack the suspension feeding mechanisms to compete for the same food resources. Several more populations of glass sponges occur at these depths throughout the Salish Sea (Leys *et al.*, 2004), which means additional populations of *A. occidentalis* may yet be discovered.

My direct observation of prey capture by *A. occidentalis* makes it only the second cladorhizid species in which predation has been verified with direct experimentation. My observation strengthens the generality of this feeding process in the family. It also lends support to the supposition that the specimens held in captivity for months at low temperature in darkness remained healthy and that larval development and release probably followed their normal courses. Like *A. hypogea* (Vacelet & Duport, 2004; Martinand-Mari *et al.*, 2012), the cells of *A. occidentalis* are dynamic and migrate back and forth along the laterally-extended bundles of tylostyle spicules for both feeding and

reproduction. However, whether tissue in *A. occidentalis* is also actively experiencing apoptosis or programmed cell death is unknown.

The frequency of atypical body forms occurring (~10%) in the field emphasizes the need for sampling of multiple individuals and the use of microscopic spicule analysis for taxonomy due to the potential variability of body shape within a species. Although the mechanism causing these variable morphotypes occur is unknown, symmetrical branching morphotypes are known for *Chondrocladia lyra* Lee, Reiswig, Austin, & Lundsten 2012 (Lee *et al.*, 2012) and an asymmetrically branching morphotype has been documented in *Abyssocladia naudur* Vacelet 2006 (Vacelet, 2006). My discovery of shallow populations of carnivorous sponges enables us to address the extent of morphotype variation in this species in the future.

Reproductive strategies

My temporal sampling suggests seasonality in the reproductive cycle could be occurring in the sponge populations we studied. The November peak in the proportion of adults with embryos can be linked to light as a cue for larval release since the upper 30 m of the water column at these sites experience their lowest level of primary productivity and highest levels of light transmissivity and photosynthetically active radiation from October to December (www.stratogem.ubc.ca; Watanabe, 1978). Exposure to sunlight after a collection dive and repeated exposure to light during observations may have caused larvae to be prematurely released from our September adult sponges, which would explain their smaller sizes compared to the larvae released in our November adult sponges. Similarly, light sensitivity in the multiciliated larvae may have prevented them from swimming while under observation. Although deep-sea populations of *A.*

occidentalis would never be exposed to the visible light spectrum found in the upper 30 m of the water column, reproduction in *A. occidentalis* is probably sensitive to at least some part of the electromagnetic spectrum range present at deeper depths. I note that our sampling was limited to only five months (July to November) and that *A. occidentalis* has also been described as a contemporaneous hermaphrodite from specimens sampled in July and August (Riesgo *et al.*, 2007). A follow-up study involving at least a year of continuous sampling with a focus on spectral sensitivity would determine if there is seasonality in the reproduction cycle of *A. occidentalis*.

Like other poecilosclerids, the microsclere spicules (anisochelae) are first formed in the larval stage of *A. occidentalis*. However, because suspension feeding does not occur in *A. occidentalis*, the energetic investment associated with their development and growth seems likely to be different than those of non-carnivorous sponges. After metamorphosis, non-carnivorous sponges feed using a functional aquiferous system (including choanochyte chambers) to fuel rapid growth and development (Simpson, 1984). In *A. occidentalis*, particularly during the larval stage, the development of anisochelae would be an energetic priority, as these would be carried over through metamorphosis and play an immediate and important role in prey capture for the juvenile sponge. Migration of the internal anisochelae in a larva to the external surface of a metamorphosed sponge would also be required for the spicules to function in prey capture. Despite the drastic differences in the adult body plan and feeding strategies of carnivorous sponges compared to the rest of the Porifera, the parenchymella larva of *A. occidentalis* remains similar to that of most demosponges (Ereskovsky, 2010). The main notable difference is of the multiciliated cells in the outer tissue layer of the larva. Such

cells are known among sponge larvae only in the cladorhizid *A. occidentalis* (Riesgo *et al.*, 2007; present study) and the hexactinellid *Oopsacas minuta* (Boury-Esnault & Vacelet, 1994). However, as the larvae of both these sponge groups are non-feeding, we suggest that the selection pressure for carnivory (i.e., low food availability in the deep sea) in the cladorhizids exerted their strongest evolutionary influence on the adult phenotype.

Propagule dispersal in carnivorous sponges

Cellular reaggregation is characteristic of members of the phylum Porifera (Wilson, 1907) and has been shown to enhance the dispersal of sexual propagules (Maldonado & Uriz, 1999). Spontaneous destruction and reorganization of tissue is also known for several demosponges, where it is involved in remodeling of the aquiferous system in order to adjust water pumping efficiency, restoration of canals lost during sexual reproduction, and production of new biomass (Simpson, 1984). It is therefore not surprising that we found spontaneous destruction and reorganization of tissue in *A. occidentalis*. The novelty of our discovery is in the utilization of this ability as the primary mechanism for larval release and asexual reproduction in *A. occidentalis*, and possibly all carnivorous sponges.

Until my study, an alternative mechanism for larval dispersal in sponges that lack choanocyte chambers and an aquiferous system has not been documented because of the scarcity of observations made on living carnivorous sponges. Both sexual reproduction resulting in extensive destruction of the parent tissue and asexual budding are uncharacteristic of other poecilosclerids (Fell, 1993; Ereskovsky, 2010), but given the absence of oscula (which serve as the typical release point for larvae in suspension-

feeding sponges) in carnivorous sponges, the disassociation of adult tissue is presumably necessary in order for the larvae to escape. I do not attribute tissue regression to starvation because all our adults were unfed but only those that released larvae showed senescence coinciding with mature larvae release. The reaggregation of destructured tissue into asexual propagules maximizes the reproductive output of *A. occidentalis* and likely contributes to its success in colonizing habitats throughout its wide depth range. In the deep sea, where resources are scarce, a combined strategy of using both sexual and asexual reproduction would maximize reproduction efficiency and increase the probability of establishing new populations.

Acknowledgements

I thank J. Lisaingo, J. Wong, I. Redan, and V. Mucciarelli for SCUBA collection of adult sponges; I. Redan and M. Blazecka for providing dive footage; D. Varela and J. Long for their microscopy expertise and use of their inverted microscope; S. Leys, E. Lanna, B. McGowan, and L. Page for SEM advice; and N. Korniyuk for translation of Russian literature. I am grateful to P. Chevaldonné for sharing the locations of recently discovered populations of carnivorous sponges in the Atlantic Ocean. Feedback and comments from K.S.P. Gale, J. Vacelet, L. Watling, A. Riesgo, and B. Pernet improved this manuscript. This research was funded by an NSERC PGS-D to J.W.F.C. and an NSERC Discovery Program grant to H.M.R.

Literature cited

Avidemux (2012) Available online at http://fixounet.free.fr/avidemux/. Accessed 25 November 2012.

Backran-Petricioli T, Vacelet J, Zibrowius H, Petricili D, Chevaldonné P, & Rada Tonći (2007) New data on the distribution of the 'deep-sea' sponges *Asbestopluma hypogea* and *Oopsacas minuta* in the Mediterranean Sea. *Marine Ecology*, **28**, 10-23.

Beveridge IA (2007) Acoustic observations of zooplankton distributions in Saanich Inlet, an intermittently anoxic fjord. Masters thesis, University of Victoria, Victoria, BC, Canada. 147 pp.

Boury-Esnault N, Vacelet J (1994) Preliminary studies on the organization and development of a hexactinellid sponge from a Mediterranean cave, *Oopsacas minuta*. In: Sponges in Time and Space. Van Soest R. van Kempen T, & Braekman, J, eds., pp. 407-415. Balkema Press, Rotterdam.

Chu JWF, Leys SP (2010) High resolution mapping of community structure in three glass sponge reefs (Porifera, Hexactinellida). *Marine Ecology Progress Series*, **417**, 98-113.

Dayton PK, Robilliard, GA, Paine, RT, Dayton LB (1974) Biological accommodation in the benthic community at Mcmurdo Sound, Antarctica. *Ecological Monographs*, **44**, 105-128.

Dayton PK (1979) Observations of growth, dispersal and population dynamics of some sponges in McMurdo Sound, Antarctica. In: Biologie des Spongiaires (Sponge Biology) 291. Levi C & Boury-Esnault N, eds., pp. 271-282. Colloq. Int. Cent. Natl. Rech. Sci., Paris

De Robertis A, Eiane K, Rau GH (2001) Eat and run: anoxic feeding and subsequent aerobic recovery by *Orchomene obtusus* in Saanich Inlet. *Marine Ecology Progress Series*, **21**, 221-227.

Ereskovsky AV (2010) The comparative embryology of sponges. Springer-Verlag, Dordrecht, 300 pp.

Fell PE (1993) Porifera. In: Reproductive biology of invertebrates, 6A: Asexual propogation and reproductive strategies. Adiyodi KG & Adiyodi RG, eds., pp. 1-44, Oxford & IBH, New Delhi.

Johannessen SC, Masson D, Macdonald RW (2006) Distribution and cycling of suspended particles inferred from transmissivity in the Strait of Georgia, Haro Strait and Juan de Fuca Strait. *Atmosphere-Ocean*, **44**, 17-27.

Koltun VM (1970) Sponge fauna of the north-western Pacific from the shallows to the ultra-abyssal depths. Proceedings of the Institute of Oceanology, *Academy of Sciences of the USSR*, **86**, 165-221.

Kos T (2011) PK_Tether. Available online at http://www.pktether.com/. Accessed 26 July, 2011.

Kübler B, Barthel D (1999) A carnivorous sponge, *Chondrocladia gigantea* (Porifera: Demospongiae: Cladorhizidae), the giant deep-sea clubsponge from the Norwegian Trench. *Memoirs of the Queensland Museum*, **44**, 289–298.

Lambe L (1893) Sponges from the Pacific coast of Canada. *Proceedings and Transactions of the Royal Society of Canada*, **11**, 25-43.

Lee WL, Reiswig HM, Austin WC, Lundsten L (2012). An extraordinary new carnivorous sponge, *Chondrocladia lyra*, in the new subgenus *Symmetrocladia* (Demospongiae, Cladorhizidae), from off of northern California, USA. *Invertebrate Biology*, **131**, 259-284.

Leys SP, Wilson K, Holeton C, Reiswig HM, Austin WC, Tunnicliffe V (2004) Patterns of glass sponge (Porifera, Hexactinellida) distribution in coastal waters of British Columbia, Canada. *Marine Ecology Progress Series*, **283**, 133-149.

Leys SP, Cheung E, Boury-Esnault N (2006) Embryogenesis in the glass sponge *Oopsacas minuta*: Formation of syncytia by fusion of blastomeres. *Integrative and Comparative Biology*, **46**, 104-117.

Maldonado M, Uriz MJ (1999) Sexual propagation by sponge fragments. *Nature*, **398**, 476.

Maldonado M 2006. The ecology of the sponge larvae. *Canadian Journal of Zoology*, **84**, 175-194.

Martinand-Mari C, Vacelet J, Nickel M, Wörheide G, Mangeat P, Baghdiguian S (2012) Cell death and renewal during prey capture and digestion in the carnivorous sponge *Asbestopluma hypogea* (Porifera: Poecilosclerida). *Journal of Experimental Biology*, **215**, 3937-3943.

Riesgo A (2010) Phagocytosis of sperm by follicle cells of the carnivorous sponge *Asbestopluma occidentalis* (Porifera, Demospongiae). *Tissue and Cell*, **42**, 198-201.

Riesgo A, Taylor C, Leys SP (2007) Reproduction in a carnivorous sponge: the significance of the absence of an aquiferous system in the sponge body plan. *Evolution and Development*, **9**, 618-631.

Simpson TL (1984) The cell biology of sponges. Springer Verlag: New York, 662 pp.

Vacelet J (1996) Deep-sea sponges in a Mediterranean cave. In: Deep-sea and Extreme Shallow-water Habitats: Affinities and Adaptations. Uiblein F, Ott J, Stachowitsch, eds., pp. 299-312. Austrian Acad. Sci., Vienna.

Vacelet J (2006) New carnivorous sponges (Porifera, Poecilosclerida) collected from manned submersibles in the deep Pacific. *Zoological Journal of the Linnean Society*, **148**, 553-584.

Vacelet J (2007) Diversity and evolution of deep-sea carnivorous sponges. In: Porifera Research: Biodiversity, Innovation and Sustainability (Custódio MR, Lôbo-Hajdu, G. Hajdu E, & Muricy G, eds.), pp. 107-115. Museu Nacional. Rio de Janiero.

Vacelet J, Boury-Esnault N (1995) Carnivorous sponges. *Nature*, **373**, 334-335.

Vacelet J, Boury-Esnault N (1996) A new species of carnivorous sponge (Demospongiae: Cladorhizidae) from a Mediterranean cave. Bulletin van het Koninklijk Belgisch Instituut voor Natuurwetenschappen. Biologie Bulletin de l'Institut Royal des Sciences Naturelles de Belgique. Biologie, 66(sup), 109-115.

Vacelet J, Boury-Esnault N, Harmelin JG (1994) Hexactinellid cave, a unique deep-sea habitat in the scuba zone. *Deep-Sea Research Part I*, **41**, 965-973.

Vacelet J, Duport E (2004) Prey capture and digestion in the carnivorous sponge *Asbestopluma hypogeal* (Porifera: Demospongiae). *Zoomorphology*, **123**, 179-190.

Van Soest RWM, Baker BJ (2011) A new carnivorous shallow-water sponge from McMurdo Sound, Antarctica (Porifera, Poecilosclerida). *Marine Biodiversity*, **41**, 495-501.

Watanabe LN (1978) Factors controlling the winter dominance of nanoflagellates in Saanich Inlet, British Columbia. Masters thesis, University of British Columbia, Vancouver, BC, Canada. 104 pp.

Wilson HV (1907) On some phenomena of coalescence and regeneration in sponges. *Journal of Experimental Zoology*, **5**, 245-258.

Appendix D Supporting Material

Additional Supporting Information may be found in the online version of this article: http://onlinelibrary.wiley.com/doi/10.1111/ivb.12045/suppinfo

Video D.1**.** Sampling for the carnivorous sponge *Asbestopluma occidentalis* in the field by SCUBA. Individuals of *A. occidentalis* can be found as small stalks growing on hard substratum in the Salish Sea. Using the tip of a dive-knife, one can sample individual sponges by flicking them off the substratum. The detached sponges are neutrally buoyant and can be captured in plastic bags. **Please refer to video file: *ivb12045-sup-0001-VideoS1-avi*.**

Video D.2**.** *Asbestopluma occidentalis* with captured prey. Hatched nauplii of *Artemia* sp. can be used to feed *A. occidentalis* in the laboratory. Digestion of the nauplii occurs over several days. Video was taken with a Pentax K-7 camera with a reverse mounted Pentax SMC-M 28 mm F3.5 lens on top of extension tubes. **Please refer to video file: *ivb12045-sup-0002-VideoS2-avi.***

Video D.3**.** Time-lapse video of prey escaping from *Asbestopluma occidentalis*. Nauplii of *Artemia* sp. are passively captured by the external anisochelae spicules of *A. occidentalis*. However, partially ensnared nauplii can escape subsequent predation by vigorously swimming. Individual sponges were placed in petri dishes filled with nauplii of *Artemia* sp. and photographed every 30 s. Photos were then combined into a 25 fps time-lapse video. **Please refer to video file: *ivb12045-sup-0003-VideoS3-avi.***

Appendix E: A Scientist's Guide to using Remotely Operated Vehicles (ROVs) for Benthic Imagery Surveys

Preface

Appendix E is a technical report submitted to Canadian Technical Report of Fisheries and Aquatic Sciences: Du Preez C, Chu JWF, Rose J. A scientist's guide to using remotely operated vehicles (ROVs) for benthic imagery surveys.

Dr. Cherisse Du Preez conceived the idea of the article, supplied data, and co-wrote the article. Jonathan Rose (Research Associate, University of Victoria) gave writing input.

I contributed data and co-wrote the article.

Abstract

Benthic imagery surveys performed using remotely operated vehicles (ROVs) can resolve high-resolution spatial patterns. Imagery can be processed using different methods to produce multiple biotic and abiotic datasets. These datasets are relevant for ecological studies that address species distributions, produce habitat maps, document animal behaviour, and monitor ecosystem health. Independent of researcher experience, ROV and ship time is expensive and logistically challenging. Based on our combined experiences with several ROVs owned and operated in Canada, we have developed best practices, workflow steps, and suggestions for optimizing the research potential when performing benthic imagery surveys with ROVs.

Introduction

The Canadian Exclusive Economic Zone (EEZ) expands into the Pacific, Atlantic, and Arctic oceans and is one of the largest in the world. The Canadian Healthy Ocean Network (CHONe), a five year (2009-2013) nationwide scientific initiative, addressed the biodiversity and sustainability in Canada's three oceans. One of the main tools CHONe scientists used to fill this knowledge gap were benthic imagery surveys using remotely operated vehicles (ROVs). With national and international commitments to ocean health, scientists from Canada are world leaders in the applied field of subsea technology and have extensive experience with conducting benthic imagery surveys using remotely operated vehicles (ROVs).

A benthic imagery survey is a spatial sampling technique where by the surface of the seafloor is non-invasively documented with video or still images. Benthic imagery surveys performed using ROVs can resolve high-resolution spatial patterns. Imagery can be processed using different methods to produce multiple biotic and abiotic datasets. These datasets are relevant for ecological studies that address species distributions, produce habitat maps, document animal behaviour, and monitor ecosystem health. Rigorous *in-situ* marine ecosystem surveys are difficult to perform without using non-invasive methods and are thus sought after when addressing the concerns of management and conservation groups.

ROVs are classically considered to be unmanned, ship-tethered submersibles (Fig. E.1). However, with the advent of subsea cable observatories, benthic crawlers are now considered a subcategory of ROV (e.g. NEPTUNE's Wally, a ROV tethered to the

observatory). For the purpose of this paper, we focus only on ship-tethered ROVs. For imagery surveys of the benthos, ROVs have several advantages over manned submersibles or other methods such as drop cams, towed cameras, autonomous underwater vehicles (AUVs), or cabled observatories. There is near unlimited bottom time with real-time data transmission to the ship (via the umbilical tether) as compared to manned submersibles. Precision navigation, changes in flight-pattern in real-time, as well as the high powered capabilities enable much more sophisticated imagery systems and lighting relative to AUVs. Remote operation enables higher precision in the collection of imagery and the option of deviating from the preplanned flight path compared to tow cameras. Simple drop cameras and cameras connected to cabled observatories can capture temporal data at high frequency, but only at fixed positions whereas ROV surveys capture high-resolution spatial data. Using strategic and precision sampling with ROVs can also supplement the patterns resolved by distribution mapping as opposed to the indiscrete and often destructive method of scientific trawling. Canadian ROVs have been particularly successful in this regard (Forget *et al.*, 2010; Chu *et al.*, 2011; Chu & Leys, 2012; Aranha *et al.*, 2014; Tunnicliffe *et al.*, 2014).

Independent of researcher experience, ROV and ship time is expensive and logistically challenging. Based on our experiences with several ROVs owned and operated in Canada (Fig. E.2), we have developed several best practices, workflow steps, and suggestions for optimizing the research potential when performing benthic imagery surveys with ROVs. The remotely operated platform for ocean science (ROPOS, Fig. E.1) is considered the flagship ROV operating in Canada and thus we will often refer to ROPOS' systems throughout this paper. However, our general suggestions can be applied

with any ROV platform given the presence or absence of certain systems. The majority of the studies cited throughout this paper were performed under the CHONe biodiversity theme. Our report will focus on pre-cruise planning, onboard operations, and *in situ* survey protocols to optimize raw imagery (data) acquisition. For post-cruise methods on data extraction and analyses, see Sameoto *et al.* (2008).

Methodological approach

Common systems of an ROV

In this section, we summarize common ROV systems that are relevant for benthic imagery surveys. A remotely operated vehicle (ROV) is the sum of multiple systems (Fig. E.1). Primary systems are essential for basic ROV operations and include the umbilical, thrusters, and a video camera for piloting. Secondary systems can greatly enhance the capabilities and science potential of a ROV and include additional cameras, manipulator arms, and sampling instruments. Depending on the focus and budget of the operating company, the standard configuration of a ROV may include many secondary systems with additional systems readily available upon request. Scientists can also design their own additional scientific equipment, modified to operate in conjunction with the ROV platform, to meet their specific research objectives (Yahel *et al.*, 2007). The most effective scientific ROVs are built as adaptable robotic platforms, where systems can be added, removed, exchanged, and updated as required.

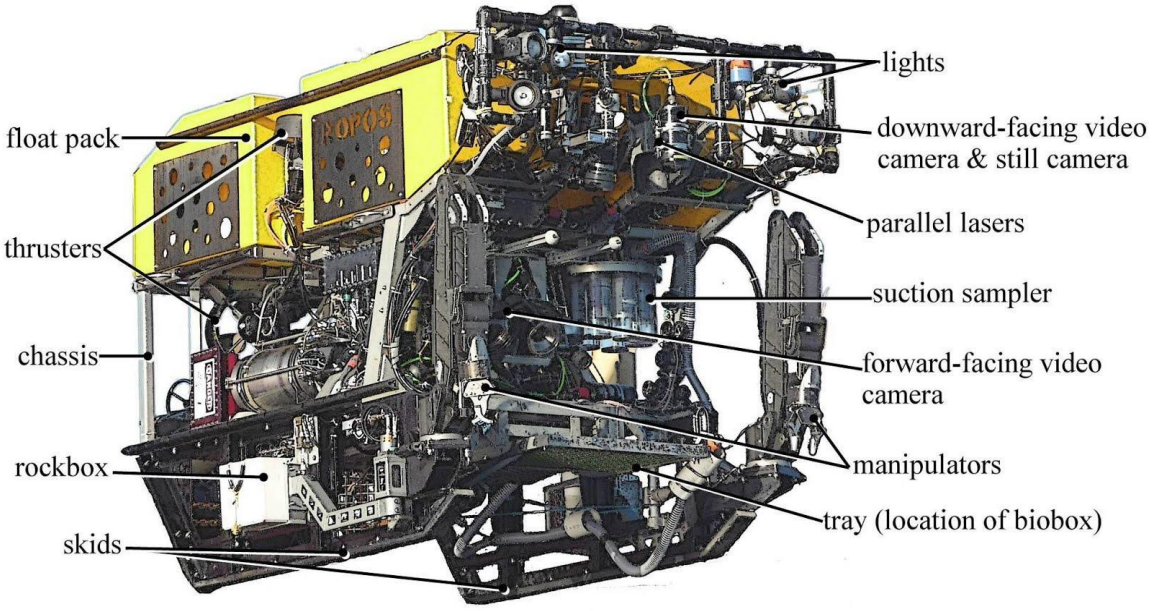

Figure E.1. The Remotely Operated Platform for Ocean Sciences (ROPOS) is a science/work-class remotely operated vehicle (ROV) developed and operated by the Canadian Scientific Submersible Facility (CSSF; dimensions: 3.1 x 1.6 x 2.2 m, 3,393 kg). Systems for benthic imagery surveys include: a primary forward-facing high-definition (HD) video camera (Insite Pacific Zeus-Plus; the pilot video camera) mounted on a pan and tilt; a secondary HD video camera (Insite Pacific Mini-Zeus) mounted on a tilt; a high-resolution digital still camera (12.1 megapixel Nikon D700) on a tilt; and over 3,700 watts of lighting (http://www.ropos.com).

Primary ROV Systems

Chassis and float Pack: ROV systems are mounted onto the chassis. The float pack provides buoyancy (influences upper and lower depth limits). Together, they make up most of the size and weight of an ROV.

Locomotion: The number and orientation of thrusters determines the speed and manoeuvrability of the ROV.

Pilot video camera: ROVs have at least one forward-facing video camera which functions as the primary field of view (FOV) for the pilot.

Floodlights: Provides artificial light to illuminate the FOV in the pilot video camera. Ambient light is minimal when at depth.

Navigation: Provides real-time geospatial information such as latitude, longitude, and depth of the ROV. Accurate navigation is needed to georeference imagery and samples collected from a cruise. Accuracy of navigation is dependent on equipment and calibration (e.g. ROPOS: ±1 % water depth, Ian Murdock pers. comm.).

Umbilical: Supplies power to the ROV and enables data exchange and remote operation between the ROV and the shipboard control station. Umbilical length may limit the maximum operating depth.

Control station: The shipboard station where the remote operations occur. Pilots and scientists share this space and include all the components that function in controlling the ROV. Several monitors will display real time information on the ROV systems, navigation, and position relative to the ship. The size and complexity depends on the ROV operations and the ship (Fig. E.2).

Secondary ROV Systems

Additional video cameras: Video cameras used for alternate viewing angles and for recording scientific imagery. Cameras may be mounted on pan/tilt heads and have zoom lenses with manual focus capabilities. High-definition (HD) cameras are becoming more readily available and are considered upgrades to the primary

cameras found on stock ROVs which may still be operating in standard-definition (SD; e.g. Super Mohawk, Fig. E.2G).

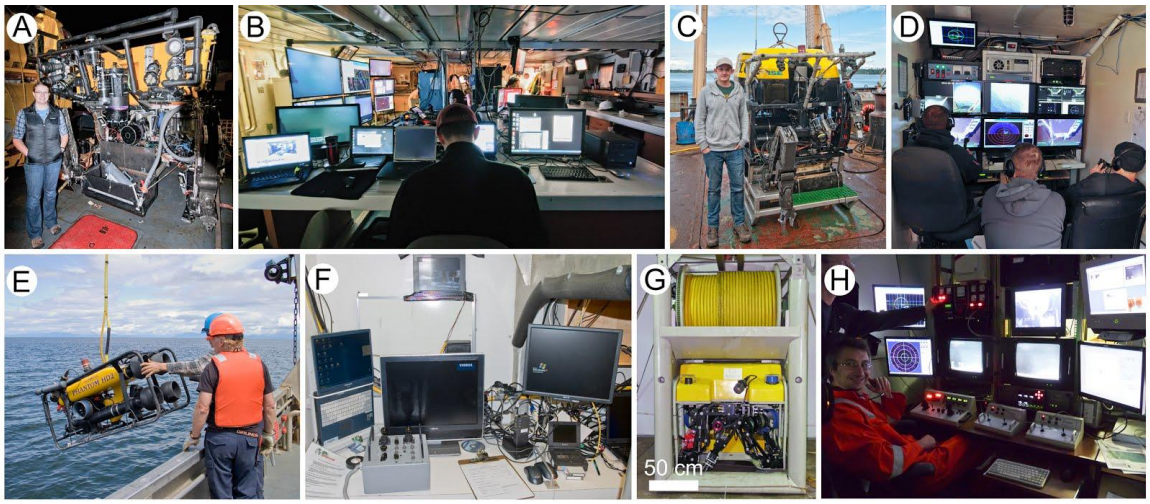

Figure E.2. Examples of Canadian remotely operated vehicles (ROVs) and their respective shipboard control stations. (A, B) ROPOS operates out of Sidney, British Columbia (BC) and has a maximum operating depth (MOD) of 5000 m. (C,D) The Oceanic Explorer operates out of Vancouver, BC, and has a MOD of 1000 m. (E,F) A Phantom HD2 operating out of the Pacific Biological Station in Naniamo, BC, with a MOD of 300 m. The Phantom is a common model and owned by several other institutions (e.g. Bamfield Marine Sciences Centre in Bamfield, BC). (G,H) A Super Mohawk owned and operated off the Canadian Coast Guard Ship Amundsen (registry port: Ottawa, Ontario) with a MOD of 1600 m. Photo credits: (A-C, E-F) J.W.F. Chu, (D) A.O.V. Bui, (G-H) C. Du Preez. An example of the control station and operating layout of ROPOS can be viewed at: https://vimeo.com/47740690.

Digital still camera (DSC): DSCs capture high resolution photographs (ROPOS has a 12 megapixel, MP, DSC) which is far superior than the low resolution of frame grabs from HD video (< 2 MP). DSC functions can be manually controlled by a scientist or automated (taking images at preset intervals) and may include a strobe (e.g. Pacific Biological Station's Phantom HD2, Fig. E.2E).

Additional lights: Additional Lights may be required to illuminate the FOV of additional cameras. Video cameras require floodlights while still cameras can function with floodlights or strobes. Due to high particulates in parts of the water column, the orientation of the lights requires calibration to maximize the clarity in the FOV.

Parallel lasers: Provides a scale reference. It is common practice to attach a set of parallel lasers to the camera housing (or camera mount) to project a known scale within the FOV of the camera. More advanced image-scaling options can be provided by multi-laser configurations and associated software (e.g. Laser Measure(C) developed by MBARI, Barker *et al.*, 2001).

Imagery recording devices: Video imagery is relayed in real-time from the ROV, via the umbilical, to a recording device at the control station. Still imagery can also be relayed in real-time or stored in-camera and downloaded upon recovery of the ROV.

Data-logging system: Software for real-time data annotation which is used by scientists during dives. It can contain useful information such as real-time user annotations, dive information, data, and events (with or without images) in a centralized, searchable, and easy to navigate interface. For example, the Canadian Scientific Submersible Facility (CSSF), who operates ROPOS, provides their Integrate Real-time Logging System (IRLS) for scientists. Fisheries and Oceans Canada developed Video Miner and ClassAct Mapper.

Manipulators: Manipulator arms are controlled by an operator and can be used to collect voucher specimens during surveys. More technical manipulators have some form of operator feedback to allow the operator to perform delicate manoeuvres.

Manipulators can be used to directly collect specimens (Aranha *et al.*, 2014) or can be used to operate collection devices such as a suction sampler or Ekman grab (Chu & Leys, 2010, 2012; Chu *et al* , 2011). Voucher specimens are usually stored in a biobox, rockbox, or sampler containers mounted on the ROV.

Other systems: Examples of other common systems include an altimeter, CTD (conductivity, temperature, and depth sensors), oxygen sensors, sediment corers, plankton nets, Imagenex sonar, SIP water samplers (Yahel *et al.*, 2007; Chu *et al.*, 2011), and temperature probes (Tunnicliffe *et al.*, 2014).

Pre-cruise planning

Prior to the ROV cruise, establishing realistic survey objectives and methodology is mandatory. The best practice approach is to have multiple contingency plans that accommodate for the potential dive time lost to technical problems, poor weather, or other unpredictable events. The end-products of a survey will highly depend on the capabilities of not only the ROV but also the experience of the ROV pilots. If possible, the cruise plan should be discussed with the ROV operation during the planning stage.

Considerations when planning

ROV capabilities: ROV options for benthic imagery surveys include a variety of vehicles, from micro-class to work-class. Smaller ROVs are generally easier and less expensive to operate. Larger ROVs maybe better suited for gathering large amounts of scientific imagery for a couple reasons: 1) larger ROVs have

increased stability and handling, especially under adverse flow conditions, and 2) larger ROVs can support, and thus are equipped with, superior imaging systems and are likely to have a more precise navigation system for georeferencing the imagery. When developing realistic research objectives, the ROV systems, configuration, limitations, and the experience of the pilots are all important factors to consider. Most ROV operations will have a detailed website to assist scientists in familiarizing themselves with the ROV's capabilities.

Collaboration among scientists: Collaborations are typical of ROV expeditions. Dive time is often split among multiple research programs within a cruise. It is imperative to have a clear plan on how time, resources, and dive products will be divided among scientists.

Multipurpose dives: Certain ROV system configurations may interfere with a benthic imagery survey. For example, mounting a front biobox may partially block the field of view (FOV) of downward camera angles. Once submerged, the refraction of light through the water-lens interface will cause objects to appear magnified (Christ & Wernli, 2014). Many ROV cameras are set to autofocus and a large obstruction in the foreground can cause the rest of the image to blur. This is particularly important to consider when using a camera set to automatic image capture or auto presets.

Dive conditions: Bathymetry, tides and currents, seasonal weather/ocean conditions, hazards, and water quality will influence a benthic survey. For example, high turbid water (found in harbours and deltas) will affect the quality of imagery. Dissolved organic matter increases light absorption and suspended matter

increases light scattering, which affects the ability to capture clear images (Christ & Wernli, 2014). Certain lighting configurations can mitigate these problems, but this needs to be addressed prior to the dive because the position of the lights is fixed once the ROV is launched. *A priori* awareness of these conditions will maximize the efficiency of a cruise.

Metadata: Adding accurate metadata to the video can be challenging. Common approaches include adding an overlay of the information onto the video or encoding it as a closed caption channel. The direct overlay usually has a negative impact on the video quality. Another option is to encode the information as an audio stream which will require dedicated hardware to decode after the cruise. A data-logging system (e.g. IRLS) is another means of recording metadata. If the ROV operation does not supply a data-logging system, the scientist will have to find or create one to suit their research needs.

Recording imagery: Standard-definition (SD) recording is relatively simple and inexpensive with viable options including digital video (DV) tapes, digital video disks (DVDs), and digital video recorders (DVRs). High-definition (HD) video streams require recording systems to compress the raw video-source into manageable file-sizes. These recording systems are more complex, costly, and require technical expertise to operate. ROPOS uses a Digital Rapids StreamZ system to record HD-video but there are other options such as a Matrox MXO2 or a Panasonic P2 system. Some of these devices record to flash memory, which can then be copied to a hard drive or directly to hard disk. The selection of a coder-decoder (codec) is another important consideration when recording HD-videos.

By default, ROPOS uses a 50Mbps MPEG2 broadcast quality stream which results in a high quality, easy playback, and broad compatibility. Alternative codec options include h.264 or AVC-intra which may fit alternative editing or image quality needs. Depending on the level of video compression, HD video can require substantially more data storage space than SD video. For example, a HD video source encoded with a 50 Mbps MPEG2 stream requires 4 GB of hard drive space for every 10-11 mins of footage. Hard drives are inexpensive relative to the total expense of a ROV expedition, thus having redundant hard drives should be factored into the cruise budget.

Voucher specimen collections: Voucher specimens assist in species identification and can supplement the patterns resolved from benthic imagery survey (Chu *et al.*, 2011; Chu & Leys, 2012). Specimen collections require collection permits, planning for appropriate sample sizes and locations to collect during each dive, and preparation (fixatives and transporting of specimens) well in advance of the cruise. Sampling capabilities and sample-storage compartments on the ROV will limit the maximum number of samples in a dive.

Cruise plan: Each lead scientist is required to submit a cruise plan to the chief scientist, who then provides a copy to the ROV operation as well as the ship's captain. The cruise plan for benthic imagery survey dives should include (1) approximate launch and recovery target times, (2) dive objectives, (3) site waypoints (latitude, longitude, depth), (4) the survey protocol (detailed in the section below), and (5) maps with relevant figures to clarify any complexity in the dive plan (e.g. Fig. E.3B,C). The plan should also include the specific systems required for the

survey. This will allow the ROV technicians to plan for adequate time before the cruise (or before specific dives) to configure the ROV to suit the dive objectives. Considering that most biologically relevant data extracted from imagery are in units of area (Sameoto *et al.*, 2008), calibrating the scaling lasers mounted on the camera systems is paramount. Time permitting, it would be ideal to have the lasers recalibrated prior to every dive.

Survey Protocols

A clear and concise survey protocol should be provided as part of the cruise plan. Prior to a dive, feasibility of the survey protocol should be discussed with the ROV operators and ship captain to anticipate potential problems and dive time constraints.

Considerations for optimizing the survey

Survey design: Due to cost and time constraints, ROV survey designs are usually based on transects or grids (Fig. E.3B,C). Both survey designs benefit from prior knowledge of the bathymetry at the dive site, the planned route for the ROV and thus the ship, and distances between specific waypoints.

Deviations from the survey design: Freedom to deviate from the survey design allows for exploration and close-up investigation of the benthos (Fig. 4.A). However, it can reduce the time allotted for completion of the original survey objectives. Accurate estimates of the time required to complete each dive objective would determine if deviations are acceptable during the dive. Deviations may be in the form of leaving the transect or grid, changing the camera settings (e.g. focus, tilt, zoom),

or turning off the lasers. If deviations from the planned transect or grid is not permitted, an alternative would be to ask the ROV navigator to create a waypoint and return to the site after completion of the survey.

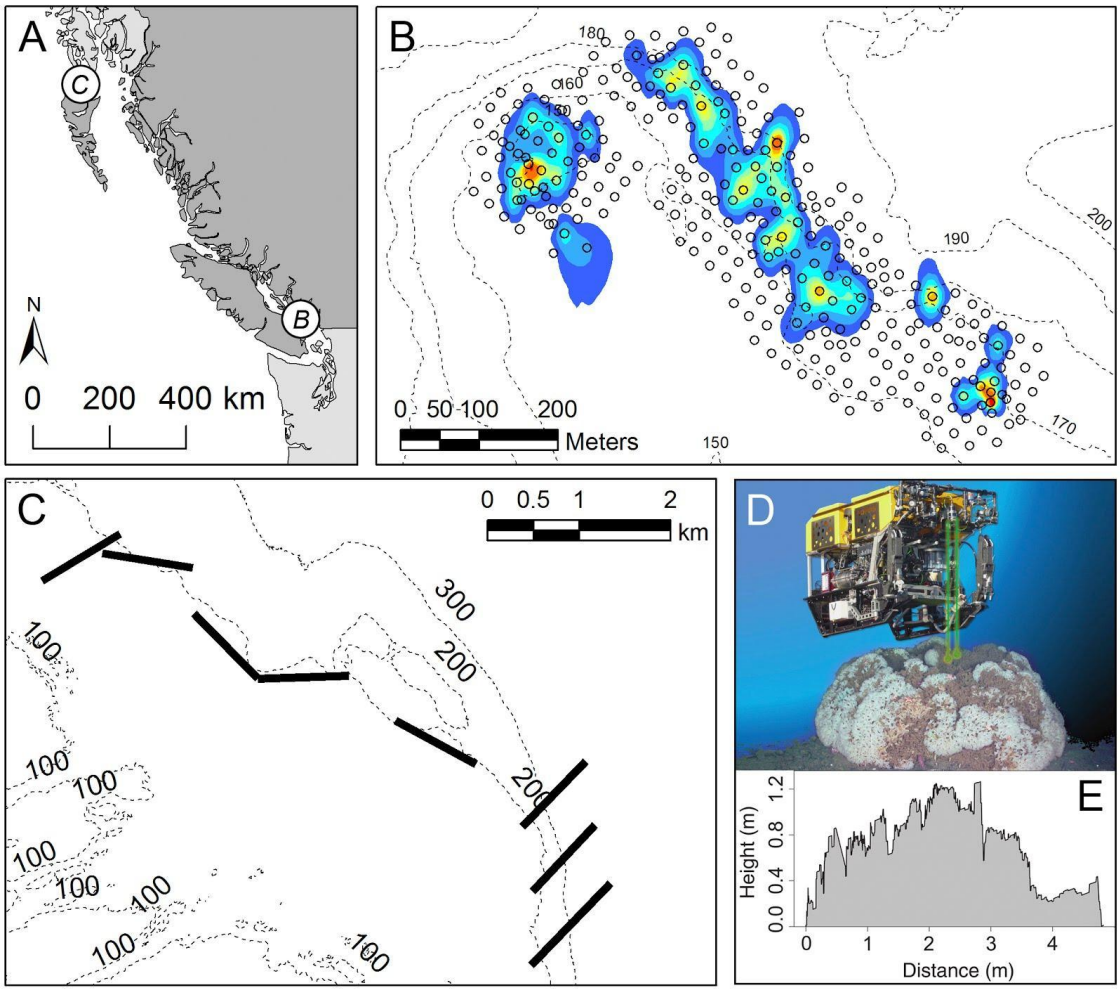

Figure E.3. Remotely operated vehicle (ROV) survey designs for benthic imagery surveys. (A) Locations of example surveys done off the Pacific coast of Canada using the ROV ROPOS (where italicized letters refer to the subsequent panels). (B) A simple stratified sampling grid of points (open circles) where photographs were taken with the downward-facing digital still camera. Live sponge cover was delineated from the images and sponge distribution maps generated post cruise (colored contours). (C) Preplanned 1 km linear video transects (black lines) for (D) a benthic video survey using the downward-facing video camera and microtopographic laser scanning (MiLS) survey protocol to measure and (E) profile cm-scale seafloor roughness (rugosity). Modified from (B) Chu & Leys (2010); and (C-E) Du Preez & Tunnicliffe (2011, 2012).

Number of survey sites: Surveying at one site continuously yields more imagery but limits the spatial coverage of the study. Transiting between multiple survey sites extends the spatial coverage but reduces the time allotted to a single site and may include the need to recover and relaunch the ROV. For ROPOS, the average descent rate is approximately 45-60 mins for every 1,000 m of water column depth and the average ROV velocity at depth when transiting between sites is ~1 m s^{-1}. Decisions to remain at depth or recover the ROV should factor in the distance and time required to transit between sites.

Voucher specimen collection: A sampling protocol (including a description of the specimen, when and where it can be expected, and how it should be collected) is required to ensure accuracy and efficiency in the collection, with minimal impact to the surrounding environment (Fig. E.4B).

Considerations for optimizing imagery

Most benthic imagery surveys target the megafauna assemblage (sizes class >5 cm), thus our suggestions are for optimizing the ROV parameters for surveys of this type. High resolution still photos may resolve smaller sizes (1-2 cm) and capture the morphological characteristics required for species-level taxonomy.

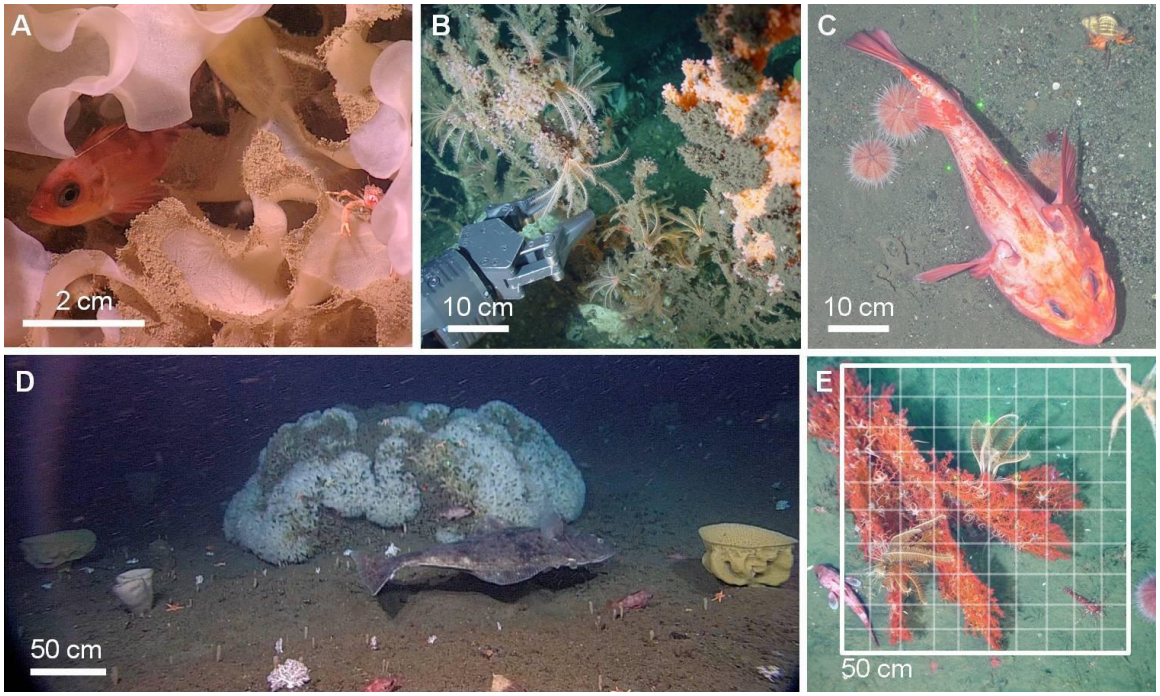

Figure E.4. Example of imagery collected during benthic surveys with the ROV ROPOS. (A) A close-up (full zoom) using the forward-facing video camera. (B) Collection of a dead coral branch next to living coral using manipulator arm. (C) The narrow field of view (FOV) of the downward-facing video camera with lasers (horizontal lasers are 10 cm). (D) The wide FOV of the forward-facing video camera. (E) A high-resolution digital still image (DSC) with a digital quadrat grid overlay (horizontal lasers are 10 cm scale; quadrat is 50 cm x 50 cm). Imagery is from a 2008 survey at Learmonth Bank, British Columbia (Du Preez & Tunnicliffe, 2011; Aranha *et al.*, 2014; Neves *et al.*, 2014).

ROV movement: During a survey, the ROV speed, height above the bottom, and orientation is dependent on the research objectives and methods (e.g. the MiLS survey protocol, Du Preez & Tunnicliffe 2012). General rules of thumb for ROV movement during a benthic imagery surveys are velocities no faster than 0.5 to 1 knots and keeping the ROV height above bottom to ≤ 1 m. Increasing ROV speed introduces the potential for blurred imagery yet may allow for more area to be covered. The higher the ROV altitude, the larger the field of view (FOV) with the trade-off of decreased pixel density to resolve fine scale features. Depending on

the environment, the operational ROV height above bottom may need to factor in the avoidance of fragile structures (hydrothermal vent chimneys, corals, sponges). The relative orientation of the ROV can affect the image quality. The best practice is to keep a stable plane parallel to the bottom. This will usually be horizontal, but in the case of a sloped bottom, it is recommended to survey up a slope. Cameras are normally mounted on forward brow of ROVs, thus moving upslope ideally minimizes the vertical distance between seafloor and camera. When moving down a slope, the seafloor to camera distance is larger and reduces the amount of lighting reaching the benthos. When moving down a slope over very steep terrain, the seafloor may not be visible at all. Depending on the position of the camera on the ROV and whether it has a tilt function, it may be possible to tilt the camera and survey a vertical wall (Yahel *et al.*, 2007), however, the altimeter may not read bottom depth if hovering above the seafloor above a certain depth (25 m for ROPOS).

Setting down or on the fly: When taking digital still images, there are tradeoffs between landing the ROV or taking the images while in motion. Setting down may bias observations, allowing time for mobile animals to avoid or to be attracted to the ROV (Stoner *et al.*, 2008). Fragile environments such as coral and sponge habitat, fast water currents, or equipment limitations can prevent the ROV from remaining stationary in the water column. When setting down is not an option, extra demand is placed on the user of the DSC system and supplementary lighting. Sensors in newer camera models have excellent low light imaging capabilities and make it possible to take sharp images while the ROV is in motion (e.g. ROPOS). A

supplemental strobe (flash) may improve the quality of the still images but may affect the quality of the video. In scenarios where the ROV is in motion and the still camera lacks a strobe, the camera operator may be able to compensate with manual exposure settings (increasing shutter speed/ISO) but this requires an understanding of exposure.

Camera orientation: A camera facing downward has a narrower FOV when compared to a forward-facing camera at a slightly oblique angle (Fig. E.4B,C). A downward-facing camera provides a more accurate estimate of area coverage, which is important for calculating density and distribution of animals. However, a forward-facing camera increases the probability of capturing mobile animals in the FOV (Stoner *et al.*, 2008).

Camera setting: Cameras on ROVs will default to automatic settings. Auto settings are designed for ease of use yet may yield poor images under varying conditions such as fast ROV movement or high levels of suspended material in the water column. User input may help with the consistency of image capture and decrease the frequency of poor images. However, manual control settings require knowledge of photographic principles to maximize the potential of capturing quality imagery under different water conditions. When detailed or demanding images are required in challenging conditions, scientists have hired professional photographers/videographers to operate the cameras.

Manual or automated timer: Both options are usually available on a ROV digital still camera (DSC) system. The manual setting allows for adaptation during a dive, but

requires diligence. The automated timer is restrictive and may function poorly in waters with low visibility, but it removes sampling bias and some user errors.

Quadrats: Quadrats can be used to increase the precision of area measurements in imagery. A physical quadrat can be used in the FOV or calibrated scaling lasers can be used to overlay a digital quadrat grid during image processing (Fig. E4E).

Scientist roles during dives

Most ROV controls stations will be space limited. The chief scientist (or dive lead scientist) will usually have a seat at the ROV control station (Fig. E.2B,D ,H) and have several key roles including providing information to the ROV operator regarding the dive plan and survey protocol, factoring in alternative scenarios when the unexpected occurs, and facilitating communications between the ROV operations with the rest of the scientific crew.

Additional tasks for the science crew may include: (1) assisting in the communication between scientists, the ROV operator, the ROV deck crew, and the ship crew, (2) monitoring the imagery recording and ensuring the video is being recorded once the ROV is at the bottom, (3) managing the data by ensuring raw video is recorded as manageable file sizes, (4) real-time data-logging and annotation and recording of audio in the control room, (5) requesting for sampling of voucher specimens at opportune moments (Fig. 4.B) and recording the proper metadata (time, site, ROV sample container), (6) operating the digital still camera (DSC), and (7) assisting the ROV technicians on deck during the descent and ascent of the ROV.

Cruise checklist

Addressing metadata issues prior to the end of the cruise facilitates post-cruise data extraction and analysis. An example checklist of several items is noted below. Some of these items need only be checked once during a cruise while others may require multiple checks if the configuration of the ROV systems changes between dives.

- Record the specifications of the ROV equipment (camera make and model, type of lasers, navigation system, etc.).
- For every set of parallel lasers, measure the distance for scale.
- Measure the location of the cameras on the ROV relative to instruments of interest (e.g. altimeter, CTD, oxygen probes) and the height above the bottom of the ROV (skids).
- Determine if there is a delay between the navigation and the imagery data.
- Determine if and how the imagery is georeferenced, and what the means are to decode the embedded data (e.g. GPS data encoded in the audio signal of the video requires a decoder). If post-cruise georeferencing of files is required, collect the navigation files and the required information to georeference the imagery yourself.
- Determine the accuracy of the ROV navigation (usually expressed as a function of water depth).
- Determine the imagery format (video and still images) and whether they are proprietary files. Proprietary imagery files require specific software to view and edit.

- Download a copy of all the data (e.g. imagery, navigation files, and data-logging) collected for your survey (e.g. hard drives, CDs, DVDs). If this is not possible before the end of the cruise, have a clear plan organized between the chief scientist and ROV technicians for post-cruise handling and delivering of imagery and data.
- Record the names and the contact information of the chief scientist, lead scientists, other science personnel involved in the ROV operations, and the ROV technicians.
- Determine the ownership of the imagery and metadata. This is important when using imagery for publications and outreach.

Applications

The science of CHONe focused on biodiversity for the sustainability of Canada's three oceans. Of CHONe's 35 collaborative research projects conducted by over 150 researchers, many used remotely operated vehicles (ROVs) to conduct benthic imagery surveys. CHONe researchers successfully surveyed the benthos of many vulnerable deep-sea marine ecosystems using five different ROVs (Chu & Leys, 2010; Forget *et al.*, 2010; Chu *et al.*, 2011; Du Preez & Tunnicliffe, 2011; St. Germain, 2011; Piepenburg *et al.*, 2011; Forget & Juniper, 2013; Lacharitè & Metaxas, 2013; Neves *et al.*, 2014; Du Preez *et al.*, 2014; Tunnicliffe *et al.*, 2014). Maps produced from these benthic imagery surveys are commonly used when addressing issues pertaining to management and conservation. Specific CHONe examples include measuring seafloor bathymetry and rugosity at a cm-scale without disturbing the seafloor (Fig. E3D,E), the area-coverage mapping of live sponges over the km-scale in the glass sponge reefs of British Columbia (Fig. E.3B), and ground-truthing of remote sensing data used to create sponge and coral habitat maps over the scale of 10's of km (Neves *et al.*, 2014). In addition, novel techniques were developed

to efficiently and efficiently utilize the benthic imagery collected (Gobi, 2010; Du Preez & Tunnicliffe, 2012). Combined, ROV benthic imagery surveys have been a central research tool in the three interrelated CHONe research themes of marine biodiversity, population connectivity, and ecosystem function in the Atlantic, Pacific, and Arctic Ocean waters of Canada (http://chone.marinebiodiversity.ca/publications).

Summary and recommendations

Although the vast majority of the deep sea (depths > 200 m) remains poorly documented, ocean exploration is rapidly advancing with the current pace of technological innovation. High resolution time-series are now streaming from advanced subsea cabled observatories such as VENUS and NEPTUNE and can supplement the spatial patterns resolved by ROV mapping (Matabos *et al.*, 2011, 2012; Robert & Juniper, 2012; Robert *et al.*, 2012). With the volumes of imagery data that are now typical of deep-sea ecological research, the motto of "garbage in, garbage out" can easily be applied to the data collected from benthic imagery surveys performed by ROVs. It is imperative that the deep-sea community develop standardized and efficient workflows to maximize the acquisition of quality information from the deluge of raw data. To this effect, our suggested protocols and workflow can be interpreted as guidelines that were developed and successfully applied in the field under the CHONe imperative.

Acknowledgements

We gratefully acknowledge Verena Tunnicliffe and Sally Leys for their support, funding, and invaluable expertise in Remotely Operated Vehicle (ROV) operations. We thank personnel of the ROVs for all their assistance: Ian Murdock and CSSF-ROPOS; Wolfgang Carolsfeld, James Pegg and the Pacific Biological Station; the Super Mohawk ROV team on the Canadian Coast Guard Ship (CCGS) Amundsen, ITB Subsea, and the Simon Fraser University (SFU) ROV team. We also thank the crew of the CCGS John P. Tully, Vector, Hudson, and Amundsen, R/V Thompson; and the personnel at VENUS and NEPTUNE. Research is sponsored by the Natural Sciences and Engineering Research Council (NSERC) through the Canadian Healthy Oceans Network (CHONe). Additional support was provided by University of Victoria fellowships and NSERC postgraduate scholarships to C. Du Preez and J.W.F. Chu.

Literature cited

Aranha R. Edinger E, Layne G, Piercey G (2014) Growth rate variation and potential paleoceanographic proxies in *Primnoa pacifica*: Insights from high-resolution trace element microanalysis. *Deep-Sea Research Part II: Topical Studies in Oceanography*, **99**, 213-226.

Barker BAJ, Davis DL, Smith GP (2001) The calibration of laser-referenced underwater cameras for quantitative assessment of marine resources. *In* Proceedings of OCEANS 2001, MTS/IEEE Conference and Exhibition, vol. 3. Honolulu, HI, USA, 5–8 November 2001. pp. 1854-1859.

Chu JWF, Leys SP (2010) High resolution mapping of community structure in three glass sponge reefs (Porifera, Hexactinellida). *Marine Ecology Progress Series*, **417**, 97-113.

Chu JWF, Leys SP (2012) The dorid nudibranchs *Peltodoris lentiginosa* and *Archidoris odhneri* as predators of glass sponges. *Invertebrate Biology*, **131**, 75-81.

Chu JWF, Maldonado M, Yahel G, Leys SP (2011) Glass sponge reefs as a silicon sink. *Marine Ecology Progress Series*, **441**, 1-14.

Christ RD, Wernli RL (2014). Video. *In* The ROV manual: a user guide for remotely operated vehicles. 2nd Ed. Butterworth-Heinemann, Amsterdam. pp. 249-283.

Du Preez C, Tunnicliffe V (2011) Shortspine thornyhead and rockfish (Scorpaenidae) distribution in response to substratum, biogenic structures and trawling. *Marine Ecology Progres Series*, **425**, 217-231.

Du Preez C (2012) A new video survey method of microtopographic laser scanning (MiLS) to measure small-scale seafloor bottom roughness. *Limnology and Oceanography Methods*, **10**, 899-909.

Du Preez C, Curtis JMR, Davies SC, Clarke ME, Fruh EL (2014) Cobb Seamount species inventory. *Canadian Technical Report Fisheries and Aquatic Sciences*, **3122**, 1-108.

Forget NL, Juniper SK (2013) Free-living bacterial communities associated with aggregations of *Ridgeia piscesae* undergoing different environmental conditions at Main Endeavour Vent field, Juan de Fuca Ridge. *Microbiologyopen*, **2**, 1-17.

Forget NL, Murdock SA, Juniper SK (2010) Bacterial diversity in Fe-rich hydrothermal sediments at two South Tonga Arc submarine volcanoes. *Geobiology*, **8**, 417–32.

Gobi AF (2010) Towards Generalized Benthic Species Recognition and Quantification Using Computer Vision. *In*: Proceedings of OCEANS 2010 Conference, Sydney, Australia, 24-27 May 2010. pp. 94–100.

Lacharitè M, Metaxas A (2013) Early life history of deep-water gorgonian corals may limit their abundance. *PLoS ONE*, **8**, e65394.

Matabos M, Tunnicliffe V, Juniper SK, Dean C (2012) A year in hypoxia: epibenthic community responses to severe oxygen deficit at a subsea observatory in a coastel inlet. *PLoS ONE*, **7**, e45626.

Matabos M, Aguzzi J, Robert K, Costa C, Menesatti P, Company JB, Juniper SK (2011) Multi-parametric study of behavioural modulation in demersal decapods at the VENUS cabled observatory in Saanich Inlet, British Columbia, Canada. *Journal of Experimental Marine Biology & Ecology* **401**, 89–96.

Neves BM, Du Preez C, Edinger E (2014) Mapping coral and sponge habitats on a shelf-depth environment using multibeam sonar and ROV video observations: Learmonth Bank, Northern British Columbia, Canada. *Deep-Sea Research Part II: Topical Studies in Oceanography*, **99**, 169–183.

Piepenburg D, Archambault P, Ambrose WG, Blanchard AL, Bluhm BA, Carroll ML, Conlan KE, Cusson M, Feder HM, Grebmeier JM, Jewett SC, Lévesque M, Petryashev VV, Sejr MK, Sirenko BI, Włodarska-Kowalczuk M (2010) Towards

a pan-Arctic inventory of the species diversity of the macro- and megabenthic fauna of the Arctic shelf seas. *Marine Biodiversity*, **41**, 51–70.

Robert K, Juniper SK (2012) Surface-sediment bioturbation quantified with cameras on the NEPTUNE Canada cabled observatory. *Marine Ecology Progress Series*, **453**, 137–149.

Robert K, Onthank KL, Juniper SK, Lee RW (2012) Small-scale thermal responses of hydrothermal vent polynoid polychaetes: Preliminary *in situ* experiments and methodological development. *Journal of Experimental Marine Biology & Ecology*, **420**, 69–76.

Sameoto JA, Lawton P, Strong MB (2008) An approach to the development of a relational database and GIS applicable scheme for the analysis of video-based surveys of benthic habitats. *Canadian Technical Report Fisheries & Aquatic Sciences*, **2818**, 1-34.

St. Germain C (2011) Reproductive and physiological condition and juvenile recruitment in the hydrothermal vent tubeworm *Ridgeia piscesae* Jones (Polychaeta: Siboglinidae) in the context of a highly variable habitat on Juan de Fuca Ridge. MSc Thesis. University of Victoria, Victoria BC, Canada.

Stoner, A.W., Ryer, C.H., Parker, S.J., Auster, P.J., and Wakefield, W.W. 2008. Evaluating the role of fish behavior in surveys conducted with underwater vehicles. *Canadian Journal of Fisheries & Aquatic Science*, **65**, 1230-1243.

Tunnicliffe V, St. Germain C, Hilãrio A (2014) Phenotypic variation and fitness in a metapopulation of tubeworms (*Ridgeia piscesae* Jones) at hydrothermal vents. *PLoS ONE*, **9**, e110578.

Yahel G, Whitney F, Reiswig HM, Eerkes-Medrano DI, Leys SP (2007) *In situ* feeding and metabolism of glass sponges (Hexactinellida, Porifera) studied in a deep temperatre fjord with a remotely operated submersible. *Limnology & Oceanography*, **52**, 428-440.